

GPO PRICE \$ _____

OTS PRICE(S) \$ _____

Hard copy (HC) 16.00

Microfiche (MF) 1.25

PHILCO

A SUBSIDIARY OF *Ford Motor Company,*

AERONUTRONIC DIVISION

N65-26079

FACILITY FORM 602

(ACCESSION NUMBER)
203
(PAGES)
Cr 63388
(NASA CR OR TMX OR AD NUMBER)

(THRU)
1
(CODE)
33
(CATEGORY)

Publication No. U-3020

FINAL TECHNICAL REPORT

**ANALYSIS OF THE PROJECT
FIRE RE-ENTRY PACKAGE FLOW FIELD**

PREPARED FOR: National Aeronautics and Space Administration
Langley Research Center
Langley Station
Hampton, Virginia

UNDER CONTRACT: NAS 1-3419

PREPARED BY: W. C. Kuby
S. R. Byron
R. M. Foster
R. F. Hoglund
M. Holt


APPROVED BY: 
M. H. Johnson, Director
Physics Laboratory

October 8, 1964

ABSTRACT

26079

The objective of the Project Fire study reported herein is to predict theoretically the state of the gas in the flow field surrounding an Apollo type vehicle entering the earth's atmosphere at hypersonic velocity and to predict the related radiative and convective heating rates and their distribution over the body. In this study, two points on a nominal re-entry trajectory are considered. In the first case, the aerodynamic velocity is 34,582 fps and the altitude is 171,111 feet. Under these conditions, the chemistry is expected to be in equilibrium over the blunt body and the flow field is analyzed by Dorodnitsyn's method of integral relations as applied to the hypersonic blunt body problem. The flow over the back of the body is computed by the method of characteristics assuming attached flow. The second point on the trajectory is at an aerodynamic velocity of 37,439 fps and an altitude of 259,113 feet. The flow field in this case is not in equilibrium and the solution takes full account of the nonisentropic interaction between the chemical reactions and the flow field. The flow equations are again made manageable through the method of integral relations; chemical kinetic and vibrational non-equilibrium equations are integrated directly. Based on the flow field calculations the convective and radiative heat fluxes are determined.



PROJECT FIRE FLOW FIELD PREDICTION AND ANALYSIS

PREFACE

In order to expand the technical base upon which the Project Fire reentry heating data will be analyzed, contracts were awarded to the Lockheed Missiles and Space Company, the General Electric Company, and the Philco Corporation (Contracts NAS1-3417, 3418 and 3419 respectively) to compute the flow field about the reentry package along with the associated magnitude and distribution of radiative and convective heating for selected points on the nominal reentry trajectory. The contracts, which were awarded as a result of competitive bidding, provided for independent analyses embracing a number of different methods. Copies of the computing machine programs used have been supplied to NASA.

All contractors performed the necessary computations for the conditions defined at the time the maximum radiative heating rate is expected ($t = 25$ seconds, $V = 34,582$ ft/sec, $h = 171,611$ ft, and $\alpha = 0^\circ$). Lockheed also made calculations for a 5° angle of attack case. In addition, calculations were made by Lockheed and Philco for the point at which the maximum radiation from nonequilibrium gas chemistry is expected ($t = 15$ seconds, $V = 37,439$ ft/sec, $h = 259,113$ ft, and $\alpha = 0^\circ$). The two above conditions were obtained from a pre-flight trajectory and do not reflect the exact conditions for Flight 1.

These independent predictions made for identical conditions of reentry-body size and shape, altitude, and velocity are expected to be very useful not only in the interpretation of the Project Fire data but also to provide, for the first time, a direct comparison between the different theoretical approaches employed.

Copies of the reports by each of the three contractors have been reviewed by LRC.

TABLE OF CONTENTS

<u>Section</u>	<u>Page</u>
1. INTRODUCTION	1
2. DISCUSSION OF ANALYSES	5
2.1 Equilibrium Flow Field Program.	5
2.1.1 Basic Flow Equations	7
2.1.2 Thermochemical Equilibrium Gas Properties. . .	17
2.1.3 Boundary Conditions and Numerical Integration Procedure	18
2.1.4 Shock Layer Property Calculation	20
2.2 Non-Equilibrium Blow Field Program.	22
2.2.1 Basic Flow Equations	24
2.2.2 Chemical Kinetic Rate Equations.	31
2.2.3 Boundary Conditions and the Numerical Integration Procedure	35
2.2.4 Shock Layer Property Calculation	37
2.2.5 Continuation of the Non-Equilibrium Program beyond the Sonic Corner	41
2.3 Non-Equilibrium Air Chemistry	44
2.3.1 Equilibrium Constants.	45
2.3.2 Vibration Relaxation Rates	46
2.3.3 Chemical Reaction Rates.	47
2.3.4 Vibration-Dissociation Coupling.	49
2.4 Radiation Properties.	51
2.4.1 Band Radiation	52
2.4.2 Continuum Radiation.	53
2.4.3 Radiative Flux Computation	56
2.4.4 Non-Equilibrium Radiation	58
2.5 Convective Heat Transfer.	60
2.6 Supersonic Flow Field	64
2.7 Low Reynolds Number Effects	70
3. DISCUSSION OF RESULTS.	76
3.1 Case I - Equilibrium Flow	76
3.2 Case III - Non-Equilibrium Flow	82

TABLE OF CONTENTS (continued)

<u>Section</u>	<u>Page</u>
REFERENCES	85
TABLES	93
FIGURES.	117
APPENDIX A - Thermodynamic Air Properties for the Equilibrium Blunt Body Program	177
APPENDIX B - Normal Shock and Blunt Body Stagnation Point Equilibrium Air Properties	185

LIST OF FIGURES

FIGURE 1.	BODY AND SHOCK GEOMETRY FOR EQUILIBRIUM PROGRAM	-117-
FIGURE 2.	BODY, SHOCK AND STREAMLINE GEOMETRY FOR NON-EQUILIBRIUM PROGRAM	-117-
FIGURE 2a.	CASE III GEOMETRY AT CORNER OF BODY	-118-
FIGURE 3.	ENERGY LEVEL DIAGRAM - DEFINITION OF RADIATION TERMS	-119-
FIGURE 4.	COORDINATE SYSTEM FOR RADIATION INTEGRATION	-120-
FIGURE 5.	CHARACTERISTIC CELL - INTERIOR POINT	-121-
FIGURE 6.	CHARACTERISTIC CELL - SHOCK POINT	-121-
FIGURE 7.	CHARACTERISTIC CELL - BODY POINT	-121-
FIGURE 8.	TEMPERATURE PROFILES IN THE PERFECT GAS SHOCK LAYER - HIGHLY COOLED BODY	-122-
FIGURE 9.	CASE I VEHICLE GEOMETRY	-123-
FIGURE 10.	CASE III VEHICLE GEOMETRY	-124-
FIGURE 11.	PRESSURE DISTRIBUTION ALONG THE BODY SURFACE, (CASE I)	-125-
FIGURE 12.	TEMPERATURE DISTRIBUTION ALONG THE BODY SURFACE, (CASE I)	-126-
FIGURE 13.	DENSITY DISTRIBUTION ALONG THE BODY SURFACE, (CASE I)	-127-
FIGURE 14.	SHOCK DETACHMENT DISTANCE, $(\bar{\epsilon}/\bar{R}_{os})$, (CASE I)	-128-
FIGURE 15.	COORDINATE SYSTEM (CASE I)	-129-
FIGURE 16.	PRESSURE DISTRIBUTION ACROSS THE SHOCK LAYER, (CASE I)	-130-
FIGURE 17.	TEMPERATURE DISTRIBUTION ACROSS THE SHOCK LAYER, (CASE I)	-131-
FIGURE 18.	DENSITY DISTRIBUTION ACROSS THE SHOCK LAYER, (CASE I)	-132-
FIGURE 19.	STREAMLINE POSITIONS OVER AFTER-BODY (CASE I)	-133-
FIGURE 20.	LOG PRESSURE VS. AXIAL DISTANCE IN FLOW OVER THE AFTER-BODY (CASE I)	-134-

FIGURE 21.	TEMPERATURE VS. AXIAL DISTANCE IN FLOW OVER THE AFTER-BODY (CASE I)	-135-
FIGURE 22.	DENSITY VS. AXIAL DISTANCE IN FLOW OVER AFTER-BODY (CASE I)	-136-
FIGURE 23.	REYNOLDS NUMBER DISTRIBUTION, PROJECT FIRE, (CASE I)	-137-
FIGURE 24.	CONVECTIVE HEAT FLUX DISTRIBUTION ON BLUNT FACE, PROJECT FIRE, (CASE I)	-138-
FIGURE 24a.	VELOCITY DISTRIBUTION ALONG THE BODY SURFACE (CASE I)	-139-
FIGURE 25.	CONVECTIVE HEAT FLUX DISTRIBUTION ON AFTERBODY, PROJECT FIRE, (CASE I)	-140-
FIGURE 26.	DISTRIBUTION OF RADIATIVE FLUX (CASE I)	-141-
FIGURE 27.	SPECTRAL INTENSITY OF RADIATION TO STAGNATION POINT (CASE I)	-142-
FIGURE 28.	COORDINATE SYSTEM FOR COMPUTATION OF RADIATION TO BACK WALL OF VEHICLE	-143-
FIGURE 29.	RADIATION TO REENTRY BODY INCLUDING AFTER-BODY (CASE I)	-144-
FIGURE 30.	PRESSURE DISTRIBUTION ALONG THE BODY SURFACE, (CASE III)	-145-
FIGURE 31.	TEMPERATURE DISTRIBUTION ALONG THE BODY SURFACE, (CASE III)	-146-
FIGURE 32.	DENSITY DISTRIBUTION ALONG THE BODY SURFACE, (CASE III)	-147-
FIGURE 33.	SHOCK DETACHMENT DISTANCE, $(\bar{e}/\bar{R}_{\bullet s})$, (CASE III)	-148-
FIGURE 34.	STREAMLINE LOCATIONS IN THE SHOCK LAYER, (CASE III)	-149-
FIGURE 35.	STAGNATION STREAMLINE PROPERTY DISTRIBUTION (CASE III)	-150-

- FIGURE 36. TEMPERATURE, DENSITY AND LOCATION DISTRIBUTIONS ALONG THE $\theta_1 = 0.01$ STREAMLINE AS A FUNCTION OF θ , THE BODY COORDINATE (CASE III) -151-
- FIGURE 37. $\gamma_{e^-}, \gamma_{N_2}, \gamma_{N_2^+}, \gamma_{O_2}, \gamma_{O_2^+}, \gamma_{O^+}$ DISTRIBUTIONS ALONG THE $\theta_1 = .01$ STREAMLINE AS A FUNCTION OF θ , THE BODY COORDINATE (CASE III) -152-
- FIGURE 38. $\gamma_N, \gamma_O, \gamma_{N^+}, \gamma_{NO^+}, \gamma_{NO}$ DISTRIBUTIONS ALONG THE $\theta_1 = .01$ STREAMLINE AS A FUNCTION OF θ , THE BODY COORDINATE (CASE III) -153-
- FIGURE 39. TEMPERATURE, DENSITY, AND LOCATION DISTRIBUTIONS ALONG THE $\theta_1 = 0.01$ STREAMLINE AS A FUNCTION OF θ , THE BODY COORDINATE (CORRECTED RATES) (CASE III) -154-
- FIGURE 40. $\gamma_{e^-}, \gamma_{N_2}, \gamma_{O^+}, \gamma_{N_2^+}, \gamma_{O_2}, \gamma_{O_2^+}$ DISTRIBUTIONS ALONG THE $\theta_1 = .01$ STREAMLINE AS A FUNCTION OF θ , THE BODY COORDINATE (CORRECTED RATES) (CASE III) -155-
- FIGURE 41. $\gamma_N, \gamma_O, \gamma_{N^+}, \gamma_{NO^+}, \gamma_{NO}$ DISTRIBUTIONS ALONG THE $\theta_1 = .01$ STREAMLINE AS A FUNCTION OF θ , THE BODY COORDINATE (CORRECTED RATES) (CASE III) -156-
- FIGURE 42. TEMPERATURE, DENSITY, AND LOCATION DISTRIBUTIONS ALONG THE $\theta_1 = .05$ STREAMLINE AS A FUNCTION OF θ , THE BODY COORDINATE (CASE III) -157-
- FIGURE 43. $\gamma_N, \gamma_O, \gamma_{N^+}, \gamma_{NO^+}, \gamma_{NO}$ DISTRIBUTIONS ALONG THE $\theta_1 = .05$ STREAMLINE AS A FUNCTION OF θ , THE BODY COORDINATE (CASE III) -158-
- FIGURE 44. $\gamma_{e^-}, \gamma_{N_2}, \gamma_{N_2^+}, \gamma_{O_2}, \gamma_{O_2^+}, \gamma_{O^+}$ DISTRIBUTIONS ALONG THE $\theta_1 = .05$ STREAMLINE AS A FUNCTION OF θ , THE BODY COORDINATE (CASE III) -159-
- FIGURE 45. TEMPERATURE, DENSITY AND LOCATION DISTRIBUTIONS ALONG THE $\theta_1 = .11$ STREAMLINE AS A FUNCTION OF θ , THE BODY COORDINATE (CASE III) -160-
- FIGURE 46. $\gamma_N, \gamma_O, \gamma_{N^+}, \gamma_{NO^+}, \gamma_{NO}$ DISTRIBUTIONS ALONG THE $\theta_1 = .11$ STREAMLINE AS A FUNCTION OF θ , THE BODY COORDINATE (CASE III) -161-

- FIGURE 47. $\gamma_{e^-}, \gamma_{N_2}, \gamma_{N_2^+}, \gamma_{O_2}, \gamma_{O_2^+}, \gamma_{O^+}$ DISTRIBUTIONS ALONG THE $\theta_1 = .11$ STREAMLINE AS A FUNCTION OF θ , THE BODY COORDINATE (CASE III) -162
- FIGURE 48. TEMPERATURE, DENSITY, AND LOCATION DISTRIBUTIONS ALONG THE $\theta_1 = .23$ STREAMLINE AS A FUNCTION OF θ , THE BODY COORDINATE (CASE III) -163
- FIGURE 49. $\gamma_{e^-}, \gamma_{N_2}, \gamma_{N_2^+}, \gamma_{O_2}, \gamma_{O_2^+}, \gamma_{O^+}$ DISTRIBUTIONS ALONG THE $\theta_1 = .23$ STREAMLINE AS A FUNCTION OF θ , THE BODY COORDINATE (CASE III) -164
- FIGURE 50. $\gamma_N, \gamma_O, \gamma_{N^+}, \gamma_{NO}, \gamma_{NO^+}$ DISTRIBUTIONS ALONG THE $\theta_1 = .23$ STREAMLINE AS A FUNCTION OF θ , THE BODY COORDINATE (CASE III) -165
- FIGURE 51. TEMPERATURE, DENSITY, AND LOCATION DISTRIBUTIONS ALONG THE $\theta_1 = .348$ STREAMLINE AS A FUNCTION OF θ , THE BODY COORDINATE (CASE III) -166
- FIGURE 52. $\gamma_N, \gamma_O, \gamma_{N^+}, \gamma_{NO}, \gamma_{NO^+}$ DISTRIBUTIONS ALONG THE $\theta_1 = .348$ STREAMLINE AS A FUNCTION OF θ , THE BODY COORDINATE (CASE III) -167
- FIGURE 53. $\gamma_{e^-}, \gamma_{N_2}, \gamma_{N_2^+}, \gamma_{O_2}, \gamma_{O_2^+}, \gamma_{O^+}$ DISTRIBUTIONS ALONG THE $\theta_1 = .348$ STREAMLINE AS A FUNCTION OF θ , THE BODY COORDINATE (CASE III) -168
- FIGURE 54. TEMPERATURE, DENSITY, AND LOCATION DISTRIBUTIONS ALONG THE $\theta_1 = .4535$ STREAMLINE AS A FUNCTION OF θ , THE BODY COORDINATE (CASE III) -169
- FIGURE 55. $\gamma_N, \gamma_O, \gamma_{N^+}, \gamma_{NO}, \gamma_{NO^+}$ DISTRIBUTIONS ALONG THE $\theta_1 = .4535$ STREAMLINE AS A FUNCTION OF θ , THE BODY COORDINATE (CASE III) -170
- FIGURE 56. $\gamma_{e^-}, \gamma_{N_2}, \gamma_{N_2^+}, \gamma_{O_2}, \gamma_{O_2^+}, \gamma_{O^+}$ DISTRIBUTIONS ALONG THE $\theta_1 = .4535$ STREAMLINE AS A FUNCTION OF θ , THE BODY COORDINATE (CASE III) -171

FIGURE 57.	CONVECTIVE HEAT FLUX DISTRIBUTION ON BLUNT FACE, PROJECT FIRE, (CASE III)	-172-
FIGURE 58.	REYNOLDS NUMBER DISTRIBUTION ON BLUNT FACE, PROJECT FIRE, (CASE III)	-173-
FIGURE 59.	DISTRIBUTION OF RADIATIVE FLUX OVER RE-ENTRY BODY	-174-
FIGURE 60.	SPECTRAL INTENSITY OF RADIATION TO STAGNATION POINT	-175-
FIGURE 61.	NORMAL DISTRIBUTION OF VOLUME EMISSION FOR CASE III	-176-

LIST OF TABLES

TABLE I	CHEMICAL KINETIC RATE CONSTANTS USED FOR COMPUTING THE REACTION RATES AND VIBRATION RELAXATION TIMES
TABLE II	MOLECULAR VIBRATION AND DISSOCIATION CONSTANTS AND HEATS OF FORMATION ($^{\circ}\text{K}$)
TABLE III	CASE I AND III FLIGHT CONDITIONS
TABLE IV	STATE OF THE GAS BETWEEN THE SHOCK AND THE FRONT FACE (CASE I)
TABLE V	STATE OF THE GAS ALONG STREAMLINES OVER THE AFTER-BODY (CASE I)
TABLE VI	CONVECTIVE HEAT TRANSFER DISTRIBUTION (CASE I)
TABLE VII	DISTRIBUTION OF RADIATIVE FLUX OVER RE-ENTRY BODY
TABLE VIII	SPECTRAL INTENSITY OF RADIATION TO STAGNATION POINT (CASE I)
TABLE IX	STATE OF THE GAS AT THE SHOCK AND BODY
TABLE X	NON-EQUILIBRIUM GAS PROPERTIES ($\xi = 0.5$), ($\xi = 0.75$) ($\xi = 0.90$)
TABLE XI	CONVECTIVE HEAT TRANSFER DISTRIBUTION (CASE III)
TABLE XII	DISTRIBUTION OF RADIATIVE FLUX OVER RE-ENTRY BODY (CASE III)
TABLE XIII	SPECTRAL INTENSITY OF RADIATION TO STAGNATION POINT (CASE III)

LIST OF SYMBOLS

English Letters

a	speed of sound
a_o	radius of first Bohr orbit
B	Planck function
B_e	rotational constant for given electronic state
c	$\rho_{t\infty}/\overline{MW}$; also velocity of light
c_p	specific heat at constant pressure
$c_{p\alpha}$	specific heat of the α th specie ($\overline{c}_p/\overline{R}_o$), dimensionless
\overline{c}_p	$\sum_{\alpha=1}^s \chi_{\alpha} c_{p\alpha} / \sum_{\alpha=1}^s \chi_{\alpha}$
e_{v_j}	vibration energy of the j species ($\overline{e}_{v_j}/\overline{R}_o \overline{T}_{t\infty}$), dimensionless
e	charge of an electron
h	enthalpy $[\overline{h}/(\overline{q}_m^2/2)]$, dimensionless; also Planck's constant
h_{α}	enthalpy of the α th specie ($\overline{h}_{\alpha}/\overline{R}_o \overline{T}_t$), dimensionless
H	enthalpy ($\overline{H}(\text{cal/gm}) \overline{MW}_{\infty} / \overline{RT}_t$), dimensionless
I	radiation intensity
k	$(\chi_{\infty} - 1)/2\chi_{\infty}$; also Boltzmann's constant
k_f, k_b	forward and backward rate coefficients $[\overline{k}/(\overline{q}_m/\overline{r}_s)]$, dimensionless
\overline{K}_i	equilibrium constant of the i reaction (moles/cm ³)
m	electronic mass
M	Mach number
\overline{MW}	molecular weight
n	coordinate perpendicular to body; also number of atoms per molecule, 1 or 2
N_o	Avogadro's number
N	number density of species

LIST OF SYMBOLS (continued)

English Letters

p	pressure, $(\bar{p}/\bar{\rho}_\infty \bar{q}_m^2)$ section 2.1; also $(\bar{p}/\bar{p}_{t_\infty})$ section 2.2, dimensionless
\bar{p}	pressure
q	total velocity $(u^2 + v^2)^{1/2}$, (\bar{q}/\bar{q}_m) , dimensionless
$q_{v'v''}$	Frank-Condon factor
Q	partition function
Q_{ij}	rate of production of the X_j species from the i th reaction $(\bar{Q}_{ij}(\text{moles/sec cm}^3)/\bar{q}_m \bar{\rho}_{t_\infty} / \bar{r}_s \bar{MW}_\infty)$
r	number of reactions; also local radius of curvature (\bar{r}/\bar{r}_s)
r_o	classical electron radius
$R_{v'v''}$	electronic transition moment
R_∞	Rydberg constant
\bar{R}_o	universal gas constant
\bar{R}	$\bar{R}_o/\bar{MW}_\infty$
R	local radius of curvature
s	coordinate along the body (\bar{s}/\bar{r}_{so}) , dimensionless; also number of species
S	specific entropy $[\bar{S}/(\bar{R}_\infty/2)]$; also resultant spin of a given electron state
t	time
\bar{T}	temperature ($^\circ\text{K}$)
T	temperature, $\bar{T}/(\bar{q}_m^2/\bar{R}_\infty)$ section 2.1; also (\bar{T}/\bar{T}_t) section 2.2, dimensionless
u	velocity: in n - or ξ - direction (\bar{u}/\bar{q}_m) , section 2.1; or, in r - or ξ - direction (\bar{u}/\bar{q}_m) , section 2.2, dimensionless
u_s	shock velocity

LIST OF SYMBOLS (continued)

English Letters

v	velocity: s -direction (\bar{v}/\bar{q}_m) section 2.1; or in θ -direction (\bar{v}/\bar{q}_m) section 2.2, dimensionless
V	volume
y	perpendicular distance from the axis of symmetry to point (s,n)
Z	distance along a streamline; also charge of ion (effective charge of neutral)

Greek Letters

α	angle between the streamline velocity vector and the s -direction velocity component
α_{jk}	atoms of the k^{th} atomic component per molecule of the j^{th} species
δ_α	concentration of the α^{th} species $\left[\bar{X}_\alpha (\text{g-moles/cm}^3) \bar{M}W_\infty / \bar{p} (\text{g/cm}^3) \right]$, moles per original moles
δ_∞	ratio of specific heats
δ	degeneracy of a given electronic state
ϵ	energy
$\bar{\epsilon}$	shock detachment distance ($\bar{\epsilon}/\bar{r}_{so}$), dimensionless
θ	polar coordinate (referred to axis of symmetry and the center of curvature of body); also streamline angle with respect to horizontal
μ	absorption coefficient; also Mach angle
ν_i, ν_i	stoichiometric coefficients
ξ	coordinate normal to the body, ($\xi = n/\bar{\epsilon}$), section 2.1; or $(r - r_o)/\bar{\epsilon}$, section 2.2, dimensionless
ρ	density, ($\bar{\rho}/\bar{\rho}_\infty$), section 2.1; or $(\bar{\rho}/\bar{\rho}_{t\infty})$, section 2.2, dimensionless
$\bar{\rho}$	density
σ	shock angle between the shock tangent and the axis of symmetry

LIST OF SYMBOLS (continued)

Greek Letters

σ_A	absorption cross section
σ_E	emission cross section
τ_j	vibration relaxation time of the j^{th} species ($\tau_j = \bar{\tau}_j q_m / \bar{r}_s$), dimensionless
ϕ	angle between body tangent and axis of symmetry
ψ	stream function
$\tilde{\omega}$	wave number
ω	shock angle
Ω	solid angle

Subscripts

e	equilibrium; also electronic
i	reaction number
j or α	species number
m	maximum
n	normal to shock
p or T	denote partial differentiation with respect to T or p
r	rotational
t	total (stagnation quantities)
tg	tangential to the shock
v	vibrational
l	conditions immediately behind shock
o	conditions on body surface
s	conditions on axial streamline
∞	freestream conditions
[]	concentration of species

LIST OF SYMBOLS (continued)

Superscripts

—	(barred) dimensional quantities
*	conditions at singular point (sonic point for equilibrium and frozen flow)
'	primed quantities denote differentiation with respect to s; also denotes excited electronic state
"	denotes lower electronic state

SECTION 1

INTRODUCTION

The objective of the Project Fire study reported herein is to predict theoretically the state of the gas in the flow field surrounding an Apollo type vehicle entering the earth's atmosphere at hypersonic velocity and to predict the related radiative and convective heating rates and their distribution over the body. In this study, two points on a nominal re-entry trajectory are considered. In the first case, the aerodynamic velocity is 34,582 fps and the altitude is 171,111 feet. Under these conditions, the chemistry is expected to be in equilibrium over the blunt body and the flow field is analyzed by Dorodnitsyn's method of integral relations as applied to the hypersonic blunt body problem. The extent of any non-equilibrium region at this flow condition was estimated to be less than 3% of the shock layer based on the normal shock studies of Allen, Rose, and Camm.^{(1.1)*} Properties of the gas in equilibrium condition are determined by analytical expressions which have been fitted to the thermochemical equilibrium gas tables. Since the solution for Case I involves the determination of the heat flux over the entire body, the portion of the flow beyond the corner was computed by the method of characteristics. The expansion at this corner is very rapid, and thus it was assumed that the chemistry became frozen along a ray normal to the body at the corner, but variations in composition and the resulting frozen heat capacity ratio along this line were considered in the frozen characteristic solution. The second point on the trajectory is at an aerodynamic velocity of 37,439 fps and an altitude of 259,113 feet. The flow field in this case is not in equilibrium and the solution takes full account of the nonisentropic interaction between the chemical reactions and the flow field. The flow equations are again made manageable through the method of integral relations; chemical kinetic

*Superscripts refer to references.

and vibrational non-equilibrium equations are integrated directly. To make a proper description of the flow field and, especially, of the radiative species, a critical evaluation of the best available rate data and extrapolation for important chemical reactions have been made.

In the calculation of radiative heating, a preliminary examination of the radiative properties of air at these temperatures and densities indicates that the air will be optically thin so that reabsorption of the radiation need not be included. After completing the computation this was not found to be true at all wavelengths. Radiation mechanisms that are considered include molecular band transitions and continuum radiation resulting from electron-neutral and electron-ion free-free transitions, photo attachment of electrons to oxygen atoms, and electron-ion free-bound (deionization) transitions. The spectral distribution of radiative flux is determined in 2000 cm^{-1} intervals and integrated over all wave numbers at the selected vehicle locations to obtain the local total radiative heat flux. The convective heating at the stagnation point is calculated by the analysis of Hoshizaki.^(1.2) The laminar flow heating distribution is calculated by a step-wise solution of Lees' technique^(1.3) while the turbulent boundary layer heating is calculated by the method of Rose, Probstein and Adams.^(1.4) For the solutions included, the flow was laminar throughout.

One of the most difficult aspects of the Project Fire Case I and III problem was the prediction of the subsonic and transonic flow fields. The equations of motion describing the inviscid adiabatic hypersonic flow over a blunt body are of the mixed elliptic-hyperbolic type and are exceedingly difficult to solve. The types of numerical solutions that can be used to solve the blunt body problem are usually classified as inverse and direct methods.^(1.5) In the inverse method, the shock shape is initially assumed known and the flow variables are expanded in a series and integrated from the shock to points in the flow field corresponding to the body streamline. Although the inverse solution is exact, the problems of convergence of the series and of the extreme sensitivity of the resulting body shape to the assumed shock shape have limited the application of the method. The source of the convergence problem has been identified and can usually be avoided,^(1.5) but the problem of assuming a shock shape to give a complicated body geometry such as the sharp or abruptly rounded shoulder associated with the

Project Fire re-entry body is presently not possible. It is this abruptly rounded corner body characteristic that necessitates the use of the direct method in the Project Fire problem. In the direct method, the body shape is specified and the shock shape and shock layer properties are calculated. Although a number of direct methods have been proposed in the literature (i.e., streamtube-continuity iteration methods and relaxation techniques), perhaps the most successful and powerful direct means of handling these equations is by the method of integral relations due to Dorodnitsyn.^(1.6) This method is particularly useful for bodies with a sharp or abruptly rounded shoulder, and, hence, has been selected to calculate the Project Fire thermochemical equilibrium and non-equilibrium flow fields. Before proceeding to the description of each of these programs a few general remarks about the method of integral relations as applied to the blunt body problem will be made.

The method of integral relations is used to transform the partial differential flow equations to a system of approximate ordinary differential equations. This transformation is accomplished by dividing the region between the shock and the body into N strips and integrating the partial differential equations with respect to the space variable in the strip direction. The integrands are then approximated by interpolation formulae involving the integrand values at the strip boundaries and a set of ordinary differential equations is obtained. To minimize the errors introduced by the integral approximations, the strips should be taken in the direction in which the flow quantities have the least variation, since the values of the flow variables obtained in the interpolation direction are less accurate than those calculated in the direction of integration. In hypersonic equilibrium and frozen blunt body flows, the major property variation occurs along the body rather than across the shock layer, and, hence, the strips should be taken normal to the body (Scheme I). A second feature of the integral relation hypersonic flow field solutions is that a one strip approximation usually gives quite accurate results.^(1.7) Thus, an accurate thermochemical equilibrium hypersonic blunt body flow field solution can be obtained by approximating the region between the shock and the body as a single strip. In the non-equilibrium solution, on the other hand, the flow properties vary considerably from the shock to the body, and, hence there is strong

justification for taking the strips in the body direction (Scheme II) rather than normal to the body (Scheme I). (1.7) The first approximation non-equilibrium solution reported here, however, utilizes a single strip taken in the direction normal to the body. There is some justification for this assumption in the single strip approximation, however, since one need only integrate the flow and chemical kinetic rate equations along the axis of symmetry and body streamlines and a considerable simplification is obtained with little sacrifice in accuracy. The axis of symmetry integration quite accurately establishes the shock layer flow properties and the fact that all integrations are accomplished on streamlines minimizes the numerical integration stability problems associated with the finite chemical reactions.

A description of the analytical methods as well as the numerical results for the two cases studied are presented in this report.

SECTION 2

DISCUSSION OF ANALYSES

A description of the analytical methods utilized in the determination of the Project Fire Case I (thermochemical equilibrium) and Case III (non-equilibrium) solutions is presented in the following sections. These analyses developed for both equilibrium and non-equilibrium conditions include the determination of the inviscid subsonic flow field for an axisymmetric, hypersonic blunt body by the method of integral relations, the determination of the non-equilibrium gas properties, the computation of the gas radiative properties, and the computation of the convective heat flux. In addition a discussion of the so called "second order effects" is included.

2.1 EQUILIBRIUM FLOW FIELD PROGRAM

There are a number of important blunt body re-entry trajectories in which the subsonic region of the flow field is in thermochemical equilibrium (i.e., ICBM and Lunar Re-entries) and, hence, in which equilibrium air properties must be utilized in describing the flow field. Method of integral relations equilibrium blunt body solutions have recently been reported in the literature by Belotserkovskii^(2.3) and Shih and Baron.^(2.4) The integral relation equations developed by both authors are essentially the same, and they differ only in the methods of evaluating the equilibrium properties. Belotserkovskii utilized the equilibrium air equation of state developed by Naumova^(2.5) which gives approximate analytical equations relating enthalpy and density to pressure and temperature over a large property range. Shih and Baron, on the other hand, chose to evaluate the equilibrium air properties directly from the partition functions, but to simplify the calculation did not include ionization. The equilibrium blunt body solution developed in this paper is a first approximation solution based largely on Belotserkovskii's approach, with attention given to particular applications needed here. In the first approximation the basic dependent variables are the surface and shock velocity, pressure, temperature, shock detachment distance and shock angle. The equations for these unknowns are derived from two integral relations (obtained from a modified radial momentum

equation and the continuity equation), from the shock equations and the thermodynamic relations set out in Naumova's tables. These tables are also needed to determine thermodynamic variables behind the shock.

Two points in the flow field require special consideration, namely the point behind the normal shock and the stagnation point. At the normal shock point the shock relations do not give the thermodynamic quantities explicitly and these must be found by iteration. A plausible value for density is first assumed. The mass conservation condition then gives the normal velocity, the momentum conservation condition the pressure, and the energy equations the enthalpy. The temperature is found implicitly from Naumova's formula. The resulting value and the pressure are then substituted in Naumova's formula for the density, which should agree with the assumed value. At the stagnation point the entropy is known (equal to the value at the normal shock point) and the enthalpy has the stagnation value ahead of the shock. Both these functions can be expressed in terms of pressure and temperature by Naumova's tables and this yields two implicit equations for the stagnation values, which are determined by an iterative process.

For a given body and flight condition the shock detachment distance on the axis must be chosen to satisfy one of two conditions at the body sonic point. If the body is smooth the sonic point must be located so that the integral curve for the surface velocity is regular there. If the body has a sharp corner then the solution must be adjusted to attain sonic conditions at the corner. In the latter case the surface velocity has a square root type singularity at the point. Following Belotserkovskii's recommendations the original procedure for finding the correct solutions on smooth contours has been considerably simplified. Previously it was necessary to stop a given integration ahead of the sonic point and extrapolate the solution up to that point by means of series expansions. These took time and labor to construct and had to be evaluated for each choice of detachment distance, until that corresponding to the correct saddle point conditions at the sonic point had been determined. Under the revised procedure, as applied to the first approximation, the integration corresponding to each detachment distance is continued until either the velocity derivative changes sign or, until it attains the value unity. The desired integration always lies between those satisfying these two conditions so that progressively closer lower upper bounds on the detachment distance can be found. No extrapolation and series expansions are required to carry out the new scheme. The various aspects of the program are described in the following paragraphs.

The description of the equilibrium flow field program is divided into four major parts: (1) basic flow equations, (2) thermochemical equilibrium gas properties, (3) boundary conditions and the numerical integration procedure, and (4) shock layer properties.

2.1.1. Basic Flow Equations

The steady adiabatic inviscid flow equations have been written in streamline or boundary layer coordinates. In this orthogonal coordinate system, which is shown in Figure 1, the body is assumed to be axially symmetric, "s" is the arc length along the body measured from the axis of symmetry and "n" is the normal to the body measured from the body surface. We also use the coordinates, y, ϕ , where y is the distance from the axis of symmetry to the point (s,n), and ϕ is the angle between the tangent to the body and the axis of symmetry.

The flow variables u and v are the velocity components in the n and s directions respectively. The thermodynamic variables, $\bar{p}, \bar{\rho}, \bar{h}, \bar{S}, \bar{T}$ denote pressure, density, enthalpy, specific entropy and temperature respectively. The angle between the shock wave and the axis of symmetry is denoted by σ . The flow quantities are in dimensionless form with velocities referred to the maximum velocity, \bar{q}_{\max} , the density $\bar{\rho}$ referred to the freestream density, $\bar{\rho}_{\infty}$; the pressure \bar{p} referred to twice the dynamic head, $\bar{\rho}_{\infty} \bar{q}_{\infty}^2$, the temperature \bar{T} referred to $\bar{q}_{\infty}^2 / \bar{R}_{\infty}$, the enthalpy, \bar{h} , referred to the stagnation enthalpy, $\bar{q}_{\infty}^2 / 2$, and entropy \bar{S} referred to $\bar{R}_{\infty} / 2$. Here $\bar{R}_{\infty} = \bar{R}_0 / \bar{MW}_{\infty}$ where \bar{R}_0 is the universal gas constant and \bar{MW}_{∞} is the molecular weight of the freestream gas. All lengths are made dimensionless by referring them to the body radius of curvature at the stagnation point.

The flow equations utilized in the equilibrium program are continuity equation, the n -momentum equation, Bernoulli's equation or the energy equation on a streamline, the equation of state and the conservation of entropy equation.

The continuity equation in boundary layer coordinates is ^(2.11)

$$\frac{\partial}{\partial s}(y \bar{\rho} v) + \frac{\partial}{\partial n}(y \bar{\rho} u [1 + \frac{n}{R}]) = 0 \quad 2.1$$

while the n -momentum equation is

$$v \frac{\partial u}{\partial s} + (1 + \frac{n}{R}) u \frac{\partial u}{\partial n} - \frac{v^2}{R} = \frac{(1 + \frac{n}{R})}{\bar{\rho}} \frac{\partial \bar{p}}{\partial n} \quad 2.2$$

The first step in utilizing the method of integral relations is to convert the continuity and n-momentum equation to divergence form. The continuity equation is already in proper form and the n-momentum equation is transformed to the divergence form by combining it with the continuity equation. To simplify the notation, the continuity and n-momentum equation in divergence form are expressed as

$$\frac{\partial \mathcal{L}}{\partial s} + \frac{\partial (AL)}{\partial n} = 0 \quad 2.3$$

and

$$\frac{\partial Z}{\partial s} + \frac{\partial (AH)}{\partial n} = Y \quad 2.4$$

where the new variables are defined as

$$\begin{aligned} Z &= y \rho u v \\ H &= y (p + \rho u^2) \\ \mathcal{L} &= y \rho v \\ L &= y \rho u \\ Y &= (G/R) + (Ap \cos \emptyset) \\ G &= y (p + \rho v^2) \\ A &= 1 + n/R \\ R &= \text{body radius of curvature} = - ds/d\emptyset. \end{aligned} \quad 2.5$$

In the analysis which follows, suffix 0 refers to conditions on the body, while suffix 1 refers to conditions immediately behind the shock. The distance of a general point from the axis of symmetry is given by

$$y = y_0(s) + n \cos \emptyset \quad 2.6$$

Before deriving the integral relations we change the independent variables in Eqs. 2.3, 2.4 from s, n , to s, ξ where

$$n = \xi \epsilon \quad 2.7$$

Then,

$$\left(\frac{\partial}{\partial s} \right)_n = \left(\frac{\partial}{\partial s} \right)_\xi - \frac{\xi \epsilon'^*}{\epsilon} \frac{\partial}{\partial \xi} \quad 2.8$$

*Primed quantities denote differentiation with respect to s .

$$\left(\frac{d}{ds}\right)_s = \frac{1}{\varepsilon} \frac{d}{d\xi} \quad . \quad 2.9$$

The transformed equations 2.3 and 2.4 are

$$\frac{d\mathcal{L}}{ds} - \xi \frac{d}{d\xi} \left(\frac{\varepsilon'}{\varepsilon} \mathcal{L} \right) + \frac{d}{d\xi} \left(\frac{A\mathcal{L}}{\varepsilon} \right) = 0 \quad 2.10$$

$$\frac{dZ}{ds} - \xi \frac{d}{d\xi} \left(\frac{\varepsilon'}{\varepsilon} Z \right) + \frac{d}{d\xi} \left(\frac{AH}{\varepsilon} \right) = Y \quad 2.11$$

Since ξ is the distance from the body to the shock measured along the normal, then $\xi = 0$ on the body and $\xi = 1$ on the shock. To apply the method of integral relations in the first approximation, interpolate linearly for \mathcal{L} , Z and Y between the body and the shock using the formulae

$$\mathcal{L} = \mathcal{L}_0 + (\mathcal{L}_1 - \mathcal{L}_0)\xi \quad 2.12$$

$$Z = Z_0 + (Z_1 - Z_0)\xi \quad 2.13$$

$$Y = Y_0 + (Y_1 - Y_0)\xi \quad 2.14$$

then substitute in 2.10 and 2.11 and integrate with respect to ξ from 0 to 1. We obtain the relations

$$\begin{aligned} \frac{d}{ds} \left(\frac{1}{2}(\mathcal{L}_0 + \mathcal{L}_1) \right) - \frac{\varepsilon'}{\varepsilon} \mathcal{L}_1 + \frac{\varepsilon'}{\varepsilon} \left(\frac{1}{2}(\mathcal{L}_0 + \mathcal{L}_1) \right) \\ + \frac{A_1 \mathcal{L}_1 - A_0 \mathcal{L}_0}{\varepsilon} = 0 \end{aligned} \quad 2.15$$

$$\begin{aligned} \frac{d}{ds} \left(\frac{1}{2}(Z_0 + Z_1) \right) - \frac{\varepsilon'}{\varepsilon} Z_1 + \frac{\varepsilon'}{\varepsilon} \left(\frac{1}{2}(Z_0 + Z_1) \right) \\ + \frac{A_1 H_1 - A_0 H_0}{\varepsilon} = \frac{1}{2}(Y_1 + Y_0) \end{aligned} \quad 2.16$$

These may be written

$$\mathcal{L}'_1 = -\mathcal{L}'_0 + \frac{\varepsilon'}{\varepsilon} (\mathcal{L}_1 - \mathcal{L}_0) - \frac{2}{\varepsilon} (A_1 \mathcal{L}_1 - A_0 \mathcal{L}_0) \quad 2.17$$

$$z_1' = \frac{\mathcal{E}'}{\mathcal{E}} z_1 - \frac{2}{\mathcal{E}} (A_1 H_1 - A_o H_o) + (Y_1 + Y_o) \quad 2.18$$

where $z_o' = z_o = 0$

The differential equations 2.17 and 2.18 can be expressed entirely in terms of the dependent variables \mathcal{E} , σ and v_o .

The differential equation for \mathcal{E} is given by the geometrical relation

$$\frac{d\mathcal{E}}{ds} = A_1 \tan(\sigma - \phi) \quad 2.19$$

The differential equation for v_o is derived from the definition

$$\mathcal{L}_o = y_o \rho_o v_o \quad 2.20$$

$$\text{Then } \mathcal{L}_o' = y_o' \rho_o v_o + y_o \rho_o' v_o + y_o \rho_o v_o' + y_o v_o' \rho_o \quad 2.21$$

Since the body surface is a streamline, we know from the Bernoulli equation that

$$dp_o = - \rho_o v_o dv_o \quad 2.22$$

and from the entropy equation that

$$dS_o = 0 \quad 2.23$$

The speed of sound, a_o , is given as

$$a_o^2 = \frac{dp_o}{d\rho_o} \quad 2.24$$

Combining these equations, we obtain the equation

$$d\rho_o = - \frac{\rho_o v_o}{a_o^2} dv_o \quad 2.25$$

Substituting 2.21 for ρ_o' ,

the differential equation for v_o is given as

$$v_o' = \frac{\frac{\mathcal{L}_o'}{y_o \rho_o} - \frac{y_o \rho_o v_o'}{y_o \rho_o}}{1 - \frac{v_o'^2}{a_o^2}} \quad 2.26$$

where y_o' is specified by the body geometry, and a_o , the speed of sound on the body streamline, is given by a

$$a_o^2 = \frac{\rho_o h_T^*}{D \rho_o + \rho_T} \quad 2.27$$

where $D = \rho_p h_T - \rho_T h_p$
 \mathcal{L}_o' is determined from the continuity integral relation differential equation 2.17 where

$$\mathcal{L}_o' = -\mathcal{L}_1' + \frac{\mathcal{E}'}{\mathcal{E}} (\mathcal{L}_1 - \mathcal{L}_o) - \frac{2}{\mathcal{E}} (A_1 L_1 - A_o L_o)$$

To evaluate \mathcal{L}_1' , we utilize the definition

$$\mathcal{L}_1 = y_1 \rho_1 v_1$$

Then

$$\begin{aligned} \mathcal{L}_1' &= y_1' \rho_1 v_1 + y_1 v_1 \frac{d\rho_1}{d\sigma} \frac{d\sigma}{ds} + y_1 \rho_1 \frac{dv_1}{ds} = \rho_1 v_1 \left\{ y_o' + \cos\theta \frac{d\mathcal{E}}{ds} + \frac{\mathcal{E}}{R} \sin\theta \right\} \\ &+ y_1 v_1 \frac{d\rho_1}{d\sigma} \frac{d\sigma}{ds} + y_1 \rho_1 (v_1 \frac{d\sigma}{ds} - \frac{u_1}{R}) \end{aligned} \quad 2.28$$

and finally

$$\begin{aligned} \mathcal{L}_1' &= \rho_1 v_1 \cos\theta \frac{d\mathcal{E}}{ds} + y_1 \left\{ v_1 \frac{d\rho_1}{d\sigma} + \rho_1 v_1 \right\} \frac{d\sigma}{ds} \\ &+ \rho_1 v_1 y_o' + \frac{\rho_1}{R} (\mathcal{E} v_1 \sin\theta - y_1 u_1) \end{aligned} \quad 2.29$$

The final form of the equation is

$$\frac{dv_o}{ds} = \frac{E_o}{F_o} \quad 2.30$$

*The subscript T(or p) denotes partial differentiation with respect to T(or p) while holding p (or T) constant.

where

$$E_o = \frac{(\mathcal{L}_o' - y_o' \rho_o v_o) a_o^2}{y_o \rho_o} \quad 2.31$$

and

$$F_o = a_o^2 - v_o^2 \quad 2.33$$

On the axis of symmetry, equation 2.31 is indeterminate and must be replaced by the limiting form of the equation.

The limiting form of equation 2.31 is, when $s = 0$

$$E_o = \left\{ \frac{\mathcal{L}_o''}{\rho_o} - v_o' \right\} a_o^2 \quad 2.34$$

To evaluate \mathcal{L}_o'' , we use equation 2.17. When $s = 0$ we have

$$\mathcal{L}_1'' = -\mathcal{L}_o'' - \frac{2}{\mathcal{E}} \left\{ (A_1 L_1)' - (A_o L_o)' \right\} \quad 2.35$$

$$\text{Now } A_1 L_1 = A_1 \rho_1 u_1 y_1$$

$$\text{Hence } (A_1 L_1)'_{s=0} = A_1 \rho_1 u_1 y_1'$$

$$\text{where } y_1 = y_o + \mathcal{E} \cos \theta$$

$$\text{so that } (y_1)'_{s=0} = 1 - \mathcal{E} (d\theta/ds)_{s=0} = 1 + \mathcal{E}/R = A_1$$

$$\text{Hence } (A_1 L_1)'_{s=0} = A_1^2 \rho_1 u_1$$

$$\text{Similarly } (A_o L_o)'_{s=0} = \rho_o u_o = 0$$

Equation 2.35 then reduces to

$$\mathcal{L}_o'' = -\mathcal{L}_1'' - \frac{2A_1^2 \rho_1 u_1}{\mathcal{E}} \quad 2.36$$

Now, when $s = 0$

$$\mathcal{L}_1'' = Z_1''/u_1 \quad 2.37$$

Here Z_1'' is determined from equation 2.18, namely

$$Z_1'' = -\frac{2}{\mathcal{E}} \left\{ (A_1 H_1)' - (A_o H_o)' \right\} + Y_1' + Y_o'$$

$$\text{where } (A_1 H_1)' = A_1^2 (p_1 + \rho_1 u_1^2)$$

$$(A_o H_o)' = p_o$$

$$Y_1' = 2A_1 p_1 / R$$

$$Y_o' = 2p_o / R$$

Hence

$$Z_1'' = -\frac{2}{\mathcal{E}} \left\{ A_1^2 (p_1 + \rho_1 u_1^2) - p_o \right\} + \frac{2}{R} (A_1 p_1 + p_o) \quad 2.38$$

The equation for \mathcal{L}_o'' is then

$$\mathcal{L}_o'' = - (Z_1'' / u_1) - 2A_1^2 \rho_1 u_1 / \mathcal{E} \quad 2.39$$

where Z_1'' is given by equation 2.38

From equation 2.34 and 2.30, when $s = 0$

$$F_o v_o' = \left\{ \frac{\mathcal{L}_o''}{\rho_o} - v_o' \right\} a_o^2$$

Hence, when $s = 0$

$$\frac{dv_o}{ds} = \frac{\mathcal{L}_o''}{2\rho_o} \quad 2.40$$

where \mathcal{L}_o'' is given by equation 2.39 and Z_1'' is determined from equation 2.38.

In the present system of coordinates, the differential equation for σ can be deduced from the momentum integral relation differential equation 2.18 and the shock boundary conditions. Since the body contour is a coordinate line $u_o = 0$,

$$Z_o = 0$$

$$\text{Now } Z_1 = y_1 \rho_1 u_1 v_1$$

so that

$$z_1' = \frac{dz_1}{ds} = (\rho_1 u_1 v_1) \frac{dy_1}{ds} + y_1 \frac{d}{ds} (\rho_1 u_1 v_1) \quad 2.41$$

$\frac{dy_1}{ds}$ can be expressed in terms of $\frac{d\epsilon}{ds}$ from equation 2.6, the definition

of y . The term $\frac{d}{ds} (\rho_1 u_1 v_1)$ can be expressed in terms of σ using the shock boundary condition. At this point we introduce equations relating the boundary layer coordinate velocity components to the velocity components q_{tg} , q_n tangential and normal to the shock.

Thus,

$$u_1 = q_{tg} \sin(\sigma - \emptyset) - q_n \cos(\sigma - \emptyset) \quad 2.42$$

$$v_1 = q_{tg} \cos(\sigma - \emptyset) + q_n \sin(\sigma - \emptyset) \quad 2.43$$

The conditions across the shock are given by

Continuity

$$\rho q_n = q_\infty \sin \sigma \quad 2.44$$

Momentum

$$\text{Normal:} \quad p = p_\infty - \rho q_n^2 + (q_\infty \sin \sigma)^2 \quad 2.45a$$

$$\text{Tangential:} \quad q_{tg} = q_\infty \cos \sigma \quad 2.45b$$

Energy

$$h = 1 - q^2 \quad 2.46$$

In this derivation, p and T are assumed to be the independent properties where h and ρ are known functions of p and T . From the shock relations, we find

$$\frac{dp_1}{d\sigma} = \mathcal{S}_2 - q_\infty \sin \sigma \frac{dq_n}{d\sigma} \quad 2.47a$$

$$\frac{dT_1}{d\sigma} = (1/h_T) \left[\mathcal{S}_1 - h_p (dp/d\sigma) - 2 q_n (dq_n/d\sigma) \right] \quad 2.47b$$

$$\frac{d\rho_1}{d\sigma} = \rho_p (dp_1/d\sigma) + \rho_T (dT_1/d\sigma) \quad 2.48$$

$$\frac{dq_{tg}}{d\sigma} = -q_{\infty} \sin \sigma \quad 2.49$$

$$\frac{dq_n}{d\sigma} = \frac{q_{\infty} h_T \cos \sigma - q_n (D \delta_2 + \rho_T \delta_1)}{\rho h_T - q_n (D q_{\infty} \sin \sigma + 2 \rho_T q_n)} \quad 2.50$$

where $D = \rho_p h_T - \rho_T h_p \quad 2.51$

$$\delta_1 = q_{\infty}^2 \sin 2\sigma \quad 2.52$$

$$\delta_2 = \delta_1 - q_n q_{\infty} \cos \sigma \quad 2.53$$

From equations 2.42 and 2.43

$$\begin{aligned} \frac{du_1}{ds} = & \left\{ \frac{dq_{tg}}{d\sigma} \sin(\sigma - \phi) - \frac{dq_n}{d\sigma} \cos(\sigma - \phi) \right\} \frac{d\sigma}{ds} + \left\{ q_{tg} \cos(\sigma - \phi) \right. \\ & \left. + q_n \sin(\sigma - \phi) \right\} \left(\frac{d\sigma}{ds} - \frac{d\phi}{ds} \right) \end{aligned} \quad 2.54$$

or

$$\frac{du_1}{ds} = U_1 \frac{d\sigma}{ds} - v_1 \frac{d\phi}{ds} \quad 2.55$$

and

$$\frac{dv_1}{ds} = v_1 \frac{d\sigma}{ds} + u_1 \frac{d\phi}{ds} \quad 2.56$$

where

$$U_1 = \frac{dq_{tg}}{d\sigma} \sin(\sigma - \phi) - \frac{dq_n}{d\sigma} \cos(\sigma - \phi) + v_1 \quad 2.57$$

$$v_1 = \frac{dq_{tg}}{d\sigma} \cos(\sigma - \phi) + \frac{dq_n}{d\sigma} \sin(\sigma - \phi) - u_1 \quad 2.58$$

Substituting for $\frac{du}{ds}$ and $\frac{dv}{ds}$ in equation 2.41, we find that

$$\begin{aligned} z_1' = & (\rho_1 u_1 v_1) \frac{dy_1}{ds} + y_1 \left\{ u_1 v_1 \frac{d\rho_1}{d\sigma} \frac{d\sigma}{ds} + \rho_1 u_1 u_1 \frac{d\sigma}{ds} - \rho_1 v_1^2 \frac{d\phi}{ds} \right. \\ & \left. + \rho_1 u_1 v_1 \frac{d\sigma}{ds} + \rho_1 u_1^2 \frac{d\phi}{ds} \right\} \end{aligned} \quad 2.59$$

Differentiating equation 2.6 with respect to "s", we obtain

$$\frac{dy_1}{ds} = \frac{dy_0}{ds} + \cos\theta \frac{d\epsilon}{ds} - \sin\theta \frac{d\theta}{ds} \quad 2.60$$

and solving equation 2.59 for $d\sigma/ds$, we find that

$$\frac{d\sigma}{ds} = \frac{C_1}{B_1} \quad 2.61$$

with

$$C_1 = Z_1' - \rho_1 u_1 v_1 \cos\theta \frac{d\epsilon}{ds} - \rho_1 u_1 v_1 \frac{dy_0}{ds} - \frac{1}{R} \left\{ y_1 \rho_1 (v_1^2 - u_1^2) + \rho_1 u_1 v_1 \epsilon \sin\theta \right\} \quad 2.62$$

and Z_1' is given by integral relation equation 2.18

$$B_1 = y_1 \left\{ u_1 v_1 \frac{d\rho_1}{d\sigma} + \rho_1 v_1 u_1 + \rho_1 u_1 v_1 \right\} \quad 2.63$$

As was the case for the velocity derivative, $d\sigma/ds$ is indeterminate on the axis of symmetry and the limiting form must be used.

Equation 2.61, when $s = 0$, is written

$$\frac{d\sigma}{ds} = \frac{C_1'}{B_1'}$$

Now, from 2.62, when $s = 0$

$$C_1' = Z_1'' - A_1 \rho_1 u_1 v_1 \frac{d\sigma}{ds} + \frac{2}{R} A_1 \rho_1 u_1^2$$

From 2.63

$$B_1' = A_1 \rho_1 u_1 v_1$$

Hence, when $s = 0$

$$\frac{d\sigma}{ds} = \frac{Z_1'' + 2(A_1 \rho_1 u_1^2)/R}{\rho_1 u_1 v_1 2A_1} \quad 2.64$$

where Z_1'' is again determined from equation 2.38.

2.1.2. Thermochemical Equilibrium Gas Properties

The equation of state utilized in the equilibrium solution was obtained from analytical functions of the thermodynamic properties of air given by Naumova.^(2.5) The independent properties are temperature and pressure and cover the property range of $300^\circ\text{K} \leq T \leq 20,000^\circ\text{K}$ and $.001 \text{ atm} \leq P \leq 1000 \text{ atm}$. This property domain covers the environmental conditions encountered by re-entry vehicles for an extensive range of speeds and altitudes. This approximate equation of state includes dissociation and ionization and correlates within one percent of results obtained from a free-energy minimization thermochemical equilibrium computer program (Ref. 2.6). This is one of the most useful equilibrium real gas subroutines currently available in this country, not only because of its high accuracy and wide range of gas properties, but because it requires a very small amount of computer memory space and calculation time.

The details of the property analytic functions and the required property derivatives are given in Appendix A and B respectively. The differential equations describing the rate of change of the thermodynamic properties along the shock and the body are given below.

The shock property differential equations are obtained from equations 2.47a and 2.47b and are given as

$$\frac{dp_1}{ds} = \int_2 \frac{d\sigma}{ds} - q_\infty \sin \sigma \frac{dq_n}{d\sigma} \frac{d\sigma}{ds} \quad 2.65$$

and

$$\frac{dT_1}{ds} = \left(\frac{1}{h_T} \right) \left[\int_1 - h_p (dp/d\sigma) - 2q_n (dq_n/d\sigma) \right] \frac{d\sigma}{ds} \quad 2.66$$

The body property differential equations are obtained from the Bernoulli and energy equation on the body streamline and are given as

$$\frac{dp_o}{ds} = - \rho_o v_o \frac{dv_o}{ds} \quad 2.67$$

$$\frac{dT_o}{ds} = - \frac{1}{h_T} (2 - \rho_o h_p) v_o \frac{dv_o}{ds} \quad 2.68$$

Once p and T have been found, the thermodynamic variables ρ and h are determined from the equation of state.

2.1.3. Boundary Conditions and Numerical Integration Procedure

In the first approximation integral relation equilibrium blunt body solution, we have to solve the seven simultaneous first order non-linear ordinary differential equations given by equations 2.19, 2.30, 2.61, 2.65, 2.66, 2.67, and 2.68. The dependent variables are ξ , σ , v_o , p_1 , T_1 , p_o , T_o and the independent variable is s . To complete the formulation of the problem, the boundary conditions must be specified. In the equilibrium blunt body problem, the values of σ , v_o , p_1 , T_1 , p_o , T_o are specified on the axis of symmetry where $s = 0$. The detachment distance ξ_s , however, is not known initially and the final boundary condition is determined by the sonic point on the body. Thus the blunt body flow equations represent a two point boundary value problem in which the boundary conditions are given on the axis of symmetry and at the sonic point. The sonic point boundary conditions differ according to whether the prescribed body contour is smooth, with continuous slope, or sharp with discontinuous slope. For smooth corner bodies, the sonic point boundary condition requires a singular solution that passes regularly through the singular sonic point on the body. For sharp corner bodies in which the corner occurs before the smooth corner sonic point, the boundary condition is that the flow be sonic at the corner. The calculation procedures used to establish the required boundary conditions are as follows:

Stagnation Streamline Boundary Conditions

At $s = 0$

$$\sigma = \pi/2$$

$$v_o = 0$$

Normal Shock Properties

p_1 and T_1 are determined from an iterative solution of the momentum, 2.44, energy 2.46 and state equations across a normal shock and this procedure is described in detail in Appendix C.

Stagnation Point Properties

The stagnation point properties are uniquely determined by the stagnation enthalpy which is given by the freestream conditions and the stagnation streamline entropy which can be calculated from the normal shock properties. The procedure for determining p_o and T_o from h_o and S_o is given in Appendix C. The procedure for determining the entropy from the pressure and temperature involves the evaluation of an integral equation which is quite time consuming on the computer. A more efficient method of evaluating the stagnation properties is obtained by noting that the properties between

the normal shock and stagnation point do not change appreciably and, hence, the compression process is characterized by a constant real gas isentropic exponent. The pressure at the stagnation point is thus given in terms of p_1 , ρ_1 , q_∞ , γ by the equation

$$\frac{p_0}{p_1} = 1 + \left(\frac{q_\infty^2}{2 p_1 \rho_1} \right) + \frac{1}{2 \gamma} \left(\frac{q_\infty^2}{2 p_1 \rho_1} \right)^2 + \frac{2 - \gamma}{3 \gamma} \left(\frac{q_\infty^2}{2 p_1 \rho_1} \right)^3 + \dots \quad 2.69$$

where the first three terms give the stagnation pressure to four significant figures. Given the stagnation pressure and enthalpy, the stagnation temperature is determined by an iterative, the procedure given in Normal Shock description of Appendix C.

Sonic Point Boundary Conditions

Case (i) Smooth Contour

Equation 2.30 has a saddle point singularity at the sonic point on the body and the remaining condition needed to fix the solution is that the integral curve for v_0 should be regular at this point. This condition determines the shock detachment distance ξ on the axis. The required regular solution is found by the following iterative procedure.

Firstly, estimate a plausible value of ξ . With this and the other known initial values on the axis of symmetry integrate equations 2.19, 2.30, 2.61, 2.65, 2.66, 2.67 and 2.68 numerically (a fourth order Runge-Kutta scheme was used in the present program) until either (a) $E_0 = 0$ or (b) $F_0 - E_0$ changes sign from positive to negative. If (a) is satisfied, increase ξ by one unit in the last figure, or if (b) is satisfied, decrease ξ by the same amount and repeat the integration. Continue until two successive runs are obtained with one in category (a) and the other in category (b). The corresponding values of ξ are then upper and lower bounds of the required detachment distance. The integration should now be carried out with the mean of these two values. This run will also be in (a) or (b) so that closer bounds on the true ξ can be found. This procedure can be continued to determine ξ to any desired degree of accuracy. Once this value of ξ has been found the integration can be continued beyond the saddle point as follows. Stop the numerical program one step ahead of the estimated saddle point and use results upstream to extrapolate

values of the dependent variables one step beyond the point, then resume the numerical integration.

Case (ii). Sharp Corner

In the sharp corner case the sonic point on the body is no longer determined by regularity conditions but is fixed at the sharp corner. This means that in Eq. 2.30 $F_0 = 0$ at a fixed "s" and it is impossible simultaneously to satisfy the condition $E_0 = 0$, so that dv_0/ds has an infinite derivative. It can be shown that v_0 approaches the sonic speed in proportion to the square root of the distance from the sonic point.^(2.7) Accordingly, for a plausible choice of ξ , the integration of equations 2.19, 2.30, 2.61, 2.65, 2.66, 2.67 and 2.68 is continued until either (a) $E_0 = 0$ or (b) $a_0 - v_0 < 0.1 a_0$. If case (a) applies reduce the detachment distance until a run in category (b) is obtained. For this run, stop the integration at the first point where conditions (b) applies and extrapolate $a_0 - v_0$, using the square root law up to the point $a_0 - v_0 = 0$. If this is upstream of the required point, repeat the integration with an increased detachment distance. Correspondingly, if the point is downstream of the sharp corner, reduce the detachment distance. A few iterations are sufficient to find the value of ξ_0 giving sonic conditions at the sharp corner.

2.1.4. Shock Layer Property Calculation

The first approximation integral relation solution completely specifies the properties p , T , h , ρ , u and v at the shock and on the body, but does not give the properties in the shock layer. Since there are six unknown flow field properties p , T , h , ρ , u and v , six independent equations are required. Although any combination of the conservation equations and integral relation approximations could be selected, the simplest set was selected for this program; namely, the linearized set of algebraic equations for Λ , Z , and Y , and, the energy equation and the equation of state. The required equations are:

$$Z \equiv y \rho u v = Z_1(s) \xi \quad 2.70$$

$$\Lambda \equiv y \rho v = \Lambda_0(s) + [\Lambda_1(s) - \Lambda_0(s)] \xi \quad 2.71$$

$$Y = \frac{Y(p + \rho v^2)}{R(s)} + \left(1 + \int \frac{\mathcal{E}(s)}{R(s)}\right) p \cos \theta(s) = Y_0(s) + (Y_1(s) - Y_0(s)) \xi \quad 2.72$$

where $Z_1, \mathcal{A}_1, \mathcal{A}_0, Y_0, Y_1, R, \mathcal{E}, \theta$ are all known functions of s .

$$h + v^2 + u^2 = 1 \quad \text{Energy Equation} \quad 2.73a$$

$$\rho = \rho(p, T)$$

$$h = h(p, T)$$

$$y = y_0(s) + \int \mathcal{E}(s) \cos \theta(s)$$

} Equation of State

$$\text{Geometry} \quad 2.73b$$

where $y_0(s), \mathcal{E}(s)$ and $\theta(s)$ are given functions of s . Therefore, the unknowns are

$$h, \rho, p, T, v, u, y = f(\xi, s)$$

A sketch of the body and shock geometry is shown in Figure 1.

To solve the equations at a given point in the shock layer (s, ξ) an iterative scheme will be used.

(a) For a given point in the shock layer (s, ξ) ,

(b) Find u from

$$u = \frac{Z_1(s) \xi}{\mathcal{A}_0(s) + (\mathcal{A}_1(s) - \mathcal{A}_0(s)) \xi}$$

(c) Assume

$$v = v_0(s) + (v_1(s) - v_0(s)) \xi$$

(d) Calculate

h from equation 2.73a

(e) Calculate ρ from equations 2.71 and 2.73b

(f) Find p and T given ρ and h from an iterative procedure using the equation of state.

(g) Calculate a new v from equation 2.72 where

$$v^2 = \frac{R(s)}{Y(s)} \left[Y_0(s) + (Y_1 - Y_0) \int - (1 + \int \frac{\epsilon(s)}{R(s)} p \cos \phi(s) \right] - \frac{p}{\rho}$$

(h) Substitute this new value of v into step (d) and repeat the cycle until v converges with 0.5%.

When $s = 0$, these equations become indeterminate and the following equations must be used.

(a) Same

(b) $u = \frac{z_1''}{\lambda_0'' + (\lambda_1'' - \lambda_0'')} \int$ where z_1'' , λ_1'' , λ_0'' are known functions of s .

(c) $v = 0$

(d) $h = 1 - u^2$

(e) $p = \frac{\rho_0 + \{p_1(1 + \epsilon) - p_0\} \int}{1 + \int \epsilon}$

(f) Same

2.2 NON-EQUILIBRIUM FLOW FIELD PROGRAM

The treatment of general non-equilibrium flow of air, or other multi-component gas, past blunt bodies requires more far reaching changes to existing methods than those sufficing in the frozen or equilibrium chemistry regimes. The chemical kinetic effects influence the fluid motion, since reaction rates depend on the streamline pattern and the velocity field. Several authors have recently considered non-equilibrium effects in blunt body flows. Freeman (Ref. 2.8) treated the flow of the ideal dissociating gas introduced by Lighthill with a single reaction obeying a simple rate equation. This is an extension of the treatment of perfect gas flow by the Newtonian approximation. Lin and Teare (Ref. 2.9) calculated reaction rates round a blunt body with a predetermined pressure field and streamline pattern; they therefore neglected any interaction effects. More recently Lick (Ref. 2.10) generalized the inverse method to treat a reacting gas including dissociation and recombination. Wurster and Marrone, and Hall, Eschenroeder and Marrone (Refs. 2.11, 2.12, 2.13, 2.14, 2.15) in a series of detailed studies extended Lick's treatment to deal with higher order reactions allowing for vibrational degrees of freedom out of equilibrium and for ionization.

In the present paper the direct integral relations method is extended to treat non-equilibrium flow past blunt bodies of revolution. Chemical kinetics are treated in essentially the same general manner proposed by Wurster and Marrone and attention is focused on the changes required in the method of integral relations to handle a multi-component gas. To an extent the fluid motion equations can still be treated separately from the chemical kinetic equations since the latter do not contain any derivatives of pressure, density or velocity components. The method of integral relations is only applied to one momentum equation and the continuity equation. The chemical kinetic equations are integrated as they stand. At each stage of the integration the kinetic equations are treated first to determine the new species production rates. The latter are then introduced into the energy equation to obtain increments in the flow velocity variables. The remaining equations are then handled in much the same manner as in the perfect gas case. The direct method is applied in the first approximation in which certain combinations of the flow variables are assumed to vary linearly between the body surface and shock wave. The equations of motion are satisfied exactly on the body surface and the shock wave. Immediately behind the shock wave it is assumed that the translational and rotational energy modes are in equilibrium and that the chemical species and the vibration energy modes are frozen at their freestream values. Therefore, the values of the flow variables at the shock can be determined from the Rankine-Hugoniot equations for a constant specific heat perfect gas. The body properties and the shock shape are determined from the Bernoulli equation, the Rankine-Hugoniot shock equations, the geometry, and the r-momentum and continuity first approximation integral relation equations. The resulting system of equations to be solved consists of seven simultaneous first order non-linear ordinary differential equations. All but one of the boundary conditions needed to integrate these equations are given on the axis of symmetry. The remaining condition is determined from the condition of transition through the sonic line. The equation for the transverse velocity component on the body surface has a saddle point near the sonic line and it is required to find integral curves passing regularly through this point. The shock detachment distance is adjusted until the required sonic behavior is obtained.

Recently, two direct solutions of the blunt body problem have appeared in literature. The treatment of non-equilibrium hypersonic flow past blunt bodies by the method of integral relations has been considered by Belotserkovskii and Dushin (Ref. 2.16). They applied the method to flow of dissociating air, using the second scheme, in which the integral relations are evaluated along strips parallel to the body surface, while the actual numerical integration is carried out along normals to the surface. As previously mentioned, a number of arguments can be offered in support of the second scheme since concentrations vary much more rapidly normal to the body than they do parallel to it. However, the number of shock and body points determined by the scheme is limited by the order of the approximation. The second approximation given three points, the third four and so on. Calculations of non-equilibrium flow using the first scheme have been carried out by Shih and Baron (Ref. 2.4). They use the first approximation with a low temperature (no ionization) air model containing six chemical reactions.

In the present paper the integral relation method is applied with the first scheme to a complex model of air, appropriate at the extremely high velocities and altitudes associated with parabolic velocity earth re-entries. The chemical kinetics used to describe the air gas model include coupled vibration-dissociation relaxation, atom and charge exchange and atom and electron ionization. The description of the non-equilibrium program is divided into four major parts: (1) Basic Flow Equations, (2) Chemical Kinetic Rate Equations, (3) Boundary Conditions and Numerical Integration Procedure, and (4) Shock Layer Property Calculation.

2.2.1. Basic Flow Equations

In non-equilibrium blunt body flow solution, the steady adiabatic flow equations have been written in spherical polar coordinates and made dimensionless by referring the flow quantities to free stream stagnation quantities. Although boundary layer coordinates are probably more convenient for arbitrary body contours, the flow equations for this problem were treated as a simple extension of a spherical-polar coordinate perfect gas solution^(2.17) and hence it was convenient to retain these coordinates. The dimensionless variables are defined in the list of symbols and in the sketch of the coordinate system in Figure 2.

The flow equations used in the first approximation non-equilibrium solution are the continuity equation, the r-momentum equation, Bernoulli's equation, the energy equation, the state equations, and the chemical reaction and vibration energy rate equations.

The continuity equation in spherical polar coordinates is

$$\frac{\partial}{\partial r} (r^2 \rho u \sin \theta) + \frac{\partial}{\partial \theta} (r \rho v \sin \theta) = 0 \quad 2.74$$

while the r-momentum equation is

$$\rho u \frac{\partial u}{\partial r} + \rho \frac{u}{r} \frac{\partial u}{\partial \theta} - \frac{\rho v}{r} + k \frac{\partial p}{\partial r} = 0 \quad 2.75$$

As was noted in Section 2.1 a., the continuity and r-momentum equations must be converted to divergence form. In simplified notation, the divergence form of the continuity equation is

$$\frac{\partial}{\partial r} (r^2 h \sin \theta) + \frac{\partial}{\partial \theta} (r t \sin \theta) = 0 \quad 2.76$$

while the divergence form of the r-momentum equation is

$$\frac{\partial}{\partial r} (r^2 H \sin \theta) + \frac{\partial}{\partial \theta} (r S \sin \theta) - r g \sin \theta = 0 \quad 2.77$$

where

$$\begin{aligned} H &= kp + \rho u^2 \\ s &= \rho uv \\ t &= \rho v \\ h &= \rho u \\ g &= 2kp + \rho v^2 \end{aligned} \quad 2.78$$

The method of integral relations is now applied to the continuity and the r-momentum equation. Firstly, the independent variables are changed from r, θ to f, θ . Applying the first approximation, these equations, are integrated with respect to f between the limits 0 and 1. The unknown functions in the integrands t, s and g are assumed to be linear functions of f . The coefficients in these functions depend on their values on the body surface (suffix 0) and at the shock (suffix 1). The integral relations relate the derivatives of these coefficients with respect to θ . The integral relation

obtained from the first approximation continuity equation is

$$t_o'^* = \frac{-(3,2)^{**}}{(3,1)} t_1' + \beta_1 \quad 2.79$$

where

$$\begin{aligned} \beta_1 = & \frac{(3,2)}{(3,1)} (t_1 - t_o) \frac{\mathcal{E}'}{\mathcal{E}} - \left[\frac{(3,2)}{(3,1)} \cot \theta - \frac{3(2,1) r_o'}{(3,1) \mathcal{E}} \right] t_1 \\ & - \left[\cot \theta + \frac{3(2,1) r_o'}{(3,1) \mathcal{E}} \right] t_o - \frac{6(1,1)^2 h_1}{(3,1) \mathcal{E}} + \frac{6(1,0)^2 h_o}{(3,1) \mathcal{E}} \end{aligned} \quad 2.80$$

The expression for t_1' is obtained similarly to \mathcal{A}_1 derivation in Section 2.1 a. The definition t_1 is combined with the shock relations (see p.30) giving

$$t_1' = \bar{G}_1 \sigma' - h_1 \quad 2.81$$

where

$$\bar{G}_1 = \rho_1 \left[\frac{2(1 - q_\infty^2) \cot \sigma \operatorname{cosec}^2 \sigma}{1 + (1 - q_\infty^2) \cot^2 \sigma} v_1 - n_1 \right] \quad 2.82$$

The integral relation r-momentum differential equation is

$$s_o' = - \frac{(3,2)}{(3,1)} s_1' + \alpha_1 \quad 2.83$$

where

$$\begin{aligned} \alpha_1 = & \frac{(3,2)}{(3,1)} (s_1 - s_o) \frac{\mathcal{E}'}{\mathcal{E}} - \left[\frac{(3,2)}{(3,1)} \cot \theta - \frac{3(2,1) r_o'}{(3,1) \mathcal{E}} \right] s_1 \\ & - \left[\cot \theta + \frac{3(2,1) r_o'}{(3,1) \mathcal{E}} \right] s_o - \frac{6(1,1)^2}{(3,1)} \frac{H_1}{\mathcal{E}} + \frac{6(1,0)^2}{(3,1)} \frac{H_o}{\mathcal{E}} \\ & + g_o + \frac{(3,2)}{(3,1)} g_1 \end{aligned} \quad 2.84$$

The differential equations (2.79) and (2.83) can be expressed entirely in terms of the dependent variables \mathcal{E} , σ , u_o , v_o , p_o , ρ_o , the species concentrations δ_j , and the species vibration energies e_j .

*The prime superscript refers to differentiation with respect to θ .

** $(a,b) = ar_o + b\mathcal{E}$.

The differential equation for detachment distance, \mathcal{E} , is given by the geometrical relation

$$\frac{d\mathcal{E}}{d\theta} = -r'_0 - (r_0 + \mathcal{E}) \cot(\sigma + \theta) \quad 2.85$$

The differential equation for v_0 is derived from the energy equation, the Bernoulli equation and the equation of state.

Energy Equation

In dimensionless form the energy equation is

$$kH + \frac{1}{2} q^2 = \frac{1}{2} \quad 2.86$$

where
$$H = \sum_{\alpha=1}^s \gamma_{\alpha} h_{\alpha} \quad 2.87$$

and
$$h_{\alpha} = c_{p_{\alpha}} T + (n_{\alpha} - 1) e_{\alpha} + h_{\alpha}^0 \quad 2.88$$

The perfect gas equation of state is

$$T = \frac{p}{\rho \sum_{\alpha=1}^s \gamma_{\alpha}} \quad 2.89$$

If we define

$$c_{p_{\alpha}} \equiv \frac{5 + 2(n_{\alpha} - 1)}{2} \quad 2.90$$

and
$$\bar{c}_p \equiv \frac{\sum_{\alpha=1}^s \gamma_{\alpha} c_{p_{\alpha}}}{\sum_{\alpha=1}^s \gamma_{\alpha}} \quad 2.91$$

and we combine the differential form of energy and the equation of state we find that for the body streamline

$$v_0 \frac{dv_0}{d\theta} + \frac{k\bar{c}_p}{\rho} \left\{ \frac{dp}{d\theta} - \frac{p}{\rho} \frac{d\rho}{d\theta} \right\} + k \mathcal{H}' = 0 \quad 2.92$$

$$\text{where } H' \equiv \sum_{\alpha=1}^s [h_{\alpha} - \bar{c}_p T] v_{\alpha}' + \sum_{\alpha=f+1}^g \gamma_{\alpha} (n_{\alpha} - 1) e_{v_{\alpha}}' \quad 2.93$$

The derivative $dp_o/d\theta^*$ is given in terms of $dv_o/d\theta$ by the Bernoulli equation

$$\frac{dp_o}{d\theta} = - \frac{\rho_o v_o}{k} \frac{dv_o}{d\theta} \quad 2.94$$

and the expression for $d\rho_o/d\theta$ is obtained from the definition of t_o and is given as

$$\rho_o' = \frac{t_o'}{v_o} - \frac{\rho_o v_o'}{v_o} \quad 2.95$$

When these equations are substituted in the energy equation 2.92, the following equation is derived for v_o'

$$\frac{dv_o}{d\theta} = \frac{E_o}{F_o} \quad 2.96$$

$$\text{where } E_o = \frac{k \bar{c}_p v_o}{(\bar{c}_p - 1)} \left[\frac{p_o t_o'}{\rho_o t_o} - \frac{H_o'}{\bar{c}_p} \right] \quad 2.97$$

$$\text{and } F_o = a_o^2 - v_o^2 \quad 2.98$$

$$\text{where } a_o^2 \equiv \frac{k \bar{c}_p p_o}{(\bar{c}_p - 1) \rho_o} \quad 2.99$$

On the axis of symmetry $dv_o/d\theta$ is indeterminate and must be replaced by a limiting form of the equation. Since H_o' is an even function, the equation reduces to

$$\frac{dv_o}{d\theta} = \frac{t_o'}{\rho_o} \quad 2.100$$

*In this study, the original first approximation solution was obtained by simplifying a second approximation formulation in which it was necessary to evaluate p_o' from the θ -momentum equation integral relation. In the first approximation, however, the θ -momentum integral relation introduces approximations that need not be made, and, hence, the Bernoulli equation which involves no approximations has been used.

where the determinate expression for t_o' is determined in a similar manner to that described in section 2.1a and is given by

$$t_o' = - \frac{(3,2)}{(3,1)} t_1' + \bar{\beta}_1 \quad 2.101$$

where t_1' is given by equation 2.81 and

$$\bar{\beta}_1 = - \frac{3(1,1)h_1}{(3,1)\mathcal{E}} + \frac{3(1,0)^2 h_o}{(3,1)\mathcal{E}} \quad 2.102$$

The differential equation for $d\sigma/d\theta$ is obtained from the r-momentum equation, and the shock boundary conditions. The procedure for deriving the differential equation is similar to that given in section 2.1a and only the resulting equations will be given here. The one major difference, other than the coordinates, however, is the shock boundary conditions. In the non-equilibrium problem the shock thickness is assumed to be small compared to the vibration energy and chemical reaction relaxation distances and, hence, vibration energy modes and the chemical species can be assumed to be frozen through the shock. Therefore, only the translation and rotational energy modes are assumed to attain their equilibrium values through the shock. Thus, the equation of state utilized in the shock relations is the perfect gas equation with constant specific heats. The shock relations in non-dimensional form are^(2.17)

$$p_1 = \frac{4\gamma_\infty}{\gamma_\infty^2 - 1} (1 - q_\infty^2) \frac{\gamma_\infty}{\gamma_\infty - 1} \left[\frac{q_\infty^2 \sin^2 \sigma}{1 - q_\infty^2} - \frac{(\gamma_\infty - 1)^2}{4\gamma_\infty} \right] \quad 2.103$$

$$\rho_1 = \frac{\gamma_\infty + 1}{\gamma_\infty - 1} (1 - q_\infty^2) \frac{1}{\gamma_\infty - 1} \frac{q_\infty^2}{1 + (1 - q_\infty^2) \cot^2 \sigma} \quad 2.104$$

where q_∞ is given in terms of the Mach number M_∞ as

$$q_\infty = \left[\frac{1}{\frac{2}{M_\infty^2 (\gamma_\infty - 1)} + 1} \right]^{\frac{1}{2}} \quad 2.105$$

The resulting differential equations for $d\sigma/d\theta$ is given as

$$\frac{d\sigma}{d\theta} = \frac{s_1' - \rho_1(v_1^2 - u_1^2)}{D_1} \quad 2.106$$

$$\text{where } D_1 = \frac{4\gamma_\infty}{\gamma_\infty^2 - 1} q_\infty^2 (1 - q_\infty^2)^{\frac{1}{\gamma_\infty - 1}} \frac{u_1 v_1 \sin 2\sigma}{1 - q_1^2} + \rho_1 \left\{ v_1 m_1 - u_1 \left[n_1 + \frac{2v_1}{1 - q_1^2} (v_1 n_1 - u_1 m_1) \right] \right\} \quad 2.107$$

$$m_1 = \frac{dq_y}{d\sigma} \sin\theta - \frac{dq_x}{d\sigma} \cos\theta \quad 2.108$$

$$n_1 = \frac{dq_x}{d\sigma} \sin\theta - \frac{dq_y}{d\sigma} \cos\theta \quad 2.109$$

$$q_x = q_\infty \left[1 - \frac{2}{\gamma_\infty + 1} \sin^2 \left(1 - \frac{1}{M_\infty^2 \sin^2 \sigma} \right) \right] \quad 2.110$$

$$q_y = \frac{q}{\gamma_\infty + 1} \sin 2\sigma \left(1 - \frac{1}{M_\infty^2 \sin^2 \sigma} \right) \quad 2.111$$

$$\frac{dq_x}{d\sigma} = - \frac{2 q_\infty}{\gamma_\infty + 1} \sin 2\sigma \quad 2.112a$$

$$\frac{dq_y}{d\sigma} = \frac{2 q_\infty}{\gamma_\infty + 1} \left(\cos 2\sigma + \frac{1}{M_\infty^2 \sin^2 \sigma} \right) \quad 2.112b$$

$$u_1 = q_y \sin\theta - q_x \cos\theta \quad 2.113a$$

$$v_1 = q_x \sin\theta + q_y \cos\theta \quad 2.113b$$

and s_1' is given by equation 2.83. All the equations derived so far are applicable to an axisymmetric body of general shape. In the evaluation of s_1' , s_0' must be determined. The equations described s_0' are determined from the fact the body is treated as a streamline and, hence, the streamline velocity and the coordinate velocity components are related by the body geometry. For spherical bodies $s_0' = 0$ and, this problem is avoided.

On the axis of symmetry equation 2.106 is indeterminate and the limiting expression for the integral equation is determined in a manner similar to section 2.1a. and is given as

$$s_1' = \frac{(3,1)}{(3,2)} \bar{\alpha}_1 \quad 2.114$$

where

$$\bar{\alpha}_1 = - \frac{3(1,1)^2}{(3,1)} \frac{H_1}{\mathcal{E}} + \frac{3(1,0)^2}{(3,1)} \frac{H_0}{\mathcal{E}} + \frac{g_0}{2} + \frac{(3,2)}{(3,1)} \frac{g_1}{2} \quad 2.115$$

2.2.2. Chemical Kinetic Rate Equations

In the non-equilibrium flow field solution, full account of the non-isentropic interaction between the chemical reactions and the flow field is obtained by considering chemical species and vibration energy non-equilibrium with coupled-vibration-dissociation. The rate equations are presented in non-dimensional form and the variables are defined in the list of symbols. The notation is similar to that utilized in reference 2.11 where species concentrations γ_j are given in moles per original mole of air. The discussion of the particular reactions considered in the Project Fire problem and the rates associated with these reactions and the vibration-dissociation coupling model utilized are given in the section 2.3 titled non-equilibrium Air Chemistry. A definition of the subscript notation along with the rate equations utilized are presented here.

Chemical Kinetic Subscript Notation

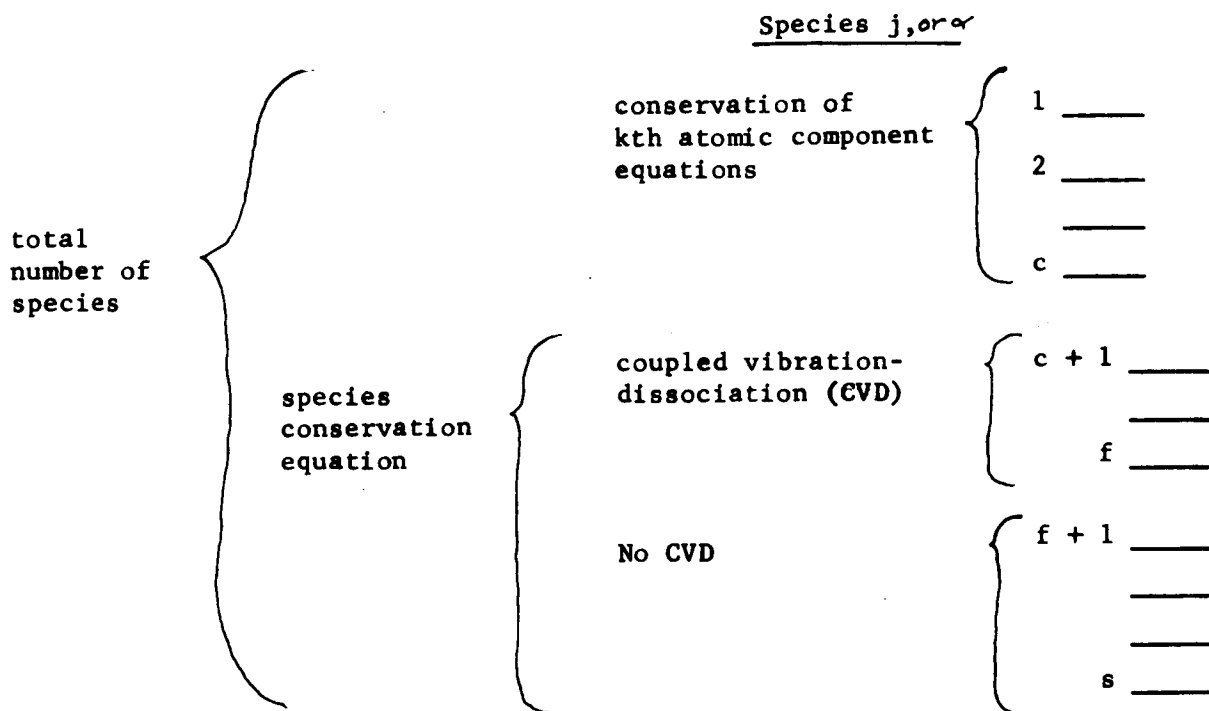
(a) Species are denoted by integers $j = 1, 2, \dots, s$.

The $j = 1, 2, 3, \dots, s$ species are further subdivided into $j = 1, \dots, c$ for conservation of the k th atomic component, and

$j = c + 1, c + 2, \dots, f$ for diatomic species in which dissociation-vibration coupling will be considered.

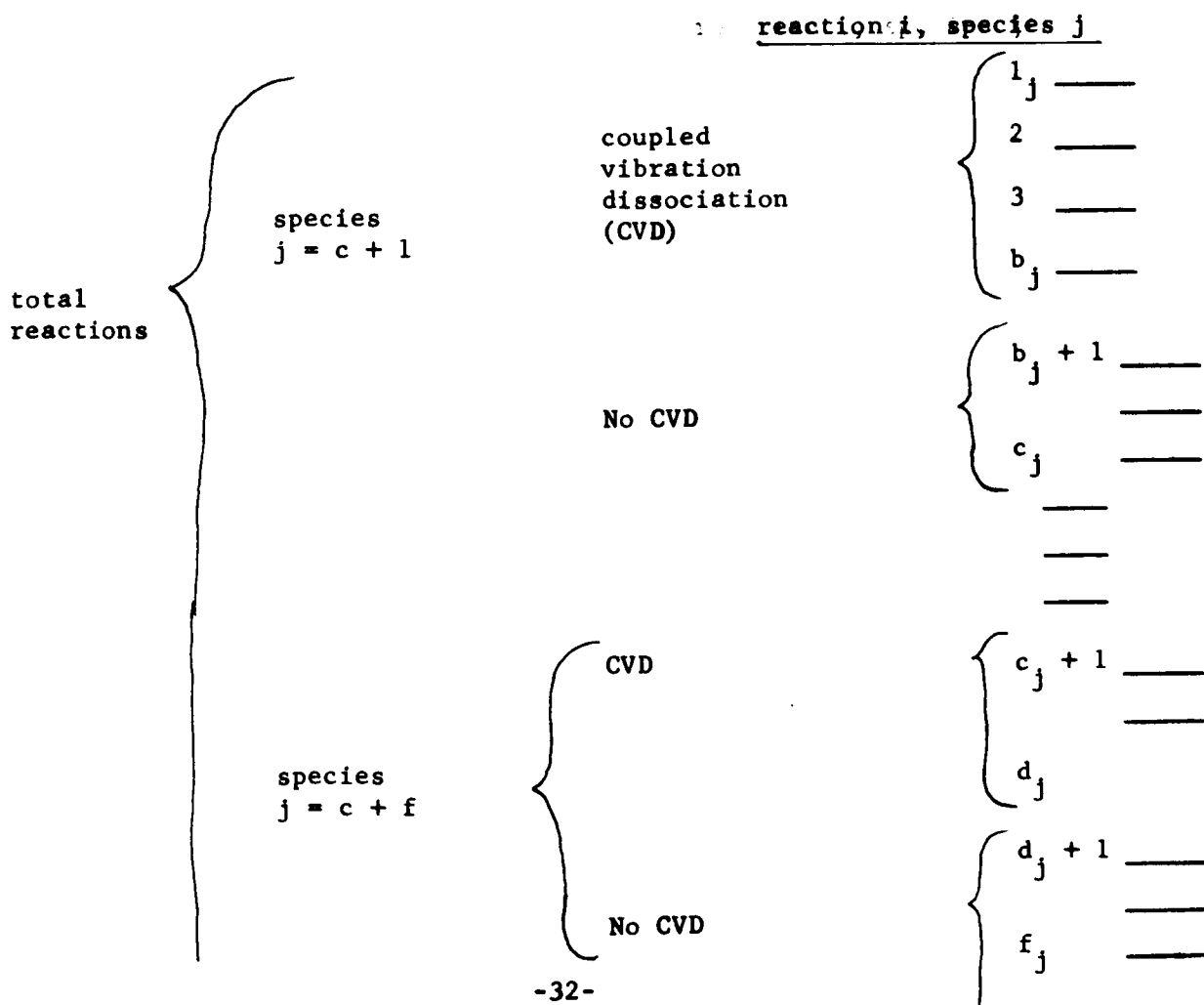
$j = f + 1, \dots, s$ uncoupled species conservation relations.

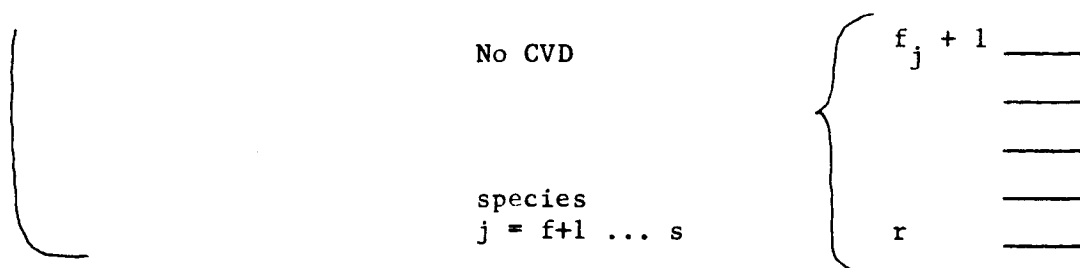
Therefore



(b) reactions are denoted by integers $i = 1, 2, \dots, r$

The reactions are grouped as follows:





Rate Equations

The system of reactions is represented as in reference 2.18 by

$$\sum_{j=1}^s \nu_{ij} M_j = \sum_{j=1}^s \nu'_{ij} M_j$$

where M_j represents the chemical species and ν_{ij} and ν'_{ij} are the stoichiometric coefficients of the reactants and products respectively. The coupled vibration-dissociation rate equations in non-dimensional form are as follows:

Coupled Species Conservation Equation

$$\frac{d \gamma_j}{dt} = q \frac{d \gamma_j}{dz} = \frac{u}{\epsilon} \frac{d \gamma_j}{d f} + \frac{v}{r} \frac{d \gamma_j}{d r} = \left[\frac{1}{1 + \frac{D_i \tau_i}{e_{vje} \gamma_j} \left| \sum_{i=1}^{c_j} \frac{Q_{ij}}{\rho} \right|} \right] \sum_{i=1}^{c_j} \frac{Q_{ij}}{\rho} + \sum_{i=f_j+1}^r \frac{Q_{ij}}{\rho} \quad (j=c+1, \dots, s) \quad 2.116$$

The species production rate is given as

$$\frac{Q_{ij}}{\rho} = \beta_{ij} (c \rho)^{\nu_i - 1} \prod_{\alpha=1}^s \gamma_{\alpha}^{\nu_{i\alpha}} \left[1 - \frac{1}{K_i} (c \rho)^{\beta_i} \prod_{\alpha=1}^s \gamma_{\alpha}^{\beta_{i\alpha}} \right] \quad 2.117$$

where $\beta_{ij} \equiv \nu'_{ij} - \nu_{ij}$

$$\nu_i \equiv \sum_{\alpha=1}^s \nu_{i\alpha}$$

$$\beta_i \equiv \sum_{\alpha=1}^s \beta_{i\alpha}$$

The vibration relaxation time τ_j is given by

$$\tau_j = (1 - \frac{1}{e^{\theta_{vj}/T}}) \frac{\bar{r}_s}{\bar{q}_m} \sum_{i=1}^{bj} z_i P_{10_i} \quad 2.119$$

where

$$z_i = \frac{a_i}{\overline{MW}_\infty} \bar{\rho}_{t\infty}^* \bar{T}_{t\infty}^{1/2} \gamma_{im} \bar{\rho} T^{1/2} \quad 2.120$$

and

$$a_i = \frac{D_i^2}{\sigma_i} \left(\frac{8\pi k}{\mu_i} \right)^{1/2} N_o \quad 2.121$$

$$\theta_{vj} = \frac{\bar{\theta}_{vj}}{\bar{T}_{t\infty}} \quad 2.122$$

$$P_{10_i} = \frac{A_i e^{-C_i/T^{1/3}}}{\bar{T}_{t\infty}^{.28} T^{.28}} \quad 2.123$$

and

$$C_i = \frac{\bar{C}_i}{\bar{T}_{t\infty}^{1/3}} \quad 2.124$$

The equilibrium vibration energy $e_{v_{je}}$ is given by

$$e_{v_{je}} = \theta_{vj} \left[\frac{1}{e^{(\theta_{vj}/T)} - 1} \right] + \frac{u_o T^2}{\theta_{vj}} \quad 2.125$$

Conservation of kth Atomic Component

$$\sum_{j=1}^s \alpha_{ik} \left[\frac{1}{\mathcal{E}} \left\{ u - \frac{v}{r} (r_o' + f \mathcal{E}') \right\} \frac{\partial \gamma_j}{\partial f} + \frac{v}{r} \frac{\partial \gamma_j}{\partial \theta} \right] = 0 \quad 2.126$$

(k = 1, 2, ..., c)

*barred quantities are dimensional

Coupled Vibration Energy Equation

$$\frac{de_v}{dt} = q \frac{de_v}{dz} = \frac{u}{\mathcal{E}} \frac{\partial e_v}{\partial \xi} + \frac{v}{r} \frac{\partial e_v}{\partial \theta} = \frac{e_{vj} - e_{vi}}{\tau_j} + \rho^{CD_j} \left[\frac{1}{1 + \frac{D_i \tau_j}{e_{vj} \gamma_j}} \left| \sum_{i=1}^{c_j} \frac{Q_{ij}}{\rho} \right| \right] \sum_{1j}^{c_j} \frac{Q_{ij}}{\rho}$$

(j = c+1...f) 2.127

The coupled species conservation and vibration energy equations are integrated point by point along the stagnation and body streamlines using the values of p_i , ρ_i , γ_i and \mathcal{E}_i at an old point, i , to obtain the new values of γ_{i+1} and \mathcal{E}_{i+1} at the next point, $i + 1$. Since in the first the approximation solution integration is only done along streamlines, the rates are given as total derivatives of streamline coordinates for spherical bodies. The temperature T is obtained from the equation of state

$$T = \frac{p}{\rho \sum_1^s \gamma_j} \quad 2.128$$

The appropriate rate constants for air system are given in Section 2.3.

2.2.3. Boundary Conditions and the Numerical Integration Procedure

Seven simultaneous first order non-linear ordinary differential equations must be solved in the first approximation integral relation solution of the non-equilibrium blunt body problem. These seven equations which are given as 2.85, 2.106, 2.96, 2.94, 2.95, 2.116, and 2.127 relate the dependent variables \mathcal{E} , σ , v_o , p_o , ρ_o , γ_j and e_j to the independent variable θ . To complete the formulation of this first order problem one boundary is required for each dependent variable. As in equilibrium solution, initial values of every dependent variable except \mathcal{E}

are specified on the axis of symmetry. The final boundary condition is given by the body sonic velocity location which in turn depends on whether the prescribed body contour is smooth with continuous slope, or sharp with discontinuous slope. The sonic velocity point boundary conditions and the convergence scheme utilized for these conditions are identical to the equilibrium scheme and will not be repeated here. The calculation procedure used to determine the stagnation streamline boundary conditions is considerably more complex than the equilibrium problem and is discussed in the following paragraphs.

Stagnation Streamline Boundary Conditions

$$\text{At } \theta = 0$$

$$\sigma = \pi/2$$

$$v_o = 0$$

Normal Shock Properties

Since the chemical species and vibration energies are assumed not to change through the shock wave, γ_j and e_j are initially the same as their free stream values and p_1 , ρ_1 and u_1 can be determined directly from the perfect gas constant specific heat Rankine-Hugoniot equations given on pages 29 and 30.

Stagnation Point Properties

In the non-equilibrium solution, the stagnation properties are obtained by combining the energy and state equations with the integration of Bernoulli and the chemical and vibration non-equilibrium differential equations along the axis of symmetry from the shock to the body. To complete the formulation of the stagnation point property problem, another equation is required and the fact that velocity along the stagnation streamline is nearly linear between the shock and the body^(2.15) was utilized in this study. It is desirable to stop the stagnation streamline integration before the stagnation point is approached, because all reactions tend equilibrium in this region and the step size for stable integration is very small, and, hence, the integration time is very large. It is possible to obtain the equilibrium stagnation properties without integrating the rate equations all the way to the stagnation point by noting that pressure only changes in the four or fifth significant figure in final 10% of the stagnation streamline integration.^(2.4) Thus the all stagnation point equilibrium properties are accurately specified by the pressure obtained from the "incomplete" stagnation streamline integration and the knowledge of the

stagnation enthalpy. In this program, the stagnation point density and all the species concentrations which are required as initial conditions are computed from a free-energy minimization thermochemical equilibrium computer program. (2.6)

A few comments should be made about the numerical instability problems associated with the integration of the chemical kinetic rate equations. In this program, a variable step fourth order Runge-Kutta numerical scheme was used to integrate the differential equations. In order to avoid numerical instabilities associated with this explicit integration scheme, the integration step size was made a fraction of the distance required to relax a given specie to a zero concentration. The step size resulting from this criteria is given by

$$\Delta z = \frac{D}{s \sum_{j=1}^s \left| \frac{d\gamma_j/dz}{\gamma_j} \right|}$$

where D is an input constant. By utilizing this step size criteria together with a test on the terms in the Runge-Kutta fourth order series expansion, a stable integration was achieved in the two critical step size regions; (1) behind the shock where the rates are very large and (2) at points downstream where some reactions approached equilibrium.

2.2.4. Shock Layer Property Calculation

The first approximation integral relation solution of the non-equilibrium blunt body provides all the flow properties at the shock and body but does not specify the shock layer properties. In making the shock layer calculation, we may utilize the three linearized integral relation variables, the conservation equations, the equation of state and the rate equations. There are the seven unknown flow properties, h , T , γ_j , e_j , p , ρ , and q that must be solved for in terms of the shock layer spacial coordinates, and if the three integral relation approximations are included, there are nine independent equations that can be used. Since there are more independent equations available than there are unknowns, the problem is overspecified and we are at liberty to select any six independent equations. The method chosen to determine shock layer properties was to locate streamlines, determine velocity and density from two of integral relation approximations, obtain the enthalpy and

temperature from the state and energy equation, determine the pressure from the state equation and obtain the species and vibration energies from the integration of the rate equation along the streamline. In the following paragraphs, the streamline shock layer calculation method will be described. The streamline calculation is divided into two major parts: (1) streamline location, and (2) streamline property determination.

(1) Streamline Location

The streamline location within the shock layer was determined by locating points of constant stream function, ψ in the shock layer, which by definition are points on a given streamline. This calculation was accomplished by utilizing the continuity equation and the approximation used in the continuity equation method of integral relations solution. The geometrical quantities used in the derivation, are shown in Figure 2.

For axisymmetric flow

$$\psi_1 = \rho_\infty q_\infty \frac{y_1^2}{2} \quad 2.129$$

and from continuity through the shock layer

$$\dot{m}_1 = \pi y_1^2 \rho_\infty q_\infty = 2\pi \psi_1 = 2\pi \int_{r_0}^{r-r_0} \rho v y dr \quad 2.130$$

Transforming variables from $r-r_0$ to ξ where $\xi = r-r_0 / \mathcal{E}(\theta)$ 2.131

$$\dot{m}_1 = 2\pi \int_0^\xi \rho v y d\xi \quad 2.132$$

and

$$\psi_1 = \mathcal{E} \int_0^\xi \rho v y d\xi \quad 2.133$$

In the solution of the non-equilibrium flow field, $t \equiv \rho v$ is assumed to be linear in ξ .

Therefore,

$$t = t_0 + (t_1 - t_0) \xi \quad 2.134$$

From geometry

$$y = y_o + \xi \mathcal{E} \sin \theta. \quad 2.135$$

Substituting 2.134 and 2.135 into 2.133, we find that

$$\psi_1 = \mathcal{E} \int_0^{\xi} [t_o + (t_1 - t_o) \xi] [y_o + \xi \mathcal{E} \sin \theta] d\xi \quad 2.136$$

and

$$\begin{aligned} \psi_1 &= \frac{\rho_o q_o y_1^2(\theta)}{2} = \mathcal{E}^2(\theta) \sin \theta [t_1(\theta) - t_o(\theta)] \frac{\xi^3}{3} \\ &+ \mathcal{E}(\theta) \left\{ y_o(\theta) [t_1(\theta) - t_o(\theta)] + \mathcal{E}(\theta) t_o(\theta) \sin \theta \right\} \frac{\xi^2}{2} \\ &+ y_o(\theta) \mathcal{E}(\theta) t_o(\theta) \xi \end{aligned} \quad 2.137$$

To find $\psi = \psi_1(\xi, \theta)$, for a given a table of θ 's, calculate

$\psi_1 = \rho_o q_o y_1^2(\theta)/2$ and solve the cubic equation 2.137 for ξ at each θ and store this information.

For a given streamline it is also necessary to know $d\xi/d\theta = f_1(\theta)$ and $\tan \alpha = d\bar{n}/d\bar{s} = f_2(\theta)$. The derivative $d\xi/d\theta$ is obtained from numerically differentiating the streamline table results relating $\xi = \xi(\theta)$ for $\psi = \text{constant}$. To determine $d\bar{n}/d\bar{s}$, we note from geometry that

$$\begin{aligned} \Delta \bar{s} &= (\bar{r}_o + \xi \bar{\mathcal{E}}) \Delta \theta \\ \Delta \bar{n} &= \Delta(\xi \bar{\mathcal{E}}) = \xi \Delta \bar{\mathcal{E}} + \bar{\mathcal{E}} \Delta \xi \end{aligned}$$

Therefore

$$\tan \alpha = \frac{\Delta \bar{n}}{\Delta \bar{s}} = \frac{\xi}{(1 + \xi \bar{\mathcal{E}})} \frac{\Delta \bar{\mathcal{E}}}{\Delta \theta} + \frac{\bar{\mathcal{E}}}{(1 + \xi \bar{\mathcal{E}})} \frac{\Delta \xi}{\Delta \theta} \quad 2.138$$

The relationship between an incremental change in θ and z is obtained from the relation $\Delta \bar{s} / \Delta z = \cos \alpha = (1 + \xi \bar{\mathcal{E}}) \Delta \theta / \Delta z$. Solving for $\Delta \theta$, we obtain, $\Delta \theta = (\Delta z / [1 + \xi \bar{\mathcal{E}}]) \cos \alpha$. Therefore, at a given θ , and ψ where we already know ξ , $d\xi/d\theta$, $d\mathcal{E}/d\theta$, and \mathcal{E} , we can evaluate α and $\Delta z / \Delta \theta$.

(2) Streamline Property Determination

The properties in the shock layer have been obtained by integrating the conservation equations along a given streamline and by

using two of the linearized variables obtained from the integral relation solution. The calculation is started just behind the shock at a given θ , and the initial values of dependent variables are given by

$$\alpha_1 = \pi/2 - (\sigma + \theta) + \arctan(\rho_0 / \rho_1 \tan \sigma) \quad 2.139$$

$$q_1 = (u_1^2 + v_1^2)^{1/2} \quad 2.113$$

$$\rho_1 = \rho_1(\sigma_1, q_\infty, \gamma_\infty) \quad 2.104$$

$$p_1 = p_1(\sigma_1, q_\infty, \gamma_\infty) \quad 2.103$$

$$T_1 = T_1(p_1, \rho_1, \gamma_j) \quad 2.128$$

$$\gamma_j = \gamma_{j\infty}$$

$$e_{v_j} = e_{v_{j\infty}}$$

The calculation procedure for determination of the shock layer properties is as follows:

The equation for the velocity q , is obtained from integral relations

$$s = \rho uv = s_1 \xi$$

and

$$t = \rho v = t_0 + (t_1 - t_0) \xi$$

and the geometrical relation that

$$q = u / \sin \alpha.$$

When these equations are combined we find that

$$q = \frac{s_1 \xi}{[t_0 + (t_1 - t_0) \xi] \sin \alpha} \quad 2.140$$

where u_1 , ρ_1 and p_1 are obtained from the Rankine-Hugoniot relations 2.113, 2.104 and 2.103.

The density is derived by combining the integral relation

$$\rho v = t_0 + (t_1 - t_0) \xi$$

and the geometrical relation

$$q = v / \cos \alpha$$

to obtain

$$\rho = \frac{t_o + (t_1 - t_o)\xi}{q \cos \alpha} \quad 2.141$$

The equation used to evaluate the temperature is obtained by combining the caloric equation of state and the energy equation giving

$$T = \frac{\frac{1}{2k} (1 - q^2) - \sum_{j=1}^s \gamma_j h_j^o - \sum_{c+1}^f \gamma_j (n_j - 1) e_{v_j}}{\sum_{j=1}^s \gamma_j (1.5 + n_j)} \quad 2.142$$

The species concentration γ_j and the vibration energies e_{v_j} are obtained by integrating the rate equations 2.116 and 2.127 finally, the pressure is given by the thermal equation of state 2.128.

$$p = \rho T \sum_1^s \gamma_j$$

2.2.5. Continuation of the Non-Equilibrium Program beyond the Sonic Corner

In the preceding discussion of the non-equilibrium computation along the body and shock, the integral relations were linearized along body normals. Since this procedure is not applicable beyond the sonic corner, the method is limited by the ray through this corner. In order to obtain the state of the gas and the extent of the shock layer beyond this ray, a requirement for the radiation computation to body points near the corner, an alternate method was formulated as follows.

All quantities at the corner are determined by Prandtl Meyer relations. As a result the only unknowns are the shock detachment distance and shock angle. The geometrical relation connecting these still applies as before so just one integral relation is needed to provide the second equation. This is obtained from the continuity equation. It should be noted in this solution that the linearized functions are

$$\mathcal{L} = y e^v$$

and

$$L = y e^u$$

while in the preceding discussion only $\rho u v$ and ρu were assumed linear. This difference greatly simplifies the computation and causes little inaccuracy since y_1/y_o does not differ greatly from unity. However, this change in

assumptions does require one alteration in the determination of the streamline locations in that Ψ is now computed by setting ξ equal to unity in equation 2.137. This change is required to compensate for an approximately 2% difference in the standoff distance caused by the different assumptions. The details of the analysis follow.

In order to deal with a centered coordinate system the integral relations were assumed to hold over rays in the Mach line direction at the corner; thus in Figure 2a the angle variable θ is

$$\theta = \frac{\pi}{2} + \nu - \mu$$

and $y = y_o + n \sin(\theta + \theta_s)$

The continuity equation may be written as

$$\frac{\partial \mathcal{L}}{\partial s} + \frac{\partial}{\partial n} \left\{ 1 + \frac{n}{R} L \right\} = 0$$

where

$$\mathcal{L} = y \rho v$$

$$L = y \rho u$$

Near the corner in the Prandtl-Meyer expansion region $R \rightarrow 0$ and this equation becomes

$$\frac{\partial \mathcal{L}}{\partial \theta} + \frac{\partial}{\partial n} (nL) = 0$$

With the change of variable $\xi = n/\epsilon$, this becomes

$$\frac{\partial \mathcal{L}}{\partial \theta} - \frac{\xi \epsilon'}{\epsilon} \frac{\partial \mathcal{L}}{\partial \xi} + \frac{1}{\epsilon} \frac{\partial}{\partial \xi} (nL) = 0 \quad 2.143$$

If we assume \mathcal{L} to be linear in ξ , i.e.

$$\mathcal{L} = \mathcal{L}_o + \xi (\mathcal{L}_1 - \mathcal{L}_o)$$

equation 2.143 can be integrated from $\xi = 0$ to 1 to give

$$\frac{1}{2} \frac{d}{d\theta} (\mathcal{L}_1 + \mathcal{L}_o) - \frac{1}{2} \frac{\epsilon'}{\epsilon} (\mathcal{L}_1 - \mathcal{L}_o) + L_1 = 0$$

or

$$\mathcal{L}'_1 = -\mathcal{L}'_o + \frac{\epsilon'}{\epsilon} (\mathcal{L}_1 - \mathcal{L}_o) - 2L_1 \quad 2.144$$

Now

$$\mathcal{L}_0 = y_0 \rho_0 v_0$$

and

$$\mathcal{L}'_0 = y_0 (\rho'_0 v'_0 + v_0 e'_0)$$

where ρ_0 , v_0 , e'_0 , and v'_0 are given by the Prandtl-Meyer relations.

\mathcal{L}_1 and L_1 can be computed from the following relations

$$y_1 = y_0 + \epsilon \sin(\theta + \theta_s)$$

$$\rho_1 = \frac{\gamma + 1}{\gamma - 1} \rho_\infty \frac{q_\infty^2}{1 + (1 - q_\infty^2) \cot^2 \sigma}$$

$$v_1 = q_\infty \left[\cos \sigma \sin(\sigma + \theta + \theta_s) - \frac{\rho_\infty}{\rho_1} \sin \sigma \cos(\sigma + \theta + \theta_s) \right]$$

and

$$u_1 = q_\infty \left[-\cos \sigma \cos(\sigma + \theta + \theta_s) - \frac{\rho_\infty}{\rho_1} \sin \sigma \sin(\sigma + \theta + \theta_s) \right]$$

where the quantity q_∞ is non-dimensionalized by \bar{q}_{\max} . Thus equation 2.144 yields \mathcal{L}'_1 . Equation 2.61 (discussion of the equilibrium flow field solution) may be written as

$$\frac{d\sigma}{d\theta} = \frac{M_1}{N_1} \quad 2.145a.$$

where

$$M_1 = \mathcal{L}'_1 - \rho_1 v_1 \sin(\theta + \theta_s) \epsilon' - \rho_1 \left[\epsilon v_1 \cos(\theta + \theta_s) - y_1 u_1 \right]$$

$$\text{and } N_1 = y_1 \left[v_1 \frac{d\rho_1}{d\sigma} + \rho_1 v_1 \right]$$

$$V_1 = -q_{\infty} \sin \sigma \sin (\sigma + \theta + \theta_s) + \\ + \left[\frac{\rho_{\infty} q_{\infty} \sin \sigma}{\rho_1} \frac{d\rho_1}{d\sigma} - \frac{\rho_{\infty} q_{\infty}}{\rho_1} \cos \sigma \right] \cos (\sigma + \theta + \theta_s) - u_1$$

Finally from geometrical considerations

$$\frac{d\epsilon}{d\theta} = -\epsilon \cot (\sigma + \theta + \theta_s) \quad 2.145 \text{ b.}$$

The values of ϵ and σ can now be computed from

$$\sigma_i = \sigma_{i-1} + \left(\frac{d\sigma}{d\theta} \right) \Delta \theta$$

$$\epsilon_i = \epsilon_{i-1} + \left(\frac{d\epsilon}{d\theta} \right) \Delta \theta$$

by iteration using equations 2.145 and previous values.

2.3 NON-EQUILIBRIUM AIR CHEMISTRY

The species included in the present calculation of non-equilibrium properties of air are O , N , e^- , O_2 , N_2 , NO , NO^+ , O_2^+ , N_2^+ , O^+ , and N^+ . Continuum theory is used, with the rotational energy of all molecules everywhere equal to the local gas temperature. Vibration relaxation, dissociation, atom exchange, charge exchange, and ionization rates are included in the calculation as well as vibration-dissociation coupling. Values for rate constants were obtained from a survey of the literature, with some modification of the equations used for extrapolation to high temperatures. Simplified analytic expressions for equilibrium constants were formulated based on spectroscopic data tabulated by Steiger. (2.19)

A number of charge transfer reactions were excluded from the set of reactions finally adopted; those having a relatively large energy defect are thought to have quite low cross-sections. Electron impact excitation and ionization was to be included originally, but subsequent study revealed that there is too little information on elastic and inelastic energy transfer rates between electrons and molecules. Only associative ionization is included. Electron attachment is insignificant at the high temperatures found in the Case III flow field.

The reactions used and the corresponding forward rates and equilibrium constants are listed in Table 1. The methods used to obtain the numerical factors are discussed briefly below.

2.3.1. Equilibrium Constants

(1) Equilibrium Vibrational Energy

Spectroscopic data for the atoms and molecules considered here have been tabulated recently by Steiger.^(2.19) The vibration and vibration-rotation coupling constants for N_2 , O_2 , and NO were used to compute equilibrium vibrational energies according to statistical mechanics (see for example Mayer and Mayer^(2.20)). It should be noted that Steiger's formulation includes vibration-rotation interactions correctly in computing partition functions, but incorrectly in computing vibrational energy. The expression used in these calculations is^(2.20)

$$e_{v_{je}} = RT \left[\frac{u}{e^u - 1} + \frac{(2\gamma + 6\sqrt{\gamma\chi} + 2\kappa)}{u} \right] = RT \left[\frac{u}{e^u - 1} + \frac{u_0}{u} \right] \quad 2.146$$

where $u_j = \theta_{v_j}/T$, with θ_{v_j} values of 2335, 3541, and 2786°K for O_2 , N_2 , and NO , respectively. These values, given recently by Konowalow and Hirschfelder,^(2.21) are somewhat larger than those given by Herzberg.^(2.22) Values of u_0 are given in Table II.

The ground electronic state properties of each molecule were used in computing vibrational energies, since the constants of low excited states differ little from the ground state. The values used are given in Table II.

(2) Equilibrium Constants of Chemical Reactions

For convenience, the species considered here are divided into a group of 3 independent elements, O , N , and e^- , and a group of 8 dependent species, O_2 , N_2 , NO , NO^+ , O_2^+ , N_2^+ , O^+ , and N^+ . Although a large number of reaction paths are considered, the equilibrium state is completely specified by a total of only 8 independent equilibrium constants. Equilibrium constants for 8 reactions were selected as being independent and the remaining equilibrium constants were calculated by linear combinations of these 8, providing complete consistency in the calculations. It should be noted that Wray^(2.23) overspecified the equilibrium state by utilizing redundant equilibrium constants, i.e., the approximations used for his $K_{(5)}$, $K_{(6)}$, and $K_{(7)}$ are inconsistent with his $K_{(2)}$, $K_{(3)}$, and $K_{(4)}$.

Using Steiger's tabulation of spectroscopic data, hand calculations of equilibrium constants were made for temperatures up to 32,000°K and were fitted by polynomials. Only those excited states which made an appreciable contribution to the partition function were included and, as mentioned above, vibration and rotation constants for all molecular electronic states were assumed the same as ground state values. The first two excited electronic states of O_2 were included, as well as the first of O , none of N_2 , the first two of N , the first of NO , the first of N^+ , and the first two of O^+ . Polynomial expressions for the three associative ionization reactions were already available from Lin^(2.24) for temperatures $3000^\circ K < T < 30,000^\circ K$. These were used in a slightly simpler form. The results, given in Table I, are accurate within 10% over the temperature range $8000^\circ K < T < 32,000^\circ K$.

2.3.2. Vibration Relaxation Rates

Because of the good agreement at high temperatures obtained by Wray^(2.25) between experimental vibration relaxation times in nitric oxide and the Schwartz, Slawsky, and Herzfeld theory,^(2.26,2.27) the SSH theory was used here for vibration relaxation of all 3 molecules, O_2 , N_2 , and NO at high temperatures. Although the theory can be used to provide absolute relaxation rates, they have been normalized by experimental data at the highest temperature available. The required reduction in the results of SSH theory in order to match experiment is a factor of 2 for oxygen and 4 for nitrogen.

The expression for the vibration transition probability given by Schwartz and Herzfeld^(2.27) is

$$P_{1 \rightarrow 0} = \frac{0.716}{\left(1 + \frac{C}{T}\right)} \left(\frac{r_c}{r_o}\right)^2 \sqrt{\frac{\pi}{3}} \left(\frac{8\pi^3 \mu h}{\alpha^{*2} h^2}\right)^2 v_{1 \rightarrow 0}^2 \mathcal{X}^{\frac{1}{2}} \exp(-3\mathcal{X}) \quad 2.147$$

$$\text{where } \mathcal{X} = \left[2\pi^4 \mu (h\nu)^2 / (\alpha^*)^2 h^2 kT \right]^{1/3}$$

$$\alpha^* = 18.0/r_o \text{ for } 10,000^\circ K \leq T \leq 30,000^\circ K$$

$$\left(\frac{r_c}{r_o}\right)^2 = \left[1/2 \left(1 + \mathcal{X} \frac{kT}{\epsilon}\right)^{\frac{1}{2}} + 1/2 \right]^{-1/3}$$

$$1 + \frac{C}{T} \approx 1$$

$$v_{1 \rightarrow 0} = -\alpha A_1 \sqrt{h/8\pi^2 M_1} v_1$$

and these parameters are defined in refs. 2.26 and 2.27.

At high temperatures $P_{1 \rightarrow 0} = P_{0 \rightarrow 1}$, the ratio being $\exp(h\nu/kT)$

The final expressions used, based on eq. 2.147 and available data, (2.25, 2.28, 2.29) are

$$\text{oxygen} \quad P_{10} = 1.7 \times 10^4 \bar{T}^{-0.28} \exp(-206/\bar{T}^{1/3})$$

$$\text{nitrogen} \quad = 8.0 \times 10^4 \bar{T}^{-0.28} \exp(-273/\bar{T}^{1/3})$$

$$\text{nitric oxide} \quad = 4.5 \times 10^4 \bar{T}^{-0.28} \exp(-230/\bar{T}^{1/3})$$

These transition probabilities are used in the classical uncoupled vibration relaxation rate expressions (2.37)

$$\frac{de_{vj}}{dt} = \frac{e_{vj} - e_{vj}}{\tau_j} = (e_{vj} - e_{vj}) Z P_{0 \rightarrow 1} (1 - e^{-\theta_j/T}) \quad 2.148$$

where e_{vj} is the equilibrium vibrational energy at the local temperature, θ_j is the fundamental vibrational oscillation energy in $^\circ\text{K}$, and Z is the collision frequency given by

$$Z = 2 \frac{\nu_1 \nu_2}{\sigma_{12}} D_{12}^2 \left(\frac{2\pi kT}{\mu_{12}} \right)^{1/2}$$

where ν_1 and ν_2 are the number densities of molecules of type 1 and 2, D_{12} is the average of the molecule diameters, μ_{12} is the reduced mass of the molecule pair and k is the Boltzmann constant.

2.3.3. Chemical Reaction Rates

The forward rate constants used were compiled from several sources, with a few modifications to insure physically reasonable extrapolations to high temperature. The oxygen atom three-body recombination rate coefficients were taken directly from Lin. (2.24) However, an average value of $1.0 \times 10^{-32} T^{-1/2} \text{ cm}^3/\text{particle}$ was used for the inert catalysts N_2 , N , and NO .

For nitrogen recombination the rate constants summarized by Lin (2.24) were used in the temperature range for which dissociation rates were measured. If this form of the recombination rate is used at higher temperatures, the dissociation rate constant reaches unreasonably large values. This arises because of the $T^{-1/2}$ temperature dependence for the pre-exponential factor of the equilibrium constant of this reaction. To provide proper extrapolation of the dissociation rate constants the inverse temperature dependence of the recombination rate constants was increased by one power of T and matched to Lin's rates at 9000°K .

The rate constant for recombination to form nitric oxide with NO as catalyst was taken directly from Wray and Teare. (2.30) The value of the

rate constant for other catalysts was assumed to be the same as that for argon, measured at an average temperature of 4000°K by Freedman and Daiber.^(2.31) The temperature dependence determined by Wray and Teare was used to extrapolate to higher temperatures. The rate used here fits Freedman and Daiber's results at 4000°K , and is 4 times larger than Wray and Teare's results.^(2.30)

All of the atom and charge transfer reaction rate constants were taken directly from Lin.^(2.24) As mentioned earlier a number of charge transfer reactions were excluded owing to large energy defects. Theoretical analysis, in agreement with experiments, shows that the cross-sections are very small for charge transfer involving atoms and monatomic ions if the energy defect exceeds a small fraction of kT .^(2.32) There is no experimental evidence to the contrary for charge transfer involving molecules and molecular ions. Therefore only charge transfer reactions having an energy defect less than 1 eV were retained, after examining all processes, including those involving low excited states.

The only ionization processes included were the associative ionization reactions. Lin's rate constants^(2.24) were used, but were extrapolated to high temperatures in a different manner. Lin extrapolates using the dissociative recombination rate constant. However, because the pre-exponential factors in the equilibrium constants increase rapidly with increasing temperature, the associative ionization rate constants obtained by Lin also increase with temperature, leading to unreasonably large cross-sections. It is thought preferable to extrapolate using the associative ionization rates determined in the temperature range $4000\text{--}5000^{\circ}\text{K}$, using a $T^{-\frac{1}{2}}$ pre-exponential temperature dependence.

Although electron impact excitation and ionization processes are probably significant for these conditions, insufficient information is currently available to warrant their inclusion. It is known that multiple excitation is the dominant electron impact ionization process for monatomic gases^(2.35) and is expected to dominate in diatomic gases. Calculations of the necessary cross-sections are currently being carried out at Philco Research Laboratories, but are not yet complete. In addition, because there is insufficient information on the rate of transfer of energy from molecular species to free electrons, it is not possible to determine the electron temperature accurately. Further theoretical and experimental work on excitation rates in diatomic gases is needed to complete the set of chemical reaction rate constants.

2.3.4. Vibration-Dissociation Coupling

The coupling between vibration relaxation processes and dissociation processes, known for some time, has recently been treated theoretically^(2.34,2.35) and observed experimentally in argon oxygen mixtures at temperatures up to 18,000°K.^(2.28,2.36) The coupling model used here is considerably simpler than the earlier theoretical treatments, although essentially the same in fundamentals. As was done by Treanor and Marrone^(2.35) the vibrational energy lost through the dissociation process is included in the vibrational relaxation rate equation. However in the present model it is assumed that the probability of dissociation is large only for high vibrational levels as opposed to other treatments which assume that "dissociation occurs with equal probability from any vibrational level in any collision that has sufficient translational energy to effect the dissociation".^(2.35)

The above assumption is based on the knowledge that the probability of a collisional transition to an adjacent quantum level is much greater than that for a change of two or more vibrational quanta.^(2.37) Similarly the cross-section for dissociation from a very high vibrational level is considerably larger than that from a low level because weak (distant interaction) forces are sufficient to effect the energy exchange required for dissociation of the high level.

With this model, all molecules dissociated must climb through the vibration ladder, the energy being fed to dissociation, through vibration relaxation, from the translational energy of the gas. Thus the vibrational coupling limits the rate of dissociation to a value which can be supplied energy-wise by vibration relaxation. This limitation is expressed as

$$\bar{E} \frac{d [X_2]^*}{dt} = [X_2] \frac{de_v}{dt} \quad 2.149$$

where \bar{E} is the dissociation energy of molecule X_2 and de_v/dt is the rate of production of vibrational energy per molecule. The limitation in dissociation relaxation time given by equation 2.149 can be combined with the uncoupled dissociation rate $(d[X_2]/dt)_u$, to determine the dissociation rate over the full range of conditions,

$$\frac{d [X_2]}{dt} = - \left\{ \frac{\bar{E}}{[X_2] \frac{de_v}{dt}} + \left(\frac{d [X_2]}{dt} \right)_u^{-1} \right\}^{-1} \quad 2.150$$

At low temperatures the uncoupled rate is very small, the second term on the right of equation 2.150 dominates, and equation 2.150 correctly gives the

*The units of the bracketed quantities are particles per original particle of air.

uncoupled rate. At high temperatures equation 2.150 reduces to equation 2.149 without the inequality.

The vibrational relaxation rate equation, including the energy lost by dissociation, is given by Treanor and Marrone^(2.35) as

$$\begin{aligned} \frac{de_v}{dt} = \frac{e_v - e_{v,j}}{[X_2]} - \frac{\bar{E}(T_T, T_v)}{[X_2]} \left[\left(\frac{d[X_2]}{dt} \right)_f \right] + \frac{\bar{G}(T_T)}{[X_2]} \left(\frac{d[X_2]}{dt} \right)_r \\ + \frac{e_{v,j}}{X_2} \left[\left(\frac{d[X_2]}{dt} \right)_f - \left(\frac{d[X_2]}{dt} \right)_r \right] \end{aligned} \quad 2.151$$

where the subscripts f and r refer to the dissociative and the recombination process respectively, T_T and T_v are the translation and vibrational temperatures respectively. The assumption that dissociation occurs primarily from upper vibrational levels also implies that the energies \bar{E} and \bar{G} are the same and are close to the dissociation energy. In the region of the flow for which vibration-dissociation coupling is significant the values of \bar{E} and \bar{G} are small compared with the dissociation energies. For this reason the last two terms of eq. 2.151 were not included in the expression used to obtain computer results. The error introduced into eq. 2.151 by this omission is less than 30% in the coupled dissociation rate, considerably less than other uncertainties (factor of 3 or more) in these rate coefficients.

2.4 RADIATION PROPERTIES

A computer program has been written under this study to compute the radiation from high temperature air both at equilibrium and non-equilibrium conditions. The former is typical of that required for the lower altitude computations while the latter applies to the high altitude, Case III determination. The particular electronic transitions considered in this computer program were dictated by the limits imposed by the two cases under consideration. In the equilibrium case the temperatures are of the order of $12,000^{\circ}\text{K}$, throughout the gas cap. Several authors such as Meyerott, ^(2.38) et.al. have indicated at these conditions the radiation from high temperature air is essentially all continuum. This continuum results primarily from electron-ion free-bound transitions, but also one must consider electron-neutral and electron-ion free-free transitions as well as the capture of electrons by oxygen atoms. In the higher altitude case the gas is considered frozen chemically going through the shock and only the translational and rotational degrees of freedom allowed to equilibrate. As a result the temperatures behind the shock are very large, of the order of $65,000^{\circ}\text{K}$, and there exists molecular species. As the flow continues in the shock layer the vibrational and electronic degrees of freedom are excited and the molecular species are dissociated. Thus in the non-equilibrium radiation it is important that molecular band radiation is also considered.

The radiation computer program developed under this study allows one to compute the radiation from high temperature air by all of these processes. A preliminary examination of the Project Fire flight conditions indicated that the densities are sufficiently low that the radiating air will be optically thin. An exception to this assumption is apparent in the final analyses as discussed in the next section. Consequently, the individual absorption coefficients can be summed and the emission computed from this. The point radiation so computed is then integrated over space to determine the local flux, either spectral or total, to a given body location.

For the non-equilibrium case the radiation is computed from the equilibrium program using the non-equilibrium specie concentrations and a modification to account for the non-equilibrium concentration of excited electronic states required in the band radiation determination.

Following is a detailed discussion of the theoretical equations used in this computer program, as well as a discussion of the various input parameters that are involved. In each case the best values which are given in the literature have been used in this computer program.

2.4.1. Band Radiation

Over the past several years the radiation from air, N_2 and at O_2 has been the subject of numerous theoretical and experimental studies. The results of these studies have indicated that the important band transitions that should be considered are the following: the O_2 Schumann-Runge, the $NO(\gamma)$, the $NO(\beta)$, the $N_2(1+)$, the $N_2(2+)$, and the $N_2^+(1-)$. The research done on these band systems has yielded electronic transition moments and/or f-numbers for these bands which radiate strongly in the temperature range of 4,000 and 9,000°K. Keck, Allen and Taylor^(2.39) have recently summarized the results of these experimental programs and reduced the data in terms of electronic transition moments. This compilation of data is believed to be the best available and was used in the computation for the values reported herein. Since the Frank-Condon factors and spectrographic data used in this study were the same as those used by Keck, Allen and Taylor and the methods of computing the r-centroid values for the molecules were similar, reference will only be made to the previously mentioned paper.

The spectral absorption coefficients in electronic band systems of diatomic emitters have been computed in the past by models that may be described as the just overlapping line model or a model utilizing a smeared out rotational structure. Both of these models are discussed by Patch, Shackleford and Penner^(2.40) and are shown to yield the same equations for the determination of the true spectral absorption coefficient. This equation is given as follows for a given electronic transition and for a single v', v'' transition:

$$\mu_{\omega, v' v''} = \pi r_o f_{v' v''} \frac{N}{Q_v'' Q_r'' (B_e' B_e'')} e^{-\frac{h\nu}{kT} (\tilde{\omega}_0 - \tilde{\omega})} e^{-\frac{(\epsilon_v' + \epsilon_r')}{kT}} q_{v' v''}$$

2.152

Keck et.al.^(2.39) shows that the f-number for such a transition is related to the electronic transition moment by the following expression which is given as a function of the r-centroid.

$$f_{v'v''} = \frac{\tilde{\omega}}{3R} \left| \frac{R_{v'v''}}{e a_0} \right|^2 q_{v'v''} \quad 2.153$$

Introducing these quantities into Eqn. 2.152 and noting that the lower state v'' may not be the ground state and thus is related to the ground state through the Maxwell-Boltzmann distribution, the following equation is obtained

$$\mu = \psi \tilde{\omega} e^{-K\tilde{\omega} - \zeta} \quad 2.154$$

where

$$\psi = \frac{\pi r_0}{3 R_e} \frac{R(\bar{r})}{e a_0}^2 N \frac{S''(2S'' + 1)}{S(2S + 1)} \frac{e^{-\epsilon_e''/kT}}{Q_v Q_r} \frac{q_{v'v''}}{B_e' - B_e''}$$

$$K = \left[\frac{B_e''}{B_e' - B_e''} \right] \times \frac{hc}{kT}$$

$$\zeta = \frac{hc}{kT} \left[\tilde{\omega}_{..} + (\tilde{\omega}_{v'} - \tilde{\omega}_{0'}) - \frac{B_e'}{B_e' - B_e''} \tilde{\omega}_{v'v''} \right]$$

(See Figure 3 for a definition of various wave numbers).

In the present work this absorption coefficient was averaged over a 2,000 wave number interval and determined by the following formula

$$\bar{\mu} = \mu_0 \left[\frac{1 + K \tilde{\omega}_0 - (1 + K \tilde{\omega}_0 + K \Delta \tilde{\omega}) e^{-K \Delta \tilde{\omega}}}{K^2 \tilde{\omega}_0 \Delta \tilde{\omega}} \right] \quad 2.155$$

Finally, the total absorption for the given band over the averaged wave number was given as the sum of the individual $v'v''$ transitions

2.4.2. Continuum Radiation

The continuum radiation mechanisms that are considered in this report are the electron neutral and the electron-ion free-free transitions, the radiation from the capture from the electrons by oxygen atoms, and the electron-ion free-bound (deionization) transitions. The first two of these mechanisms are particularly important at temperatures of less than 9,000°K for equilibrium air while the last as pointed out by Meyerott et.al. (2.38) become predominant at temperatures greater than 10,000 to 12,000°K.

As in the band systems computations, an absorption coefficient was computed for each of the radiation mechanisms described above. The contribution from O^- was obtained from the following formula.

$$\mu = \sigma [O^-]$$

where σ , the total detachment cross section, was obtained from the measurements of Branscomb et.al.^(2.41) at low energies and the calculated cross section of Bates and Massey^(2.42) at higher energies as reported by Armstrong, Sokoloff, Nicholls, Holland and Meyerott.^(2.43) The ion and neutral free-free transitions were computed using Kramer's formula (Eqn. 2.156) and, in the case of the neutral free-free, the effective charges for the atoms reported by Keck, et.al.^(2.39)

$$\mu = \frac{8\pi}{3\sqrt{3}} \frac{e^6}{m^4 c^4 h \omega^3} (2\pi mkT)^{-\frac{1}{2}} [e^-] Z^2 [N_i] \quad 2.156$$

Again noting that the air is optically thin at all wave numbers, the total absorption coefficient is obtained by summation.

The continuum radiation from electron-ion free-bound transitions was determined by interpolation and extrapolation of the results presented by Breene, et.al.^(2.44) For this determination the hydrogenic cross-sections for recombination as computed by Bates et.al.^(2.45) were used to determine the ionization cross-sections (i.e., absorption cross-section) from the following

$$\sigma_A = \frac{m E_k c^2}{h^2 \omega} \times \sigma_E$$

Where E_k is an energy term dependent on the frequency of the absorption edge for the lower electronic level considered. The computed spectral and total radiation is reported at 10,000 and 25,000°K. It was found that this radiation could be scaled by the ratio of the product of the number densities of the species of importance over the wave number range of interest. Since the temperature range of interest was near the 10,000°K level in the equilibrium solution, this temperature was used as a base and the intensity computed from the following:

$$I_{\omega, N^+} = I_{\omega, N^+, 10,000} \frac{[N^+][e^-]}{.86 \times 10^{33}}$$

and

$$I_{\omega, 0^+} = I_{\omega, 0^+, 10,000} \frac{[0^+][e^-]}{.523 \times 10^{33}}$$

where the constants are the products of the equilibrium concentrations at 10,000°K respectively. The above method was used to simplify the computer program with little inaccuracy.

The invariance of the free-bound radiation with temperature can be shown analytically. Breene^(2.44) computes the radiation as follows

$$I_{\omega} = \sigma_A [N_N] Q B (1 - e^{-\frac{h c \omega}{k T}})$$

If we define the equilibrium constant as

$$K_{eq} = \frac{[N_N^+][N_e^-]}{[N_N]} \sim T^{3/2} e^{-\frac{1}{kT} \{h c \omega_t + E^*\}}$$

where $h c \omega_t$ is the energy of the electronic transition and E^* is the energy of the absorbing state above the ground state, and we introduce the partition function of the absorbing state as

$$Q \sim T^{3/2} e^{-\frac{E^*}{kT}}$$

then

$$I_{\omega} \sim \sigma_A [N_N^+][N_e^-] e^{\frac{h c \omega_t}{kT}} e^{-\frac{h c \omega}{kT}}$$

It is apparent from the computations of Breene that the radiation from a particular radiating state decreases rapidly with wave length; thus

$$\frac{h c \omega_t}{kT} \approx \frac{h c \omega}{kT}$$

Finally it is apparent that the radiation from free-bound transitions can be

given by

$$I_{\omega} \sim \sigma_A [N_N^+] [N_e^-]$$

which is invariant with temperature. Although this result is only approximate for the exact spectral distribution (errors of the order of a factor of 2 were noted at specific wave numbers, the total radiation resulting is essentially exact with the computation of Breene in the temperature range of 10,000°K to 30,000°K.

2.4.3. Radiative Flux Computations

If we consider only the equilibrium radiation from gases which are optically thin at all wave lengths, one can write the radiation per unit volume as the following

$$\frac{d I}{d V \frac{d \nu}{d \omega}} = \mu'_{\omega} \frac{d B}{d V \frac{d \nu}{d \omega}}$$

where

$$\frac{d B}{d V \frac{d \nu}{d \omega}} = 2 h c^2 \omega^3 \left(e^{\frac{h c \omega}{k T}} - 1 \right)^{-1}$$

is the blackbody intensity and

$$\mu'_{\omega} = \mu_{\omega} \left(1 - e^{-\frac{h c \omega}{k T}} \right)$$

is the apparent absorption coefficient in terms of the true absorption coefficient. The absorption coefficient computed using the previously mentioned absorption models yields the true absorption coefficient. Finally the total absorption coefficient for all bands and continuum mechanisms (except deionization) at a given wave number, i.e., over a wave number interval, were obtained by summing the individual contributions, and the flux determined from equations. The flux per unit volume is then the sum of the above and the deionization determinations.

The values of the radiation per unit volume so computed for various points in the shock layer were then numerically integrated over space to determine the spectral and total flux to a given body location. The radiation

to a given point is given by

$$dq = I \frac{\cos \theta'}{r^2} dV \quad 2.157$$

where I is the volume emission

θ is the angle between the body normal and the line between the radiating volume dV and the body location and r is the distance along the latter line.

If one considers the spherical coordinate system with its center at the center of curvature of the body face as shown in Figure 4, Eqn. 2.157 can be written as (I is not a function of β because of axisymmetry)

$$dq = R^2 \sin \theta I(\theta, R) \frac{(R^2 - R_o^2 - a) + b \cos \beta}{2 R_o [a + b \cos \beta]^{3/2}} d\theta dR d\beta \quad 2.157a$$

where $a = R_o^2 + R^2 - 2 R R_o \cos \theta \cos \theta_o$

$$b = -2 R R_o \sin \theta \sin \theta_o$$

The appropriate limits of β , R , and θ are as follows:

$$\beta = 0 \text{ to } \beta_{\max}$$

$$\text{where, if } R \cos(\theta + \theta_o) < R_o, \beta_{\max} = \arccos \left[\frac{R_o - R \cos \theta \cos \theta_o}{R \sin \theta \sin \theta_o} \right]$$

$$\text{if } R \cos(\theta + \theta_o) \geq R_o, \beta_{\max} = \pi$$

$$R = R_o \text{ to } R_s$$

$$\theta = 0 \text{ to } \theta_{\max}$$

$$\text{where } \theta_{\max} = \arccos \left(\frac{R_o}{R_s} \right) + \theta_o$$

Equation 2.157a is numerically integrated using Simpson's rule. It should be noted that at $\theta = \theta_o$, $R = R_o$, and $\beta = 0$, the integrand of equation 2.157a becomes infinite, but the radiating volume goes to zero ($\beta = \beta_{\max} = 0$). Care must be taken when numerically integrating in the region of this singularity to avoid numerical errors. To obviate this problem, integration along the

ray through this particular body point was not used, but rather the body point was chosen to be mid-way between mesh rays. Further the effect of this numerical problem was investigated by varying the proximity of the ray closest to the singularity and noting the effect on the integration for a constant value of I . Since the q for this problem should be constant over the body, any variation was necessarily caused by the singularity. It was found that as the body point moves away from a mesh ray the computed value of q at the mid-point between the mesh rays had decreased to within 5% of the analytic value for this simple case; thus the accuracy of this method is assumed to be of this order.

2.4.4. Non-equilibrium Radiation

Some years ago it was noted in observations of the variation of electron density and of band radiation behind normal shocks in air that the relaxation time to overshoot is roughly the same for both. The time to decay to equilibrium is also very nearly the same. These early observations are borne out well by the more recent and more careful studies of the ionization rise distance behind normal shocks in air by Lin^(2.46) and of band radiation rise distance by Allen, Rose, and Camm.^(2.47) Noting Lin's definitions of "ionization rise distance" and "ionization incubation distance" and examining his detailed electron density profiles, a good approximation for the "distance to reach peak ionization" is to add the incubation distance to the rise distance. The resulting distance, when transferred to a time in the laboratory frame of reference and compared with Allen's band radiation "time to peak", is in remarkably close correspondence. Over the velocity range $4.5 < u_s < 7$ km/sec where the two sets of data overlap the radiation time to peak agrees with the ionization time to peak within 30%, or better than the scatter of either set of data.

This remarkable coincidence in relaxation times strongly suggests a close coupling between electron production and excited state production processes. As noted earlier, the mechanism and rate of production of excited states of diatomic molecules has not yet been determined either theoretically or analytically. However, empirical relations to determine the population of excited molecular electronic states can be extracted from the above experimental data. Although the data is insufficient to lead to a unique empirical model, the following quite simple approach has been adopted on the basis of our studies of collisional excitation rates.

At any point in the non-equilibrium flow field the density of excited molecular states is computed from the already determined ground state density assuming the ratio to be in equilibrium at the local translational temperature. This excited state number density is reduced by the ratio of the local electron density to the equilibrium value at the stagnation point. This number density is used in computing band emission and absorption coefficients.

This model correctly predicts the overshoot in $N_2^{(1+)}$ band emission by two orders of magnitude measured by Allen, Rose and Camm. ^(2.47) It does not introduce the unrealistically large band emission immediately behind the shock front predicted by a model based on equilibrium excited state densities with respect to local ground state densities at the local temperature. The model is quite similar, in its results for normal shocks, to that given by Allen, Rose and Camm. ^(2.47) However, it has the advantage that it can be extended simply to any flow geometry resulting in significant changes in time scale from that of one dimensional flow through a normal shock. Note, however, that this model has been formulated for the region of approach to equilibrium following a strong shock and should not be extended to the computation of band radiation in an accelerating, rapidly cooling, flow region.

The model adopted here is open to question on two counts; (1) The use of the local translational temperature in determining the density of excited states, and (2) the use of a linear dependence on electron density to reduce these densities. The former is justified to some extent by the success of the same assumption in the model adopted by Allen, et.al. ^(2.47) The latter is partially justified on the basis of the similarity in shape of the electron density profiles and the radiation profiles prior to reaching a peak.

2.5 CONVECTIVE HEAT TRANSFER COMPUTATIONS

Although the percentage of particles ionized is small for Project FIRE re-entry velocities, the amount of energy invested in ionization is significant ($\sim 15\%$ by a crude estimate). Also, the presence of mobile electrons with their attendant high thermal conductivity raises the question of the effect of electron-borne heat transfer on the overall heat transfer. For these reasons, attention should be given to evaluation of the expected accuracy and validity of the correlation formulas used to calculate convective heat transfer.

The correlation formulas used to evaluate stagnation region heat transfer are those of Hoshizaki^(2.48) and Fay and Riddell.^(2.49) Hoshizaki numerically solved the stagnation point boundary layer equations for air in thermodynamic equilibrium. He used the thermodynamic and transport properties calculated by Hansen,^(2.50) and found that the heat transfer could be correlated with $\pm 6\%$ by use of a single formula. This uniform dependence of heat transfer on enthalpy level throughout the ionization regime is attributed by Hoshizaki to a cancelling of effects of decreasing viscosity-density ratio and increasing wall enthalpy gradient.

Fay and Riddell's^(2.49) binary mixture boundary layer analysis includes only the dissociation process and is therefore not expected to be applicable in the ionization regime (velocities above 30,000 ft. per sec). However Hoshizaki found that simple extrapolation of Fay and Riddell's formula, neglecting any effect of dissociation or ionization on viscosity, gave a result that agreed reasonably well with his results. Specifically, at a velocity of 37,500 ft per sec, the Fay and Riddell result thus extrapolated (with a Sutherland viscosity formula) gives a heat transfer parameter about 10% lower than Hoshizaki's for a highly cooled wall.

Now we have to ask what effect factors not included in these theories might have in order to assess the overall expected accuracy of the heat transfer calculations. Also, we should compare these formulas with the available experimental results. We can consider Hoshizaki's formula as the norm or basis in

our discussion since the agreement with it of Fay and Riddell's formula in the ionization range is little more than coincidental.

The first things that come to mind are the effects of different estimates of the transport properties and the effects of non-equilibrium reaction processes. The effect of different transport properties can be evaluated by comparing the results obtained by Pallone and Van Tassell^(2.51) using both Hansen's^(2.50) transport properties and those of Yos.^(2.52) In the velocity range of 37,500 fps, the two calculations differ by only about 8% (Hansen's properties giving the higher values), although considerably greater differences occur at higher velocities. The big factor here seems to be the equilibrium thermal conductivity which Hansen calculates to be considerably above that given by Yos for temperatures above 10,000°K.

We should note that greater differences than this 8% figure exist among the various calculations which use the same transport properties. Thus, Pallone and Van Tassell's calculation for equilibrium air, which also used Hansen's transport properties, gives a heat transfer parameter about 25% higher than Hoshizaki's (at 37,500 fps); Cohen's^(2.53) calculation using the same properties gives a result about 10% above Hoshizaki's.

We also note, somewhat parenthetically, that Fay and Kemp's^(2.54) evaluation of equilibrium heat transfer in nitrogen (which will be discussed more below) agrees almost exactly with Pallone and Van Tassell's result (the one using the transport properties of Yos) at this velocity (and lies about 15% above Hoshizaki's result). Fay and Kemp argue, justifiably, that the differences between nitrogen and air should be small in this velocity range (and this is borne out by Pallone's calculations). On the other hand, the largely discounted^(2.48, 2.54) calculation of Scala^(2.55) for equilibrium nitrogen gives results a factor of two higher than the other calculations.

Considering all these results, then, before looking at the experimental data, we estimate that Hoshizaki's formula for equilibrium air agrees with the best estimates of other investigators within about 15% (if we accept Yos' transport property calculations as preferable to Hansen's). Most likely, Hoshizaki's formula underestimates the equilibrium heat transfer by an amount of this magnitude.

But what about possible non-equilibrium effects? The only applicable non-equilibrium boundary layer solution is that of Fay and Kemp^(2.54) who considered nitrogen in stagnation regions with frozen and equilibrium boundary layers. They found that the frozen boundary layer heat transfer exceeded the

equilibrium value for velocities above about 35,000 fps. The difference between frozen and equilibrium appears to be approximately 4% at the 37,500 fps. velocity level, although the difference increases markedly for higher velocities. The reason for this difference is the appearance of a layer of atoms in the equilibrium, recombining boundary layer. Because of the relatively large charge-exchange cross section between nitrogen atoms and ions, this layer of atoms inhibits or prevents diffusion of ions toward the wall. Since the ions and electrons are coupled by Coulomb forces, electron diffusion is also inhibited. As a matter of fact, electron diffusion through atoms is eliminated in the Fay-Kemp model because they let the ion-atom cross section be infinite, i.e., no relative diffusion of ions, atoms and electrons occurs in their model. On the other hand, since no recombination occurs in the frozen boundary layer, there is a continuous diffusion of atoms, ions and electrons to the wall. Hence the greater heat transfer for a frozen boundary layer. Actually, the differences between frozen and equilibrium heat transfer would be somewhat less than given by Fay and Kemp since the charge exchange cross section is not infinite, but is (presumably) about an order of magnitude greater than the neutral-neutral cross sections.

Thus, although non-equilibrium effects are of considerable importance in ionized boundary layers, the magnitude of the difference between equilibrium and frozen layers is still small for Project FIRE conditions (too small, in fact, to be measured in the experiments).

Note should be taken of the fact that Fay and Kemp (and, of course, all the other investigators) have given no consideration to intermediate-rate or partial equilibrium processes, the presence of molecular ions, vibrational non-equilibrium, unequal electron and heavy particle temperatures and non-equilibrium conditions outside the boundary layer. While it is difficult to generalize or even predict the direction of change caused by all these effects, the general effect of non-equal electron and heavy particle temperatures is qualitatively clear.

As pointed out by Chung and Mullen,^(2.56) the pertinent parameter to characterize temperature equilibration is the ratio of the thermal conduction time (in the electron gas) to the electron-heavy particle temperature equilibration time. Because of the high thermal conductivity (or low Prandtl number) of the electron gas, unless elastic energy exchange between the electrons and heavy particles occurs quickly (high pressures) this ratio will remain small for a wide range of flight conditions. Thus, the thermal boundary layer in the electron gas will be thick compared with the neutral thermal boundary layer, i.e., the effects of the cool electrons near the wall will be felt far from the wall.

This lower electron temperature will make itself felt in a corresponding decreased thermal conductivity and an increased tendency toward electron-ion recombination. (Also, of course, a depressed electron temperature may affect the rates of other reactions significantly.) Both of these tendencies are in the direction of lower heat transfer than that predicted by the one-temperature theories.

Now for a look at the available experimental results. Rose and Stankevics^(2.57) have presented a summary plot of all available data, along with the abovementioned theories. In the velocity range of interest, the mean of the experimental data lie about 20% below the mean of the theories (and about 5% below Hoshizaki's theory). The scatter in the data is on the order of $\pm 25\%$ so definitive conclusions are hard to draw. Also, all of the data are from shock tubes which have the inherent undesirable feature of heating the gas in a two-step process (through the incident shock and then through the model bow shock).

Notice that the direction of the deviation of the experimental results from the theoretical is in the direction indicated by our discussion of unequal electron-heavy particle temperature effects. Clearly, more analysis and better data are required. However, the results that do exist tend to establish the overall validity of the theoretical heat transfer formulae (except for Scala and Warren's^(2.55)). Hoshizaki's correlation seems to agree best with the experimental data, although for no apparent good reason. Thus, in using his formula, we are hitting some sort of mean, i.e., we are perhaps 15% low compared with other theories, about 5% high compared with the mean of the experiments. Overall we can probably say that stagnation point convective heat transfer should be correctly estimated within $\pm 20\%$ in the velocity range around 37,500 fps at altitudes where low Reynolds number effects are unimportant.

All aerodynamic heating calculations were performed by means of the Aeronutronic Blunt Body Heating Computer program which contains the stagnation point methods of both Fay and Riddell^(2.49) and Hoshizaki^(2.48). Hoshizaki's solution was applied to both of the specified Project Fire cases since it has been shown above to be applicable in this flight regime. The heating distribution over the blunt face is determined by a stepwise solution of Lee's integral equation^(2.60) for laminar flow and by the method of Rose, Probstein, and Adams^(2.61) for turbulent flow. Transition to turbulent flow is based on a pre-selected momentum-thickness Reynolds number which is calculated by the method outlined in reference 2.62. The calculated results indicated that turbulent flow will not occur on the blunt face of the Project Fire re-entry vehicle at either of the flight conditions considered.

It is anticipated that separation will occur at the corner and the entire vehicle afterbody will be immersed in a separated flow field. However, afterbody heating distributions were calculated (Case I) for attached laminar flow. The attached flow calculations were an extension of the blunt face distribution using Lees' laminar solution.

2.6 SUPERSONIC FLOW FIELD

The solution for Case 1 involves the determination of the heat flux over the entire body requiring that the flow properties downstream of the body corner, that is, the supersonic portion of the flow be computed by the method of characteristics. Since the expansion at the corner is very rapid it was assumed that the chemistry became frozen along a ray normal to the body at the corner, but variations in composition and the resultant frozen heat capacity ratio along this line were considered in the frozen characteristic solution.

As discussed previously the flow properties within the gas cap as determined by the integral relations methods were not accurate enough to serve as the input to the characteristic solution for the afterbody flow. Instead the initial flow properties along a ray completely in the supersonic field were determined using the normal pressure gradients at the shock and the body. The distribution of flow properties along the normal at a body angle of 0.37 was first found. This was done by fitting a cubic equation for the pressure distribution using the computed pressures and the normal pressure gradients at the shock and the body as shown in equation 2.158.

$$\bar{p} = a \xi^3 + b \xi^2 + c \xi + d \quad 2.158$$

where $a = \bar{p}'_s + \bar{p}'_B - 2(\bar{p}_s - \bar{p}_B)$

$$b = 3(\bar{p}_s - \bar{p}_B) - (\bar{p}'_s - 2\bar{p}'_B)$$

$$c = \bar{p}'_B$$

$$d = \bar{p}_B \quad \text{and} \quad \bar{p}' = -\bar{\rho} \frac{\bar{q}^2}{\bar{R}}$$

In addition it was assumed ($\bar{\rho} v$) varied linearly along the normal to the body. Coupling this with the energy equation and the equation of state (i.e., equation 2.46 and 2.160), the pressure, velocity and density distributions along the normal were determined.

$$q^2 + h = 1 \quad 2.159$$

$$\bar{p} = \bar{\rho} \frac{\bar{R}_o \bar{T}}{MW} \quad 2.160$$

In order to find the location of a body point at which the velocity was slightly supersonic a Prandtl-Meyer expansion was taken around the corner to a Mach of 1.25.

The new input line, which was completely in a supersonic region, was then chosen as the straight line connecting this body point and the shock point at a body angle of 0.37 radians. The flow property distributions along this new input line were then computed by a constant γ stream tube expansion from the original data on the 0.37 normal. By this method all flow conditions were prescribed at intervals between the body contour and the shock along a ray that was entirely supersonic. At each data point on this line the equilibrium concentrations were determined and from them a value of the heat capacity ratio, γ .

Using such input line a simple characteristics program was developed to compute the properties for a frozen expansion over the afterbody taking into account a variation in γ along the input line. The flow equations are referred to Cartesian coordinates in x and y with x along the axis of symmetry and y normal to the axis. The origin is taken at the nose of the body. The flow variables and the values of γ are given at points S, 1,2,3, --- through B along a ray which is completely supersonic.

The method of characteristics enables one to find flow conditions on a new data line, further in the supersonic region, by determining conditions at intersections of characteristics through interior points 1,2,3,..... and at a new shock point and new body point. First, consider Figure 5 which shows two interior points 1,2 on the initial line. The conditions at the point of intersection 3 of the - characteristic through 2, the + characteristic through 1 are determined using relations along the streamline segment 3,4. The equations of the characteristics are

$$\frac{dy}{dx} = \tan (\theta \mp \mu) \quad 2.161$$

where θ is the angle between the velocity vector and the x-axis and μ is the Mach angle.

To determine the position of point 3 eq. 2.161 is solved as simple difference relations:

$$\begin{aligned} y_3 - y_1 &= \left\{ \tan (\theta_1 - \mu_1) \right\} (x_3 - x_1) \\ y_3 - y_2 &= \left\{ \tan (\theta_2 - \mu_2) \right\} (x_3 - x_2) \end{aligned} \quad 2.162$$

Next the pressure and flow direction are calculated at point 3. The compatibility equations are

$$\frac{\cot \mu}{\bar{\rho} q^2} dp \mp d\theta + \frac{\sin \mu \sin \theta}{y \cos(\theta \mp \mu)} dx = 0 \quad 2.163$$

Equation 2.163 can be expressed as simple difference relations along 1,3 (upper sign) and 2,3 (lower sign). Thus

$$\frac{\cot \mu_1}{\bar{p}_1 \bar{q}_1} (\bar{p}_3 - \bar{p}_1) - (\theta_3 - \theta_1) + \frac{\sin \mu_1 \sin \theta_1}{y_1 \cos(\theta_1 - \mu_1)} (x_3 - x_1) = 0 \quad 2.164$$

and

$$\frac{\cot \mu_2}{\bar{p}_2 \bar{q}_2} (\bar{p}_3 - \bar{p}_2) + (\theta_3 - \theta_2) + \frac{\sin \mu_2 \sin \theta_2}{y_2 \cos(\theta_2 + \mu_2)} (x_3 - x_2) = 0 \quad 2.165$$

These determine p_3 and θ_3 .

The streamline through 3 (inclined at θ_3 to the x-axis) is drawn back to intersect the initial line at 4. The values of x_4, y_4 are found from

$$\frac{y_4 - y_3}{x_4 - x_3} = \tan \theta_3$$

$$\frac{y_4 - y_2}{x_4 - x_2} = \frac{y_1 - y_2}{x_1 - x_2} \quad 2.166$$

and $\bar{p}_4, \bar{e}_4, \bar{q}_4, a_4$, and γ_4 by linear interpolation between the values at 1 and 2. Since $\gamma_3 = \gamma_4$, points 3 and 4 being assumed to be on a streamline, $\bar{e}_3, a_3, \bar{q}_3$, and μ_3 can be determined from the following relations:

$$\frac{\bar{p}_3}{\bar{p}_4} = \left(\frac{\bar{p}_3}{\bar{p}_4} \right)^{1/\gamma_3} \quad 2.167$$

$$a_3^2 = \frac{\gamma_3 \bar{p}_3}{\bar{e}_3} \quad 2.168$$

$$\frac{\bar{p}_3 - \bar{p}_4}{\bar{e}_3} + \bar{q}_4 (\bar{q}_3 - \bar{q}_4) = 0 \quad 2.169$$

$$\mu_3 = \arcsin a_3 / q_3 \quad 2.170$$

This procedure gives a first estimate of conditions at point 3.

Improved values are then found by applying a mean difference process.

The values of x_3, y_3 are found from the mean difference relations

$$\begin{aligned} y_3 - y_1 &= \frac{1}{2} \left\{ \tan(\theta_1 - \mu_1) + \tan(\theta_3^{(i)} - \mu_3^{(i)}) \right\} (x_3 - x_1) \\ y_3 - y_2 &= \frac{1}{2} \left\{ \tan(\theta_2 + \mu_2) + \tan(\theta_3^{(i)} + \mu_3^{(i)}) \right\} (x_3 - x_2) \end{aligned} \quad 2.171$$

where (i) denotes values found by the previous intersection. Equation 2.163 is solved as mean difference relations along 1,3 and 2,3 such that

$$\frac{1}{2} \left\{ \frac{\cot \mu_1}{\bar{p}_1 \bar{q}_1^2} + \frac{\cot \mu_3^{(i)}}{\bar{p}_3^{(i)} \bar{q}_3^{(i)}} \right\} (\bar{p}_3 - \bar{p}_1) - (\theta_3 - \theta_1) + \frac{1}{2} \left\{ \frac{\sin \mu_1 \sin \theta_1}{y_1 \cos(\theta_1 - \mu_1)} \right. \\ \left. + \frac{\sin \mu_3^{(i)} \sin \theta_3^{(i)}}{y_3 \cos(\theta_3 - \mu_3^{(i)})} \right\} (x_3 - x_1) = 0 \quad 2.172$$

and

$$\frac{1}{2} \left\{ \frac{\cot \mu_2}{\bar{p}_2 \bar{q}_2^2} + \frac{\cot \mu_3^{(i)}}{\bar{p}_3^{(i)} \bar{q}_3^{(i)}} \right\} (\bar{p}_3 - \bar{p}_2) + (\theta_3 - \theta_2) + \frac{1}{2} \left\{ \frac{\sin \mu_2 \sin \theta_2}{y_2 \cos(\theta_2 + \mu_2)} \right. \\ \left. + \frac{\sin \mu_3^{(i)} \cos \theta_3^{(i)}}{y_3 \cos(\theta_3^{(i)} + \mu_3^{(i)})} \right\} (x_3 - x_2) = 0 \quad 2.173$$

The location of point 4 is thus found by

$$y_3 - y_4 = \frac{1}{2} \left\{ \tan \theta_3 + \tan \theta_4 \right\} (x_3 - x_4) \\ \tan \theta_4 = \frac{x_1 \tan \theta_2 - x_2 \tan \theta_1 + x_4 (\tan \theta_1 - \tan \theta_2)}{x_1 - x_2} \\ y_4 - y_2 = \left(\frac{y_1 - y_4}{x_1 - x_2} \right) (x_4 - x_2) \quad 2.174$$

Again \bar{p}_4 , \bar{p}_4 , \bar{q}_4 , a_4 , and γ_4 are determined by linear interpolation and \bar{p}_3 , a_3 , \bar{q}_3 , and γ_3 by relations connecting pt. 3 with pt. 4. Equations 2.167 and 2.168 determine \bar{p}_3 and a_3 ; \bar{q}_3 is found from

$$(\bar{p}_3 - \bar{p}_4) \left(\frac{1}{\bar{p}_3} + \frac{1}{\bar{p}_4} \right) + (\bar{q}_3^{(i)} + \bar{q}_4) (\bar{q}_3 - \bar{q}_4) = 0 \quad 2.175$$

Equation 2.170 then determines μ_3 .

The whole mean difference process can now be repeated using the revised values of quantities at point 3. The iteration is continued until the differences between values at the beginning and end of an iterative cycle are negligible.

The procedure at a shock point varies in that the new properties are found from the solution of the χ -characteristic of the last internal point and the shock relations.

In Figure 6 point S is a known point on the shock and point 2 is an adjacent internal point. Point 3 is found as the intersection of the shock tangent at S and the characteristic tangent at 2. Equation 2.165 and the shock relation written in difference form as

$$2p_0 \tan \theta_s \sec^2 \theta_s (\theta_3 - \theta_s) = F'(\chi_s)(p_3 - p_s)$$

where

$$F(\chi) = \left[\frac{\chi - 1}{\gamma M_0^2 - \chi + 1} \right]^2 \frac{2\gamma M_0^2 - (\gamma - 1) + (\gamma + 1)\chi}{(\gamma + 1)\chi + (\gamma - 1)}$$

and $\chi = p/p_0$

are used to compute \bar{p}_3 and θ_3 (Suffix 0 refers to free stream conditions). \bar{p}_3 is determined from the shock relation

$$\frac{\bar{p}_3}{\bar{p}_0} = \frac{(\gamma + 1)\chi + (\gamma - 1)}{(\gamma - 1)\chi + (\gamma + 1)} \quad 2.176$$

a_3 is found from

$$a_3^2 = \bar{p}_3 / \bar{\rho}_3 \quad 2.177$$

and M_3 from the relation

$$M_3^2 = \frac{M_0^2 \left[(\gamma + 1)\chi + (\gamma - 1) \right] - 2(\chi^2 - 1)}{\chi [(\gamma - 1)\chi + (\gamma + 1)]} \quad 2.178$$

Hence $q_3 = M_3 a_3$ and $\mu_3 = \arcsin(1/M_3)$. The new shock angle is now found from the relation

$$M_0^2 \sin^2 \omega = \frac{(\gamma + 1)\chi + (\gamma - 1)}{2\gamma} \quad 2.179$$

In order to perform a mean difference iteration, equation 2.173 is used with the following shock equation;

$$\bar{p}_0 \left\{ \tan \theta_s \sec^2 \theta_s + \tan \theta_3^{(i)} \sec^2 \theta_3^{(i)} \right\} (\theta_3 - \theta_s) + \frac{1}{2} \left\{ F'(\chi_s) + F'(\chi_3) \right\} (\bar{p}_3 - \bar{p}_s) \quad 2.180$$

The procedure at a body point is different in that the intersection of the positive characteristic from the nearest interior point and the body, a limiting streamline, is used.

In Figure 7, B is a known body point and l is an adjacent interior point. C is a new body point where conditions are to be determined.

First, since θ_C is known as the slope of the body at point C, p_C can be found from equation 2.164. (C is the known point of intersection of the + characteristics tangent through l and the body). The remaining conditions at C can then be determined; γ_C from 2.167 (note that $\gamma_C = \gamma_B$), a_3 from 2.168 and q_C from Bernoulli's equation. This can again be improved by a mean difference process using equation 2.172.

2.7 LOW REYNOLDS NUMBER EFFECTS

A group of effects appear and require consideration at high altitudes, i.e., when the Reynolds number drops below the values where separation of the shock layer flow into distinct inviscid and boundary layer regions is clearly permissible. These effects have been studied since 1954, when Ferri and Libby^(2.63) first mentioned the possibility of an interaction between the vorticity generated by shockwave curvature at the nose of a blunt body and the surface-shear generated vorticity (the boundary layer). This particular effect, it turns out, is only one of several effects of equivalent order (although quantitatively the most important one for blunt spheres in hypersonic flow). The assemblage of effects is frequently referred to as "vorticity interaction" or, more precisely, as "second order effects".

Consideration of second order effects is necessary for the high altitude condition of Project FIRE for two reasons. First of all, the convective heat transfer, as calculated from boundary layer theory, is modified by second order effects. At the Reynolds number associated with the high altitude case, this modification might be significant (up to a 30% increase by heat transfer rate according to some theories). Secondly, the thickening (at low Reynolds numbers) of the region wherein viscous and heat conduction effects are important (which is the basic reason for the breakdown of the inviscid flow-boundary layer distinction) causes a significant region of temperature and density gradients. Estimates of gas-cap radiation, which ordinarily are based on properties determined by an inviscid-flow field solution, may be significantly in error if a substantial part of the gas cap is affected by the presence of the highly-cooled wall. It is noted at the outset that, in our situation, the second order effects are augmentive to convective heat transfer and (ordinarily) attenuative to radiation heat transfer. However, the possible presence of particular important radiating species at lower temperature prevents generalization of the latter statement.

What we are concerned with here is seen most clearly by following the procedure used by Van Dyke^(2.64,2.65,2.66) and others, i.e., examining the hierarchy of successive approximations for finding an asymptotic solution to

the Navier-Stokes equations for viscous flow at large Reynolds number. This singular-perturbation problem is treated by the method of inner and outer expansions.^(2.67) Two complementary asymptotic expansions are constructed simultaneously, and matched in their overlap region of common validity. The perturbation parameter, in order to satisfy the boundary conditions, is proportional to a negative half power of the Reynolds number and for the hypersonic case, turns out to be^(2.68)

$$\epsilon = \frac{[(\gamma - 1) M_\infty^2]^{w/2}}{\sqrt{Re_\infty}}$$

for a gas obeying a power-law temperature-viscosity relationship with the exponent set equal to w .

The outer expansion, valid outside of a region of $O(\epsilon)$ next to the body is of the form

$$\phi(s, n, \epsilon) \sim \phi_1(s, n) + \epsilon \phi_2(s, n) + \dots$$

where ϕ is any pertinent flow variable and s and n are the geometrical coordinates, say, along and normal to the body surface. The corresponding inner expansion (valid in the region of $O(\epsilon)$ near the surface) is of the form

$$\phi^i(s, n, \epsilon) \sim \phi_1^i(s, N) + \epsilon \phi_2^i(s, N) + \dots$$

where $N = n/\epsilon$. When these expansions are substituted into the Navier-Stokes equations and terms involving like powers of (ϵ) are collected, the inner and outer expansions can be matched by assuming that the inner expansion for large N behaves in the same manner as the outer expansion for small n .

The first approximation in the outer expansion gives the inviscid flow equations, i.e., the equations which we actually solve (albeit by an approximate method) in the digital computer program. The second approximation in the outer expansion gives another set of inviscid equations which describe a perturbed outer flow past a body whose normal coordinate is increased by the displacement thickness of the first-order boundary layer.

The first approximation in the inner expansion gives the Prandtl boundary layer equations, which have been solved in the stagnation region to

give those heat transfer results which we use and present. The second approximation in the inner expansion gives a number of additional effects known as second order effects. These effects can be identified with longitudinal curvature, transverse curvature, velocity slip at the surface, temperature jump at the surface, entropy gradients in the (inviscid) outer flow, stagnation enthalpy gradients in the outer flow and displacement of the outer flow by the inner or boundary layer flow.

Numerical calculations of the magnitude of all these effects have been accomplished only by Van Dyke,^(2.66) Maslen^(2.69) and Lenard.^(2.70) Van Dyke^(2.71) points out that both Maslen's and Lenard's matching procedures were incorrect in that they failed to include the pressure change due to displacement. According to Davis and Flugge-Lotz,^(2.68) Lenard's values have since been corrected but have not been published as yet. Thus, at the present time, Van Dyke's results seem best to be used to estimate the relative magnitude of the various second order effects.

Taking note of the corrections listed in Reference 2.71 (p. 227), Van Dyke's calculations^(2.66) of the magnitude of second order effects for a highly cooled sphere at infinite Mach number take the form

	Ent. Grad.	Long. Curv.	Trans. Curv.	Slip & Temp. Jump
$\frac{q}{q_{b,l.}} = 1 +$	$(0.584$	$- 0.090$	$+ 0.146$	$- 0.157) \epsilon$

	Total	
$\frac{q}{q_{b,l.}} = 1 +$	0.483ϵ	2.181

where q is the best transfer rate and $q_{b,l.}$ is the corresponding heat transfer rate calculated from boundary layer theory. While external vorticity is the dominant effect, it is seen to be not the only one.

Before accepting Van Dyke's result and using it, we should recognize its limitations and compare it with existing experimental data.

To take note at this point of the absolute magnitude of these effects, we compute ϵ for the Project FIRE high altitude conditions to be 0.107 based on a combined Reynolds number $Re = \frac{V_\infty r \rho_\infty}{\mu_0} = 174$. Thus, the overall magnitude of the second order effect is about a 5% increase in stagnation region heat transfer rate, if we accept Van Dyke's results.

Van Dyke did not calculate the displacement effect because the displacement thickness was so small for the highly cooled body he considered (surface-to-stagnation-temperature ratio of 0.2). That this simplification is generally invalid was shown clearly by Davis and Flugge-Lotz.^(2.68) They found that the pressure gradient associated with displacement can change the magnitude of the entropy gradient effect by as much as a factor of two. Fortunately, they also found that the change is indeed negligible for highly-cooled bodies. Thus, we can safely ignore the displacement effect for our highly cooled body, while taking note of the fact that the vorticity interaction effect might be doubled if a situation exists wherein the body temperature rises to near-stagnation values.

To compare Van Dyke's result with those of others, we make reference to the thorough calculations of the vorticity interaction term by Davis and Flugge-Lotz^(2.68) and to the review by Van Dyke.^(2.71) Apart from Van Dyke's, the other complete analyses of second order effects are those of Lenard^(2.70) and Maslen.^(2.65) Both fail to include the correct displacement effect, but this doesn't matter for the case of a highly cooled body. In this case, their results agree very well with those of Van Dyke. By far the most complete analysis of the vorticity effect itself was carried out by Davis and Flugge-Lotz.^(2.68) They considered a variety of surface-to-stagnation temperature ratios and demonstrated the importance of displacement-induced pressures as the temperature ratio increases. Again, good agreement with Van Dyke's result for a highly cooled body is found. Of the other theories surveyed by Davis and Flugge-Lotz and by Van Dyke, only those of Ferri, et.al.^(2.72) and Cheng^(2.75) give significantly different results. The calculations of these authors give a vorticity interaction effect about four or five times as large as that calculated by the other authors for Project Fire conditions.

Comparison with experiments is something less than conclusive in resolving this difference because of the differences in experimental data, no doubt due to the considerable difficulty in making these experiments. A set of experiments by Hickman and Giedt^(2.73) and additional experiments by Tong and Giedt^(2.74) in the University of California low density wind tunnel (supply air at ambient temperature) give results that agree well with Van Dyke (and the other authors cited previously whose calculations do not disagree significantly). The scatter in the data is sufficient to prevent any choosing among these theories and calculations. Eq. 2.181 above fits Hickman's data

very well, although an estimated re-evaluation of the theoretical result by Van Dyke^(2.72) to correspond with Hickman's experimental conditions (lower Mach number and higher temperature ratio) gives a second order correction low by a factor of two or three.

Other experimental results were obtained by Ferri, et.al.^(2.72) in a hypersonic wind tunnel wherein the supply air was heated to a temperature of 2300°R. Ferri, et.al.'s. results agree with their theory, which as already mentioned, gives an effect about five times as large as that expressed by eq. 2-181. However, the theory of these authors includes only the vorticity (entropy gradient) effect. Thus, it seems coincidental that their experiments (which necessarily include all second order effects) agree with their theory.

To summarize these comparisons, then, there are two distinct sets of theories and experiments. One assemblage gives a second order increase in convective heat transfer of about 5% for high altitude Project FIRE conditions; the other set predicts an increase of 25-30%. The stronger theoretical foundation of the former results leads us to preference of this estimate. Perhaps the results of the Project FIRE experiments will settle the disagreement conclusively.

However, careful note must be taken of the fact that real gas effects (in the form of vibrational non-equilibrium) might be present in the experiments of Ferri, et.al.^(2.72) Also, note that all available treatments of second order effects apply to perfect, non-reacting gases. Surely, real gas effects will be abundant in the Project FIRE experiments. The convective heat transfer can be affected not only by the real gas constituents, per se, (i.e., through modified transport properties, species gradients, surface reactions, etc.) but also because of a new and apparently unconsidered effect, reaction-generated vorticity. Finite rate reactions generate entropy (at a rate proportional to the square of the deviation from equilibrium and inversely proportional to the reaction relaxation time). By Crocco's theorem, reactions also generate vorticity. This vorticity then can interact with the surface-shear generated vorticity in a presently undetermined fashion. These considerations make the Project FIRE heat transfer data at the same time more interesting and more difficult to analyze and interpret.

So far, we have considered only the effect of low Reynolds numbers on convective heat transfer. As mentioned earlier, the effect of wall cooling may modify the radiative heat transfer to a significant extent. We can estimate the approximate physical extent of the region of important viscous effects by noting that, if the shock layer thickness is of order unity, then the first-order boundary layer thickness is of order (ϵ) and the shockwave thickness is of order (ϵ^2). (For reference, the perfect gas shock layer thickness is about 7% of the body radius for the conditions of the high altitude case). Thus, we are considering a situation just about at the boundary between Probstein's^(2.76,2.77) "vorticity interaction" regime and the "viscous layer" regime. The shockwave is reasonably well approximated as a discontinuity; the region of viscous effects is large for the boundary layer approximation, yet small enough that an essentially inviscid region does exist in the shock layer.

To get a semi-quantitative estimate of the temperature profile, we can use the viscous layer calculations of Ho and Probstein^(2.78) or Levinsky and Yoshihara.^(2.79) These authors use the Navier-Stokes equations in a form simplified by the primary assumptions of a thin shock layer (compared to body radius) and local flow similarity. The resulting system of ordinary differential equations are integrated numerically with either free stream^(2.79) or behind-the-shock^(2.78) outer boundary conditions.

Estimated temperature profiles, obtained by interpolating and extrapolating in the plotted numerical results of these authors, are shown on Figure 8. Generally good agreement between the two results is found, at least good enough to permit estimates of the resulting modifications in shock layer radiation. Again, it should be noted that these results are for a perfect, non-reacting gas. Comparable profiles for real gases remain to be determined.

3. DISCUSSION OF RESULTS

The methods discussed in the preceding section were used to compute the convective and radiative fluxes to an Apollo configuration at two points in its re-entry trajectory. These points were specified to be at 171,111 feet and 34,582 ft/sec and 259,113 feet and 37,439 ft/sec, altitude and velocity respectively and both at zero angle of attack. The input parameters corresponding to these conditions are given in Table III. Also given were the exact configurations of the vehicle at the two positions as shown in Figures 9 and 10. These computations are referred to as Cases I and III respectively and as shown in Section 1, Case I is essentially in equilibrium while Case III is essentially in non-equilibrium.

The results of the computations for Case I and Case III are shown in the appendix. For each case the thermodynamic and chemical state of the case is defined as a function of position in the shock layer and the resulting heat flux distributions, both convective and radiative, are shown. These results were obtained using the methods described in Section 2. Sharp corner sonic point boundary conditions were used in both cases. The smooth corner saddle point boundary condition was initially utilized in the Case I solution, but the sonic point was found to be so close to the change in body curvature at the corner, that the sharp corner convergence scheme, which is more rapid and hence more economical than the saddle point scheme, was used. In each instance figures describing the coordinate system used are included. Following is a discussion of the more important features of these results.

3.1 Case I - Equilibrium Flow

The shock layer thermodynamic properties, pressure (Atm), temperature ($^{\circ}\text{K}$), and density (gm/cm^3) as obtained from the first approximation solution are presented graphically as a function of the body coordinate s, n (see Fig. 14) in Figures 16, 17 and 18 respectively. As noted previously in Section 2.1, the first approximation solution gives directly the shock and body properties, but only satisfies the conservation equations across the shock layer on an integrated or mean basis. Thus, when the shock layer properties are determined from the integral relation approximations, some deviation from a higher order direct or inverse solution would be expected. As far as it is known there are no inverse or direct sharp corner blunt body thermochemical equilibrium solutions in the literature with which to compare these results. The reported results have been compared with an $M_{\infty} = 19.36$ inverse equilibrium spherical body result ^(3.1) and with Lees' survey results in reference 3.2. The property

distributions follow the inverse solution results throughout most of the flow field, but deviate from the inverse solution in the stagnation point and sonic regions. The linear property distribution found in the stagnation region is slightly in error since it can be shown that if the velocity is linear in this region (the inverse solution gives a linear velocity and Lees predicts this result), the slope of the pressure and density curves should approach zero at or near the body. The Case I property distribution errors introduced by the first approximation solution are very small, however, because the properties along the stagnation streamline do not vary much from the shock to the body.

The first approximation property distributions obtained in the region of the rounded shoulder sonic point, although adequate for radiation calculations, were not accurate enough to start the characteristic solution. This deficiency was alleviated by replacing two of the integral relation approximations by the exact normal momentum equation and the energy equation. This alternate method is discussed in Section 2.6.

Before leaving the discussion of the shock layer properties, several points should be mentioned. At the Case I velocity and altitude, the shock layer density and temperature are such that the gas is essentially completely dissociated and is about 7% ionized on the axis and 1% near the corner behind the shock. Hypersonic flow theory^(3.3) shows that the density ratio across the shock is only a function of γ . Since, as the shock becomes more oblique, the temperature decreases and thus the degree of ionization decreases, the γ varies with body angle for this case. It can be shown that the effect of temperature is dominant and decreases γ , thus the increasing density ratio (see Fig. 18) as a function of body angle. The final feature to be noted is that the shock is nearly concentric with the front face of the body as would be expected for the high Mach number flow of this problem.

The pressure, temperature and density distributions along the body which were used in the convective heat transfer solution are given in Figures 11, 12, and 13. An examination of the pressure distribution in Figure 11 indicates the strong influence of the sharp cornered shoulder on the pressure and, hence, all the property distributions. The equilibrium pressure distribution on spheres (in contrast to sphere caps with sharply rounded shoulders such as the Case I geometry) has been calculated at hypersonic velocities by both inverse^(3.4) and direct methods^(3.5, 3.6) and

can be shown to be closely approximated by modified Newtonian solution with the centrifugal correction. The effect of the sharply rounded shoulder sonic point on the body properties is to cause a much more rapid decrease in properties than would be expected in the case of a complete sphere. In addition to causing a rapid change in body properties, the sharp corner causes the velocity gradient at the stagnation point to be larger than the complete sphere and the Newtonian result. Since the stagnation point heat transfer is proportional to the square root of the velocity gradient, for a given altitude and reentry velocity, the sharp corner sphere stagnation point heat transfer is also larger than the complete sphere case. This result is not unexpected, however, and has been observed experimentally by Boison and Curtiss^(3.7) and predicted theoretically by Probstein.^(3.8) In the sharp corner solution, the characteristic dimension is not the radius of curvature at the stagnation point as in the Newtonian result, but rather the distance from the stagnation point to the sharp corner. This functional relationship between the sharp corner and the Newtonian velocity gradient can be shown from Probstein's results for a circular disc^(3.8) to be

$$\frac{dv}{ds} \sim \frac{1}{s^*} \left(\frac{dv}{ds} \right)_{\text{Newtonian}} .$$

In the first approximation solution, the stagnation

point velocity derivative was found to be twice the Newtonian value and hence the heat transfer rate is approximately 40% larger than the Newtonian prediction. Although the velocity gradient was expected to be larger than the Newtonian value, the factor of two seems somewhat high^(3.7) and may be due to approximations inherent in the one strip integral relation solution.

The convective heat transfer flux distribution on the blunt face is shown in Figure 24. The distribution was calculated from Lee's local similarity results^(2.60) which give the ratio heat flux at any point to the stagnation point value as

$$\frac{\dot{q}}{\dot{q}_{os}} \sim \frac{pv \sin s}{\sqrt{\int_0^s pv \sin^2 s \, ds}}$$

The rather unconventional form of the heat transfer distribution as compared to a Newtonian results occurs primarily because of the form of the body velocity distribution obtained from the first approximation solution (see Figure 24a.).

The fact that the rate of increase of velocity with body coordinate, s , is greater in the region of the stagnation point than at larger values of s , rather than constant as is assumed in the Newtonian solution, appears to be the primary reason for the unconventional distribution. Since the velocity derivative obtained at the stagnation point appears to be somewhat large, the "bump" in the heat transfer distribution obtained in the region of the stagnation point is probably exaggerated.

The method of computing the radiative flux shown in Figures 26 and 27 makes use of the assumption that the gas is optically thin at all wave lengths; however, it is apparent from Figure 27 that integrated intensity in the ultra-violet would exceed black body if computed accordingly. Thus self absorption effects are important in this wave length region and should be considered. Since a numerical analysis of radiation including self-absorption was not within the scope of this study, a simple approximation was used, this being that the radiation in this wave length region was equal to the black body value. This assumption is felt to be warranted in that the path length over which radiation could reach the body is a small fraction of the standoff distance (approximately $1/6$). This distance is based on an absorption cross section of 10^{-17} cm^2 from Bates, et.al. (3.9) and a number density of absorbers typical of stagnation conditions (i.e., $.4 \times 10^{18}$). The total flux to the various points on the body were corrected by the same proportion as required at the stagnation point.

It is of further interest to note that since the temperature and density were essentially constant throughout the gas cap, one could compute the spectral and total radiative flux to the stagnation point on the basis of a single point computation. This was done by solving Eqn. 2.157 with the assumptions of constant intensity and a concentric shock and body relation. The spectral distribution so computed (using the distribution at the point at a body angle of 0.01 and next to the body) is shown in Figure 27. The points placed on this curve were computed by the actual volume integration over the shock layer. The agreement is seen to be excellent.

The solution reported here for the heat flux over the back of the body is in serious question. In order to allow a characteristic solution the flow was assumed to be attached to the back of the body. In addition, the chemistry in the inviscid field was assumed frozen at the corner and the gas immediately behind the shock was assumed to be in a pseudo equilibrium. By this is meant that the γ for the shock was set equal to

1.13, which is the value of the δ for the equilibrium gas behind the shock at the corner, and the composition was held frozen with respect to the corner values. The effect of each of these assumptions on the convective and radiative fluxes is considerable.

The assumption of attached flow seems to be in error but no direct analytical or experimental information is available. A separation at the corner may be affected by two mechanisms, by the inability of the inviscid flow to expand sufficiently rapidly, or by a viscous boundary layer effect caused by the steep external pressure gradient. The former can be evaluated by looking at the maximum Prandtl-Meyer expansion angle and comparing this to the corner angle. Although this criterion indicates no separation, experimental data at lower Mach numbers and with helium and air definitely show a separation with this configuration. (3.10-3.17) This might indicate a boundary layer fed separation, the analysis of which is not within the scope of this contract.

The effect of a separated region over the afterbody would most likely increase both the convective and radiative fluxes. If one assumes the separation streamline to be in the direction of or closer to the body flow, Chapman's shear layer stability criterion indicates that the layer will be laminar over the entire body. Applying Chapman's free shear layer heat flux approximation, the flux is then about half the flux computed for a pseudo body having the contour of the separated region. Since the convective flux is such a strong function of the body density distribution, manifested by the enormous decrease in convective flux for the attached flow case, it is clear that even half the flux for the much less expanded separated flow may be of considerable importance. Further, the increased density of the less expanded flow will increase the radiative flux by the ratio of ρ^2 for a frozen flow and ρ for an equilibrium flow.

The assumptions concerning the chemistry will have a greater influence on the radiative flux than the convective as the primary change will be in the number densities of the radiating species rather than the gas properties of the field. Since the expansion will still be severe even considering a separated region, the frozen assumption near the body will be good, but the chemistry of the flow entering through the shock

beyond the corner will be a shifting non-equilibrium flow from which a radiation overshoot may exist due to band radiation. All of these effects are difficult to evaluate without a better analysis of the separated flow region which is not within the scope of this study.

As indicated, the flow over the afterbody was computed using the above assumptions and from this the convective flux computed by continuing the boundary layer analysis around the corner. Because of the serious uncertainties in the flow field conditions, it was felt that only an estimate of the radiative flux was warranted. For this purpose a point on the afterbody just beyond the small radius section was considered. The radiation from a right cone having an altitude normal to the body and extending to the shock was computed as follows. Consider the flux equation and Figure 28.

$$dq = I \frac{\cos \theta}{r^2} dV = I \cos \theta \sin \theta dr d\theta d\alpha$$

By a Jacobian transformation to the coordinates of the cone this becomes

$$dq = I \sin \theta dh d\theta d\alpha$$

If we assume I to be a function of h only and relate this to the point radiation at the corner by the following

$$I = I_{\text{corner}} \left(\frac{\rho}{\rho_{\text{corner}}} \right)^2$$

(See radiation discussion and note that the radiation is primarily ion free-bound) one obtains

$$q = \left(\frac{I}{\rho^2} \right)_{\text{corner}} 2\pi \int_0^{\theta_{\text{cone}}} \sin \theta d\theta \int_0^h \rho^2(h) dh$$

or

$$q = 2\pi (1 - \cos \theta_{\text{cone}}) \left(\frac{I}{\rho^2} \right)_{\text{corner}} \int_0^h \rho^2(h) dh$$

The final integral was found graphically.

Before computing the radiative flux to the rear of the vehicle the effect of self absorption had to be considered particularly in the ultra violet. As was done for the gas cap, the path required to make the absorption coefficient equal to 2 was computed from the following

$$Q_a N_a L = 2$$

Q_a , the absorption cross section was obtained from Bates^(3.9) and the

number density obtained from the characteristic solution (a value near the body was chosen). The result showed a maximum path of 0.3 feet, thus the U-V radiation will be limited by self-absorption. Since the ratio of visible to U-V radiation is about 1.5, it is clear that only the visible need be considered in this approximation.

Finally, using the visible portion of the corner radiation as the I_{corner} , the flux was computed as $15 \text{ BTU/ft}^2\text{-sec}$ and is shown in Figure 29. Again it is well to note the serious uncertainties in both the convective and radiative flux over the afterbody.

3.2 Case III - Non-Equilibrium Flow

The state of the gas at various points on the body and shock is shown in Figures 30, 31 and 32. These results were obtained using the integral relation solution previously discussed which makes use of the assumption that only the translational and rotational degrees of freedom equilibrate through the shock but does allow the integration of vibrational and chemical rate equations along the body. Previous to running the complete solution, an equilibrium solution for Case III was obtained in order to compare the available chemical reaction rates at the temperature and density of the flow with the rate required to maintain the equilibrium. This comparison indicated that the flow along the body was essentially frozen at the stagnation point equilibrium composition and thus this additional assumption was used in the reported solution to reduce the cost of the computation of the shock and sonic point locations which are found by iteration.

Based on this frozen solution for the shock and body the streamlines were located within the shock layer and the chemical rate and flow equations integrated along streamlines to determine the state of the gas. The integration results showed that the normal gradients in the layer were very non-linear as evidenced in Figure 35. The velocity component normal to the normal was found to change little between the shock and the body and thus the assumption of linear e_v seems to be questionable. A more accurate answer might be obtained by a multiple strip method or a more appropriate choice of "body conditions." Since the density gradient near the body is very steep, one might choose a point just outside the body as one of the limits in the linearization without greatly changing the problem. In essence, this would

be a two strip approximation in which the inner (near body) strip is negligible in size. The very steep gradients of specie composition near the body further substantiate the assumption of frozen chemistry over the body. It is apparent that at the temperature and densities of the problem the velocities (i.e., the reciprocal of the time scale) must become very small to allow the chemistry to approach equilibrium.

Two solutions for the distribution of the state properties along the body were obtained. The first solution utilized the first approximation integral relation form of the θ -momentum equation (see p. 28). The converged solution indicated that there was a slight increase in density with increasing body angle over a portion of the subsonic flow field. Since the subsonic flow on the body is isentropic with frozen chemistry, the density should decrease with increasing body angle. The source of the problem was found to be the inaccuracies introduced by the first approximation θ -momentum equation. When this equation was replaced with the Bernoulli equation, which is exact along the body streamline, the more reasonable density distribution shown in Figure 32 were obtained. The convective and radiative heat transfer calculations were run before this density inaccuracy was resolved. The convective heat flux solution was rerun (Figure 57) with the more accurate body properties and was found to be approximately 10% lower than the initial calculation. The new flow field solution should not change the radiation results appreciably, however, since the molecular collisions occurring in the non-equilibrium shock layer are primarily binary and the radiation will be independent of density.^(3.18) The radiation calculation was not rerun due to shortages in time and funds.

In the previous discussion of the Case I solution it was noted that the convective flux may be somewhat high due to the linear approximation. It should be noted that these same arguments apply in the Case III solution.

The radiation results shown in Figures 59 and 60 were obtained by integrating the volume emission over space by using the computed volume emission at ξ of 1.0, 0.9, 0.75, 0.5 and near the body along various normals. The choice of these locations was predicated on the assumption that the flux would peak between $\xi = 0.5$ and the shock due to non-equilibrium

band radiation and then be relatively constant from 0.5 to the body. An examination of the computed results shows that this is the case (see Figure 61). A point near the body was chosen because of the very steep gradients near the body which made the radiation from the gas at the body streamline non-representative of any volume of consequence in the shock layer. In addition, the radiation at the shock was taken as zero. This assumption is based on the shock tube results discussed in Section 2.4 and ignores any precursor ionization by ultra-violet radiation. Since the radiation in the ultra-violet is very small (i.e., very little continuum), the precursor ionization is expected to be less than 0.01% and thus negligible.

The non-equilibrium radiation that was determined was found to be primarily a result of band emission. This is the result of the steep properties and concentration gradients near the body in that the major portion of the shock layer is far from equilibrium. The continuum radiation produced by ion free-bound transitions which dominated at the equilibrium conditions of this flow is thus produced over a comparatively small volume. The results obtained have been compared with those of Page^(3.18) at the conditions of this flight and found to be in excellent agreement. Page, by the use of binary scaling of his experimental results, predicts approximately 15 watts/cm²; our results show about 6 watts/cm². In either case this flux is small in comparison with the convective flux.

As discussed in Section 2.7, the increase to the convective heat transfer by second order effects is about 5% based on the best current theory. Further, the assumption of the viscous effects being limited to a boundary layer which is small compared to the shock layer thickness seems to be reasonable for this case. Consequently, the solution reported herein which is based on a boundary layer solution for the convective flux and does not correct for viscous effects in the shock layer in computing the shock volume properties is considered to be adequate.

REFERENCES

Section 1

- 1.1. Allen, R. A., Rose, P. H., and Camm, J. C., AVCO Research Report 156, (1962).
- 1.2. Hoshizaki, H., ARS J. 32, 1544 (1962).
- 1.3. Lees, L., Jet Propulsion 26, 259 (1956).
- 1.4. Rose, P., Probststein, R., and Adams, J., J. of Aero./Sci. 25, 751 (1958).
- 1.5. Hayes, W. and Probststein, R., Hypersonic Flow Theory, Academic Press, New York, 1959.
- 1.6. Dorodnitsyn, A. A., The Solution of Mathematical and Logical Problems on High-Speed Calculating Machines, All-Union Conference on "Means of Developing Soviet Design of Mathematical Machines and Equipment" Part I, pp. 44-52, Moscow, VINITTI, 1956.
- 1.7. Belotserkovskii, O. M., "Supersonic Symmetrical Flow of Perfect and Real Gases Around Blunt Bodies," Journal of Computing Mathematics and Mathematical Physics, Vol. II, No. 6, Nov.-Dec. 1962.

Section 2

- 2.1. Hayes, W. and Probstein, R., Hypersonic Flow Theory, Academic Press, New York, 1959.
- 2.2. Dorodnitsyn, A. A., The Solution of Mathematical and Logical Problems on High-Speed Calculating Machines, All-Union Conference on "Means of Developing Soviet Design of Mathematical Machines and Equipment" Part I, pp. 44-52, Moscow, VINITI, 1956.
- 2.3. Belotserkovskii, O. M., "Supersonic Symmetrical Flow of Perfect and Real Gases Around Blunt Bodies", Journal of Computing Mathematics and Mathematical Physics, Vol. II, No. 6, Nov-Dec. 1962.
- 2.4. Shih, W.C.L. and Baron, J. R., "Nonequilibrium Blunt Body Flow Using the Method of Integral Relations," AIAA Journal, 2,6, 1062, 1964.
- 2.5. Naumova, I. N., "An Approximation to the Thermodynamic Functions of Air," J. of Computing Mathematics and Mathematical Physics, USSR, 1,2, March-April, 1962.
- 2.6. Philco Free-Energy-Minimization Computer Program (SAT-01).
- 2.7. Holt, M., "Direct Calculation of Pressure Distribution on Blunt Hypersonic Nose Shapes with Sharp Corners," Journal of the Aerospace Sciences, 28,11, Nov. 1961.
- 2.8. Freeman, N.C., NATO Report No. 133, 1957.
- 2.9. Lin, S. C. and Teare, J. D., AVCO-Everett Research Note 223, August 1961.
- 2.10. Lick, W. J., F. M. 7, 128, 1960.
- 2.11. Wurster, W. H. and Marrone, P. V., Cornell Aero. Lab. Rep. QM-1373-A-1, 1959.
- 2.12. Wurster, W. H. and Marrone, P. V., Cornell Aero. Lab. Rep. QM-1373-A-2, 1960.
- 2.13. Wurster, W. H. and Marrone, P. V., Cornell Aero. Lab. Rep. QM-1373-A-4, 1961.
- 2.14. Wurster, W. H. and Marrone, P. V., Cornell Aero. Lab. Rep. QM-1626-A-2, 1962.
- 2.15. Hall, J. G., Eschenroeder, A. Q. and Marrone, P. V., "Blunt-Nose Inviscid Air Flows with Coupled Nonequilibrium Processes," Journal of the Aerospace Sciences, Sept. 1962.
- 2.16. Belotserkovskii, O. M., and Dushin, V. K., Zh. Vych Mat, 1 Mar. Fiz 4, 1, 61-77, 1964.
- 2.17. Holt, M. and Hoffman, G. H., "Calculation of Hypersonic Flow Past Spheres and Ellipsoids," IAS-ARS Meeting, Los Angeles, Paper 61-209-1903, 1961.
- 2.18. Penner, S. S., Chemistry Problems in Jet Propulsion, Pergamon Press, 1957.

- 2.19. M. H. Steiger, "On the Chemistry of Air at High Temperatures," General Applied Science Laboratories Technical Report No. 357 (1963).
- 2.20. J. E. Mayer and M. G. Mayer, "Statistical Mechanics," John Wiley and Sons, New York (1954).
- 2.21. D. D. Konowalow and J. O. Hirschfelder, "More Potential Parameters for O-O, N-N, and N-O Interactions," Physics of Fluids 4 (1961).
- 2.22. G. Herzberg, "Spectra of Diatomic Molecules," Van Nostrand, New York (1950).
- 2.23. K. L. Wray, "Chemical Kinetics of High Temperature Air," AVCO-Everett Research Laboratory, Research Report 104 (1961).
- 2.24. S. C. Lin and J. D. Teare, "Rate of Ionization behind Shock Waves in Air II. Theoretical Interpretation," AVCO-Everett Research Laboratory, Research Report 115 (1962).
- 2.25. K. L. Wray, "A Shock Tube Study of the Vibrational Relaxation of Nitric Oxide," AVCO-Everett Research Laboratory, Research Report 96, (1961).
- 2.26. R. N. Schwartz, Z. I. Slawsky, and K. F. Herzfeld, "Calculation of Vibrational Relaxation Times in Gases," J. Chem. Phys. 20, 1591 (1952).
- 2.27. R. N. Schwartz and K. F. Herzfeld, "Vibrational Relaxation Times in Gases (Three-Dimensional Treatment)," J. Chem. Phys. 22, 767 (1954).
- 2.28. M. Camac and A. Vaughan, "O₂ Vibration and Dissociation Rates in O₂-Argon Mixtures," AVCO-Everett Research Laboratory, Research Report 132 (1960).
- 2.29. V. H. Blackman, "Vibrational Relaxation in Oxygen and Nitrogen," J. Fluid Mech. 1, 61 (1956).
- 2.30. K. L. Wray and J. D. Teare, "A Shock Tube Study of the Kinetics of Nitric Oxide at High Temperatures," AVCO-Everett Research Laboratory RR95, 1961.
- 2.31. E. Freedman and J. W. Daiber, "Decomposition Rate of Nitric Oxide between 3000 and 4300°K," J. Chem. Phys. 34, 1271 (1961).
- 2.32. E. Bauer and S. Byron, "Application of Gryzinski's Semi-Classical Method to Non-Resonant Charge Transfer Processes," Bull. Amer. Phys. Soc. 9, 38 (1964).
H. Gryzinski, "Classical Theory of Atomic Collisions. I Inelastic Atomic Collisions," Institute of Nuclear Research, Report No. 448/XVIII, Warsaw, Poland (1963).
- 2.33. H. Petschek and S. Byron, "Approach to Equilibrium Ionization behind Strong Shock Waves in Argon," Annals of Physics 1, 270 (1957).

- 2.34. P. Hammerling, J. D. Teare, and B. Kivel, "Theory of Radiation from Luminous Shock Waves in Nitrogen," Phys. of Fluids 2, 422 (1959).
- 2.35. C. E. Treanor and P. V. Marrone, "The Effect of Dissociation on the Rate of Vibrational Relaxation," Phys. Fluids 5, 1022 (1962).
- 2.36. K. L. Wray, "A Shock Tube Study of the Coupling of the O_2 -Ar Rates of Dissociation and Vibrational Relaxation," AVCO-Everett Research Laboratory, Research Report 125 (1962).
- 2.37. E. Montroll and K. Shuler, "Studies in Nonequilibrium Rate Processes. I. The Relaxation of a System of Harmonic Oscillators," J. Chem. Phys. 26, 454 (1957).
- 2.38. Meyerott, R. E., Sokoloff, J., and Nicholls, R. W., "Absorption Coefficients of Air," Geophysical Research Paper No. 58, GRD-TN-60-277 (July 1960).
- 2.39. Keck, J. C., Allen, R. A. and Taylor, R. L., "Electronic Transition Moments of Air Molecules," AVCO Research Report No. 149 (March 1963).
- 2.40. Patch, R. W., Shackleford, W. L., and Penner, S. S., "Approximate Spectral Absorption Coefficient Calculations for Electronic Band Systems Belonging to Diatomic Molecules," J. Quant. Spectrosc. Radiat. Transfer, Vol. 2, pg. 263 (1962).
- 2.41. Bramscomb, L. M. and Smith, S. J., Phys. Rev. Vol. 98, pg. 1127 (1955).
- 2.42. Bates, D. R., and Massey, H.S.W., Proc. Roy. Soc., A239, pg 269 (1943); Phil Trans. Roy. Soc., A192, pg 1 (1947).
- 2.43. Armstrong, B. H., Sokoloff, J., Nicholls, R. W., Holland, D. H., and Meyerott, R. E., J.Q.S.R.T., Vol. 1, pg. 143 (1961).
- 2.44. Breene, R. G., Nardone, M., Zeldin, S., and Reethof, T. R., "Radiance of Species in High Temperature Air," General Electric Report R63SD3 (1963).
- 2.45. Bates, D. R., Buckingham, R. A., Massey, H.S.W., and Unwin, J. J., Proc. Roy. Soc. A170, pg 322 (1939).
- 2.46. Lin, S. C., and Teare, J. D., AVCO Research Report R115 (1962).
- 2.47. Allen, R. A., Rose, P. H., and Camm, J. C., AVCO Research Report 156, (1962).
- 2.48. Hoshizaki, H., ARS Journal, Vol. 32 (1962), p. 1544.
- 2.49. Fay, J. and Riddell, F., J. Aero. Sci., Vol 25 (1958), p. 73.
- 2.50. Hansen, C., NASA TR R-50 (1959).
- 2.51. Pallone, A. and Van Tassell, W., AVCO Corp. RAD Div. TM-62-75 (1962).
- 2.52. Yos, J., AVCO Corp. RAD Div. TM-63-7 (1963).

- 2.53. Cohen, N., NASA TR R-118 (1961).
- 2.54. Fay, J. and Kemp, N., AIAA Journal, Vol. 1 (1963), p. 2741.
- 2.55. Scala, S. and Warren, W., ARS Journal, Vol. 32 (1962), p. 101.
- 2.56. Chung, P. and Mullen, J., AIAA Preprint 63-161, June, 1963.
- 2.57. Rose, P. and Stankevics, J., AIAA Journal, Vol. 1 (1963), p. 2752.
- 2.58. Fay, J. A. and Riddell, F. R., "Theory of Stagnation Point Heat Transfer in Dissociated Air," AVCO Research Laboratory, Research Report 1, April 1957.
- 2.59. Hoshizaki, H., "Heat Transfer in Planetary Atmospheres at Super-Satellite Speeds," ARS Journal, Vol. 32, No. 10, October, 1962.
- 2.60. Lees, L., "Laminar Heat Transfer over Blunt-Nosed Bodies at Hypersonic Flight Speeds," Jet Propulsion, Vol. 26, No. 4, April 1956.
- 2.61. Rose, P. H., Probst, R. F., and Adams, M. C., "Turbulent Heat Transfer through a Highly Cooled, Partially Dissociated Boundary Layer," AVCO Research Laboratory, Research Report 14, January 1958.
- 2.62. Detra, R. W. and Hidalgo, H., "Generalized Heat Transfer Formulae and Graphs," AVCO Research Laboratory, Research Report 72, March 1960.
- 2.63. Ferri, A. and Libby, P., J. Aero. Sci., Vol. 21, 1954, p. 130.
- 2.64. Van Dyke, M., J. Fluid Mech., Vol. 14, 1963, p. 161..
- 2.65. Van Dyke, M., J. Fluid Mech., Vol. 14, 1963, p. 481.
- 2.66. Van Dyke, M., In Hypersonic Flow Research, Academic Press, New York, 1962, p. 37.
- 2.67. Lagerstrom, P., J. Math. Mech., Vol. 6, 1957, p. 605.
- 2.68. Davis, R. and Flugge-Lotz, I., Int. J. Heat and Mass Trans., Vol. 7, 1964, p. 341.
- 2.69. Maslen, S., AIAA J., Vol. 1, 1963, p. 33.
- 2.70. Lenard, M., Cornell University Thesis, 1962.
- 2.71. Van Dyke, M., In Rarefied Gas Dynamics, Suppl. 2, Vol. 2, Academic Press, New York, 1963, p. 212.
- 2.72. Ferri, A., Zakkay, V. and Ting, L., J. Aero. Sci., Vol. 28, 1961, p. 962 and p. 991.
- 2.73. Hickman, R. and Giedt, W., AIAA J., Vol. 1, 1963, p. 665.
- 2.74. Tong, H. and Giedt, W., AIAA J., Vol. 2, 1964, p. 185.

- 2.75. Cheng, H., In Proc. 1961 Heat Trans. and Fluid Mech. Inst., Stanford University Press, 1962, p. 161
- 2.76. Adams, M. and Probststein, R., Jet Propulsion, Vol. 28, 1958, p. 86.
- 2.77. Probststein, R. and Kemp, N., J. Aero/Space Sci., Vol. 27, 1960, p. 174.
- 2.78. Ho, H. and Probststein, R., In Rarefied Gas Dynamics, Suppl. 1, Academic Press, New York, 1961, p. 525.
- 2.79. Levinsky, E. and Yoshihara, H., In Hypersonic Flow Research, Academic Press, New York, 1962, p. 81.

Section 3

- 3.1. Philco Research Laboratory Inverse Equilibrium Blunt Body Program FM07.
- 3.2. Lees, L., "Recent Developments in Hypersonic Flow," Jet Propulsion, Nov. 1957, p. 1162.
- 3.3. Hayes, W. and Probstein, R., Hypersonic Flow Theory, Academic Press, New York, 1959.
- 3.4. Lomax, H. and Inouye, M., Numerical "Analysis of Flow Properties about Blunt Bodies Moving at Supersonic Speeds in an Equilibrium Gas, NASA TR-204, July 1964.
- 3.5. Belotserkovskii, O. M., "Supersonic Symmetrical Flow of Perfect and Real Gases around Blunt Bodies," Journal of Computing Mathematics and Mathematical Physics, Vol. II, No. 6, Nov.-Dec. 1962.
- 3.6. Shih, W.C.L. and Baron, J. R., "Nonequilibrium Blunt Body Flow using the Method of Integral Relations," AIAA Journal, 2,6, 1062, 1964.
- 3.7. Boison, C. J. and Curtiss, H. A., "An Experimental Investigation of Blunt Body Stagnation Point Velocity Gradient," ARS Journal, Feb. 1959, p. 130.
- 3.8. Probstein, R. F., "Inviscid Flow in the Stagnation Point Region of Very Blunt-Nosed Bodies at Hypersonic Flight Speeds WADC TN 56-395 ASTIA AD 97273, Sept. 1956.
- 3.9. Bates, D. R., Buckingham, R. A., Massey, H.S.W., and Unwin, J. J., Proc. Roy. Soc. A170, pg 322 (1939).
- 3.10. Lee, G., "Correlation of Heat-Transfer Data for the Apollo Afterbody at Mach numbers 8 to 20," NASA TM X-855, Feb. 1964.
- 3.11. Weston, K. C. and Fitzkee, A. L., "Afterbody Heat Transfer Measurements Obtained During Reentry of the Spacecraft of the Mercury-Atlas 5 Mission," NASA TM x-564, Dec. 1963.
- 3.12. Weston, K. C. and Swanson, J. E., "A Compilation of Wind Tunnel Heat Transfer Measurements on the Afterbody of the Project Mercury Capsule Reentry Configuration," NASA TM X-495, 1963.
- 3.13. Stephens, E. W., "Afterbody Heating Data obtained from an Atlas-Boosted Mercury Configuration in a Free Body Reentry," NASA TM x-493, 1961.
- 3.14. Jones, R. A., "Preliminary Results on Heat Transfer to the Afterbody of the Apollo Reentry Configuration at a Mach Number of 8," NASA TM X-699, 1962.

- 3.15. Garberoglio, J. E., et.al., "Hypersonic Shock Tunnel Pressure and Heat Transfer Tests of the Apollo Reentry Vehicle for North American Aviation ," Rep. AA-1712-Y-2, Cornell Aero. Lab., Dec. 1962.
- 3.16. Reller, J. O. and Seegmiller, H. L., "Pressure and Heat-Transfer Measurements on a Mercury Capsule Model," NASA TM X-647, May 1962.
- 3.17. Watson, R. and Wagner, R. D., "Pressure Distribution at a Mach Number of 24.5 on a Symmetrical Blunt-Faced Reentry Body at Angles of Attack from 0° to 40° in Helium Including an Investigation of Afterbody Sting Effects," NASA TM X-841, 1963.
- 3.18. Page, W. A., "Shock-Layer Radiation of Blunt Bodies Traveling at Lunar Return Entry Velocities," IAS 31st Annual Meeting, New York, N.Y. (1963).

TABLE I

CHEMICAL KINETIC RATE CONSTANTS USED FOR COMPUTING THE REACTION RATES
AND VIBRATION RELAXATION TIMES

The dimensional forward reaction rates are of the form $\bar{C}_{i2} \bar{C}_i \exp\left(\frac{E_i}{T}\right)$									
and the vibration relaxation time equation form is given in equation 2.119									
i	Reactions ($i = 1, \dots, r$)	\bar{C}_{i1}	\bar{C}_{i2}	\bar{C}_i	K_i	a_i	A_i	C_i	
A. Dissociation									
1.	$2O + O_2 \xrightleftharpoons[k_f]{k_r} O_2 + O_2$	0	-3/2	8×10^{19}	$8.3 \times 10^{-4} T^{-1/2} \bar{T}_{\infty}^{-1/2} \exp(59300/T \bar{T}_{\infty})$	$.4205 \times 10^{13}$	1.7×10^4	206	
2.	$2O + O \xrightleftharpoons[k_f]{k_r} O_2 + O$	0	-3/2	2.2×10^{20}	"	$.9149 \times 10^{13}$	1.7×10^4	206	
3.	$2O + N_2 \xrightleftharpoons[k_f]{k_r} O_2 + N_2$	"	-1/2	3.6×10^{15}	"	$.9468 \times 10^{13}$	1.7×10^4	206	
4.	$2O + N \xrightleftharpoons[k_f]{k_r} O_2 + N$	"	"	"	"	1.017×10^{13}	1.7×10^4	206	
5.	$2O + NO \xrightleftharpoons[k_f]{k_r} O_2 + NO$	"	"	"	"	"	"	"	
6.	$2N + N_2 \xrightleftharpoons[k_f]{k_r} N_2 + N_2$	"	-3/2	2.4×10^{20}	$5.0 T^{-1/2} \bar{T}_{\infty}^{-1/2} \exp(113200/T \bar{T}_{\infty})$	$.5291 \times 10^{13}$	8.0×10^4	273	
7.	$2N + N \xrightleftharpoons[k_f]{k_r} N_2 + N$	"	-5/2	1.0×10^{25}	"	1.131×10^{13}	8.0×10^4	273	
8.	$2N + O_2 \xrightleftharpoons[k_f]{k_r} N_2 + O_2$	"	-3/2	1.0×10^{20}	"	"	"	"	
9.	$2N + O \xrightleftharpoons[k_f]{k_r} N_2 + O$	"	"	"	"	"	"	"	
10.	$2N + NO \xrightleftharpoons[k_f]{k_r} N_2 + NO$	"	"	"	"	"	"	"	
11.	$N + O + N_2 \xrightleftharpoons[k_f]{k_r} NO + N_2$	"	-3/2	4.0×10^{20}	$0.25 \exp(75400/T \bar{T}_{\infty})$	$.9601 \times 10^{13}$	4.5×10^4	230	
12.	$N + O + N \xrightleftharpoons[k_f]{k_r} NO + N$	"	"	"	"	1.027×10^{13}	4.5×10^4	230	
13.	$N + O + O_2 \xrightleftharpoons[k_f]{k_r} NO + O_2$	"	"	"	"	"	"	"	
14.	$N + O + O \xrightleftharpoons[k_f]{k_r} NO + O$	"	"	"	"	"	"	"	
15.	$N + O + NO \xrightleftharpoons[k_f]{k_r} NO + NO$	"	"	2.0×10^{21}	"	"	"	"	
B. Atom and Charge Exchange									
16.	$N + NO \xrightleftharpoons[k_f]{k_r} N_2 + O$	"	0	1.6×10^{13}	K_6/K_{11}	"	"	"	
17.	$N + O_2 \xrightleftharpoons[k_f]{k_r} NO + O$	-3560	1	1.3×10^{10}	K_{11}/K_1	"	"	"	
18.	$NO + NO \xrightleftharpoons[k_f]{k_r} N_2 + O_2$	-43000	-5/2	2.4×10^{23}	K_{16}/K_{17}	"	"	"	
19.	$O^+ + NO \xrightleftharpoons[k_f]{k_r} O_2^+ + N$	0	1/2	3.0×10^{11}	$6.5 \times 10^{-3} T^{-1/2} \bar{T}_{\infty}^{-1/2} (1 + 1.8 \times 10^{-5} T \bar{T}_{\infty})$	"	"	"	
20.	$O^+ + N_2 \xrightleftharpoons[k_f]{k_r} NO^+ + N$	0	"	"	K_{24}/K_{16}	"	"	"	
21.	$N + N_2^+ \xrightleftharpoons[k_f]{k_r} N_2 + N^+$	0	"	"	$250 \times 10^{-6} T^{-1/2} \bar{T}_{\infty}^{-1/2} (1 + 1.3 \times 10^9 T^{-2} \bar{T}_{\infty}^{-2}) \times \exp(11900/T \bar{T}_{\infty})$	"	"	"	
22.	$O^+ + O_2 \xrightleftharpoons[k_f]{k_r} O_2^+ + O$	0	"	"	K_{19}/K_{17}	"	"	"	
23.	$N^+ + NO \xrightleftharpoons[k_f]{k_r} N_2^+ + O$	0	"	"	K_{16}/K_{21}	"	"	"	

TABLE I (continued)

i	Reactions ($i = 1, \dots, r$)	$\overline{k_F}_i$			K_i	a_i	A_i	C_i
		τ_{i1}	τ_{i2}	C				
<u>B. Atom and Charge Exchange</u>								
24.	$O^+ + NO \rightleftharpoons NO^+ + O$	0	1/2	3.0×10^{11}	$K_{19} K_{26} / K_{27}$			
25.	$N^+ + O_2 \rightleftharpoons O_2^+ + N$	0	"	"	$K_{17} K_{23} K_{27} / K_{28}$			
<u>C. Ionization Atom Impact</u>								
26.	$N + O \rightleftharpoons NO^+ + e^-$	-31900	-1/2	7.5×10^{13}	$1.8 \times 10^{-10} T_e^{1.5} (1 + 1.2 \times 10^{-4} T_e)^x \exp(-31900/T_e)$			
27.	$O + O \rightleftharpoons O_2^+ + e^-$	-82300	-1/2	5×10^{13}	$4 \times 10^{-12} T_e^2 (1 + 7 \times 10^{-5} T_e)^x \exp(-82300/T_e)$			
28.	$N + N \rightleftharpoons N_2^+ + e^-$	-67500	-1/2	1.5×10^{14}	$(6.5 \times 10^{10} T_e^{-2} + 50)^{-1} \exp(-67500/T_e)$			

TABLE II

MOLECULAR VIBRATION AND DISSOCIATION CONSTANTS
AND HEATS OF FORMATION (0°K)

Species, j	\bar{h}_j° cal/mole	$\bar{\theta}_{v,j}^{\circ}$ $^{\circ}\text{K}$	$u_{o,j}$	\bar{d}_j cal/mole
O	58980			
N	112520			
e^{-}	0.0			
O_2	0.0	2335	.039	117770
N_2	0.0	3541	.032	224815
NO	21480	2786	.037	149744
NO^{+}	234880			
O_2^{+}	277900			
N_2^{+}	359310			
O^{+}	373030			
N^{+}	448040			

TABLE III

CASE I AND III FLIGHT CONDITIONS

Case	Alt (ft)	\bar{q}_∞ (ft/sec)	\bar{p}_∞ (atm)	\bar{T}_∞ (°K)	$\bar{\rho}_\infty^3$ (g/cm ³)	a_∞ (ft/sec)	M_∞	γ_∞	\bar{q}_m (ft/sec)	\bar{MW}_∞	\bar{R}_{so} (ft)
I	171,611	34,582	5.9258×10^{-4}	270.65	7.7280×10^{-7}	1082.07	31.96	1.4	34667	28.966	2.6417
III	259,133	37,439	1.2349×10^{-5}	184.65	2.3606×10^{-8}	893.78	41.89	1.4	37492	28.966	3.0667

TABLE IV
STATE OF THE GAS BETWEEN THE SHOCK AND THE FRONT FACE
Case I

S (RAD)	N (FT)	X (FT)	Y (FT)	P (ATM)	T (DEG-K)	RH (GM/CC)
0.0	0.0	0.0	0.0	0.8210000	11205.00	0.1211158-4
0.0	0.0240920	-0.0240920	0.000000	0.8150732	11200.39	0.1203965-4
0.0	0.0481840	-0.0481840	0.000000	0.8092526	11193.24	0.1196770-4
0.0	0.0722760	-0.0722760	0.000000	0.8035353	11183.84	0.1189575-4
0.0	0.0963680	-0.0963680	0.000000	0.7979187	11172.28	0.1182381-4
0.0	0.1204600	-0.1204600	0.000000	0.7924000	11158.63	0.1175186-4
0.020000	0.0	0.0005283	0.052830	0.8195614	11202.68	0.1209361-4
0.020000	0.0241186	-0.0235855	0.053312	0.8145823	11198.53	0.1202467-4
0.020000	0.0482372	-0.0476992	0.053794	0.8093077	11191.53	0.1195600-4
0.020000	0.0723558	-0.0718130	0.054277	0.8037948	11182.12	0.1188762-4
0.020000	0.0964744	-0.0959268	0.054759	0.7980738	11170.52	0.1181956-4
0.020000	0.1205930	-0.1200405	0.055242	0.7921713	11156.91	0.1175184-4
0.040000	0.0	0.0021131	0.105638	0.8158353	11196.65	0.1204700-4
0.040000	0.0241894	-0.0220570	0.106606	0.8117849	11192.51	0.1199220-4
0.040000	0.0483789	-0.0462272	0.107573	0.8072273	11185.22	0.1193490-4
0.040000	0.0725683	-0.0703973	0.108540	0.8022833	11175.59	0.1187551-4
0.040000	0.0967578	-0.0945674	0.109508	0.7970316	11164.09	0.1181437-4
0.040000	0.1209472	-0.1187375	0.110475	0.7915370	11151.11	0.1175178-4
0.060000	0.0	0.0047536	0.158405	0.8109531	11188.70	0.1198595-4
0.060000	0.0242834	-0.0194861	0.159861	0.8082286	11184.03	0.1195224-4
0.060000	0.0485668	-0.0437258	0.161317	0.8045795	11175.69	0.1191050-4
0.060000	0.0728501	-0.0679655	0.162773	0.8002657	11165.05	0.1186235-4
0.060000	0.0971335	-0.0922052	0.164229	0.7954590	11152.86	0.1180907-4
0.060000	0.1214169	-0.1164448	0.165686	0.7902863	11139.65	0.1175167-4
0.080000	0.0	0.0084488	0.211108	0.8056236	11179.98	0.1191920-4
0.080000	0.0243786	-0.0158518	0.213056	0.8044410	11173.96	0.1191130-4
0.080000	0.0487573	-0.0401525	0.215004	0.8017023	11163.55	0.1188692-4
0.080000	0.0731359	-0.0644531	0.216953	0.7979050	11150.67	0.1185030-4
0.080000	0.0975145	-0.0887538	0.218901	0.7933595	11136.34	0.1180445-4
0.080000	0.1218931	-0.1130545	0.220849	0.7882766	11121.12	0.1175156-4

TABLE IV (continued)

STATE OF THE GAS BETWEEN THE SHOCK AND THE FRONT FACE

S (RAD)	N (FT)	X (FT)	Y (FT)	P (ATM)	T (DEG-K)	RH0 (GM/CC)
0.100000	0.0	0.0131973	0.263727	0.7999361	11170.62	0.1184792-4
0.100000	0.0244602	-0.0111406	0.266168	0.8004244	11162.47	0.1186913-4
0.100000	0.04892	-0.0354786	0.26861	0.798549	11148.9	0.118632-4
0.100000	0.0733805	-0.0598166	0.271052	0.7951348	11132.44	0.1183830-4
0.100000	0.0978407	-0.0841546	0.273494	0.7906662	11114.23	0.1179987-4
0.100000	0.1223009	-0.1084926	0.275936	0.7854510	11094.85	0.1175155-4
0.120000	0.0	0.0189972	0.316240	0.7936805	11160.25	0.1176940-4
0.120000	0.0245203	-0.0053468	0.319175	0.7959681	11149.29	0.1182288-4
0.120000	0.0490407	-0.0296908	0.322110	0.7949485	11131.58	0.1183686-4
0.120000	0.0735610	-0.0540349	0.325046	0.7918411	11110.19	0.1182472-4
0.120000	0.0980814	-0.0783789	0.327981	0.7873252	11086.37	0.1179461-4
0.120000	0.1226017	-0.1027229	0.330917	0.7818146	11060.68	0.1175177-4
0.140000	0.0	0.0258461	0.368626	0.7866133	11148.44	0.1168061-4
0.140000	0.0245559	0.0015304	0.372053	0.7908696	11134.07	0.1176993-4
0.140000	0.049112	-0.022785	0.37548	.790759	11111.3	0.118062-4
0.140000	0.073668	-0.047101	0.37891	.787942	11083.7	0.118086-4
0.140000	0.098224	-0.071416	0.38233	.783309	11052.6	0.117883-4
0.140000	0.122779	-0.095732	0.38576	.777388	11018.5	0.117524-4
0.160000	0.0	0.0337413	0.420865	0.7785397	11134.82	0.115790-4
0.160000	0.0245654	0.0094896	0.424779	0.7849838	11116.49	0.1170850-4
0.160000	0.0491308	-0.0147620	0.428693	0.7858852	11087.78	0.1176999-4
0.160000	0.0736962	-0.0390136	0.432607	0.7833838	11052.70	0.1178933-4
0.160000	0.0982616	-0.0632652	0.436520	0.7785995	11012.60	0.1178101-4
0.160000	0.1228270	-0.0875169	0.440434	0.7721793	10967.97	0.1175379-4
0.180000	0.0	0.0426796	0.472936	0.7693006	11119.09	0.1146254-4
0.180000	0.0245474	0.0185288	0.477331	0.7782014	11096.20	0.1163730-4
0.180000	0.0490948	-0.0056220	0.481726	0.7802576	11060.60	0.1172773-4
0.180000	0.0736422	-0.0297728	0.486120	0.7781258	11016.70	0.1176688-4
0.180000	0.0981896	-0.0539236	0.490515	0.7731719	10965.87	0.1177279-4
0.180000	0.1227370	-0.0780744	0.494910	0.7661733	10908.51	0.1175619-4

TABLE IV(continued)
STATE OF THE GAS BETWEEN THE SHOCK AND THE FRONT FACE

S(RAD)	N(FT)	X(FT)	Y(FT)	P(ATM)	T(DEG-K)	RHO(GM/CC)
0.200000	0.0	0.0526574	0.524818	0.7587376	11100.87	.1132911-4
0.200000	0.0244995	0.0286463	0.529685	0.7704153	11072.83	0.1155511-4
0.200000	0.0489990	0.0046352	0.534553	0.7738050	11029.32	0.1167882-4
0.200000	0.0734985	-0.0193760	0.539420	0.7721186	10975.14	0.1174111-4
0.200000	0.0979980	-0.0433871	0.544287	0.7669886	10911.67	0.1176392-4
0.200000	0.1224975	-0.0673982	0.549155	0.7593335	10839.12	0.1176012-4
0.220000	0.0	0.0636709	0.576490	0.7466559	11079.75	0.1117620-4
0.220000	0.0244179	0.0398415	0.581818	0.7614921	11045.87	0.1146040-4
0.220000	0.0488358	0.0160122	0.587147	0.7664350	10993.31	0.1162253-4
0.220000	0.0732537	-0.0078172	0.592476	0.7652944	10927.23	0.1171491-4
0.220000	0.0976716	-0.0316465	0.597805	0.7599919	10848.93	0.1175475-4
0.220000	0.1220894	-0.0554759	0.603133	0.7515980	10758.36	0.1176627-4
0.240000	0.0	0.0757155	0.627931	0.7327855	11055.10	0.1100010-4
0.240000	0.0242970	0.0521149	0.633706	0.7512419	11014.63	0.1135099-4
0.240000	0.0485939	0.0285144	0.639482	0.7580135	10951.71	0.1155779-4
0.240000	0.0728909	0.0049138	0.645257	0.7575529	10871.85	0.1167905-4
0.240000	0.0971878	-0.0186867	0.651033	0.7520956	10776.17	0.1174571-4
0.240000	0.1214848	-0.0422873	0.656808	0.7428746	10664.16	0.1177564-4
0.260000	0.0	0.0887865	0.679121	0.7167274	11026.02	0.1079560-4
0.260000	0.0241288	0.0654686	0.685324	0.7393856	10978.10	0.1122366-4
0.260000	0.0482576	0.0421508	0.691527	0.7483468	10903.26	0.1148304-4
0.260000	0.0723863	0.0188330	0.697730	0.7487548	10807.38	0.1164233-4
0.260000	0.0965151	-0.0044848	0.703933	0.7431853	10691.22	0.1173768-4
0.260000	0.1206439	-0.0278026	0.710136	0.7330439	10553.56	0.1178994-4
0.280000	0.0	0.1028785	0.730039	0.6978660	10991.07	0.1055461-4
0.280000	0.0239024	0.0799070	0.736645	0.7254630	10934.68	0.1107299-4
0.280000	0.0478049	0.0569354	0.743250	0.7370919	10846.05	0.1139521-4
0.280000	0.0717073	0.0339638	0.749856	0.7386339	10731.36	0.1160058-4
0.280000	0.0956098	0.0109922	0.756462	0.7330317	10590.82	0.1173105-4
0.280000	0.1195122	-0.0119793	0.763067	0.7218690	10422.11	0.1181090-4

TABLE IV(continued)

STATE OF THE GAS BETWEEN THE SHOCK AND THE FRONT FACE

S(RAD)	N(FT)	X(FT)	Y(FT)	P(ATM)	T(DEG-K)	RHC(GM/CC)
0.300000	0.0	0.1179861	0.780666	0.6752093	10947.90	0.1026377-4
0.300000	0.0236030	0.0954373	0.787641	0.7087671	10881.80	0.1089066-4
0.300000	0.0472059	0.0728885	0.794616	0.7237611	10777.01	0.1129017-4
0.300000	0.0708089	0.0503398	0.801591	0.7268537	10639.97	0.1155314-4
0.300000	0.0944118	0.0277910	0.808566	0.7213806	10470.00	0.1172805-4
0.300000	0.1180148	0.0052422	0.815541	0.7091058	10263.07	0.1184312-4
0.320000	0.0	0.1341031	0.830980	0.6470621	10892.34	0.0990035-4
0.320000	0.0232096	0.1120717	0.838281	0.6880405	10815.01	0.1066169-4
0.320000	0.0464191	0.0900404	0.845582	0.7074548	10690.92	0.1115973-4
0.320000	0.0696287	0.0680091	0.852883	0.7127733	10526.78	0.1149764-4
0.320000	0.0928382	0.0459777	0.860184	0.7077440	10320.51	0.1173122-4
0.320000	0.1160478	0.0239464	0.867485	0.6943048	10065.63	0.1189329-4
0.340000	0.0	0.1512231	0.880962	0.6102490	10816.11	0.0942146-4
0.340000	0.0226929	0.1298292	0.888529	0.6608860	10725.60	0.1035685-4
0.340000	0.0453857	0.1084354	0.896097	0.6864544	10577.89	0.1098755-4
0.340000	0.0680786	0.0870416	0.903665	0.6951954	10380.01	0.1142902-4
0.340000	0.0907715	0.0656478	0.911233	0.6912673	10127.81	0.1174521-4
0.340000	0.1134644	0.0442540	0.918800	0.6767744	9811.70	0.1197443-4
0.360000	0.0	0.1693392	0.930591	0.5573827	10698.62	0.0872603-4
0.360000	0.0220095	0.1487405	0.938344	0.6214751	10592.51	0.0990329-4
0.360000	0.0440191	0.1281418	0.946098	0.6564629	10414.90	0.1072922-4
0.360000	0.0660286	0.1075432	0.953851	0.6711234	10173.62	0.1132910-4
0.360000	0.0880382	0.0869445	0.961604	0.6699556	9862.13	0.1177528-4
0.360000	0.1100477	0.0663458	0.969358	0.6553044	9469.41	0.1211240-4

TABLE V
CASE I
STATE OF THE GAS ALONG STREAMLINES OVER THE AFTER-BODY

X (FT)	Y (FT)	DENSITY (G/FT ³)	PRESSURE (ATM)	VELOCITY (FPS)
				BODY
0.24495400+001	0.98010100+001	0.59423077-005	0.36282277+000	0.10586856+005
0.24498000+001	0.982886100+000	0.57640224-005	0.35095684+000	0.10557669+005
0.24475100+001	0.98469700+000	0.55662981-005	0.33785092+000	0.10524443+005
0.24445200+001	0.98868500+000	0.51537019-005	0.31065581+000	0.10451721+005
0.24392400+001	0.99494400+000	0.45770673-005	0.27295655+000	0.10340695+005
0.24289000+001	0.10050400+001	0.37661058-005	0.22070569+000	0.10161285+005
0.24125500+001	0.10158300+001	0.28848237-005	0.16504235+000	0.99198303+004
0.23897000+001	0.10273200+001	0.20198878-005	0.11192283+000	0.96076911+004
0.23607600+001	0.10330600+001	0.12310769-005	0.65239877-001	0.91887312+004
0.23522600+001	0.10333300+001	0.10555032-005	0.52427083-001	0.86123912+004
0.23443400+001	0.10330300+001	0.87351763-006	0.40063674-001	0.79525554+004
0.23351700+001	0.10320000+001	0.68261538-006	0.28221244-001	0.71684901+004
0.23235200+001	0.10296200+001	0.48625801-004	0.17427230-001	0.62142568+002
0.23076800+001	0.10242600+001	0.29260577-006	0.84582072-002	0.50180640+004
0.22799900+001	0.10085200+001	0.14747917-006	0.32820276-002	0.38586835+004
0.22429500+001	0.98446300+000	0.15087540-006	0.33910211-002	0.38971348+004
0.22071600+001	0.96121900+000	0.15113029-006	0.33995158-002	0.39002565+004
0.21505600+001	0.93095700+000	0.14132292-006	0.30903316-002	0.37915789+004
0.21128000+001	0.89904500+000	0.13675753-006	0.29494278-002	0.37395050+004
0.20549000+001	0.86234000+000	0.13091186-006	0.27718897-002	0.36713396+004
0.19900100+001	0.82020200+000	0.12573542-006	0.26174442-002	0.36095031+004
0.17755300+001	0.68091800+000	0.11745994-006	0.23759243-002	0.35072800+004
0.13802000+001	0.42418500+000	0.13771378-006	0.29791667-002	0.37509822+004
0.15994700+001	0.56658200+000	0.12183381-006	0.25028402-002	0.35620002+004

TABLE V (continued)
STATE OF THE GAS ALONG STREAMLINES OVER THE AFTER-BODY

SHOCK

0.25635400+001	0.99431000+000	0.12211538-004	0.64231221+000	0.99640937+004
0.25527000+001	0.10166400+001	0.12219647-004	0.64195863+000	0.99520001+004
0.25374400+001	0.10479500+001	0.12219327-004	0.64082600+000	0.99347020+004
0.25218900+001	0.10797900+001	0.12219343-004	0.66184374+000	0.10260526+005
0.25105100+001	0.11028400+001	0.12217724-004	0.63510417+000	0.98472882+004
0.25007300+001	0.11225200+001	0.12219374-004	0.63307512+000	0.98926650+004
0.24905500+001	0.11420900+001	0.12210224-004	0.60957600+000	0.94572794+004
0.24768500+001	0.11556000+001	0.12197532-004	0.57072623+000	0.88637577+004
0.24589500+001	0.11926800+001	0.12185849-004	0.53905516+000	0.83799111+004
0.24467700+001	0.12074500+001	0.12178429-004	0.52068662+000	0.80992935+004
0.24373700+001	0.12227400+001	0.12169151-004	0.49935739+000	0.77734395+004
0.24244600+001	0.12391300+001	0.12159615-004	0.47315493+000	0.74647992+004
0.24092000+001	0.12572900+001	0.12144904-004	0.45095070+000	0.70339131+004
0.23912300+001	0.12772500+001	0.12129792-004	0.42517606+000	0.66401435+004
0.23698900+001	0.12994400+001	0.12111923-004	0.39821156+000	0.62282031+004
0.23452800+001	0.13235200+001	0.12096410-004	0.37735622+000	0.59095854+004
0.23148000+001	0.13515100+001	0.12073205-004	0.34989850+000	0.54899589+004
0.22749500+001	0.13855300+001	0.17435299-004	0.31681485+000	0.54422162+004
0.22252400+001	0.14246900+001	0.12009894-004	0.29075558+000	0.45865596+004
0.21555900+001	0.14750800+001	0.11954647-004	0.25417254+000	0.40276698+004
0.20648155+001	0.15348800+001	0.11901458-002	0.22603580+000	0.35978169+002
0.17168100+001	0.17335200+001	0.11723606-004	0.16405451+000	0.26513580+004
0.92199900+000	0.28196100+001	0.10935064-004	0.70635563-001	0.12236694+004

TABLE V. (continued)
STATE OF THE GAS ALONG STREAMLINES OVER THE AFTER-BODY

ψ_1

0.24792861+001	0.22277100+000	0.84514020-005	0.49870506+000	0.10224891+005
0.24734027+001	0.10129097+001	0.81052398-005	0.48112238+000	0.10285688+005
0.24660362+001	0.10140236+001	0.79305068-005	0.45698075+000	0.10112338+005
0.24534501+001	0.10240421+001	0.74451661-005	0.43185776+000	0.10051016+005
0.24479014+001	0.10361242+001	0.67653396-005	0.38840325+000	0.99472906+004
0.24331066+001	0.10408501+001	0.60271504-005	0.34144293+000	0.98163436+004
0.24131038+001	0.10364646+001	0.54202713-005	0.30341687+000	0.96997905+004
0.23879600+001	0.10277240+001	0.37660256-005	0.20833333+000	0.95855964+004

ψ_2

0.23190000+001	0.10570001+001	0.12307681-005	0.51797048-001	0.72924326+004
0.22951400+001	0.10575001+001	0.96980800-006	0.37228371-001	0.66516888+004
0.22644600+001	0.10557401+001	0.74211081-006	0.25685079-001	0.59973004+004
0.22310901+001	0.10479402+001	0.54922916-006	0.17197974-001	0.54258445+004
0.21856001+001	0.10305002+001	0.37718368-006	0.10505827-001	0.48263745+004
0.21367501+001	0.10116803+001	0.27585798-006	0.68568105-002	0.43070533+004
0.20746300+001	0.98240630+000	0.21269426-006	0.48071982-002	0.39163357+004
0.20037300+001	0.95323634+000	0.17816849-006	0.37499613-002	0.36470316+004
0.17669000+001	0.85616338+000	0.16094409-006	0.31907023-002	0.34352227+004
0.13951395+001	0.78446443+000	0.17056429-006	0.32473631-002	0.32990309+004

TABLE V (continued)

STATE OF THE GAS ALONG STREAMLINES OVER THE AFTER-BODY

 ψ_3

0.23046322+001	0.11088311+001	0.31627686-005	0.13240610+000	0.73839986+004
0.22738480+001	0.12028070+001	0.27739535-005	0.11042044+000	0.70210382+004
0.22328036+001	0.12180555+001	0.23973878-005	0.90518284-001	0.66596143+004
0.21844650+001	0.12343625+001	0.20333013-005	0.71019476-001	0.61606535+004
0.21194247+001	0.12550273+001	0.17030822-005	0.55532687-001	0.57512748+004
0.20374080+001	0.12729900+001	0.13828427-005	0.41781777-001	0.53292386+004
0.17418453+001	0.12847603+001	0.77941259-006	0.19270796-001	0.43609720+004
0.23315400+001	0.11753362+001	0.35864040-005	0.15739560+000	0.77407750+004
0.25101067+001	0.10227930+001	0.10750563-004	0.60595394+000	0.99416731+004
0.24092749+001	0.10211008+001	0.11280026-004	0.63043409+000	0.99985439+004
0.24873913+001	0.10391690+001	0.11136823-004	0.63023486+000	0.99814166+004
0.24773457+001	0.10526391+001	0.10181972-004	0.57079202+000	0.98877400+004
0.24660418+001	0.10567786+001	0.82302857-005	0.45140544+000	0.96633628+004
0.24535066+001	0.10326055+001	0.74619388-005	0.40369085+000	0.95424076+004
0.24361936+001	0.11111034+001	0.69134494-005	0.37049076+000	0.94522162+004
0.24176564+001	0.11256615+001	0.67480439-005	0.31590350+000	0.92127768+004
0.24056545+001	0.11299545+001	0.54296547-005	0.27701491+000	0.89988759+004
0.23954282+001	0.11372073+001	0.57855565-005	0.25317155+000	0.87806662+004
0.23840700+001	0.11154300+001	0.47633974-005	0.23122506+000	0.85618800+004
0.23700900+001	0.11533567+001	0.43027885-005	0.20774110+000	0.83412894+004
0.23535320+001	0.111531060+001	0.40093911-005	0.18342400+000	0.80691669+004

 ψ_4

0.22863222+001	0.12480129+001	0.37671706-005	0.14986514+000	0.71284032+004
0.21972627+001	0.12941100+001	0.29660315-005	0.10440410+000	0.63073764+004
0.21307482+001	0.13239353+001	0.23534921-005	0.84720278-001	0.59451085+004
0.20461287+001	0.13562940+001	0.21683838-005	0.67411103-001	0.55706097+004
0.17334718+001	0.14849184+001	0.11356120-005	0.27373767-001	0.43135870+004

TABLE V (continued)
STATE OF THE GAS ALONG STREAMLINES OVER THE AFTER-BODY

ψ_4

0.25229010+001	0.19792236+001	0.11845005-004	0.64711042+000	0.97892649+004
0.25154470+001	0.195324890+001	0.12145613-004 ✓	0.66557971+000	0.98196508+004
0.25012887+001	0.193555341+001	0.11285556-004	0.61272670+000	0.97276520+004
0.24905615+001	0.192727949+001	0.11060532-004	0.59865085+000	0.96986613+004
0.24802521+001	0.19190326+001	0.10053200-004	0.53742372+000	0.95789834+004
0.24679915+001	0.19158668+001	0.9269733-005	0.49134322+000	0.94771431+004
0.24518694+001	0.191250716+001	0.83501865-005	0.43543519+000	0.93440313+004
0.24316549+001	0.191184011+001	0.72547182-005	0.37150382+000	0.91759210+004
0.24207024+001	0.191358138+001	0.69261912-005	0.34181149+000	0.89725347+004
0.24034488+001	0.191557951+001	0.64045114-005	0.31321107+000	0.87629686+004
0.23971133+001	0.191757006+001	0.59707104-005	0.28413504+000	0.85271857+004
0.23824552+001	0.191362218+001	0.55168753-005	0.25486824+000	0.82778176+004
0.23651229+001	0.191252071+001	0.51133837-005	0.22957746+000	0.80450326+004
0.23432966+001	0.19133790+001	0.47348014-005	0.20625250+000	0.78055659+004
0.23171095+001	0.1912601892+001	0.42457105-005	0.17710012+000	0.74743843+004

TABLE VI
CONVECTIVE HEAT TRANSFER DISTRIBUTION
CASE I

N	X (ft)	Y (ft)	S (ft)	QC (Btu/ft ² -sec)
1	0.	0.	0.	759.6330
2	-0.0016	0.0921	0.0922	758.9651
3	-0.0064	0.1842	0.1843	738.1123
4	-0.0101	0.2301	0.2304	711.8413
5	-0.0145	0.2760	0.2765	689.7961
6	-0.0226	0.3446	0.3456	662.5203
7	-0.0325	0.4130	0.4147	646.4972
8	-0.0442	0.4811	0.4838	636.3246
9	-0.0577	0.5489	0.5529	629.2803
10	-0.0730	0.6163	0.6221	623.7497
11	-0.0900	0.6833	0.6911	619.2725
12	-0.1087	0.7498	0.7603	615.8250
13	-0.1292	0.8158	0.8394	612.2538
14	-0.1514	0.8813	0.8985	607.0268
15	-0.1611	0.9830	0.9223	603.9644
16	-0.1805	0.9585	0.9811	589.4379
17	-0.2055	1.0000	1.0295	441.8734
18	-0.2888	1.0310	1.1184	144.2551
19	-0.4000	0.9850	1.2387	10.5942
20	-0.6000	0.8550	1.4773	7.5002
21	-0.8000	0.7250	1.7158	5.6779
22	-1.0000	0.5959	1.9538	4.6813
23	-1.2000	0.4660	2.1923	4.1437
24	-1.5000	0.2711	2.5502	3.9157
25	-1.8000	0.0761	2.9080	1.5887

TABLE VII

DISTRIBUTION OF RADIATIVE FLUX OVER RE-ENTRY BODY

CASE I		
<u>s_{Body}, Radians</u>	<u>R_{Body}, Ft</u>	<u>Q_B, BTU/ft²-sec</u>
0	2.6417	323
.025	2.6417	304
.075	2.6417	292
.130	2.6417	255
.170	2.6417	233
.230	2.6417	190
.330	2.6417	93

TABLE VIII

SPECTRAL INTENSITY OF RADIATION TO STAGNATION POINT
CASE I

$\tilde{\omega} \text{ cm}^{-1}$	Q_B watt-cm/ft^2
0.20000 + 004	.334 + 01
0.10000 + 005	.224 + 01
0.18000 + 005	.134 + 01
0.26000 + 005	.778 + 01
0.34000 + 005	.484 + 01
0.42000 + 005	.408 + 00
0.50000 + 005	.216 + 00
0.58000 + 005	.137 + 00
0.66000 + 005	.860 - 01
0.74000 + 005	.558 - 01
0.82000 + 005	.934 + 00
0.90000 + 005	.830 + 01
0.98000 + 005	.376 + 01
0.10600 + 006	.168 + 01
0.11400 + 006	.735 + 00
0.12200 + 006	.318 + 00
0.13000 + 006	.138 + 00
0.13800 + 006	.672 - 01
0.14600 + 006	.250 - 01

TABLE IX

STATE OF THE GAS AT THE SHOCK AND BODY

θ (RAD)	ξ	$T(^{\circ}\text{K})$	$P(\text{ATM})$	ρ (GM/CC)
0.0	0	10264	.028700	.4225-6
0.0	1	63205	.025304	1.4127-7
0.02	0	10259	.028671	.4223-6
0.02	1	63150	.025294	1.4123-7
0.04	0	10247	.028590	.4216-6
0.04	1	62966	.025269	1.4123-7
0.06	0	10227	.028456	.4204-6
0.06	1	62929	.025227	1.4123-7
0.08	0	10200	.028275	.4188-6
0.08	1	62794	.025159	1.4123-7
0.10	0	10167	.028053	.4168-6
0.10	1	62596	.025069	1.4123-7
0.12	0	10128	.027792	.4145-6
0.12	1	62301	.024950	1.4123-7
0.14	0	10085	.027494	.4118-6
0.14	1	61987	.024800	1.4123-7
0.16	0	10034	.027156	.4088-6
0.16	1	61488	.024616	1.4122-7
0.18	0	9977	.026774	.4053-6
0.18	1	60842	.024394	1.4121-7
0.20	0	9912	.026343	.4014-6
0.20	1	60528	.024134	1.4121-7

TABLE IX (continued)
STATE OF THE GAS AT THE SHOCK AND BODY

θ (RAD)	ξ	$T(^{\circ}K)$	$P(ATM)$	ρ (GM/CC)
0.22	0	9837	.025849	.3969-6
0.22	1	59457	.023829	1.4120-7
0.24	0	9749	.025280	.3916-6
0.24	1	58718	.023474	1.4119-7
0.26	0	9644	.024610	.3854-6
0.26	1	57611	.023060	1.4119-7
0.28	0	9515	.023804	.3777-6
0.28	1	56503	.022574	1.4119-7
0.30	0	9349	.022778	.3679-6
0.30	1	54786	.021989	1.4116-7
0.32	0	9118	.021405	.3544-6
0.32	1	53124	.021266	1.4116-7
0.34	0	8752	.019321	.3333-6
0.34	1	50391	.020326	1.4114-7
0.356	0	8097	.015135	.2968-6
0.356	1	48267	.019280	1.4111-7

LOG GAMMA

NON-EQUILIBRIUM GAS PROPERTIES (CASE III) $\beta = 0.5$

TABLE X

θ	TEMP	RHO	O	NO	N+	N	NO+	E-	O2+	O2	N2+	N2	O+
.01	23628.	.233-006	-0.42	-2.38	-1.71	0.16	-3.13	-1.48	-4.19	-3.59	-2.68	-2.02	-1.96
.03	23774.	.233-006	-0.42	-2.39	-1.75	0.15	-3.16	-1.48	-4.19	-3.59	-2.68	-2.02	-1.98
.05	23736.	.235-006	-0.41	-2.40	-1.78	0.16	-3.19	-1.48	-4.19	-3.60	-2.67	-2.01	-1.99
.07	23673.	.244-006	-0.41	-2.41	-1.78	0.16	-3.19	-1.48	-4.19	-3.60	-2.67	-2.01	-1.99
.09	23584.	.253-006	-0.41	-2.40	-1.77	0.16	-3.19	-1.48	-4.19	-3.60	-2.68	-2.01	-1.98
.11	23470.	.257-006	-0.40	-2.41	-1.75	0.16	-3.18	-1.49	-4.18	-3.60	-2.67	-2.00	-1.96
.13	23317.	.259-006	-0.41	-2.40	-1.73	0.16	-3.16	-1.50	-4.18	-3.60	-2.67	-1.99	-1.94
.15	23114.	.259-006	-0.40	-2.39	-1.70	0.16	-3.13	-1.50	-4.18	-3.60	-2.67	-1.98	-1.91
.17	22923.	.258-006	-0.40	-2.38	-1.68	0.16	-3.12	-1.50	-4.19	-3.60	-2.67	-1.97	-1.89
.19	22631.	.257-006	-0.40	-2.37	-1.67	0.16	-3.11	-1.51	-4.19	-3.59	-2.67	-1.96	-1.88
.21	22415.	.255-006	-0.40	-2.35	-1.66	0.16	-3.10	-1.51	-4.18	-3.57	-2.67	-1.94	-1.86
.23	22098.	.252-006	-0.40	-2.32	-1.67	0.16	-3.10	-1.52	-4.19	-3.56	-2.67	-1.92	-1.86
.25	21958.	.248-006	-0.39	-2.29	-1.69	0.16	-3.11	-1.53	-4.19	-3.54	-2.68	-1.90	-1.86
.27	21666.	.241-006	-0.40	-2.27	-1.73	0.14	-3.12	-1.55	-4.20	-3.52	-2.68	-1.86	-1.88
.29	21285.	.224-006	-0.40	-2.22	-1.79	0.15	-3.13	-1.57	-4.20	-3.48	-2.67	-1.81	-1.93
.31	20866.	.129-006	-0.40	-2.17	-1.85	0.14	-3.12	-1.59	-4.21	-3.43	-2.68	-1.75	-2.00
.33	20269.	.121-006	-0.41	-2.12	-1.92	0.13	-3.10	-1.63	-4.22	-3.38	-2.68	-1.69	-2.08
.35	19583.	.118-006	-0.41	-2.05	-2.00	0.13	-3.04	-1.67	-4.23	-3.31	-2.68	-1.60	-2.18
.37	19037.	.118-006	-0.41	-1.99	-2.07	0.12	-2.99	-1.71	-4.24	-3.23	-2.69	-1.49	-2.28
.39	18631.	.126-006	-0.42	-1.91	-2.15	0.12	-2.91	-1.76	-4.25	-3.15	-2.70	-1.39	-2.40
.41	18364.	.124-006	-0.44	-1.84	-2.24	0.10	-2.84	-1.83	-4.27	-3.06	-2.71	-1.28	-2.52
.43	18199.	.128-006	-0.45	-1.76	-2.34	0.07	-2.75	-1.91	-4.30	-2.97	-2.72	-1.16	-2.66
.45	18085.	.135-006	-0.47	-1.67	-2.43	0.05	-2.66	-1.98	-4.32	-2.85	-2.73	-1.04	-2.80
.47	18072.	.142-006	-0.47	-1.56	-2.54	0.03	-2.55	-2.05	-4.34	-2.73	-2.74	-0.90	-2.94
.49	18212.	.149-006	-0.50	-1.45	-2.64	0.01	-2.44	-2.13	-4.36	-2.61	-2.75	-0.76	-3.08
.51	18288.	.159-006	-0.51	-1.31	-2.76	-0.03	-2.32	-2.22	-4.39	-2.47	-2.77	-0.61	-3.22

LOG GAMMA

θ	TEMP	ERG	U	NO	N+	N	NO+	E-	O2+	O2	N2+	N2	U+
.01	26733.	.194-006	-0.44	-1.43	-2.37	0.17	-3.17	-2.13	-4.10	-2.53	-2.64	-1.14	-2.79
.03	26797.	.186-006	-0.47	-1.44	-2.62	0.08	-3.18	-2.14	-4.10	-2.50	-2.64	-1.12	-2.83
.05	26733.	.184-006	-0.47	-1.44	-2.65	0.08	-3.19	-2.15	-4.08	-2.48	-2.65	-1.11	-2.84
.07	26683.	.186-006	-0.44	-1.43	-2.65	0.09	-3.19	-2.15	-4.06	-2.47	-2.65	-1.10	-2.83
.09	26657.	.191-006	-0.44	-1.42	-2.64	0.10	-3.18	-2.14	-4.03	-2.46	-2.65	-1.10	-2.79
.11	26594.	.194-006	-0.45	-1.42	-2.63	0.10	-3.17	-2.13	-4.01	-2.47	-2.64	-1.10	-2.76
.13	26556.	.196-006	-0.45	-1.41	-2.61	0.10	-3.16	-2.13	-4.00	-2.48	-2.62	-1.09	-2.74
.15	26505.	.196-006	-0.45	-1.40	-2.59	0.09	-3.15	-2.12	-3.98	-2.49	-2.59	-1.08	-2.72
.17	2634.	.194-006	-0.45	-1.38	-2.56	0.10	-3.14	-2.12	-3.98	-2.50	-2.58	-1.07	-2.72
.19	26147.	.192-006	-0.44	-1.38	-2.56	0.10	-3.13	-2.12	-3.98	-2.49	-2.58	-1.06	-2.71
.21	2606.	.191-006	-0.44	-1.35	-2.57	0.09	-3.12	-2.13	-3.99	-2.48	-2.58	-1.04	-2.72
.23	25895.	.191-006	-0.45	-1.34	-2.58	0.08	-3.11	-2.14	-4.01	-2.47	-2.60	-1.02	-2.74
.25	25667.	.191-006	-0.44	-1.33	-2.61	0.07	-3.09	-2.15	-4.03	-2.45	-2.62	-1.00	-2.77
.27	25451.	.191-006	-0.44	-1.31	-2.65	0.07	-3.08	-2.17	-4.07	-2.43	-2.64	-0.96	-2.84
.29	25171.	.192-006	-0.44	-1.29	-2.69	0.06	-3.05	-2.20	-4.13	-2.40	-2.68	-0.92	-2.93
.31	2493.	.192-006	-0.47	-1.26	-2.73	0.06	-3.01	-2.24	-4.19	-2.38	-2.71	-0.89	-3.03
.33	24701.	.192-006	-0.44	-1.24	-2.79	0.06	-2.94	-2.27	-4.24	-2.34	-2.74	-0.83	-3.16
.35	2413.	.186-006	-0.47	-1.21	-2.86	0.04	-2.90	-2.31	-4.30	-2.31	-2.78	-0.78	-3.29
.37	22355.	.174-006	-0.47	-1.18	-2.94	0.04	-2.88	-2.35	-4.34	-2.28	-2.82	-0.73	-3.43
.39	20815.	.162-006	-0.48	-1.15	-3.03	0.03	-2.88	-2.41	-4.39	-2.24	-2.86	-0.68	-3.54
.41	20498.	.156-006	-0.50	-1.12	-3.12	0.01	-2.89	-2.47	-4.43	-2.21	-2.90	-0.48	-3.66
.43	20637.	.151-006	-0.52	-1.09	-3.23	-0.00	-2.90	-2.52	-4.47	-2.18	-2.94	-0.59	-3.77
.45	20923.	.148-006	-0.51	-1.06	-3.35	-0.03	-2.94	-2.59	-4.52	-2.16	-3.00	-0.57	-3.87
.47	21311.	.146-006	-0.53	-1.05	-3.46	-0.05	-2.98	-2.64	-4.55	-2.12	-3.05	-0.54	-3.96
.49	21907.	.144-006	-0.54	-1.02	-3.55	-0.08	-3.03	-2.71	-4.58	-2.09	-3.09	-0.53	-4.05
.51	22555.	.143-006	-0.54	-0.99	-3.60	-0.11	-3.09	-2.77	-4.60	-2.05	-3.15	-0.54	-4.15

LOG GAMMA

NON-EQUILIBRIUM GAS PROPERTIES (CASE III) $\mu = 0.90$													
θ	TEMP	RHO	0	NO	N+	N	NO+	E-	O2+	O2	N2+	N2	0+
.01	34023.	.163-006	-0.62	-0.91	-4.15	-0.12	-3.72	-3.10	-4.12	-1.78	-3.32	-0.53	-4.62
.03	33985.	.160-006	-0.62	-0.90	-4.17	-0.13	-3.75	-3.09	-4.10	-1.77	-3.31	-0.53	-4.63
.05	33934.	.158-006	-0.62	-0.89	-4.20	-0.15	-3.77	-3.09	-4.08	-1.77	-3.31	-0.54	-4.63
.07	33934.	.157-006	-0.61	-0.88	-4.20	-0.15	-3.79	-3.08	-4.06	-1.76	-3.31	-0.54	-4.62
.09	33896.	.158-006	-0.61	-0.88	-4.17	-0.15	-3.77	-3.06	-4.05	-1.76	-3.31	-0.54	-4.60
.11	33858.	.159-006	-0.61	-0.87	-4.15	-0.14	-3.74	-3.05	-4.04	-1.75	-3.31	-0.53	-4.58
.13	33807.	.161-006	-0.60	-0.86	-4.12	-0.13	-3.71	-3.03	-4.03	-1.74	-3.31	-0.54	-4.56
.15	33718.	.162-006	-0.60	-0.86	-4.12	-0.13	-3.69	-3.02	-4.03	-1.74	-3.31	-0.52	-4.54
.17	33633.	.163-006	-0.60	-0.86	-4.12	-0.12	-3.68	-3.03	-4.04	-1.73	-3.32	-0.52	-4.53
.19	33503.	.163-006	-0.60	-0.86	-4.13	-0.12	-3.67	-3.03	-4.05	-1.71	-3.33	-0.50	-4.53
.21	33299.	.162-006	-0.59	-0.84	-4.15	-0.12	-3.67	-3.04	-4.07	-1.70	-3.35	-0.49	-4.52
.23	33071.	.162-006	-0.59	-0.84	-4.18	-0.13	-3.68	-3.06	-4.10	-1.69	-3.36	-0.48	-4.53
.25	32766.	.161-006	-0.59	-0.84	-4.21	-0.14	-3.69	-3.08	-4.15	-1.67	-3.38	-0.46	-4.55
.27	32423.	.160-006	-0.59	-0.83	-4.26	-0.14	-3.69	-3.10	-4.20	-1.66	-3.40	-0.44	-4.57
.29	32004.	.159-006	-0.59	-0.83	-4.30	-0.16	-3.71	-3.13	-4.30	-1.64	-3.43	-0.44	-4.60
.31	31483.	.157-006	-0.60	-0.83	-4.36	-0.18	-3.72	-3.16	-4.43	-1.63	-3.46	-0.41	-4.64
.33	30772.	.156-006	-0.60	-0.83	-4.42	-0.20	-3.73	-3.20	-4.54	-1.61	-3.50	-0.39	-4.68
.35	29947.	.154-006	-0.61	-0.84	-4.48	-0.22	-3.75	-3.24	-4.62	-1.59	-3.54	-0.38	-4.73
.37	28791.	.152-006	-0.62	-0.84	-4.55	-0.24	-3.76	-3.28	-4.67	-1.57	-3.57	-0.36	-4.78
.39	27610.	.151-006	-0.63	-0.84	-4.62	-0.26	-3.78	-3.33	-4.72	-1.55	-3.62	-0.34	-4.84
.41	26949.	.149-006	-0.64	-0.85	-4.68	-0.29	-3.80	-3.38	-4.76	-1.53	-3.68	-0.29	-4.90
.43	26518.	.147-006	-0.65	-0.86	-4.75	-0.32	-3.82	-3.43	-4.79	-1.50	-3.73	-0.31	-4.96
.45	26340.	.145-006	-0.67	-0.87	-4.83	-0.34	-3.84	-3.48	-4.80	-1.47	-3.79	-0.31	-5.01
.47	26276.	.143-006	-0.68	-0.88	-4.90	-0.37	-3.86	-3.54	-4.82	-1.44	-3.86	-0.32	-5.07
.49	26314.	.141-006	-0.70	-0.89	-4.97	-0.40	-3.88	-3.59	-4.83	-1.40	-3.93	-0.32	-5.13
.51	26556.	.139-006	-0.72	-0.90	-5.05	-0.43	-3.91	-3.65	-4.84	-1.37	-4.01	-0.34	-5.19

TABLE XI
CONVECTIVE HEAT TRANSFER DISTRIBUTION

CASE III				
N	X	Y	θ	QC
	(ft)	(ft)	(degrees)	(BTU/ft ² -sec)
1	0.	0.	0.	144.1527
2	0.0001	0.0268	0.5002	144.1448
3	0.0005	0.0535	0.9998	144.1211
4	0.0010	0.0803	1.5002	144.0814
5	0.0019	0.1070	2.0001	144.0260
6	0.0029	0.1338	2.5000	143.9547
7	0.0042	0.1605	3.0310	142.8850
8	0.0057	0.1872	3.5138	141.8154
9	0.0075	0.2139	3.9752	141.1936
10	0.0095	0.2406	4.5007	140.6951
11	0.0117	0.2673	4.9941	139.9140
12	0.0141	0.2939	5.5009	139.2037
13	0.0168	0.3206	6.5118	138.4189
14	0.0262	0.4003	7.4953	135.2683
15	0.0377	0.4797	9.0	132.9333
16	0.0670	0.6376	11.9980	128.2417
17	0.1045	0.7937	14.9980	125.6401
18	0.1501	0.9477	17.5053	123.4432
19	0.1850	1.0489	20.0	118.8414

TABLE XII

CASE III

DISTRIBUTION OF RADIATIVE FLUX OVER RE-ENTRY BODY

<u>θ (Radians)</u>	<u>R_{Body} (Ft)</u>	<u>Q_p (BTU/ft²-sec)</u>
0.0	3.0667	5.32
.04	3.0667	5.14
.06	3.0667	5.23
.12	3.0667	5.30
.20	3.0667	5.19
.28	3.0667	5.09
.321	3.0667	5.19

TABLE XIII

CASE III

SPECTRAL INTENSITY OF RADIATION TO STAGNATION POINT

<u>(cm⁻¹)</u>	<u>Q_B (watt-cm/ft²)</u>
0.20000 + 004	.177 - 3
0.10000 + 005	.248 - 2
0.18000 + 005	.313 - 1
0.26000 + 005	.264 + 0
0.34000 + 005	.438 + 0
0.42000 + 005	.367 - 1
0.50000 + 005	.173 - 1
0.58000 + 005	.241 - 1
0.66000 + 005	.665 - 4
0.74000 + 005	.784 - 5
0.82000 + 005	.781 - 4
0.90000 + 005	.145 - 2
0.98000 + 005	.123 - 2
0.10600 + 006	.750 - 3
0.11400 + 006	.292 - 2
0.12200 + 006	.121 - 2
0.13000 + 006	.192 - 3
0.13800 + 006	.270 - 4
0.14600 + 006	.382 - 5

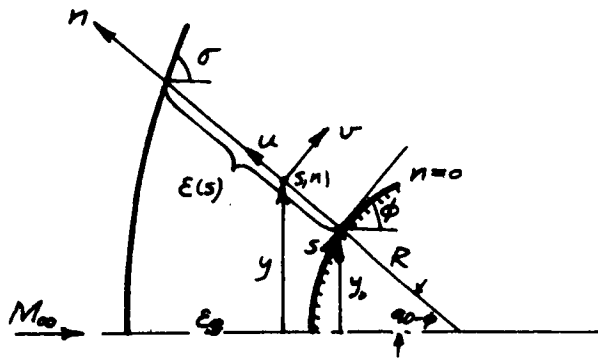
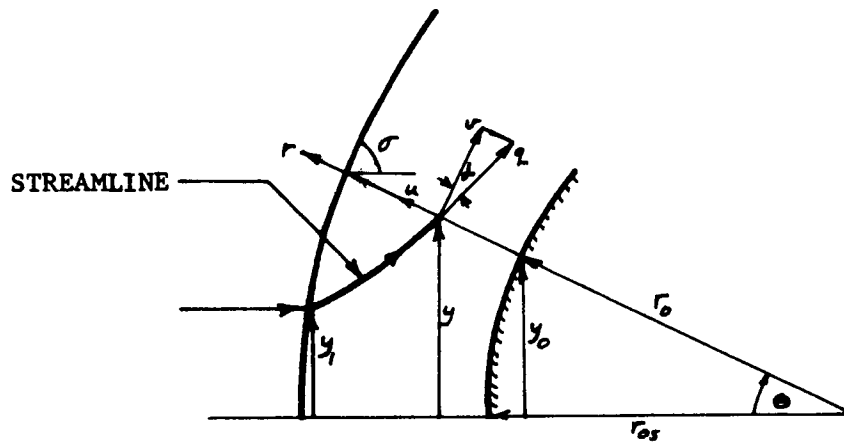
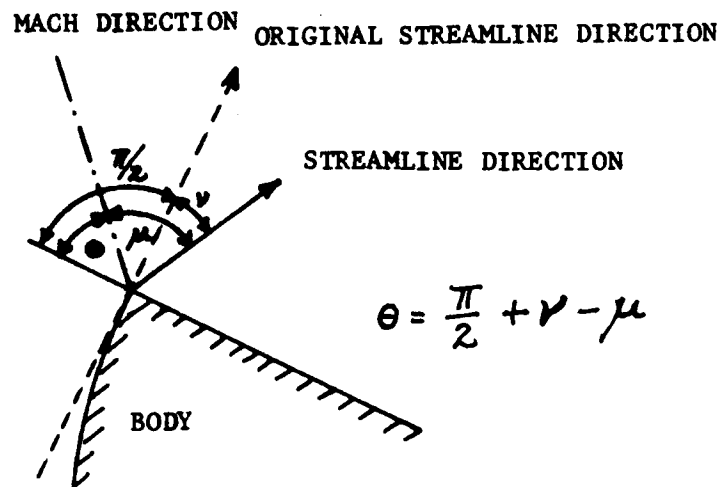


FIGURE 1. BODY AND SHOCK GEOMETRY FOR EQUILIBRIUM PROGRAM



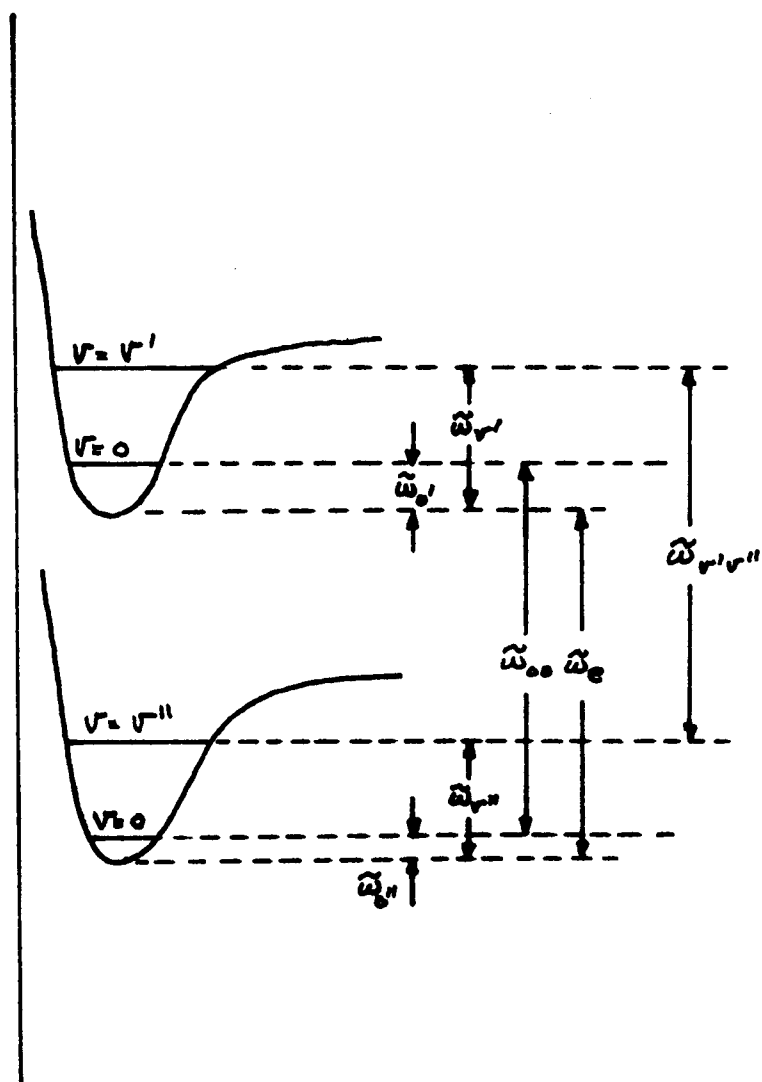
R11086

FIGURE 2. BODY, SHOCK AND STREAMLINE GEOMETRY FOR NON-EQUILIBRIUM PROGRAM



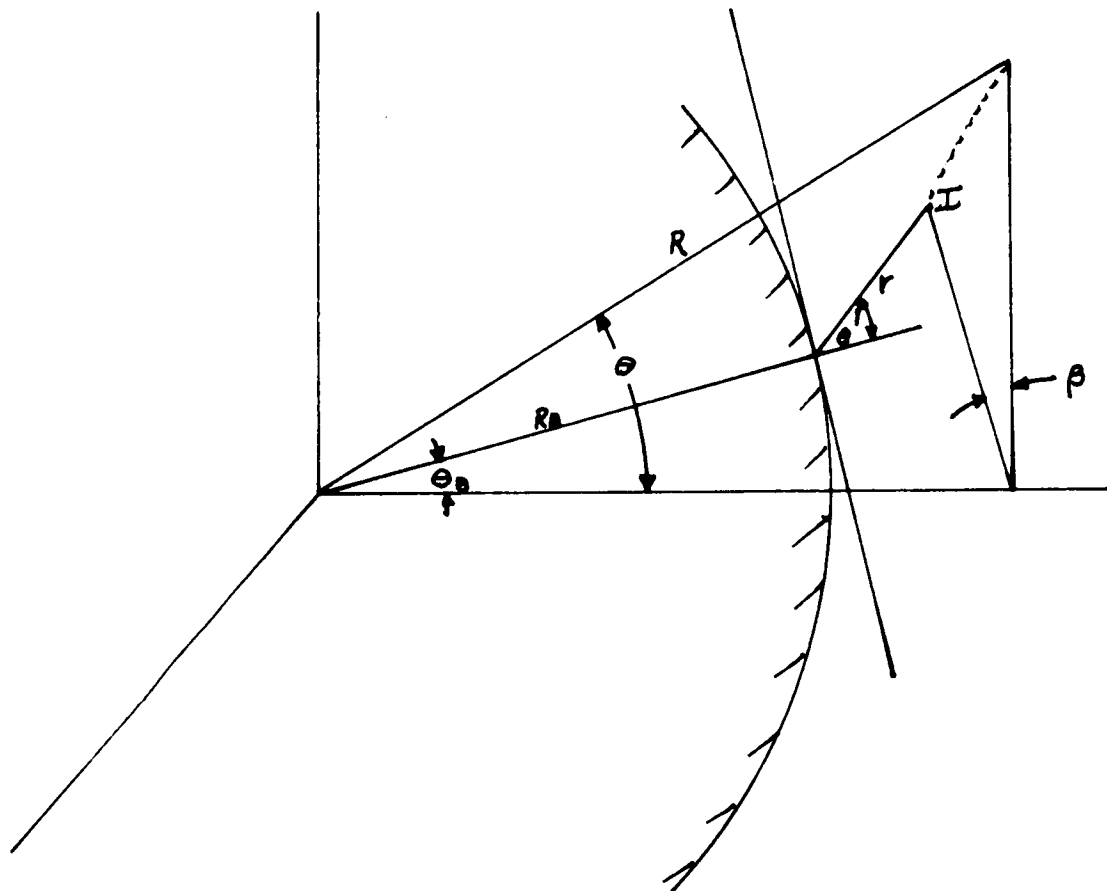
R11087

FIGURE 2a. CASE III GEOMETRY AT CORNER OF BODY



R11088

FIGURE 3. ENERGY LEVEL DIAGRAM - DEFINITION OF RADIATION TERMS



R11089

FIGURE 4. COORDINATE SYSTEM FOR RADIATION INTEGRATION

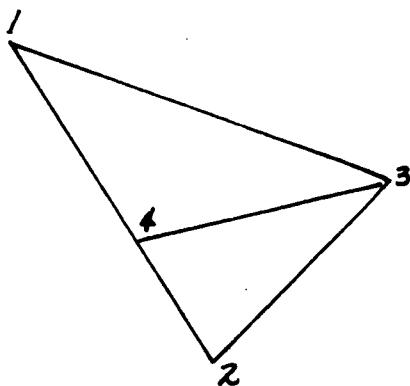


FIGURE 5. CHARACTERISTIC CELL - INTERIOR POINT

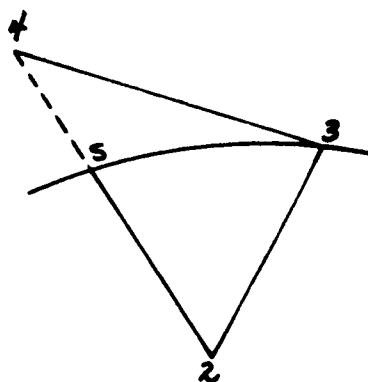
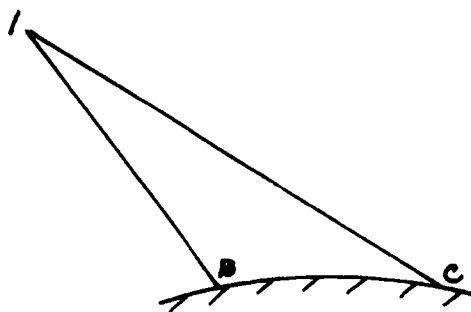
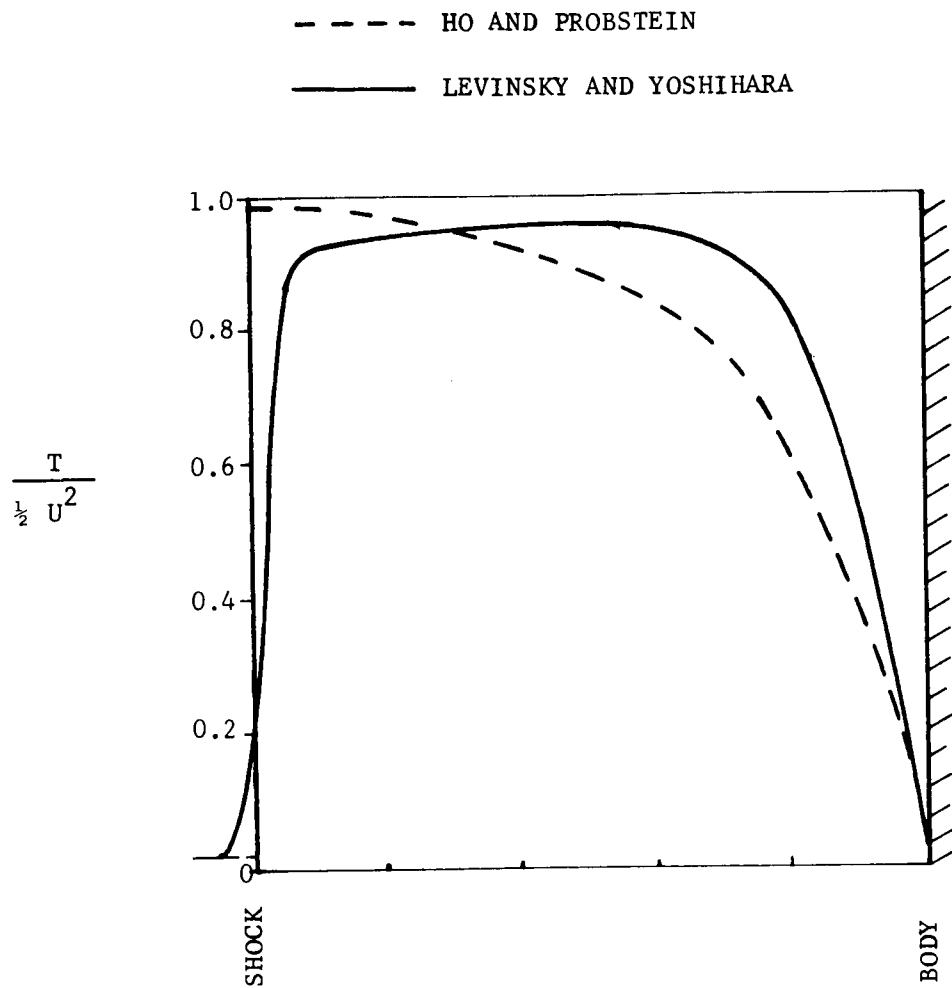


FIGURE 6. CHARACTERISTIC CELL - SHOCK POINT



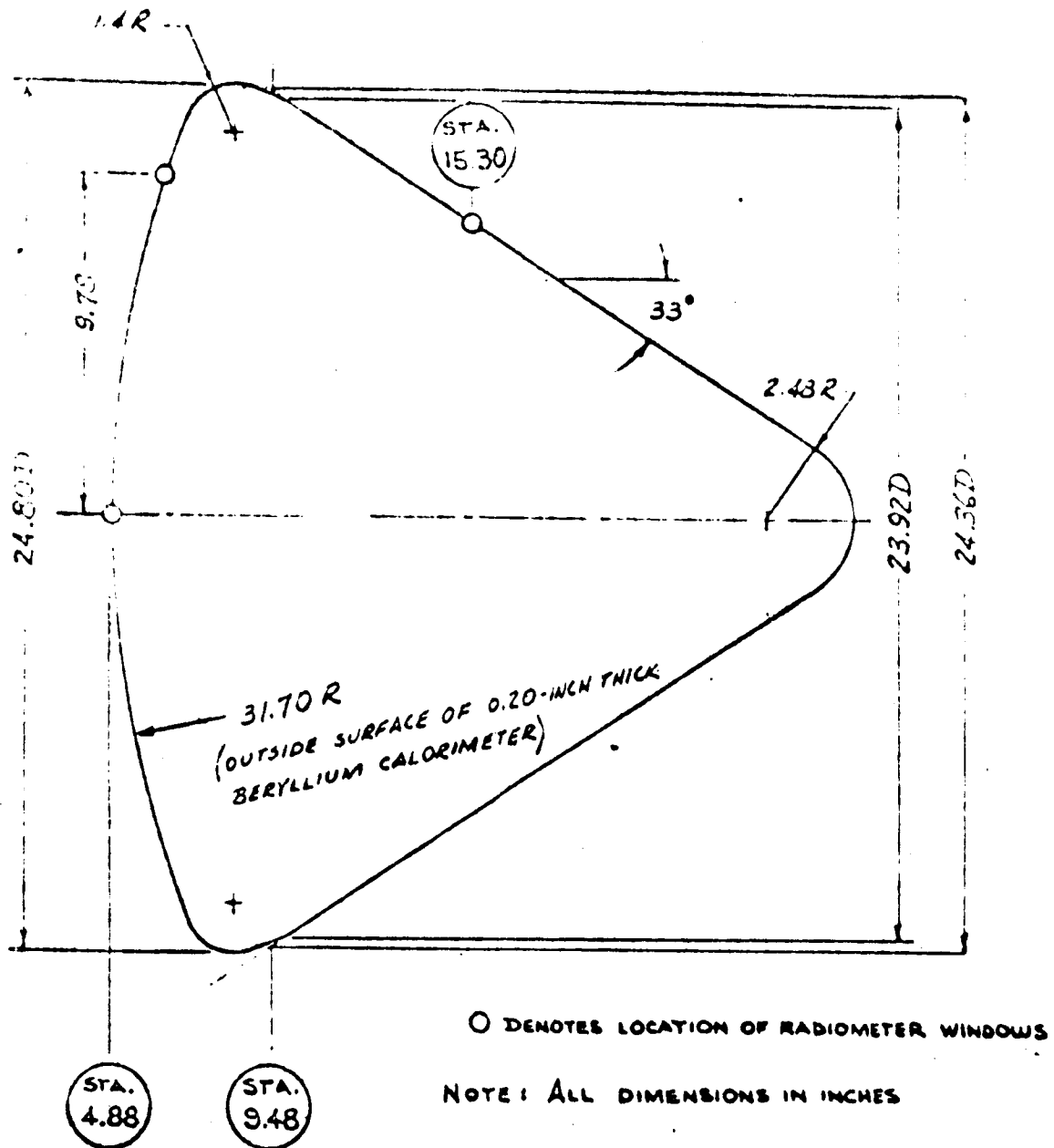
R11090

FIGURE 7. CHARACTERISTIC CELL - BODY POINT



R11091

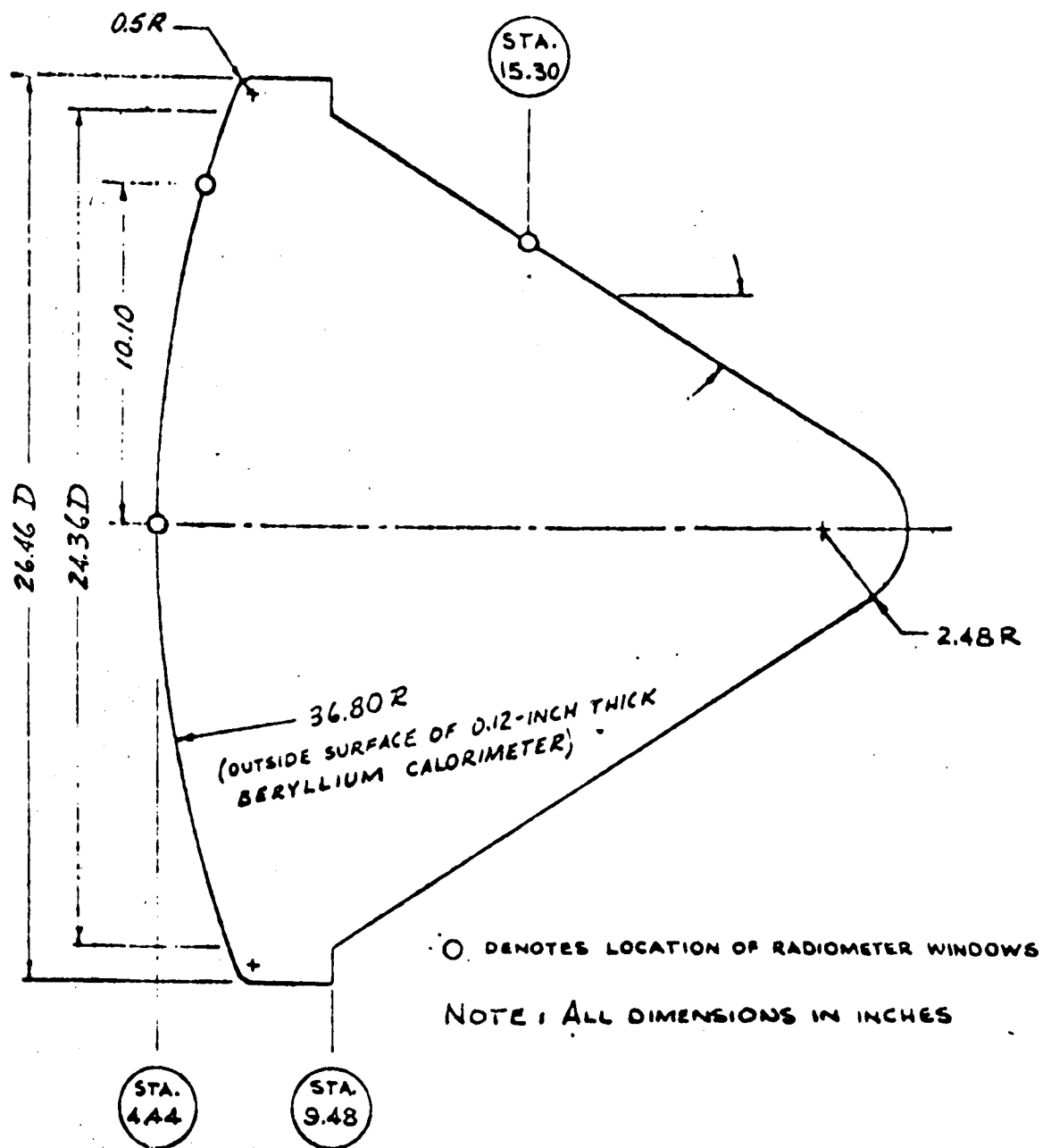
FIGURE 8. TEMPERATURE PROFILES IN THE PERFECT GAS SHOCK LAYER -
HIGHLY COOLED BODY



Shape after removal of first calorimeter and ablative layers.

R11092

FIGURE 9. CASE I VEHICLE GEOMETRY



Original shape.

R11093

FIGURE 10. CASE III VEHICLE GEOMETRY

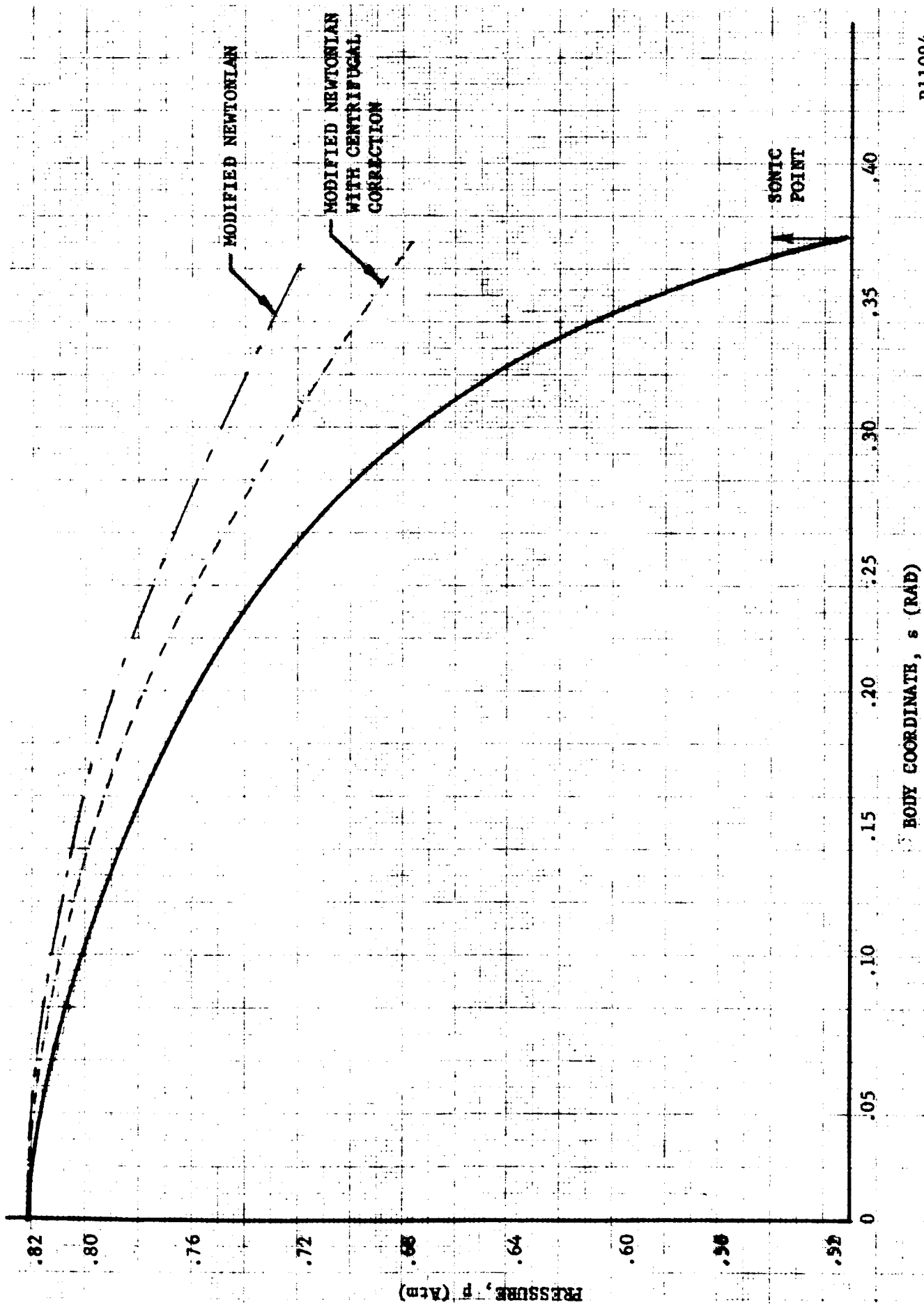


FIGURE #1. PRESSURE DISTRIBUTION ALONG THE BODY SURFACE, (CASE 1)

R11094

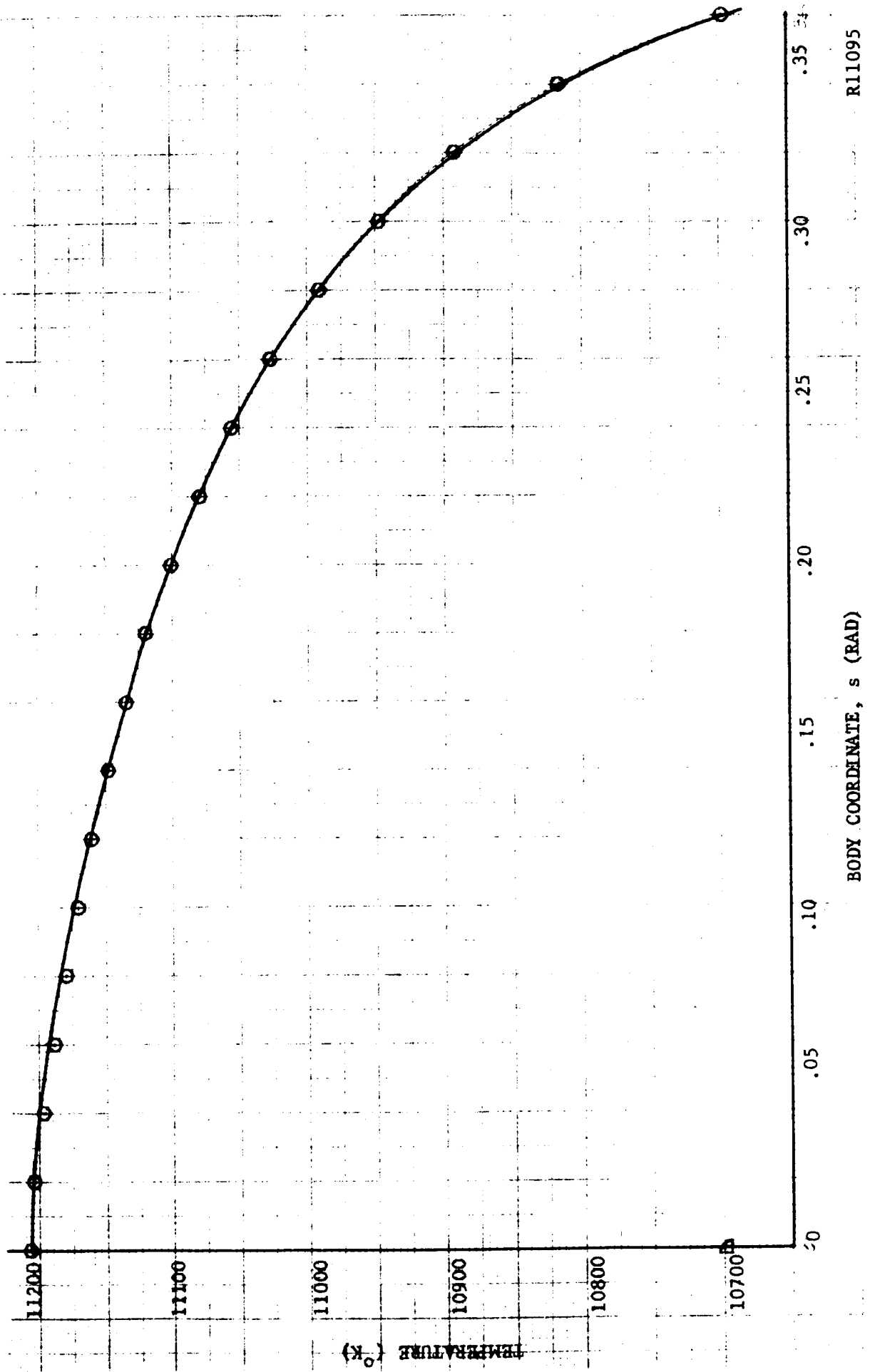
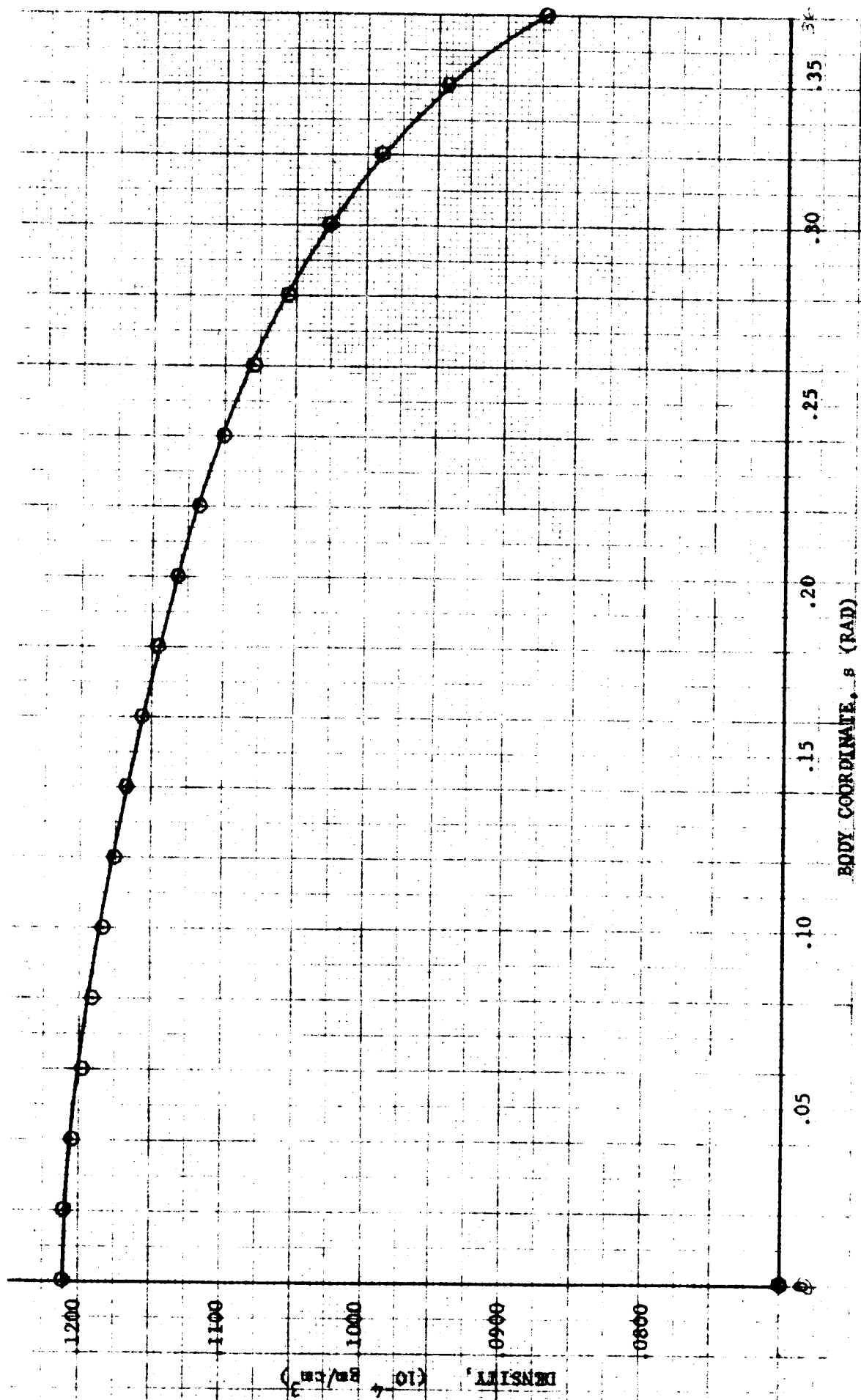
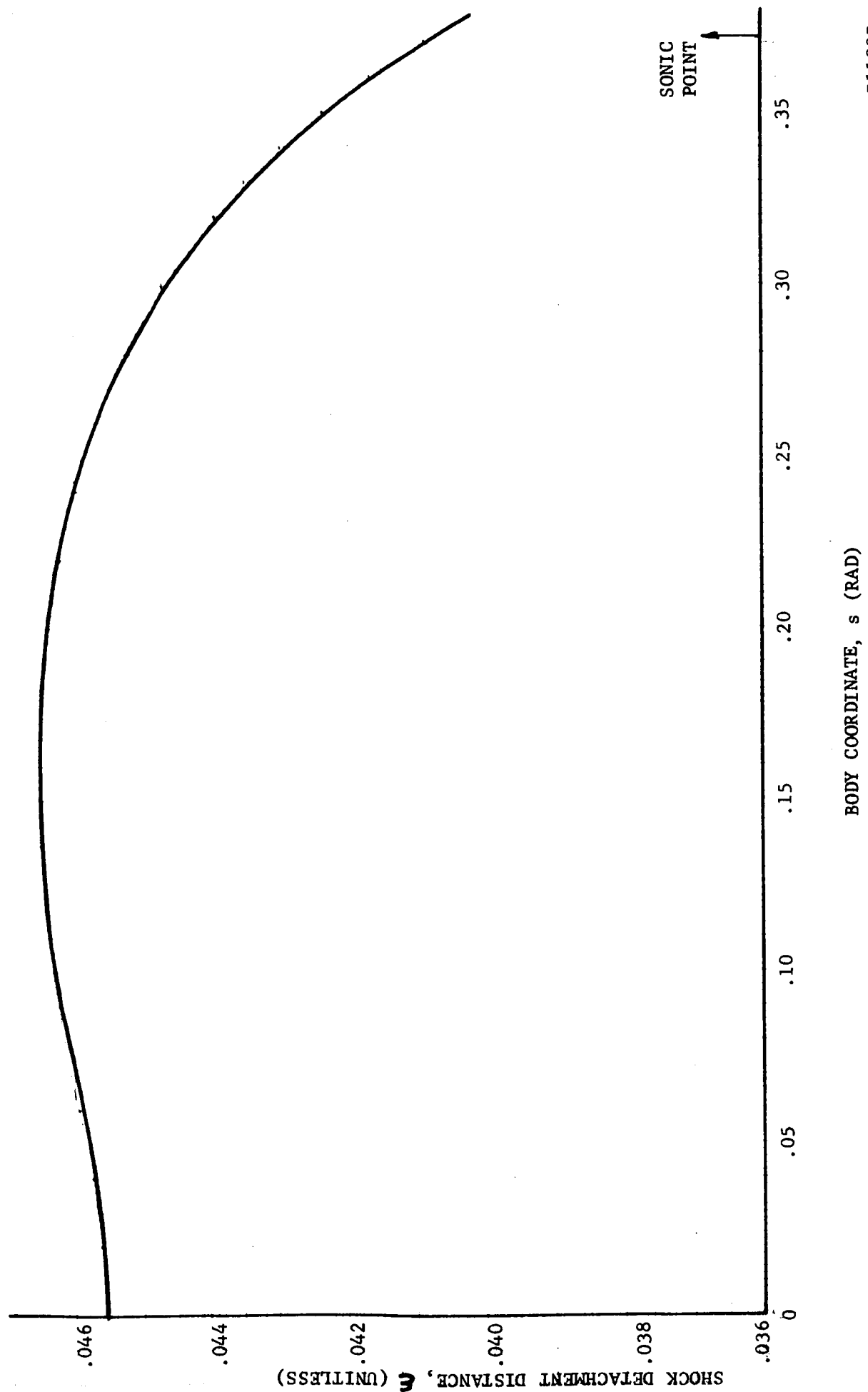


FIGURE 12. TEMPERATURE DISTRIBUTION ALONG THE BODY SURFACE, (CASE I)



R11096

FIGURE 13. DENSITY DISTRIBUTION ALONG THE BODY SURFACE, (CASE I)



R11097

FIGURE 14. SHOCK DETACHMENT DISTANCE, $\bar{\epsilon}(\bar{\epsilon}/\bar{r}_{os})$, (CASE I)

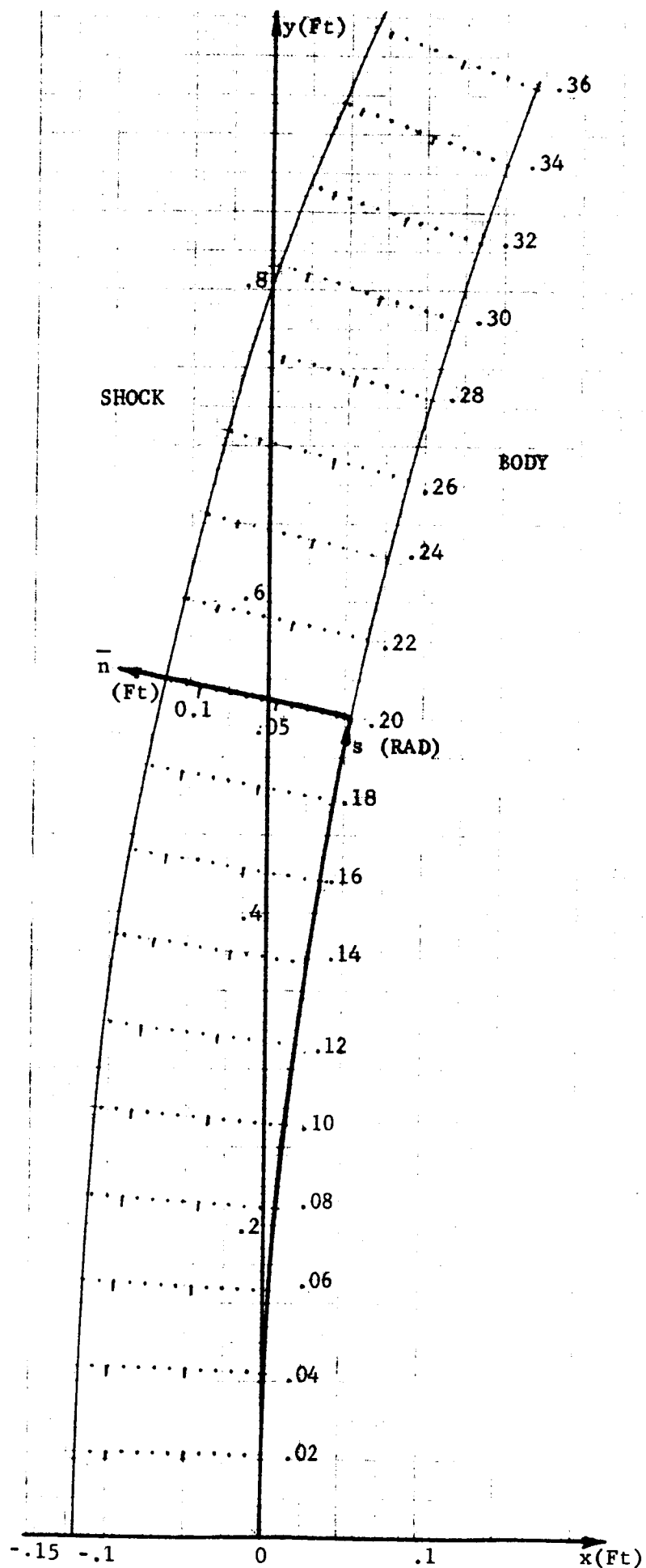


FIGURE 15. COORDINATE SYSTEM (CASE I)

R11098

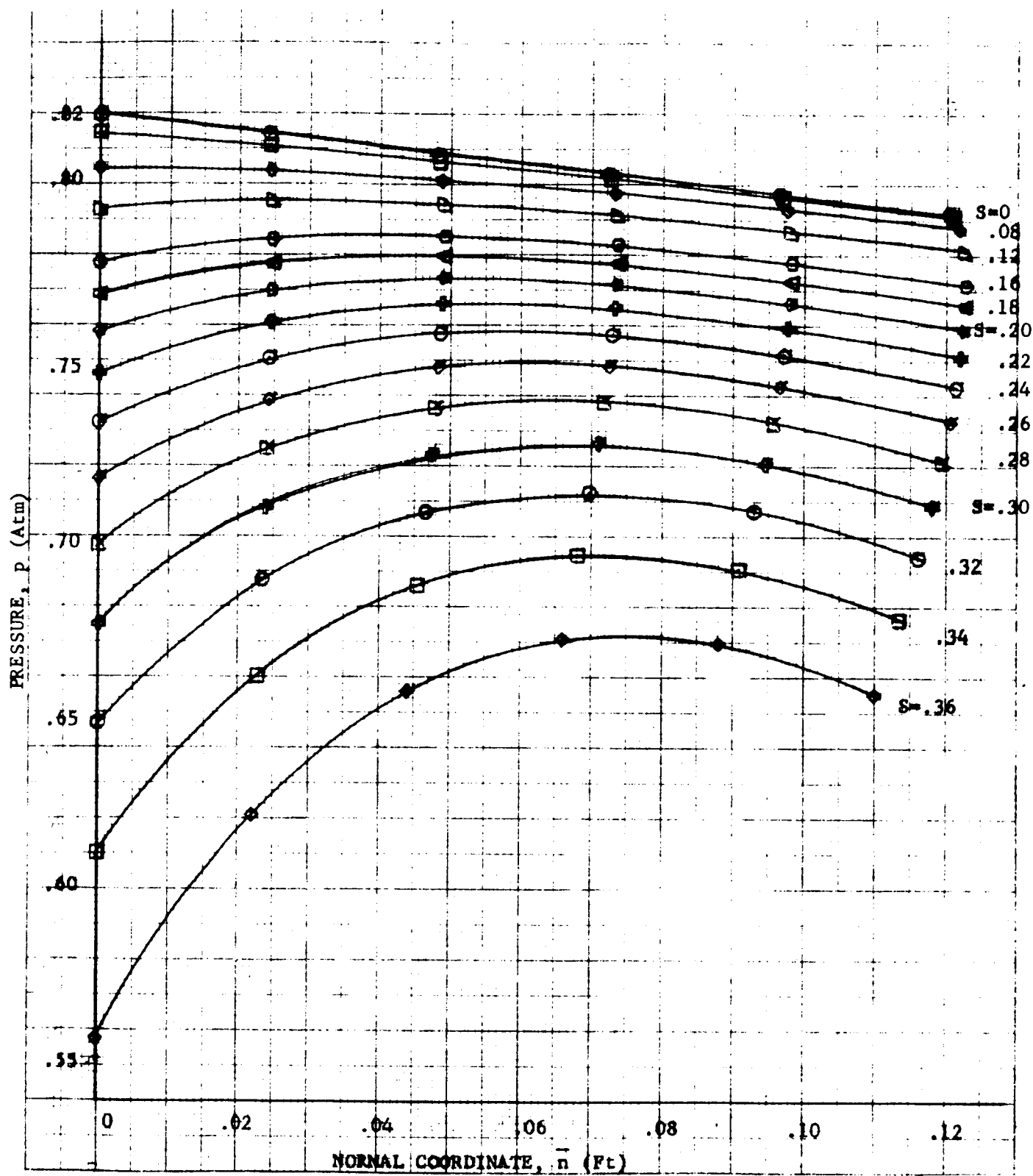


FIGURE 16. PRESSURE DISTRIBUTION ACROSS THE SHOCK LAYER, (CASE I)

R11099

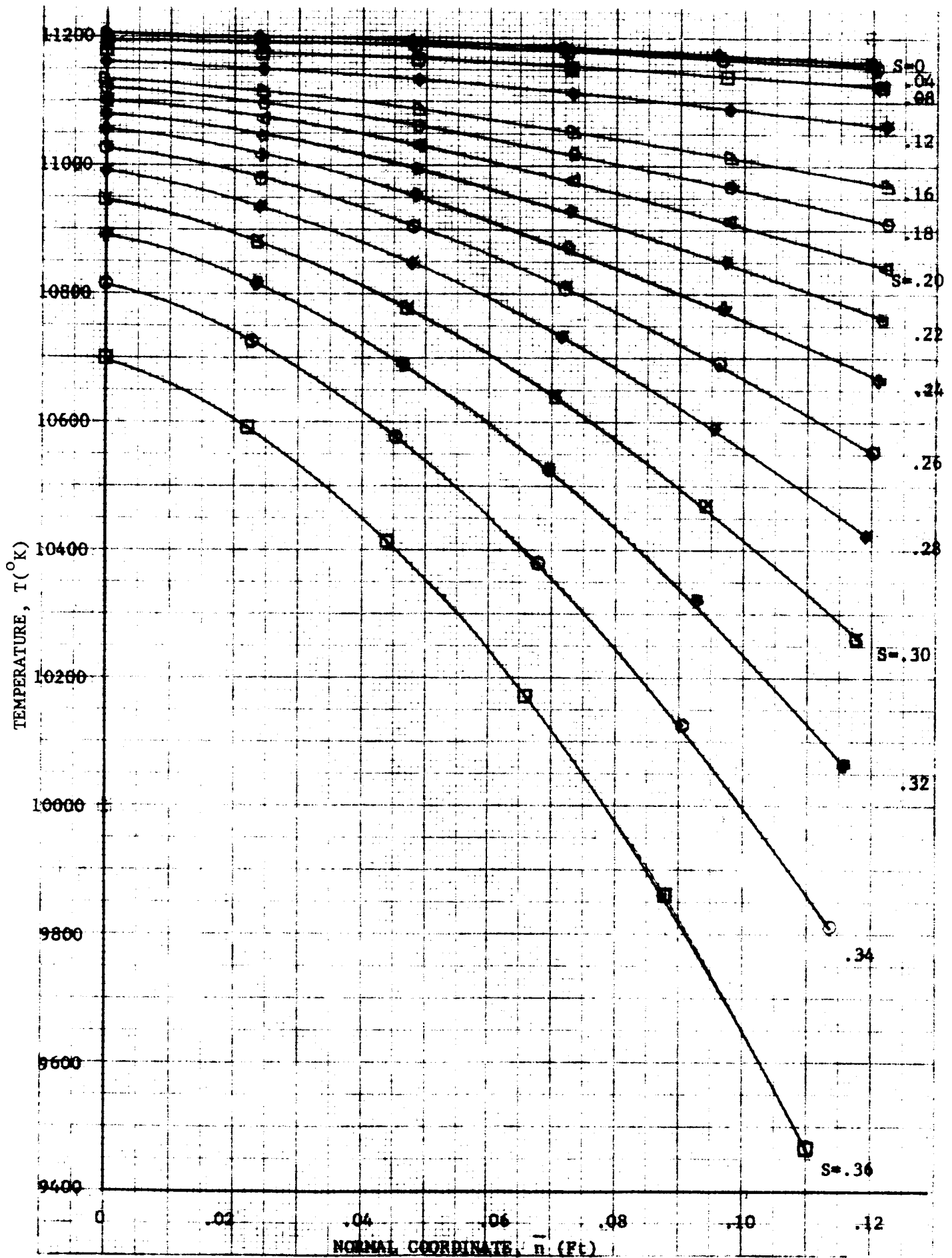


FIGURE 17. TEMPERATURE DISTRIBUTION ACROSS THE SHOCK LAYER, (CASE I)

R11100

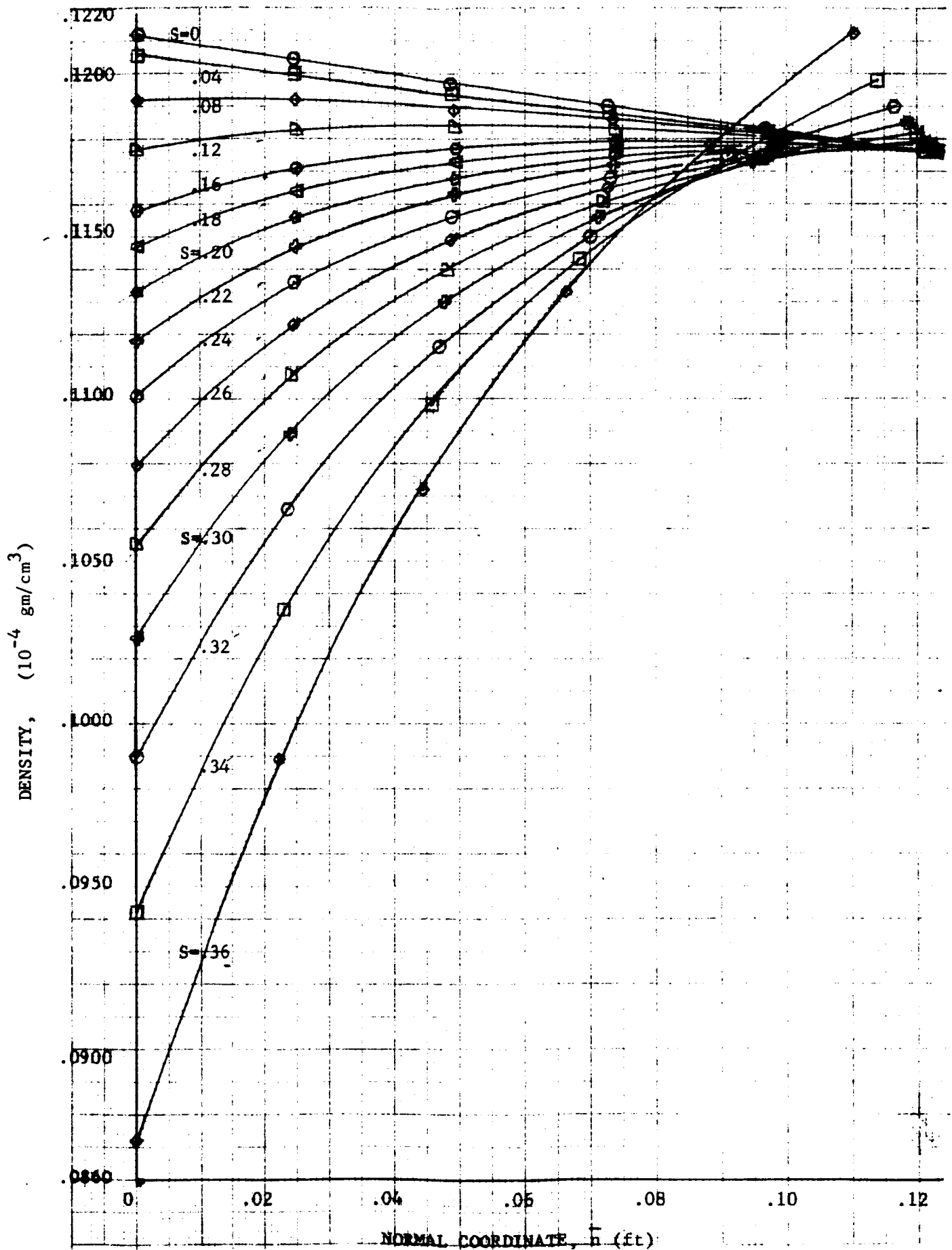
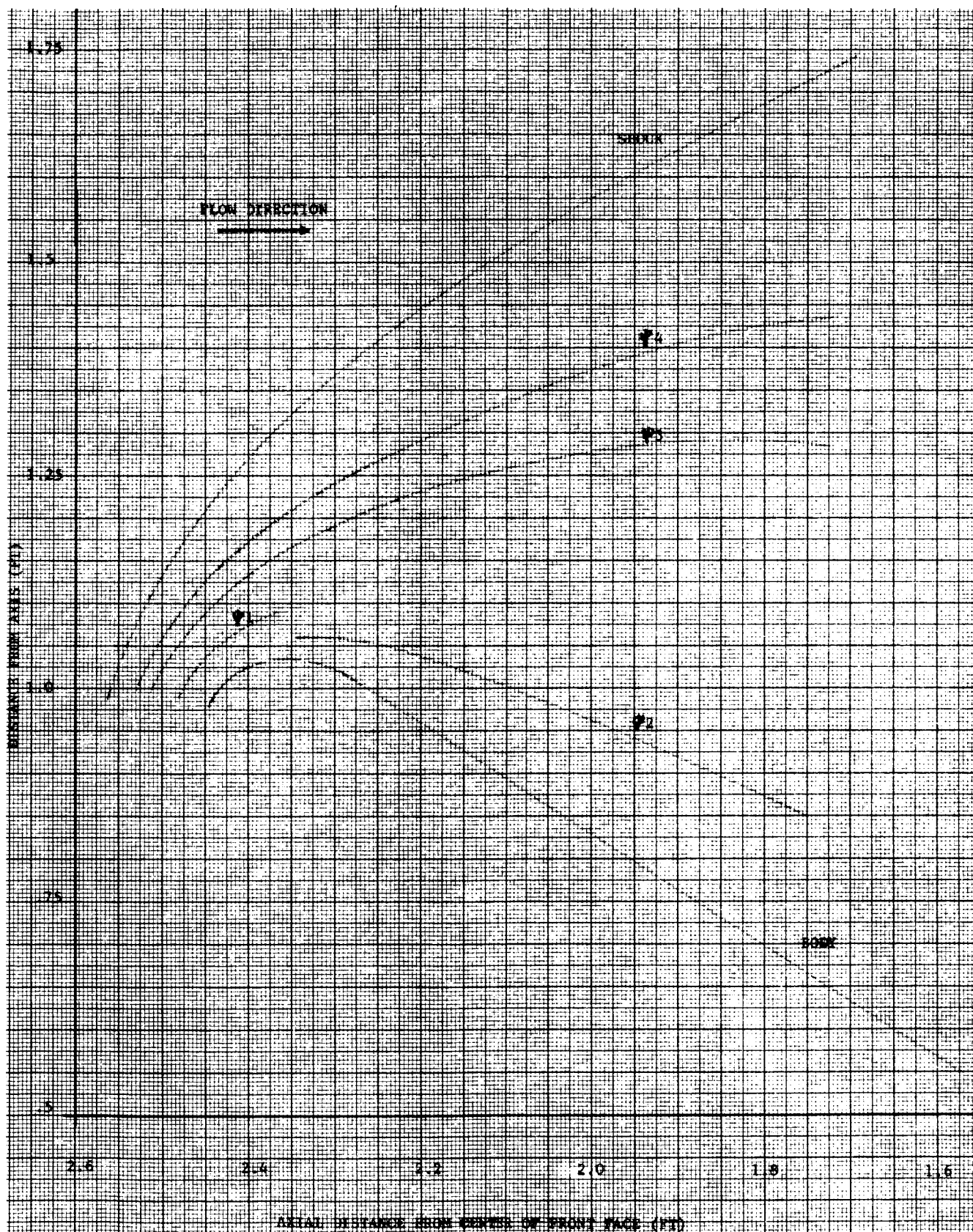


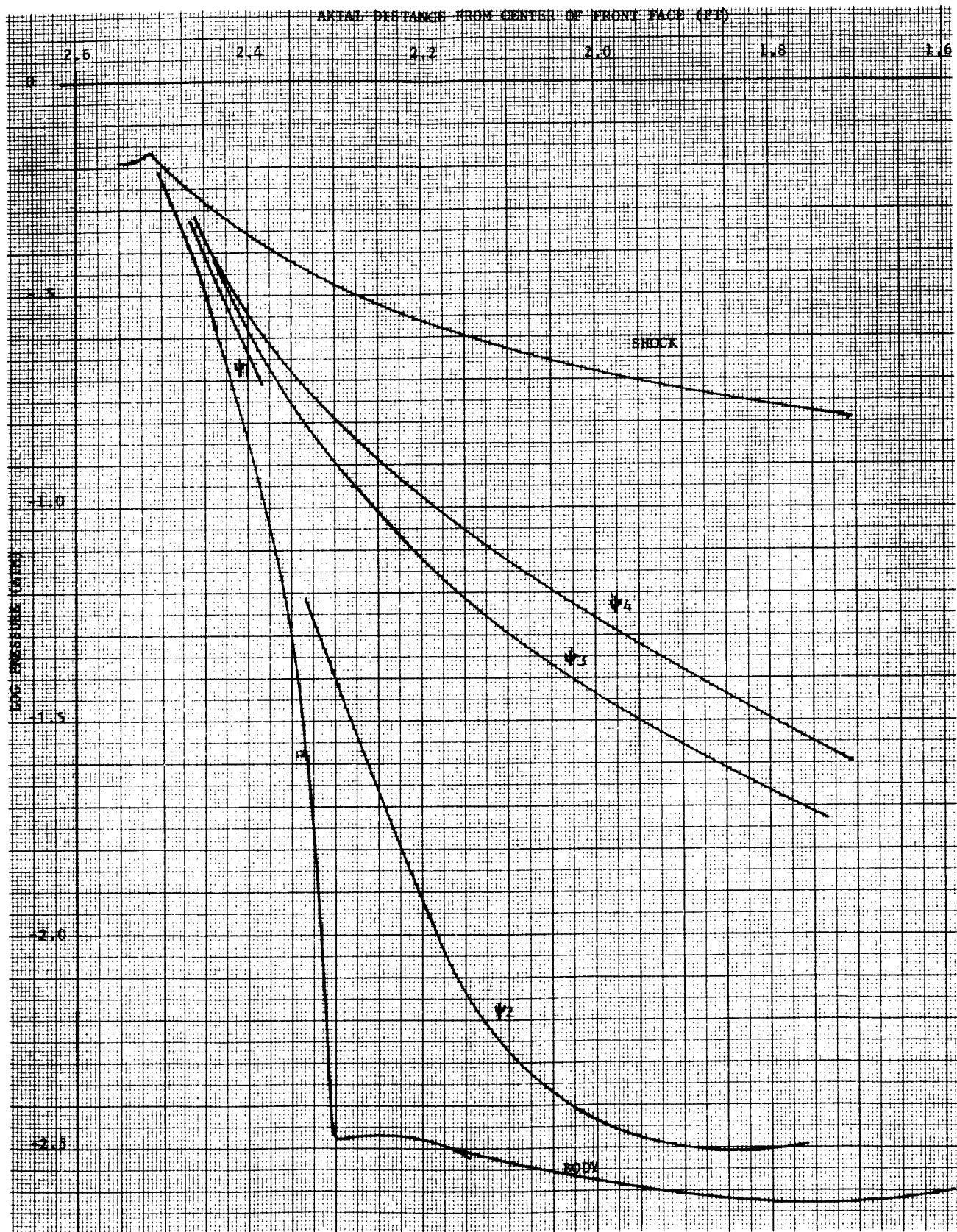
FIGURE 18. DENSITY DISTRIBUTION ACROSS THE SHOCK LAYER, (CASE I)

R11101



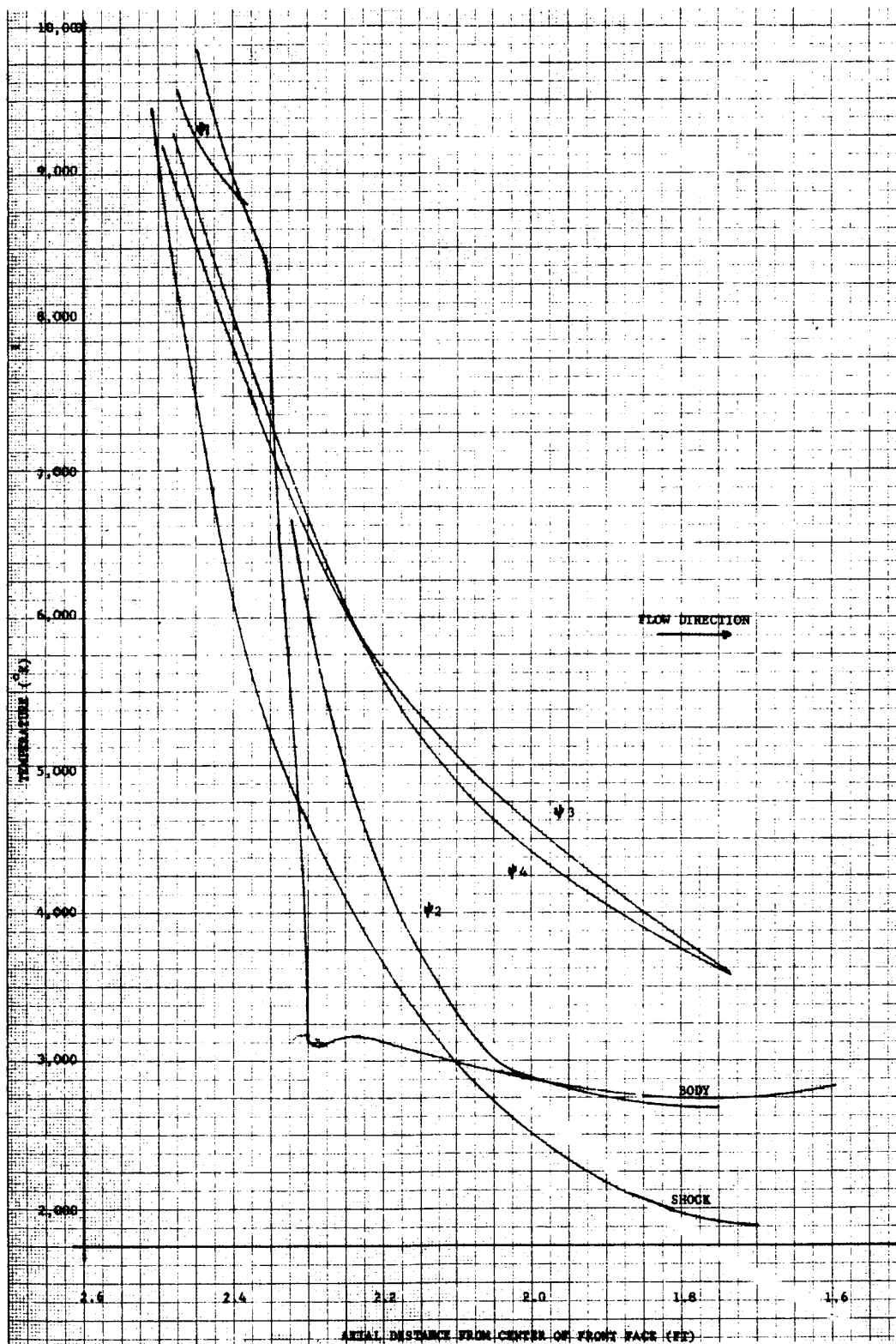
R11102

FIGURE 19. STREAMLINE POSITIONS OVER AFTER-BODY (CASE I)



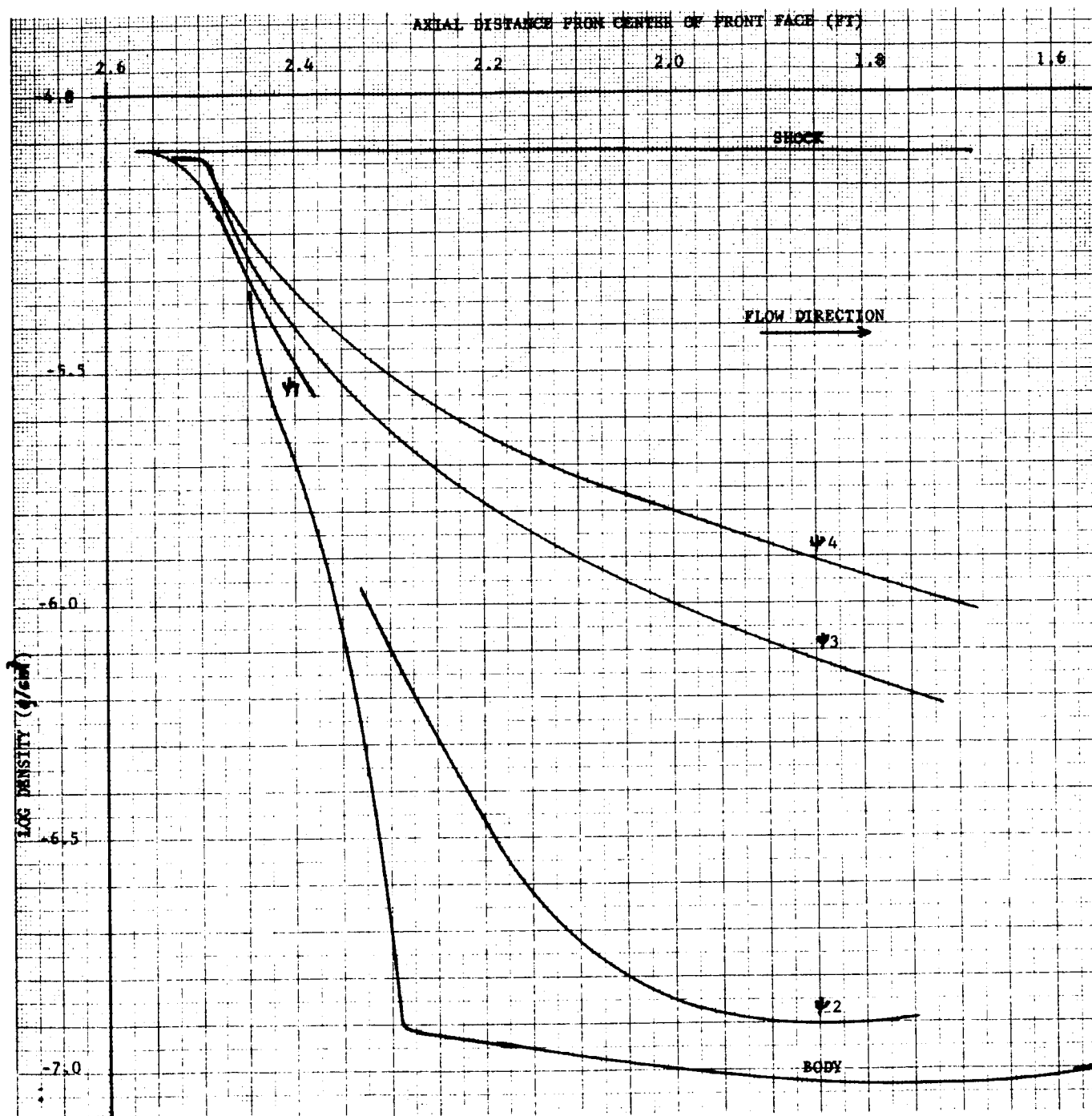
R11103

FIGURE 20. LOG PRESSURE VS. AXIAL DISTANCE IN FLOW OVER THE AFTER-BODY (CASE I)



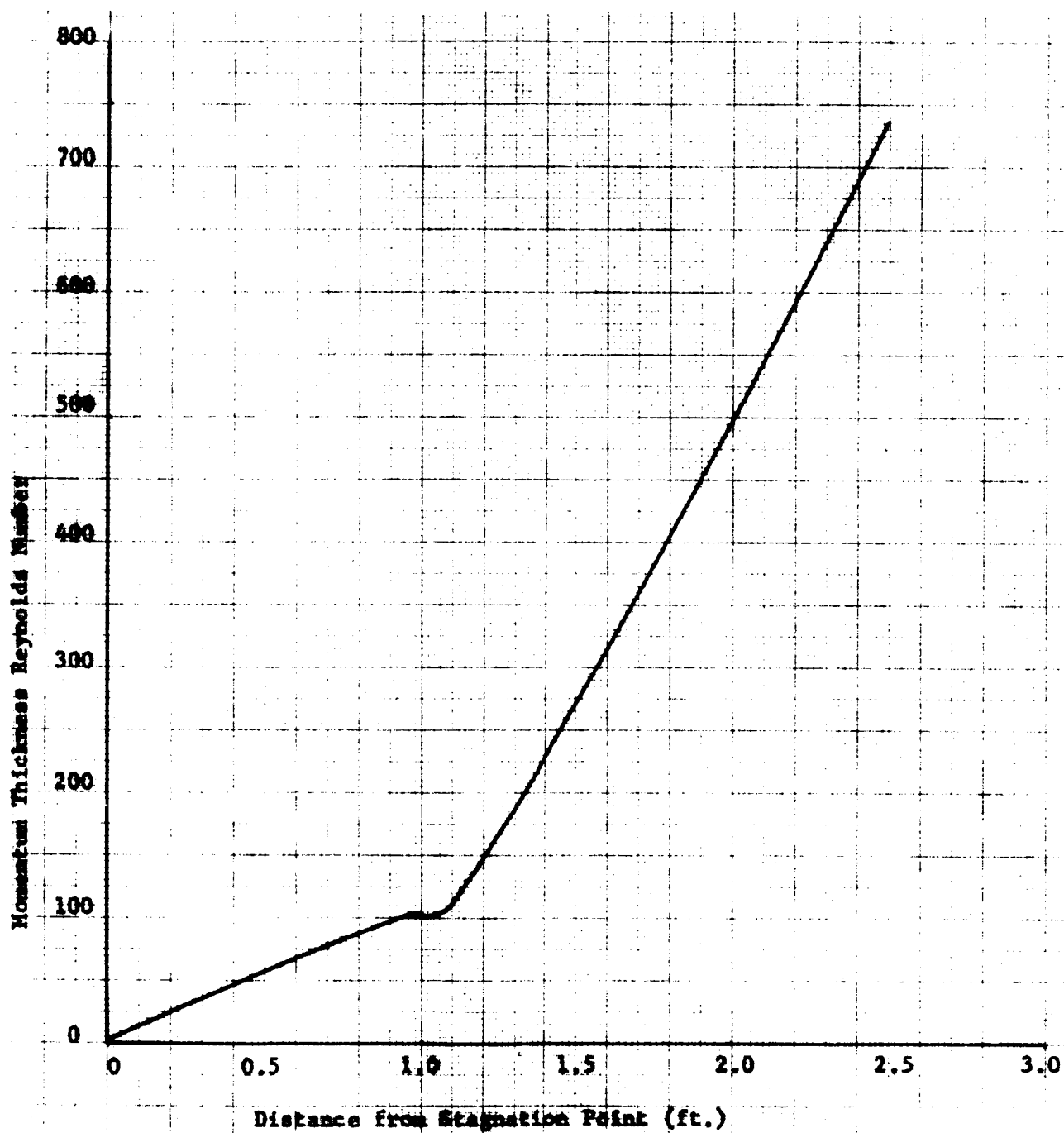
R11104

FIGURE 21. TEMPERATURE VS. AXIAL DISTANCE IN FLOW OVER THE AFTER-BODY (CASE I)



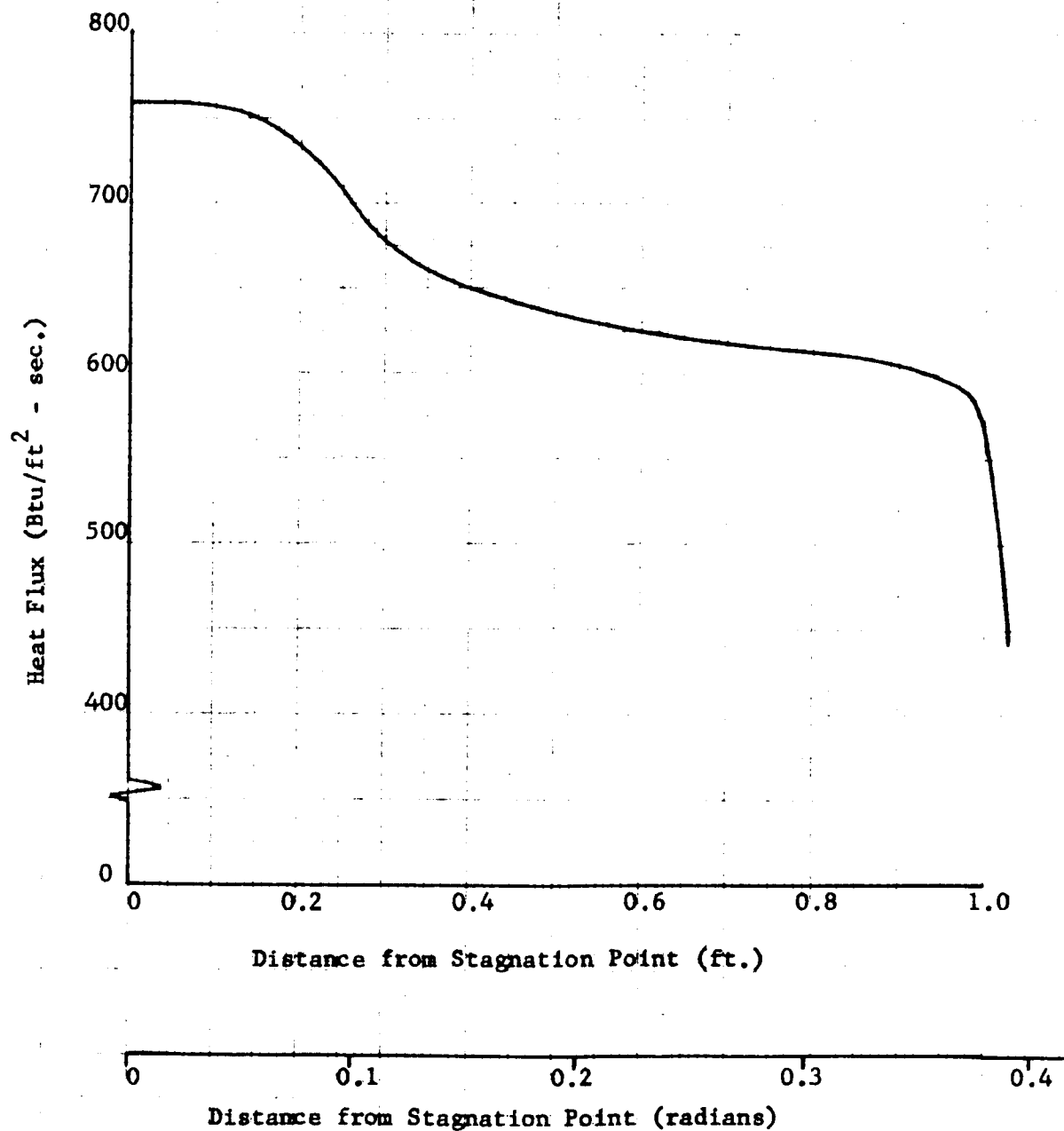
R11105

FIGURE 22. DENSITY VS. AXIAL DISTANCE IN FLOW OVER AFTER-BODY (CASE I)



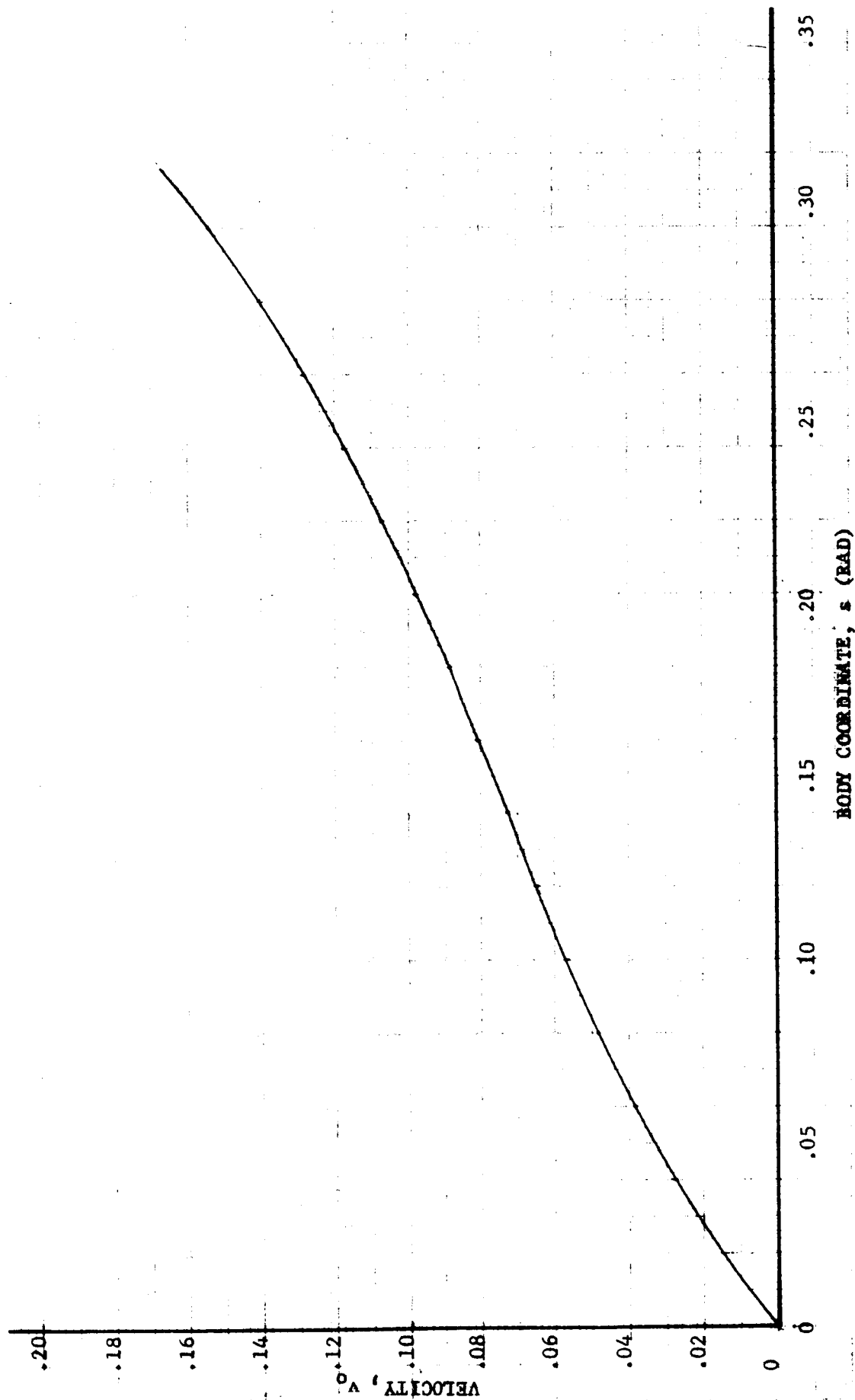
R11106

FIGURE 23. REYNOLDS NUMBER DISTRIBUTION, PROJECT FIRE, (CASE 1)



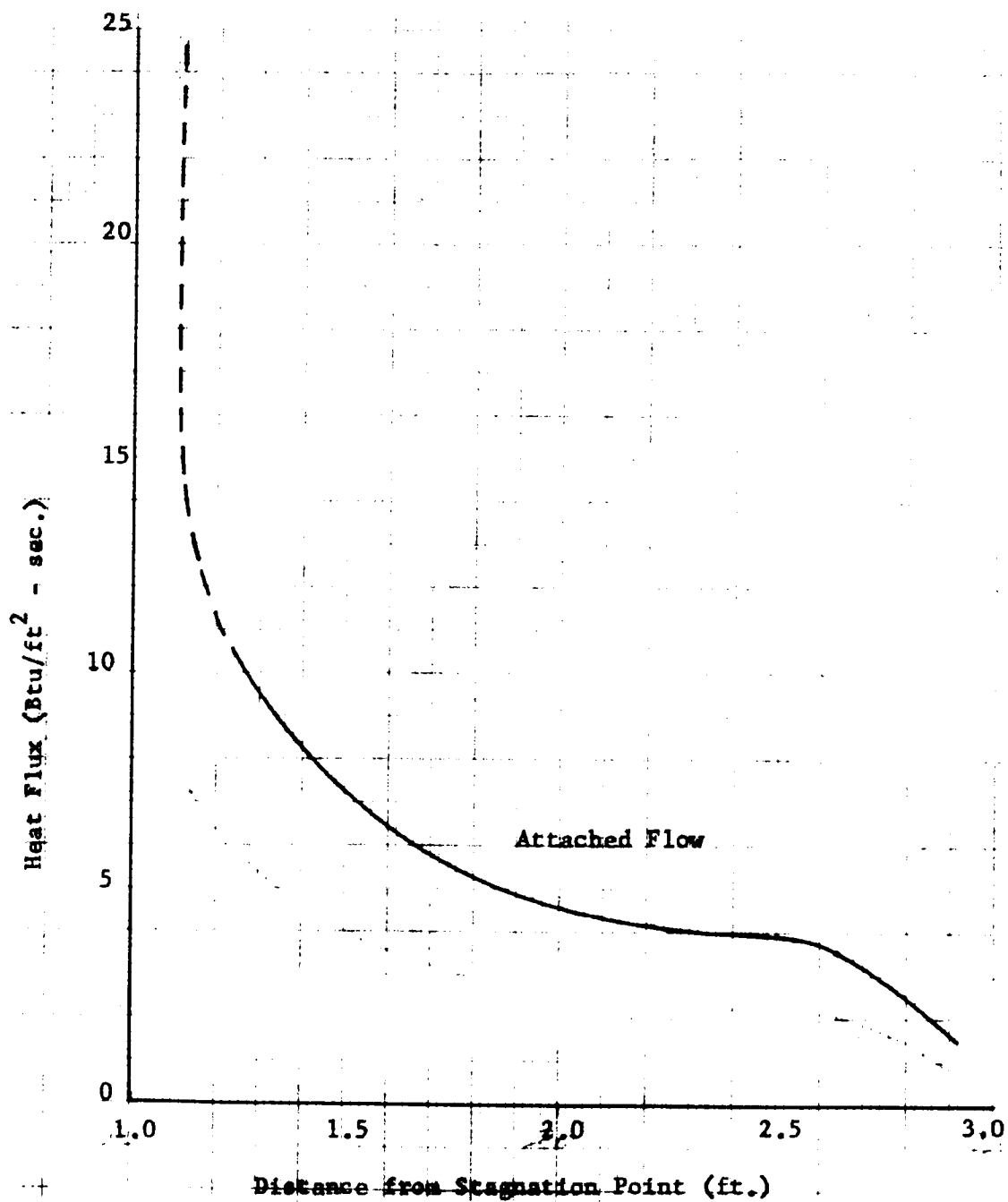
R11107

FIGURE 24. CONVECTIVE HEAT FLUX DISTRIBUTION ON BLUNT FACE, PROJECT FIRE, (CASE I)



R11108

FIGURE 24a. VELOCITY DISTRIBUTION ALONG THE BODY SURFACE (CASE I)



R11109

FIGURE 25. CONVECTIVE HEAT FLUX DISTRIBUTION ON AFTER-BODY (CASE I)

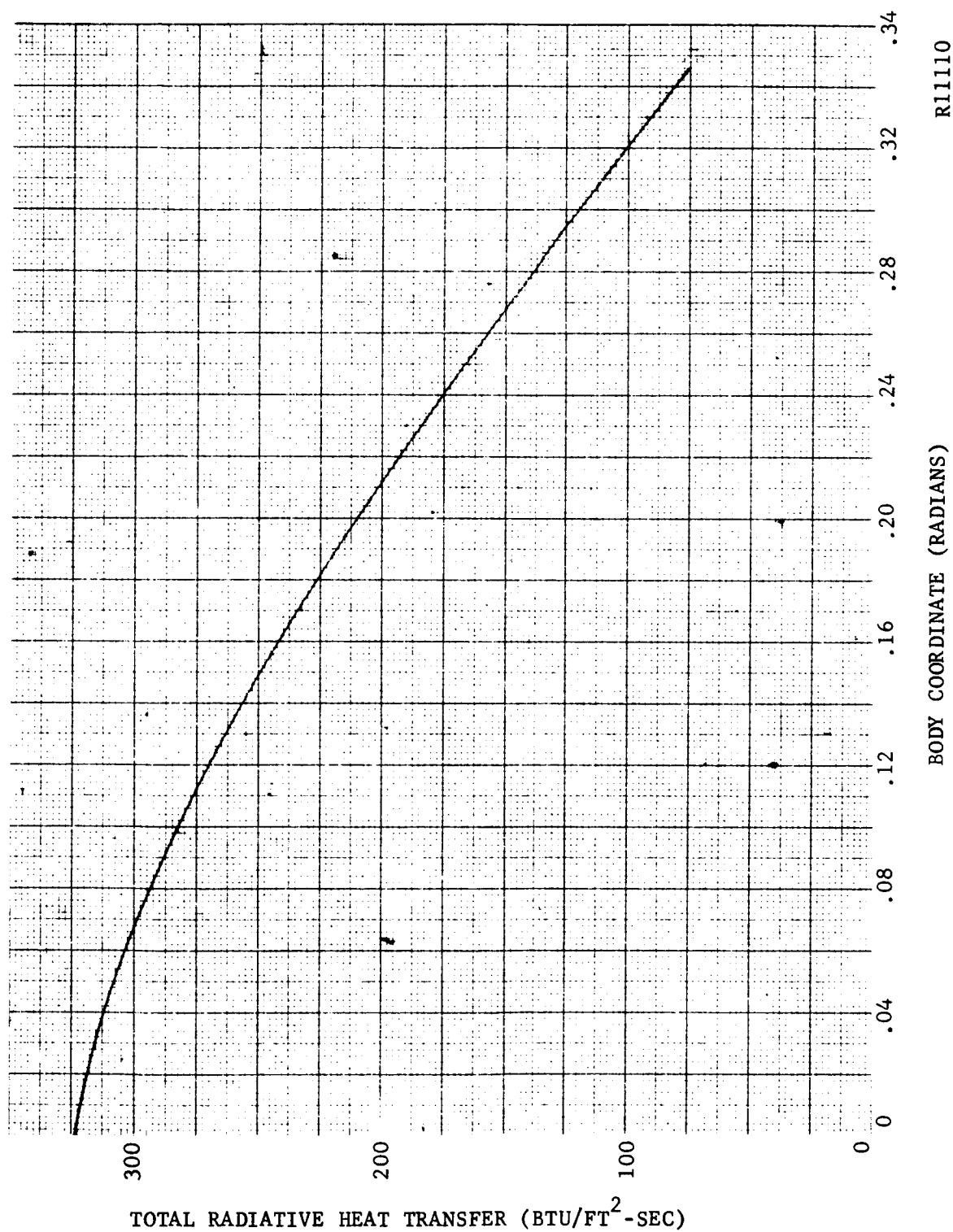


FIGURE 26. DISTRIBUTION OF RADIATIVE FLUX (CASE I)

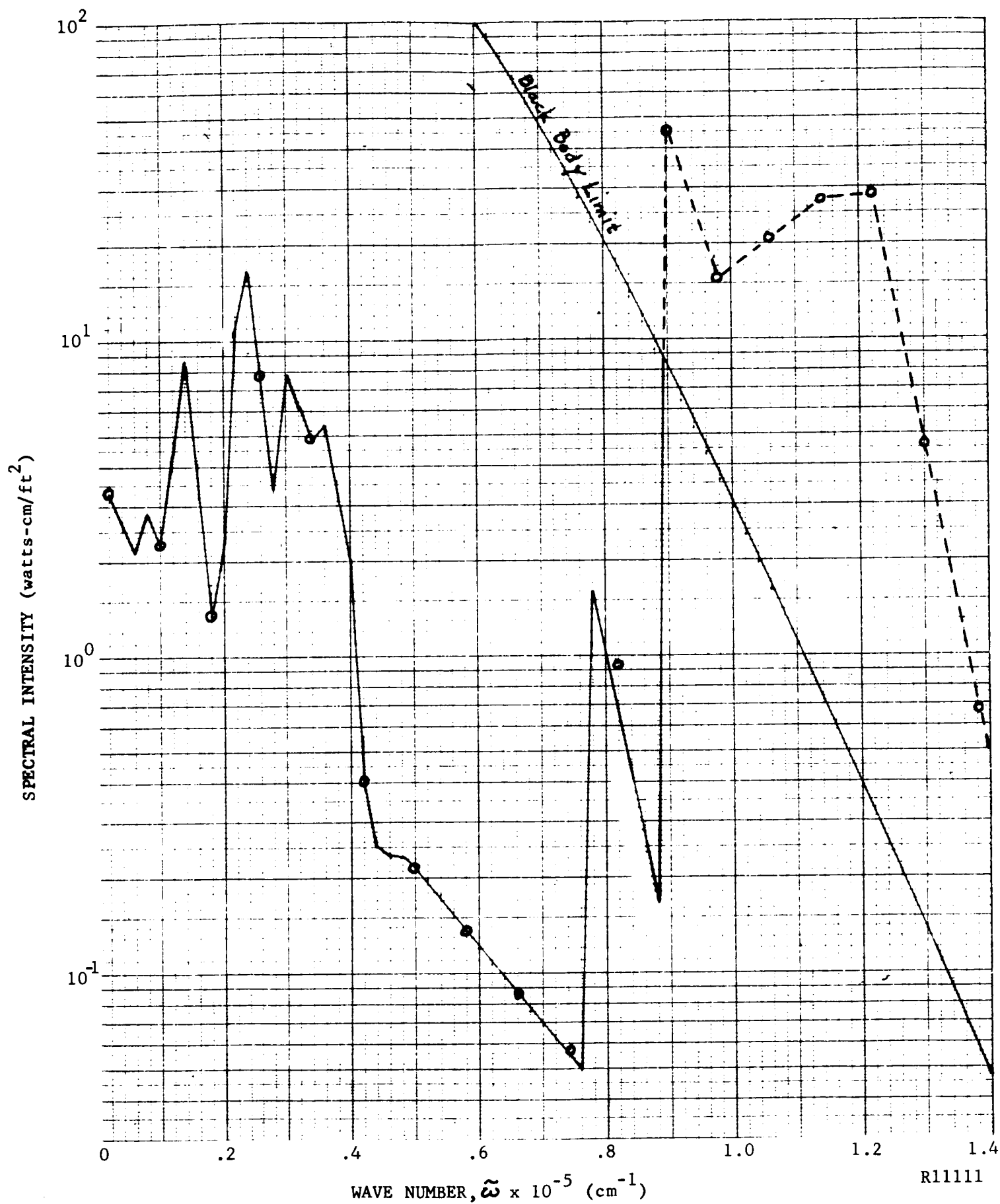
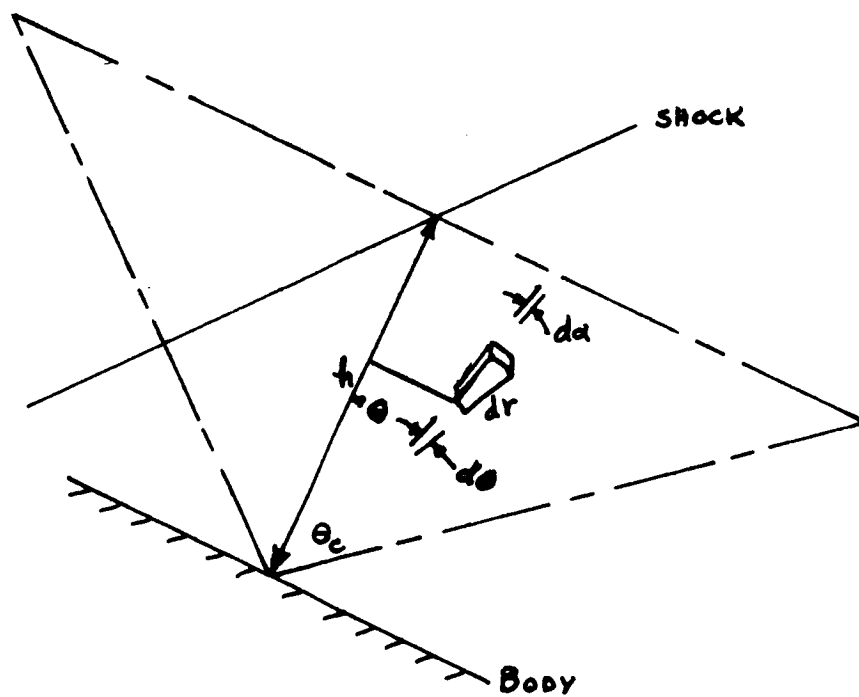
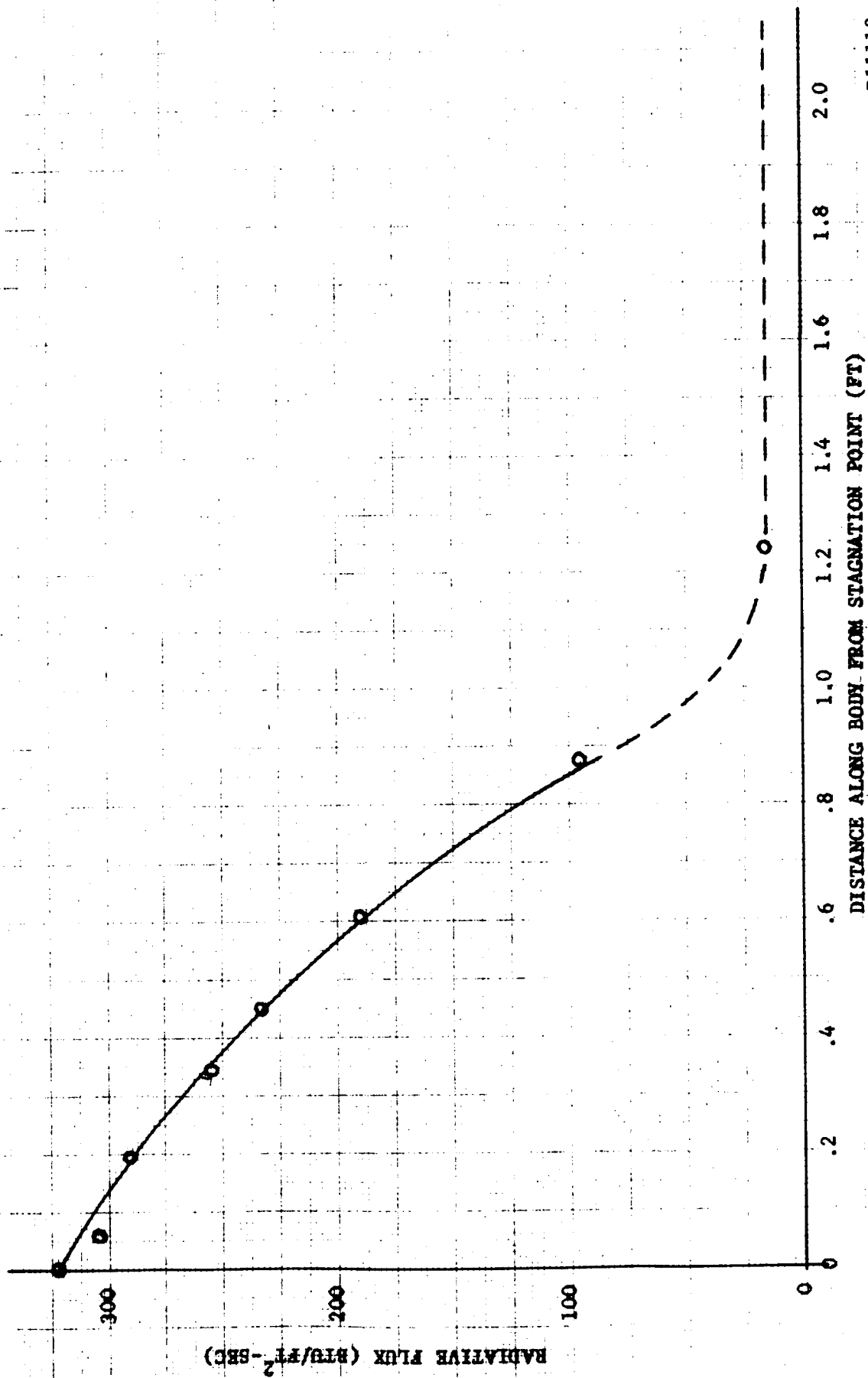


FIGURE 27. SPECTRAL INTENSITY OF RADIATION TO STAGNATION POINT (CASE I)



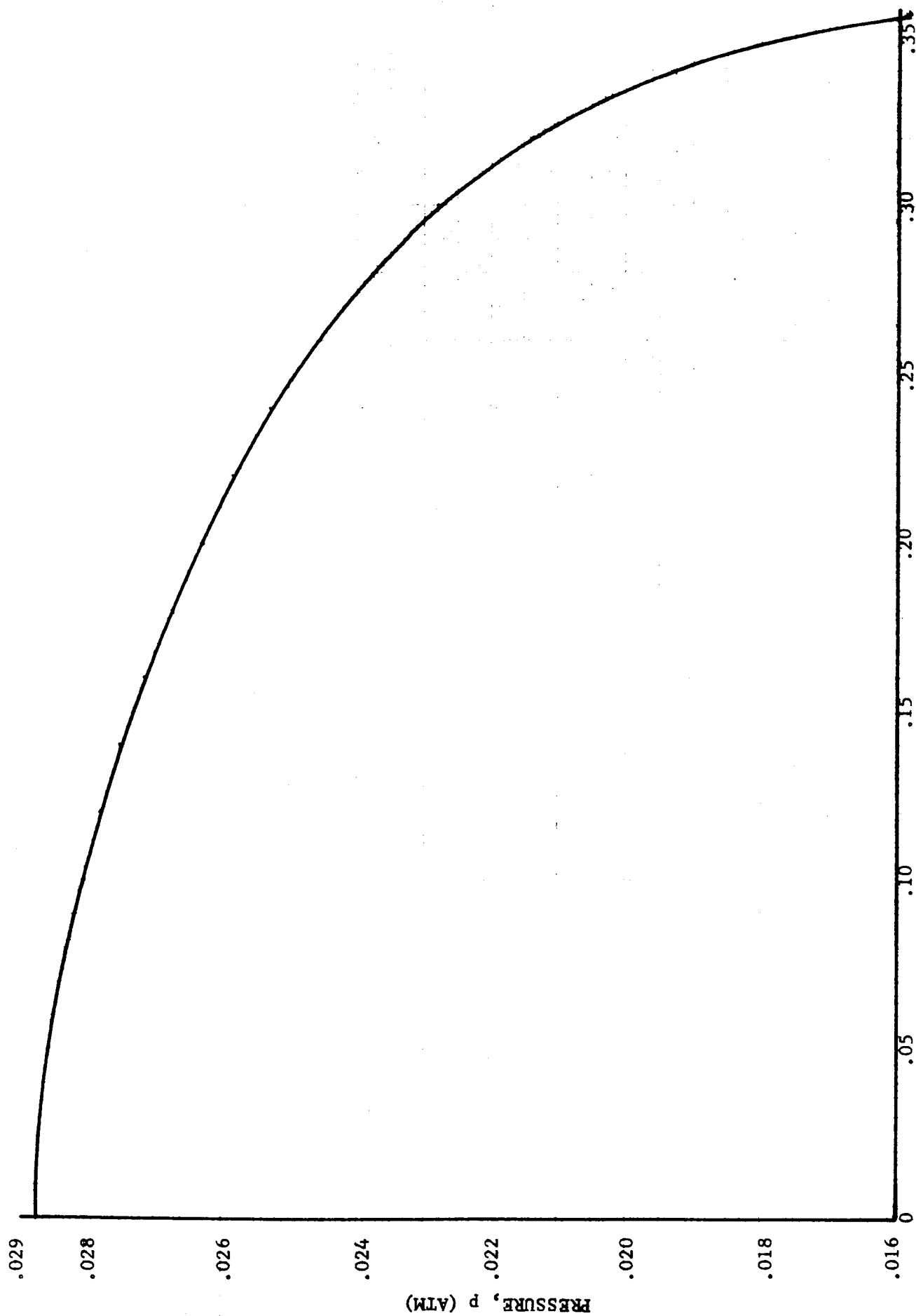
R11112

FIGURE 28. COORDINATE SYSTEM FOR COMPUTATION OF RADIATION TO BACK WALL OF VEHICLE



R11113

FIGURE 29. RADIATION TO RE-ENTRY BODY INCLUDING AFTER-BODY (CASE I)



BODY COORDINATE, θ (RAD)

FIGURE 30. PRESSURE DISTRIBUTION ALONG THE BODY SURFACE, (CASE III)

R11114

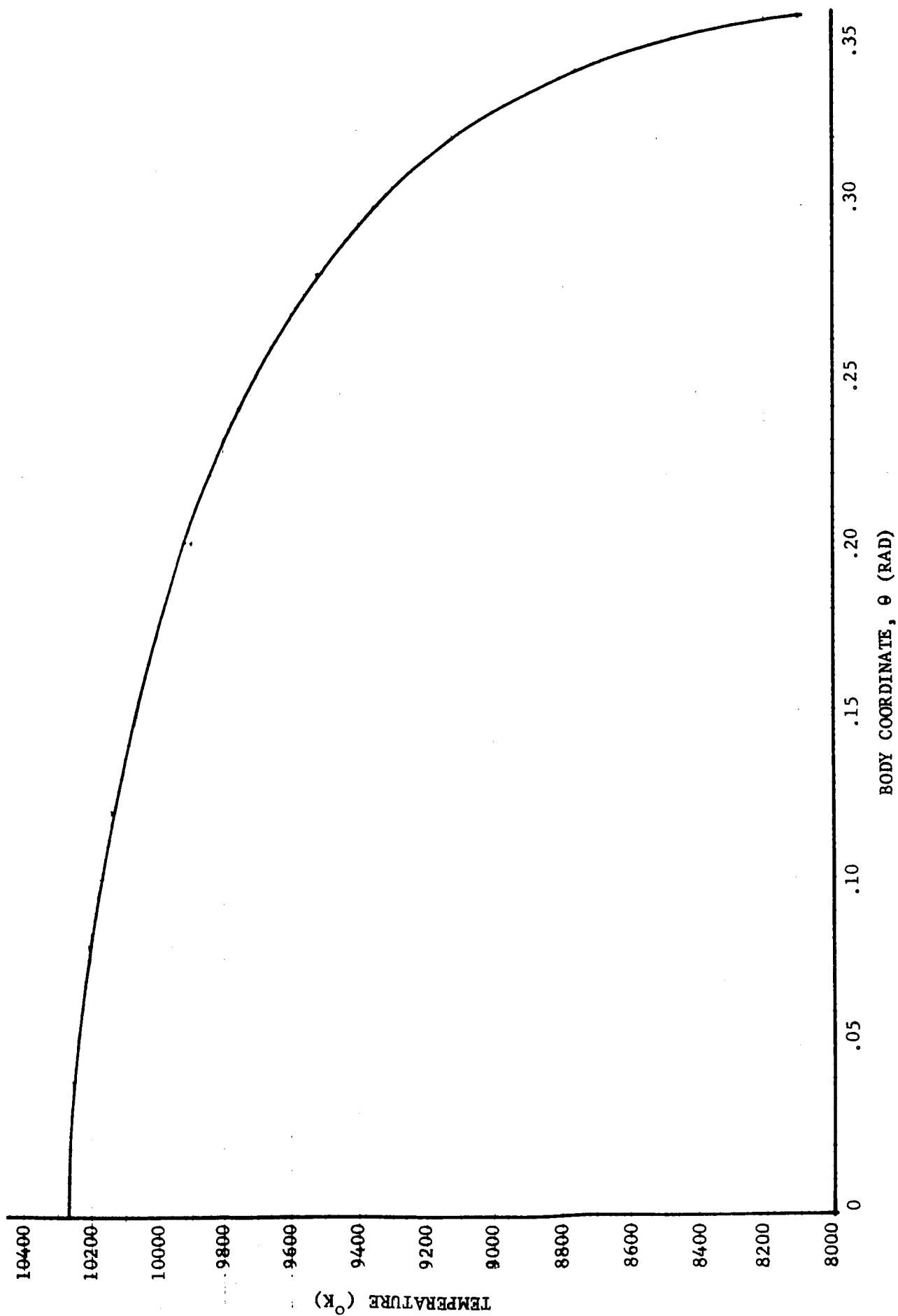
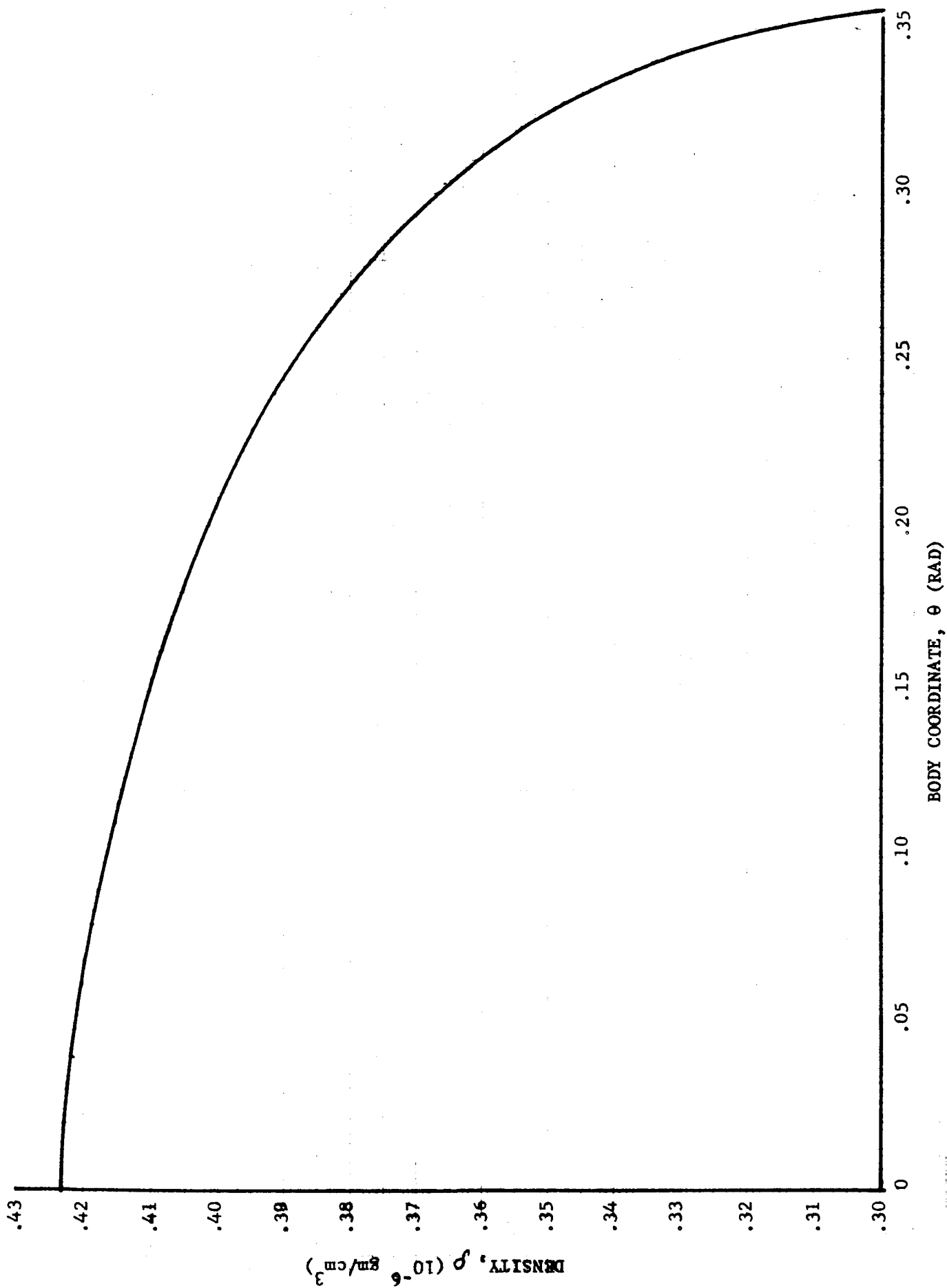


FIGURE 31. TEMPERATURE DISTRIBUTION ALONG THE BODY SURFACE, (CASE III)

R11115



R11116

FIGURE 32. DENSITY DISTRIBUTION ALONG THE BODY SURFACE, (CASE III)

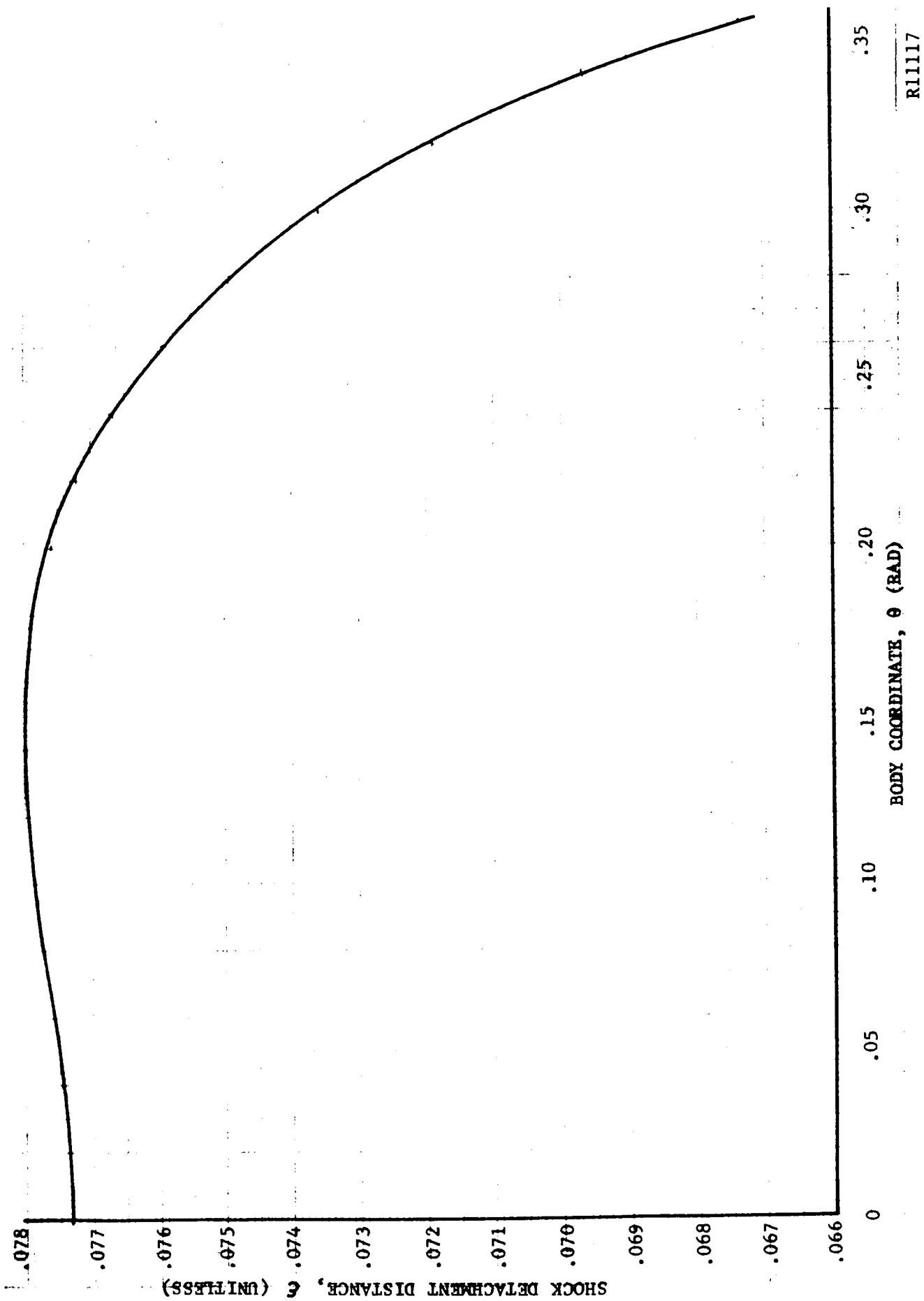
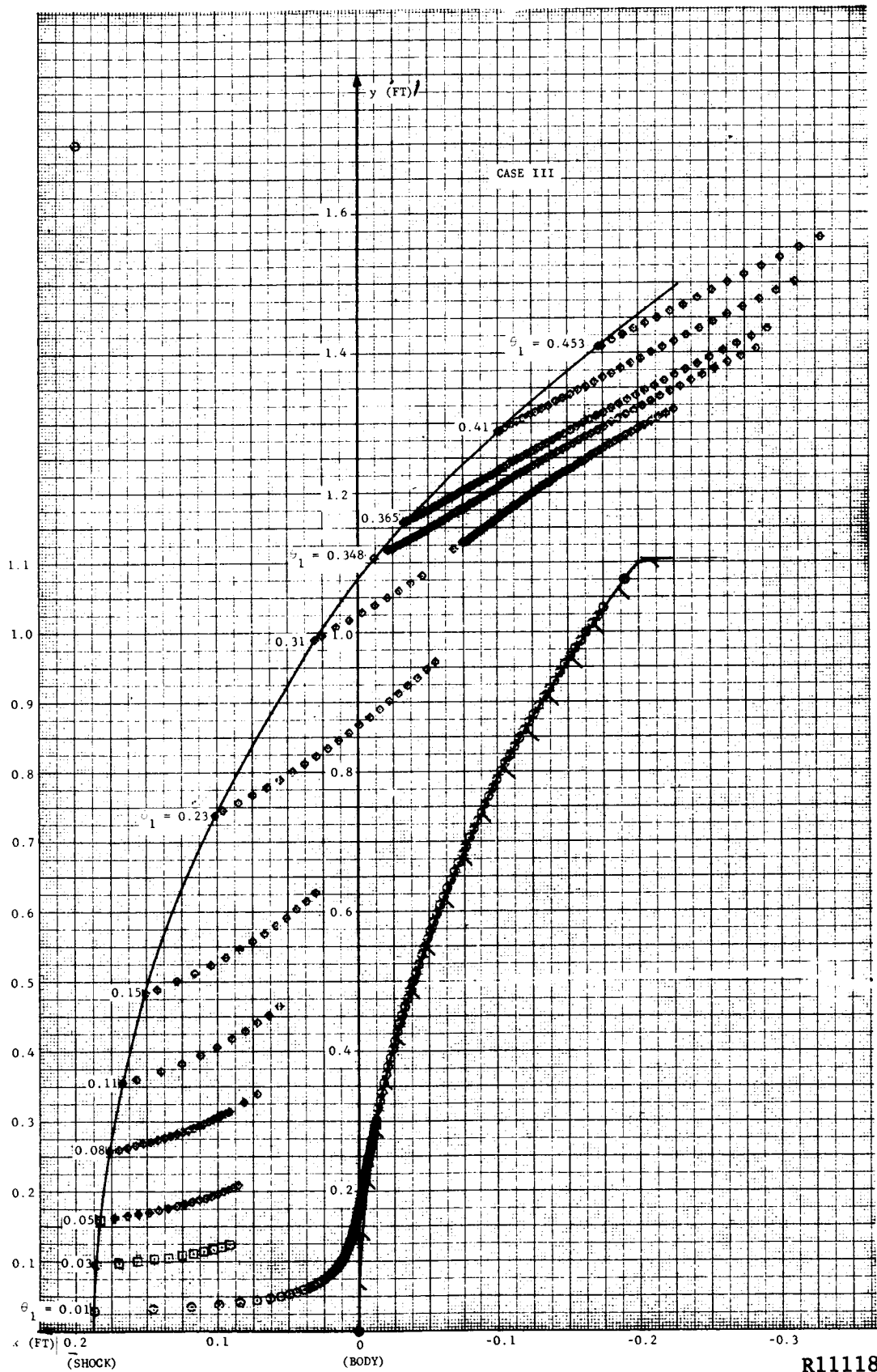


FIGURE 33. SHOCK DETACHMENT DISTANCE, $\epsilon(\bar{x}/\bar{R}_s)$. (CASE III)



R11118

FIGURE 34. STREAMLINE LOCATIONS IN THE SHOCK LAYER, (CASE III)

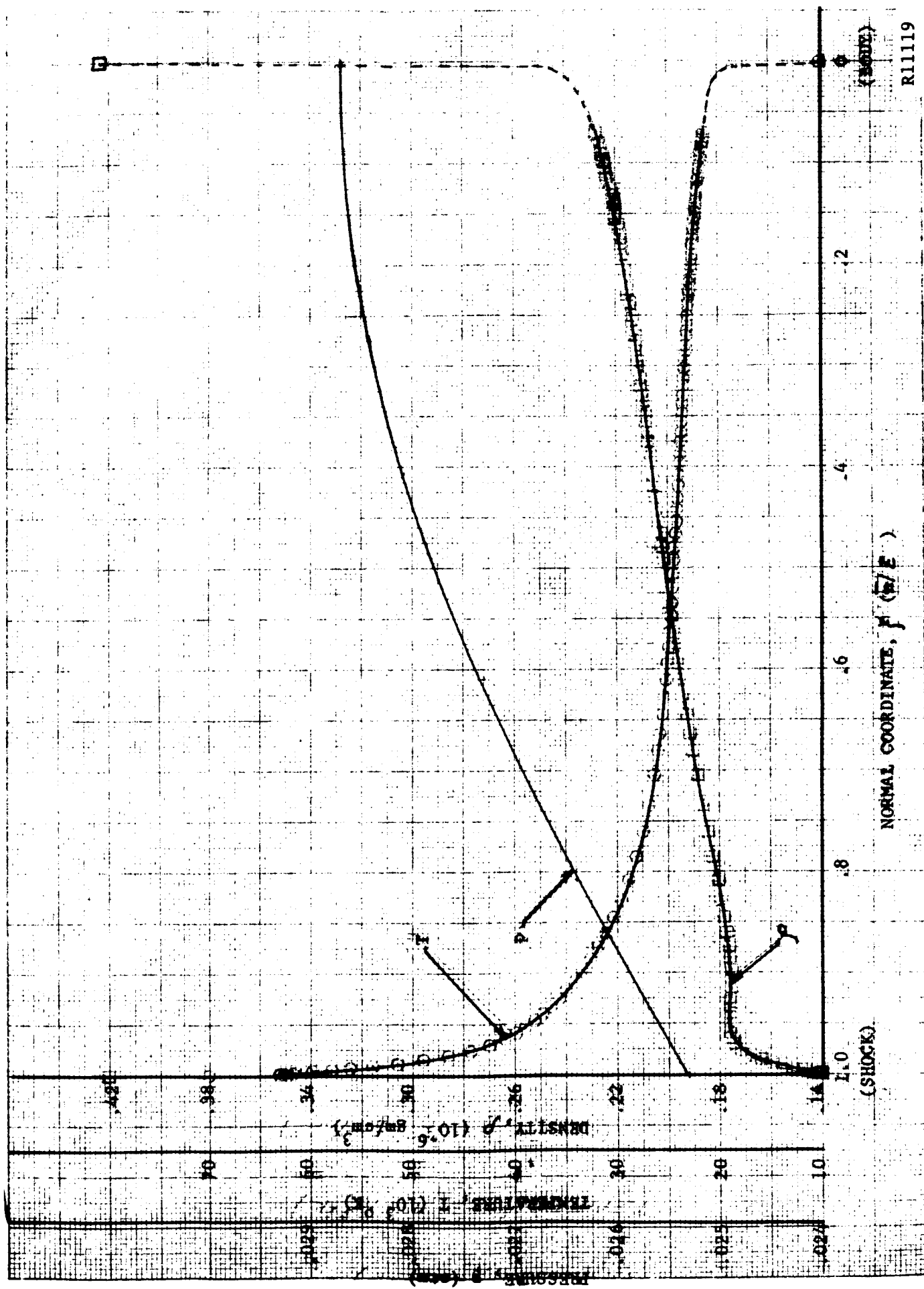
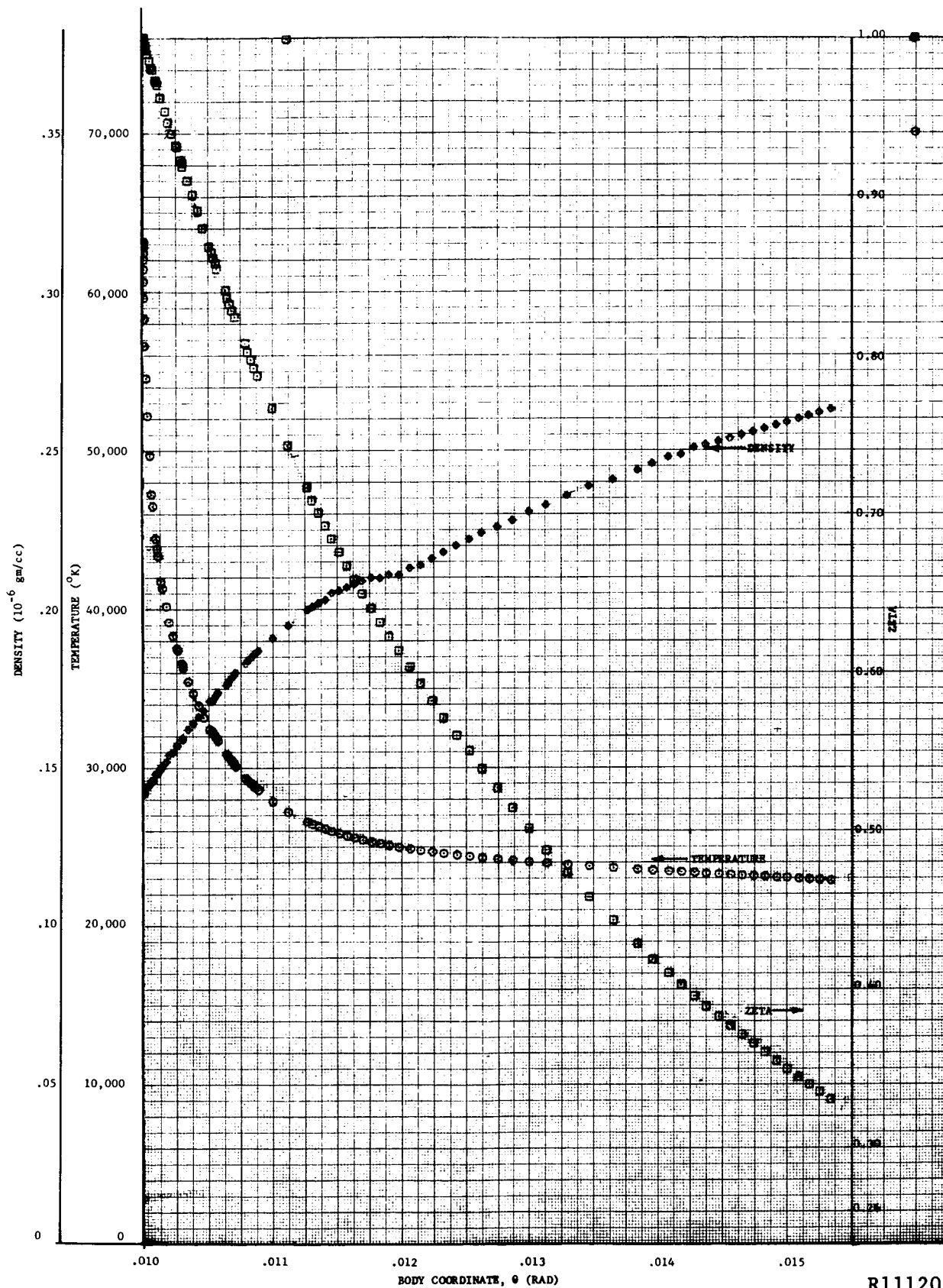


FIGURE 35. STAGNATION STREAMLINE PROPERTY DISTRIBUTION (CASE III)

R11119



R11120

FIGURE 36. TEMPERATURE, DENSITY AND LOCATION DISTRIBUTIONS ALONG THE $\theta_1 = 0.01$ STREAMLINE AS A FUNCTION OF θ , THE BODY COORDINATE (CASE III)

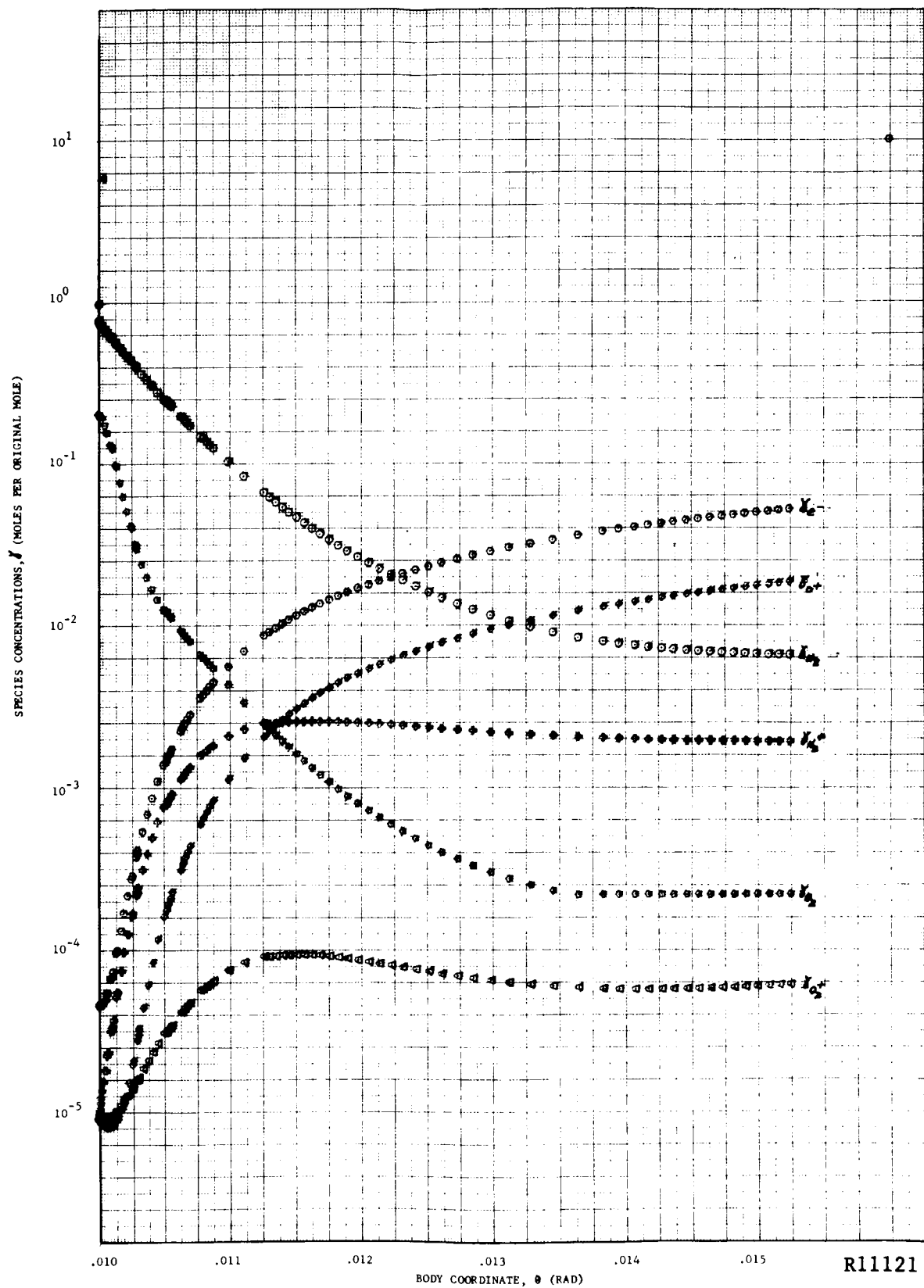


FIGURE 37. γ_{e^-} , γ_{N_2} , $\gamma_{N_2^+}$, γ_{O_2} , $\gamma_{O_2^+}$, γ_{O^+} DISTRIBUTIONS ALONG THE $\theta_1 = .01$ STREAMLINE AS A FUNCTION OF θ , THE BODY COORDINATE (CASE III)

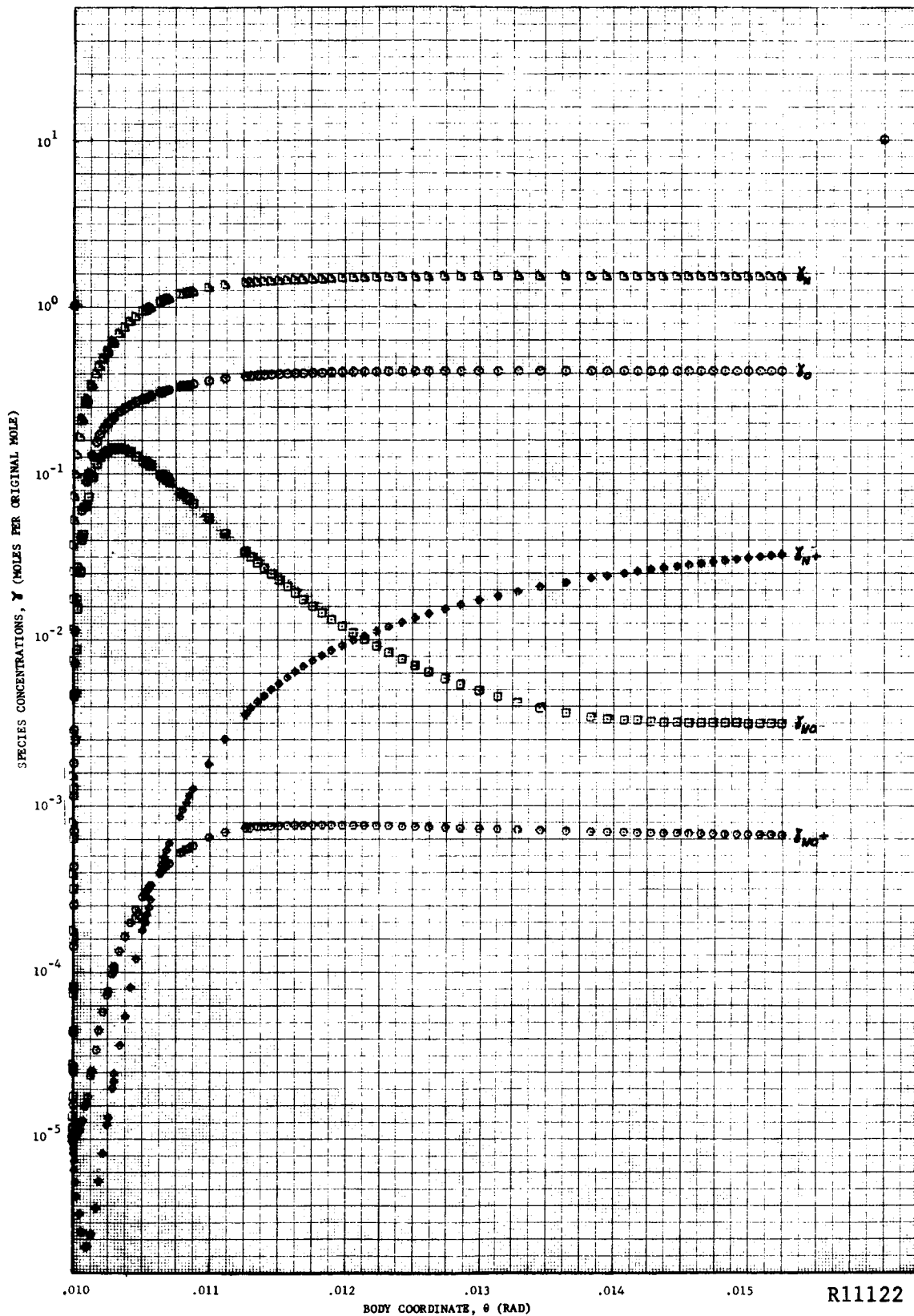


FIGURE 38. Y_N , Y_C , Y_{N^+} , Y_{NO^+} , Y_{NO} DISTRIBUTIONS ALONG THE $\theta_1 = .01$ STREAMLINE AS A FUNCTION OF θ , THE BODY COORDINATE (CASE III)

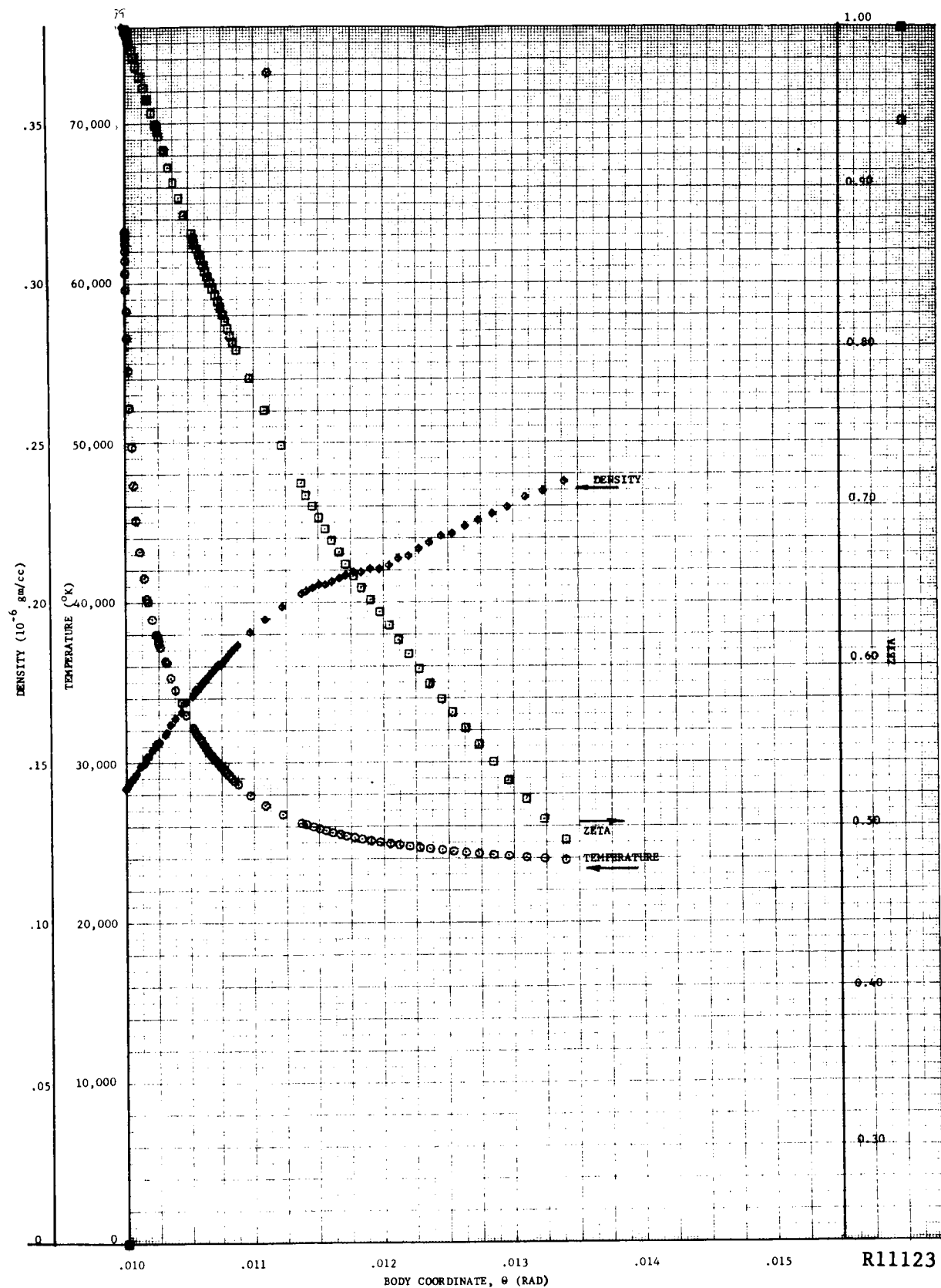


FIGURE 39. TEMPERATURE, DENSITY, AND LOCATION DISTRIBUTIONS ALONG THE $\theta_1 = 0.01$ STREAMLINE AS A FUNCTION OF θ , THE BODY COORDINATE (CORRECTED RATES) (CASE III)

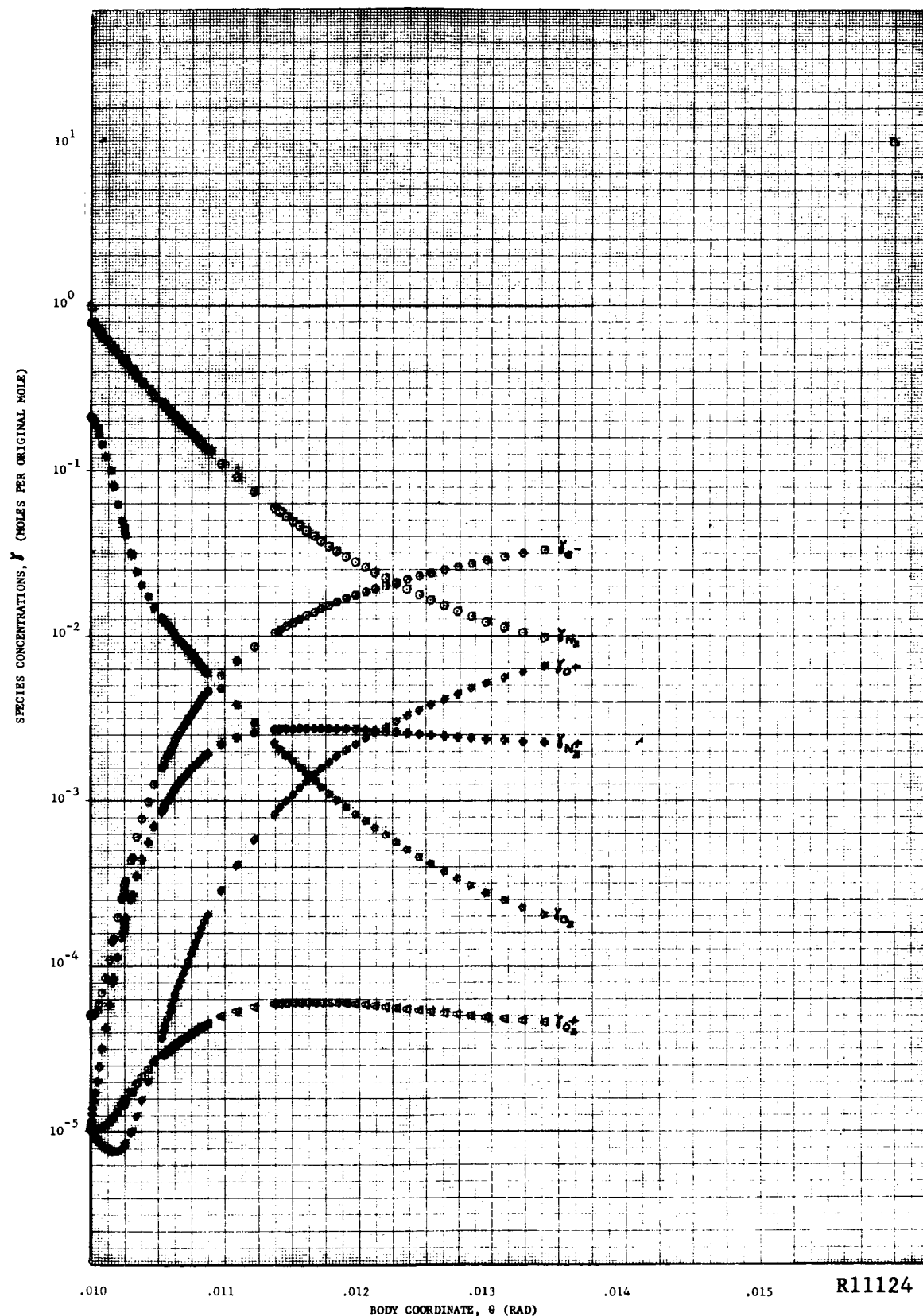


FIGURE 40. γ_{e^-} , γ_{N_2} , γ_{O^+} , $\gamma_{N_2^+}$, γ_{O_2} , γ_{O^+} DISTRIBUTIONS ALONG THE $\theta_1 = .01$ STREAMLINE AS A FUNCTION OF θ , THE BODY COORDINATE (CORRECTED RATES) (CASE III)

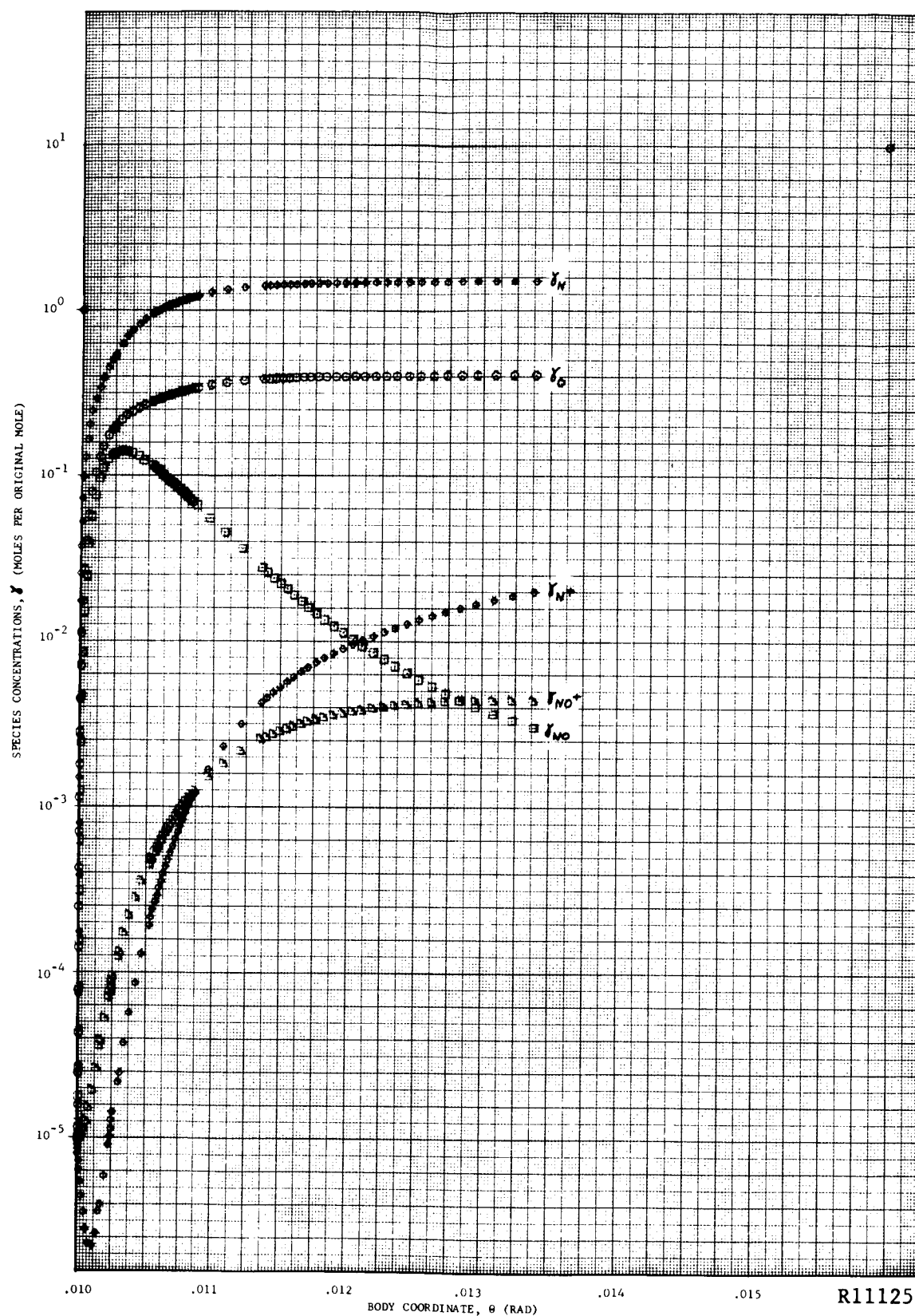


FIGURE 41. γ_N , γ_O , γ_{N^+} , γ_{NO^+} , γ_{NO} DISTRIBUTIONS ALONG THE $\theta_1 = .01$ STREAMLINE AS A FUNCTION OF θ , THE BODY COORDINATE (CORRECTED RATES) (CASE III)

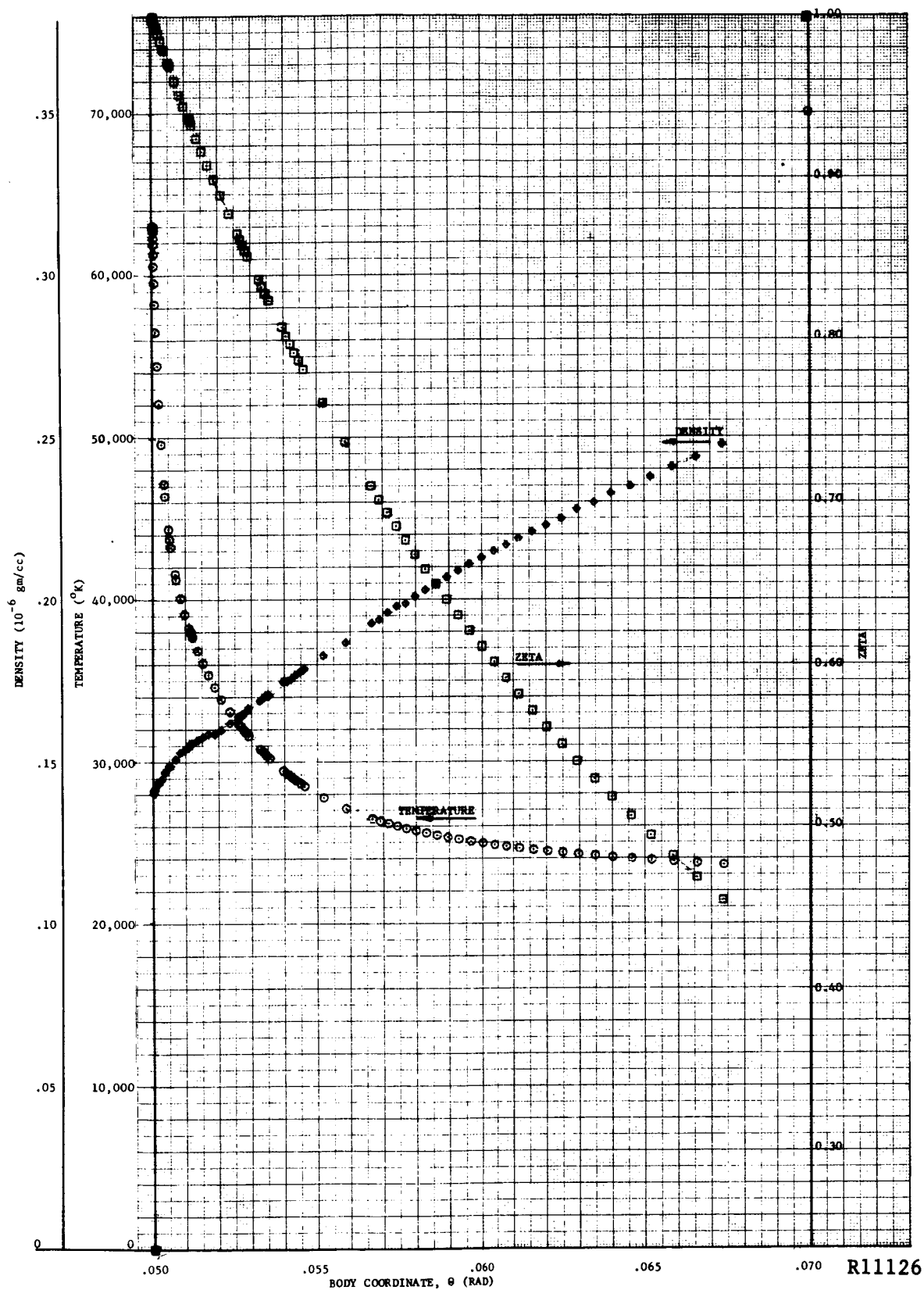


FIGURE 42. TEMPERATURE, DENSITY, AND LOCATION DISTRIBUTIONS ALONG THE $\theta_1 = .05$ STREAMLINE AS A FUNCTION OF θ , THE BODY COORDINATE (CASE III)

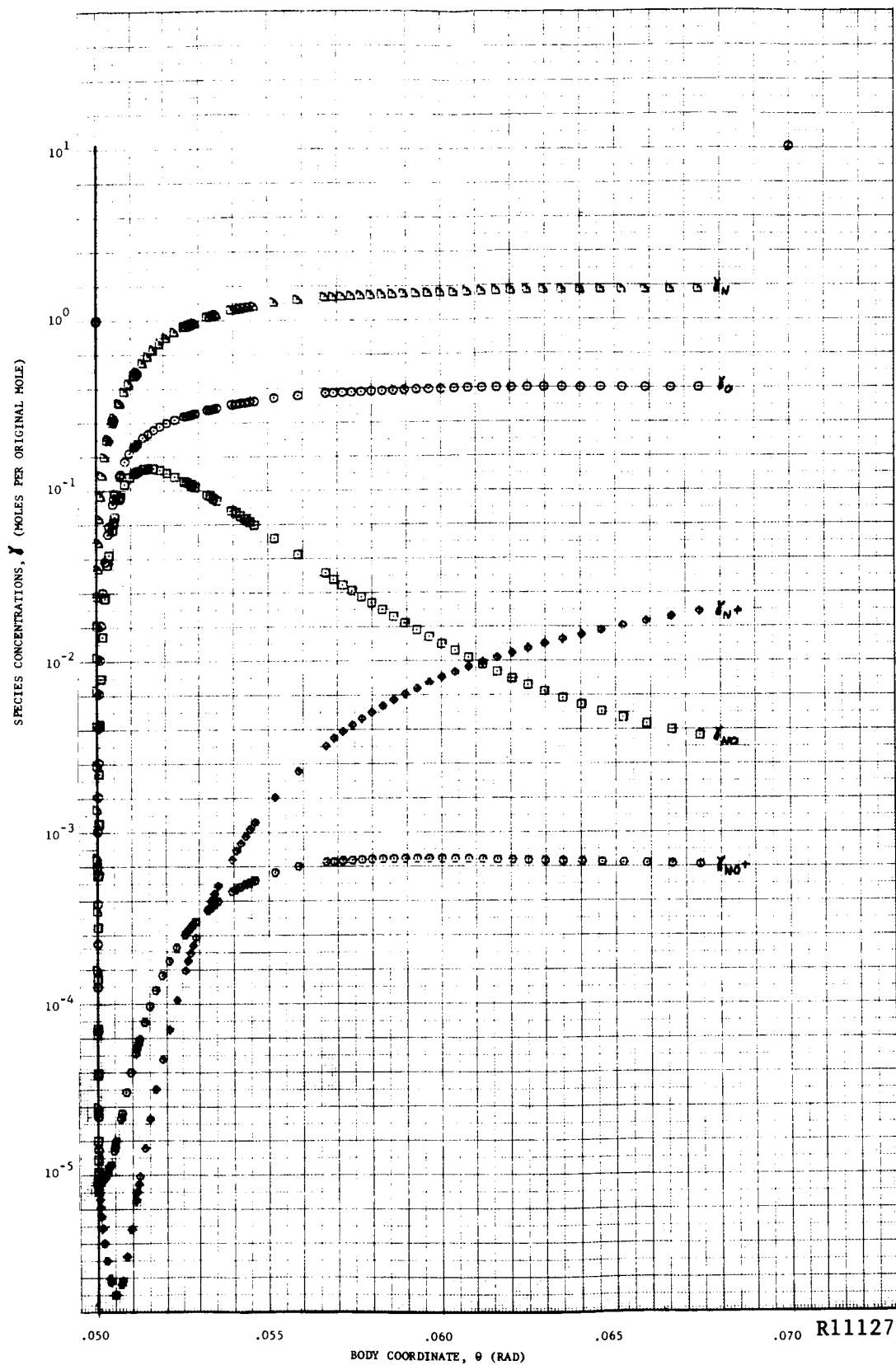


FIGURE 43. Y_N , Y_O , Y_{N^+} , Y_{NO} , Y_{NO^+} DISTRIBUTIONS ALONG THE $\theta_1 = .05$ STREAMLINE AS A FUNCTION OF θ , THE BODY COORDINATE (CASE III)

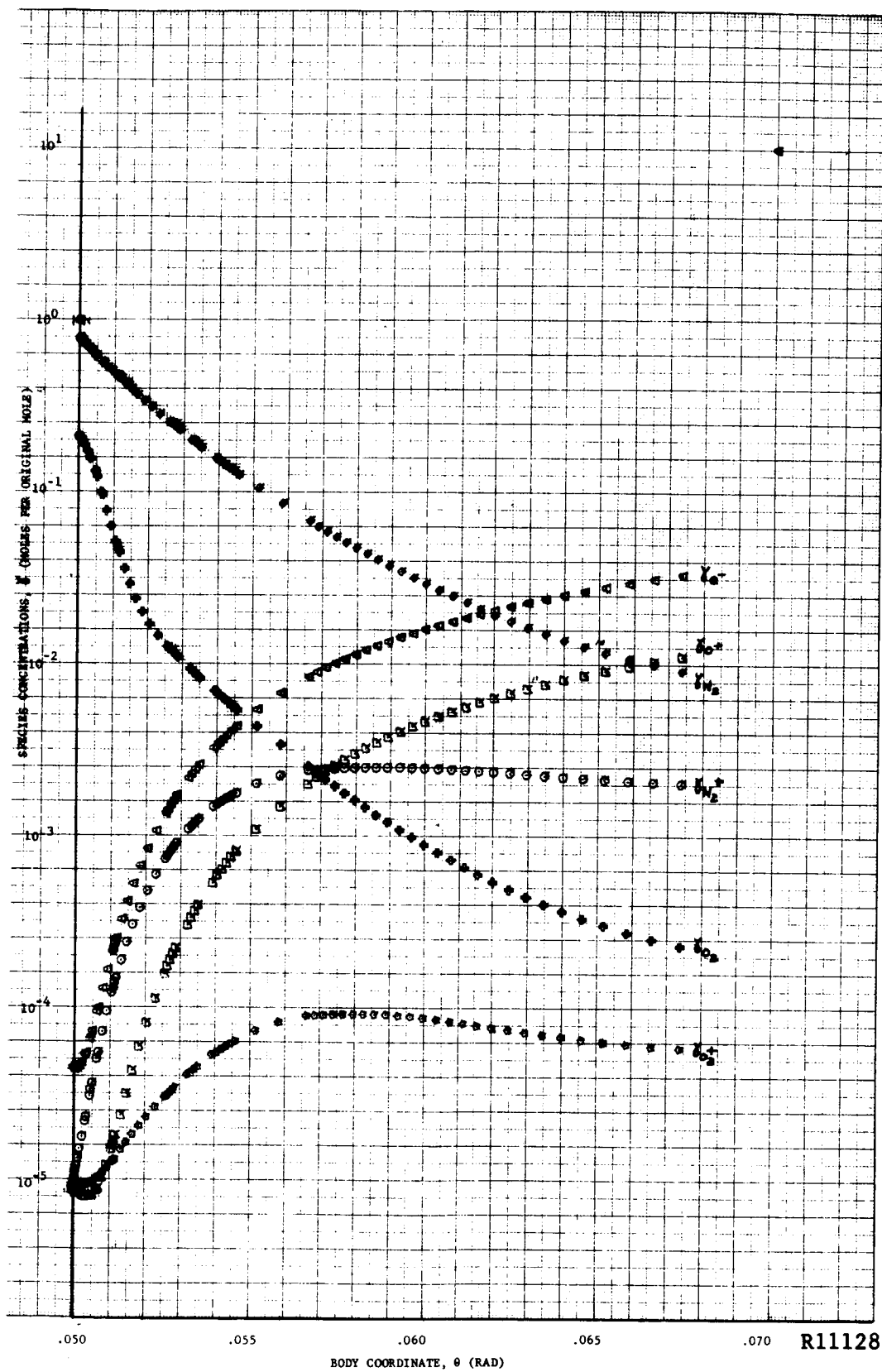


FIGURE 44. e^- , N_2 , N_2^+ , O_2 , O_2^+ , O^+ DISTRIBUTIONS ALONG THE $\theta_1 = .05$ STREAMLINE AS A FUNCTION OF θ , THE BODY COORDINATE (CASE III)

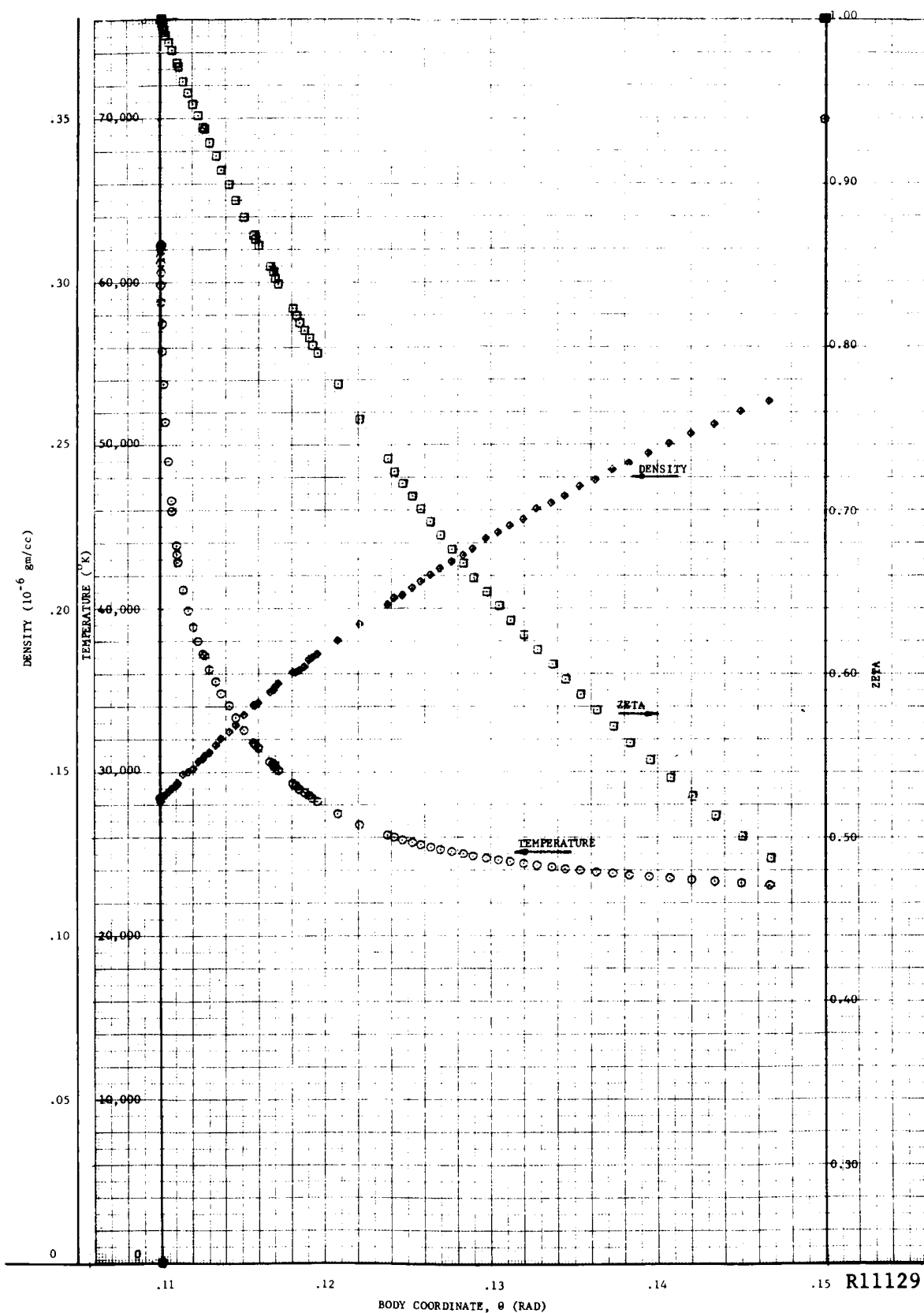
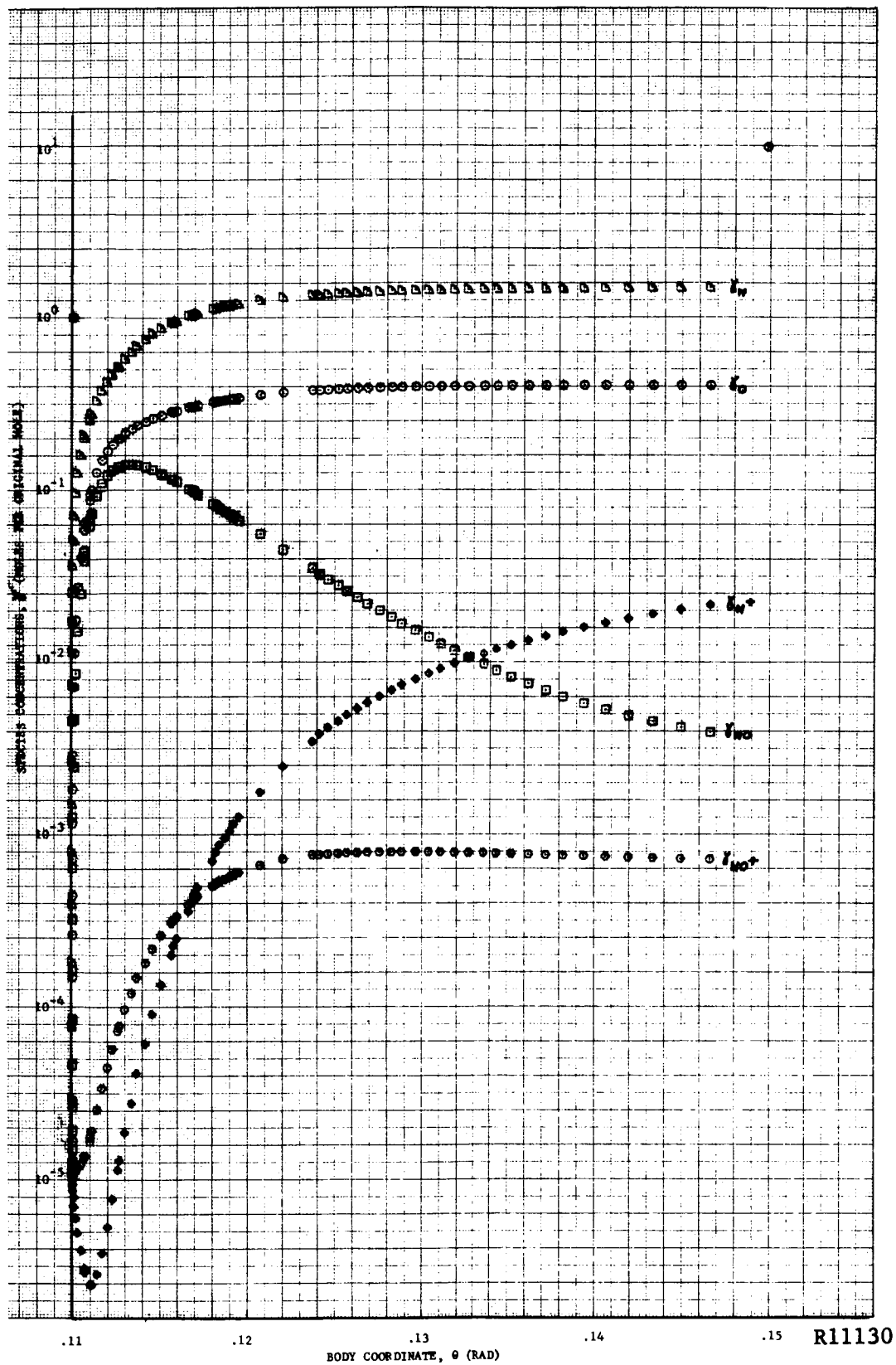


FIGURE 45. TEMPERATURE, DENSITY AND LOCATION DISTRIBUTIONS ALONG THE $\theta_1 = .11$ STREAMLINE AS A FUNCTION OF θ , THE BODY COORDINATE (CASE III)



R11130

FIGURE 46. $Y_N, Y_O, Y_+, Y_{NO}, Y_{NO+}$ DISTRIBUTIONS ALONG THE $\theta_1 = .11$ STREAMLINE AS A FUNCTION OF θ , THE BODY COORDINATE (CASE III)

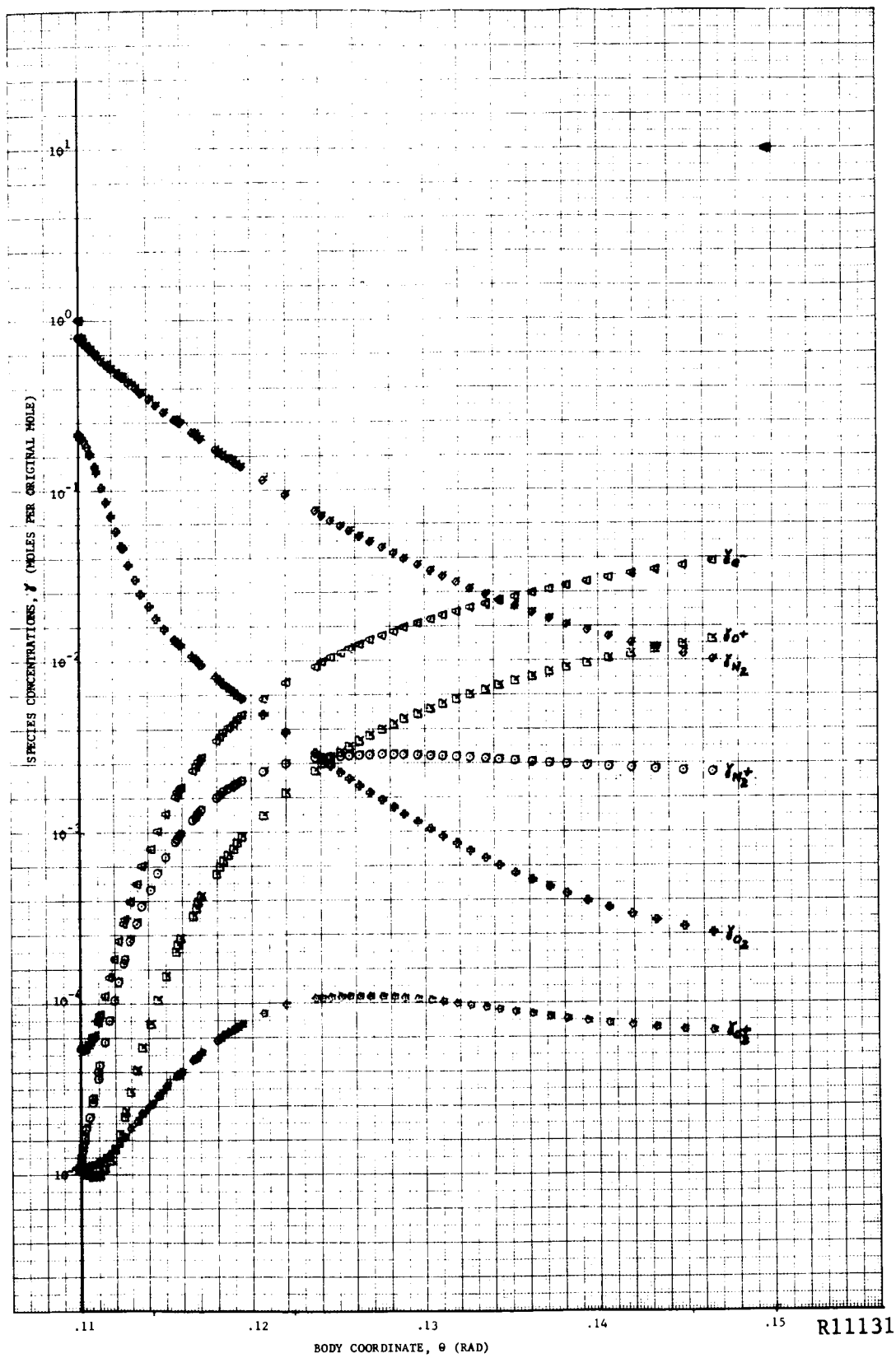


FIGURE 47. γ_{e^-} , γ_{N_2} , $\gamma_{N_2^+}$, γ_{O_2} , $\gamma_{O_2^+}$, γ_{O^+} DISTRIBUTIONS ALONG THE $\theta_1 = .11$ STREAMLINE AS A FUNCTION OF θ , THE BODY COORDINATE (CASE III)

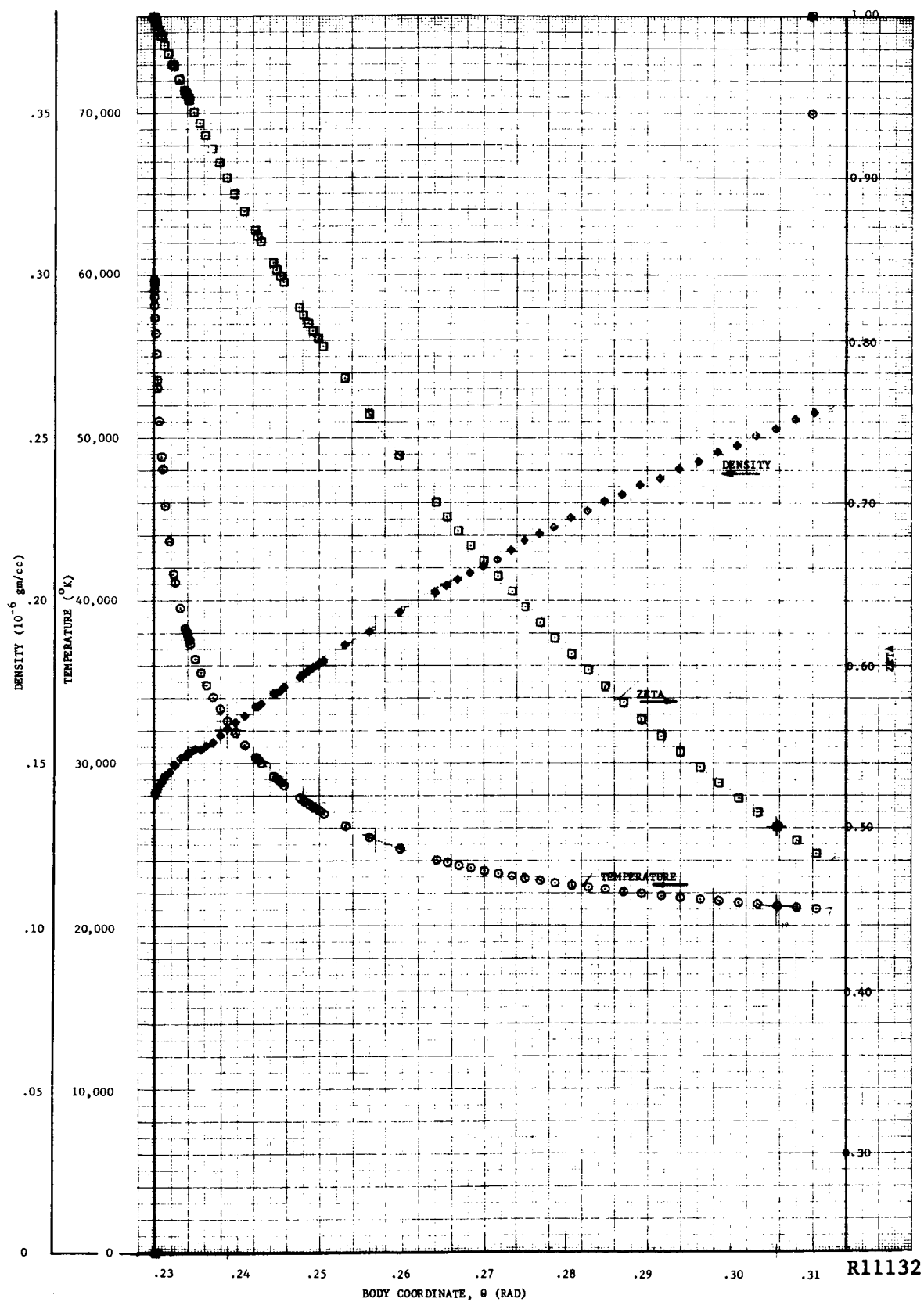


FIGURE 48. TEMPERATURE, DENSITY, AND LOCATION DISTRIBUTIONS ALONG THE $\theta = .23$ STREAMLINE AS A FUNCTION OF θ , THE BODY COORDINATE (CASE III)

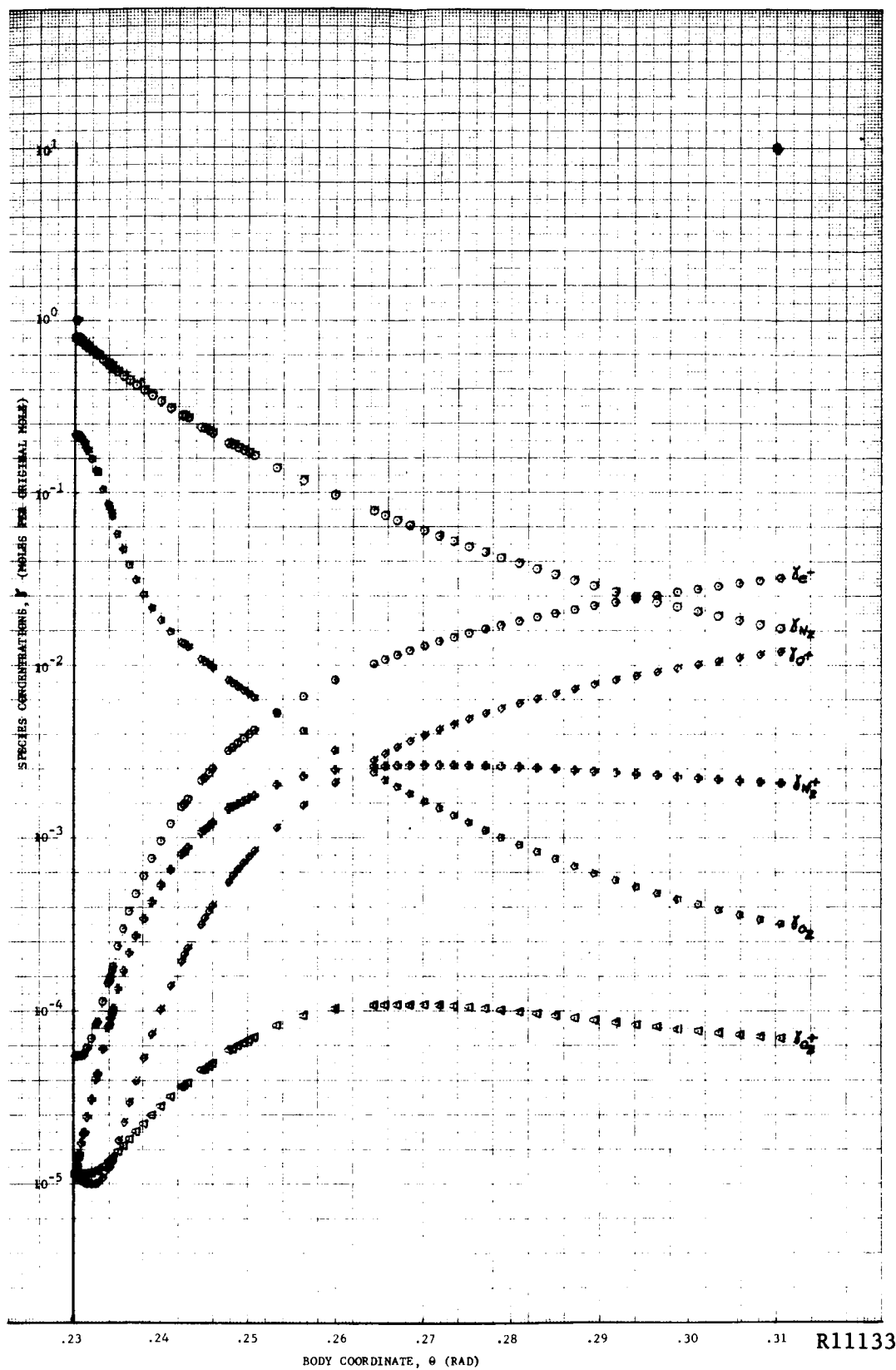


FIGURE 49. e^- , N_2 , N_2^+ , O_2 , O_2^+ , O^+ DISTRIBUTIONS ALONG THE $\theta_1 = .23$ STREAMLINE AS A FUNCTION OF θ , THE BODY COORDINATE (CASE III)

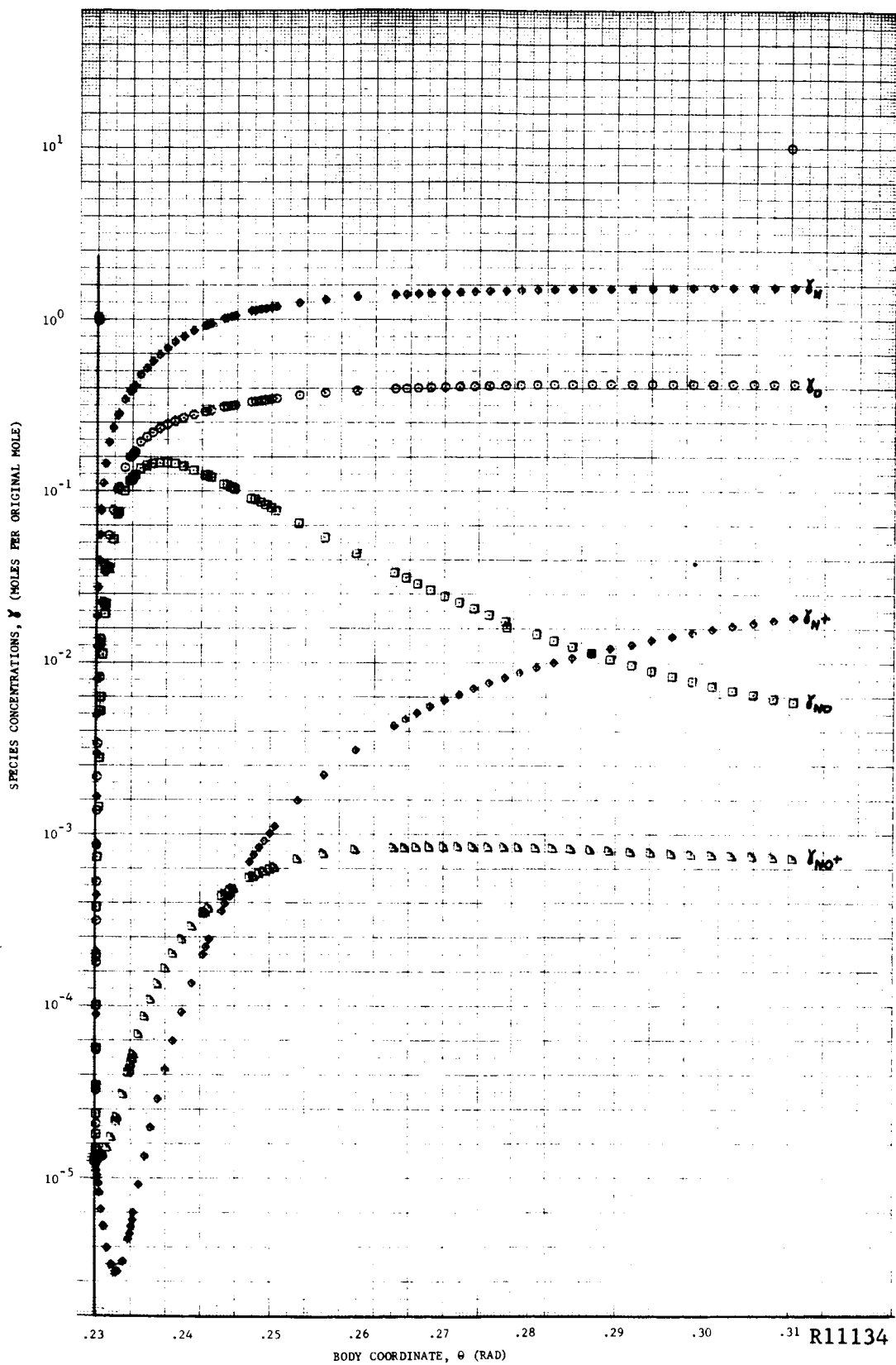


FIGURE 50. Y_N , Y_O , Y_{N^+} , Y_{NO} , Y_{NO^+} DISTRIBUTIONS ALONG THE $\theta_1 = .23$ STREAMLINE AS A FUNCTION OF θ , THE BODY COORDINATE (CASE III)

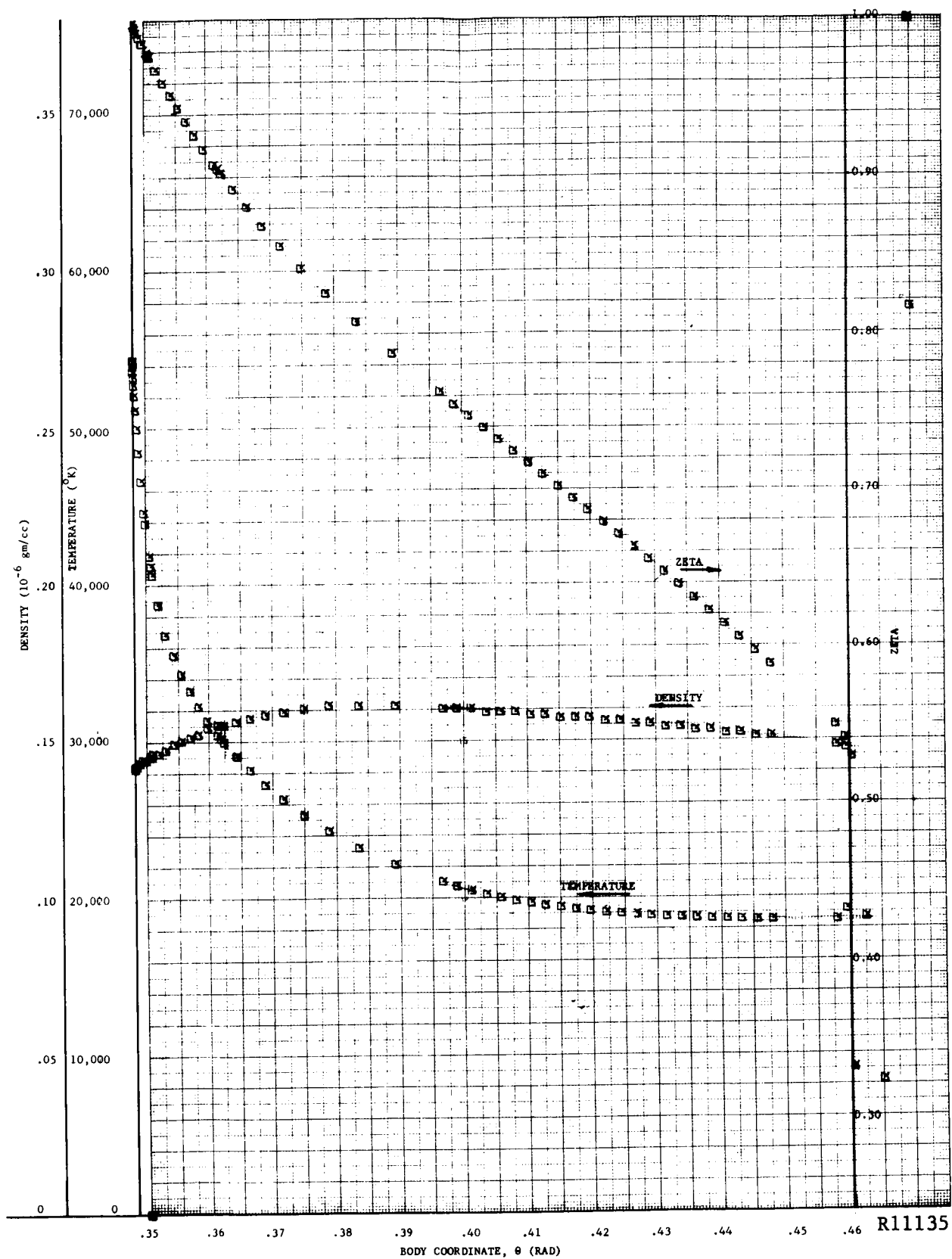
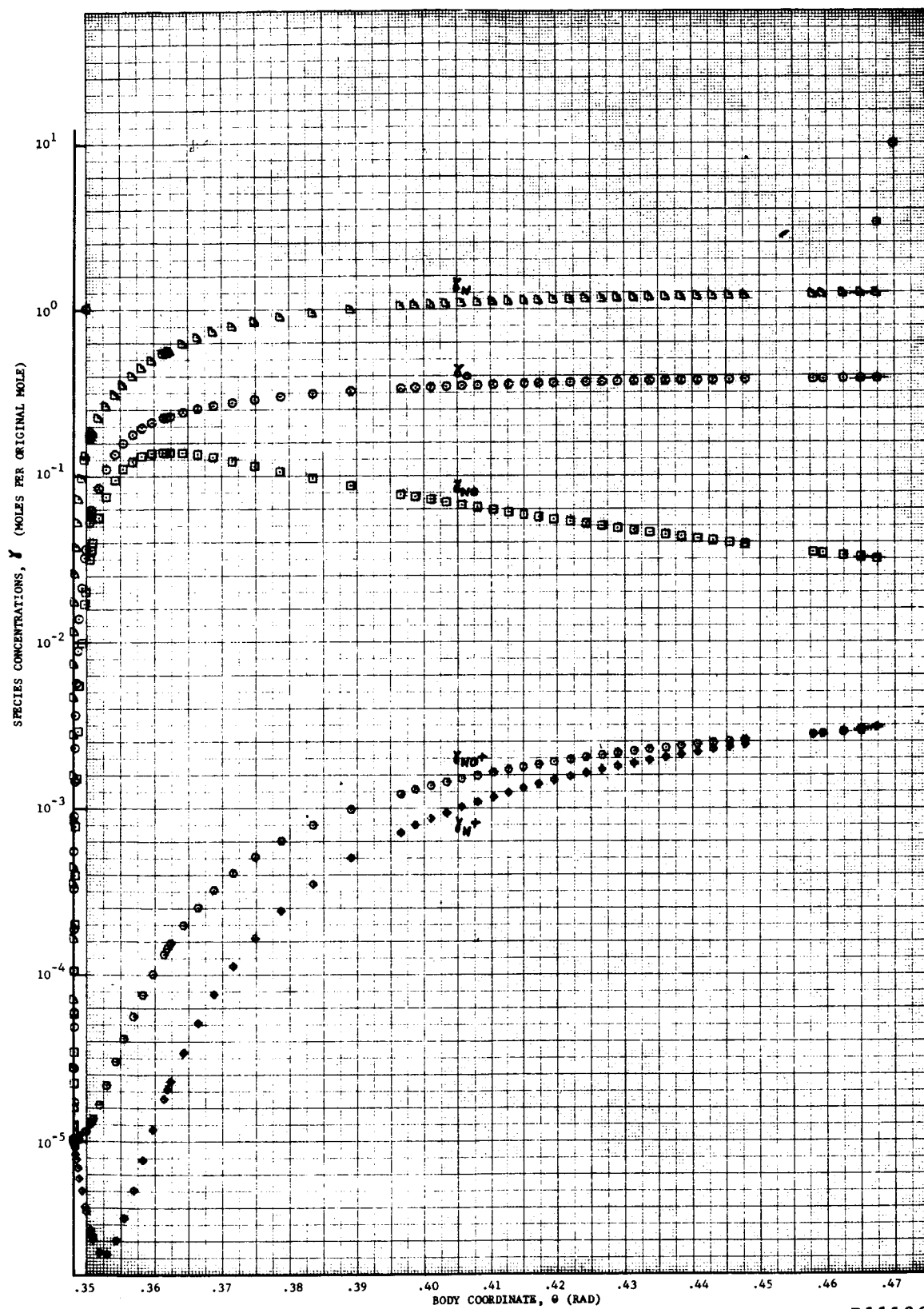


FIGURE 51. TEMPERATURE, DENSITY, AND LOCATION DISTRIBUTIONS ALONG THE $\theta_1 = .348$ STREAMLINE AS A FUNCTION OF θ , THE BODY COORDINATE (CASE III)



R11136

FIGURE 52. γ_N , γ_O , γ_{N^+} , γ_{NO} , γ_{NO^+} DISTRIBUTIONS ALONG THE $\theta_1 = .348$ STREAMLINE AS A FUNCTION OF θ , THE BODY COORDINATE (CASE III)

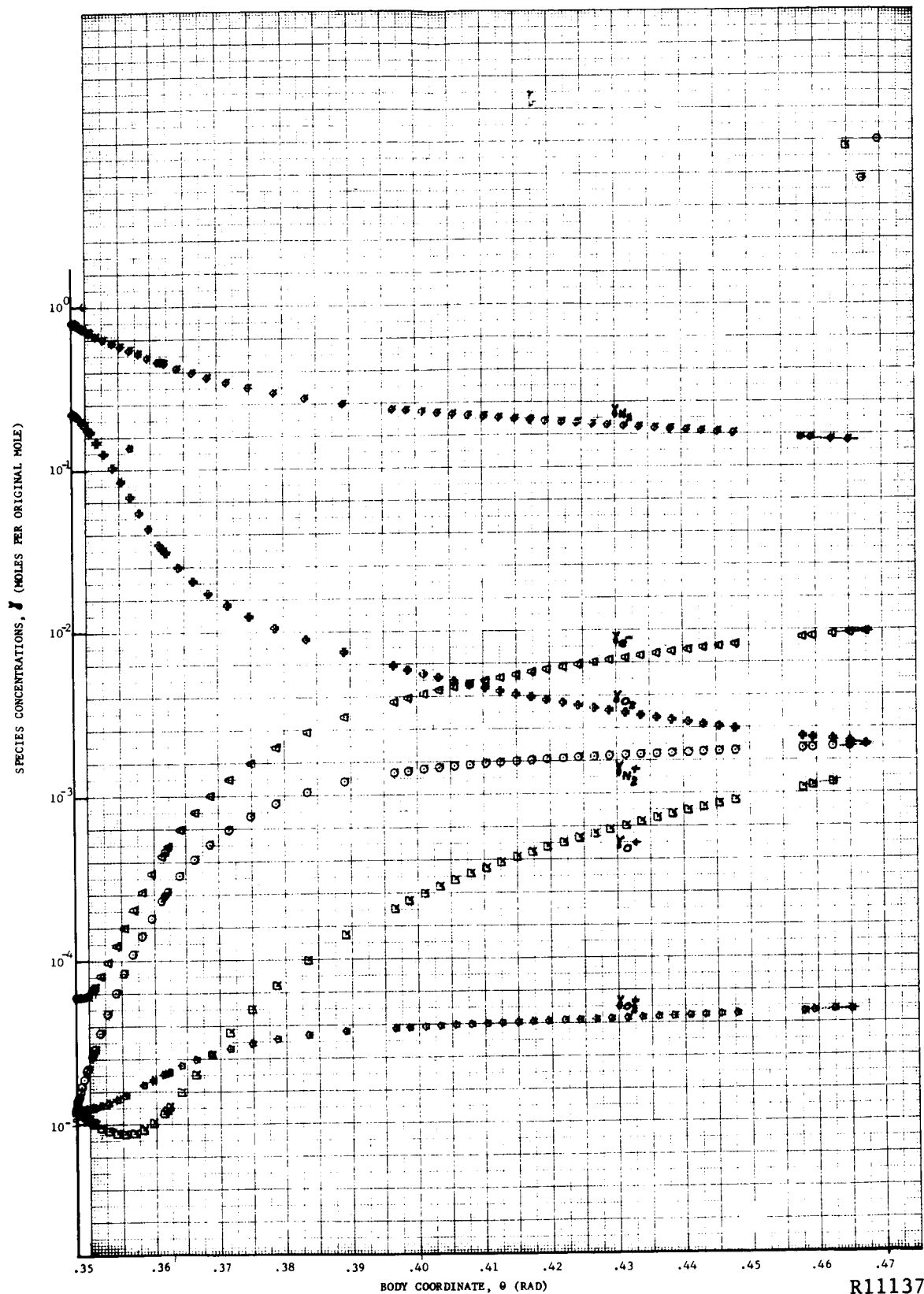


FIGURE 53. γ_{e^-} , γ_{N_2} , $\gamma_{N_2^+}$, γ_{O_2} , $\gamma_{O_2^+}$, γ_{O^+} DISTRIBUTIONS ALONG THE $\theta_1 = .348$ STREAMLINE AS A FUNCTION OF θ , THE BODY COORDINATE (CASE III)

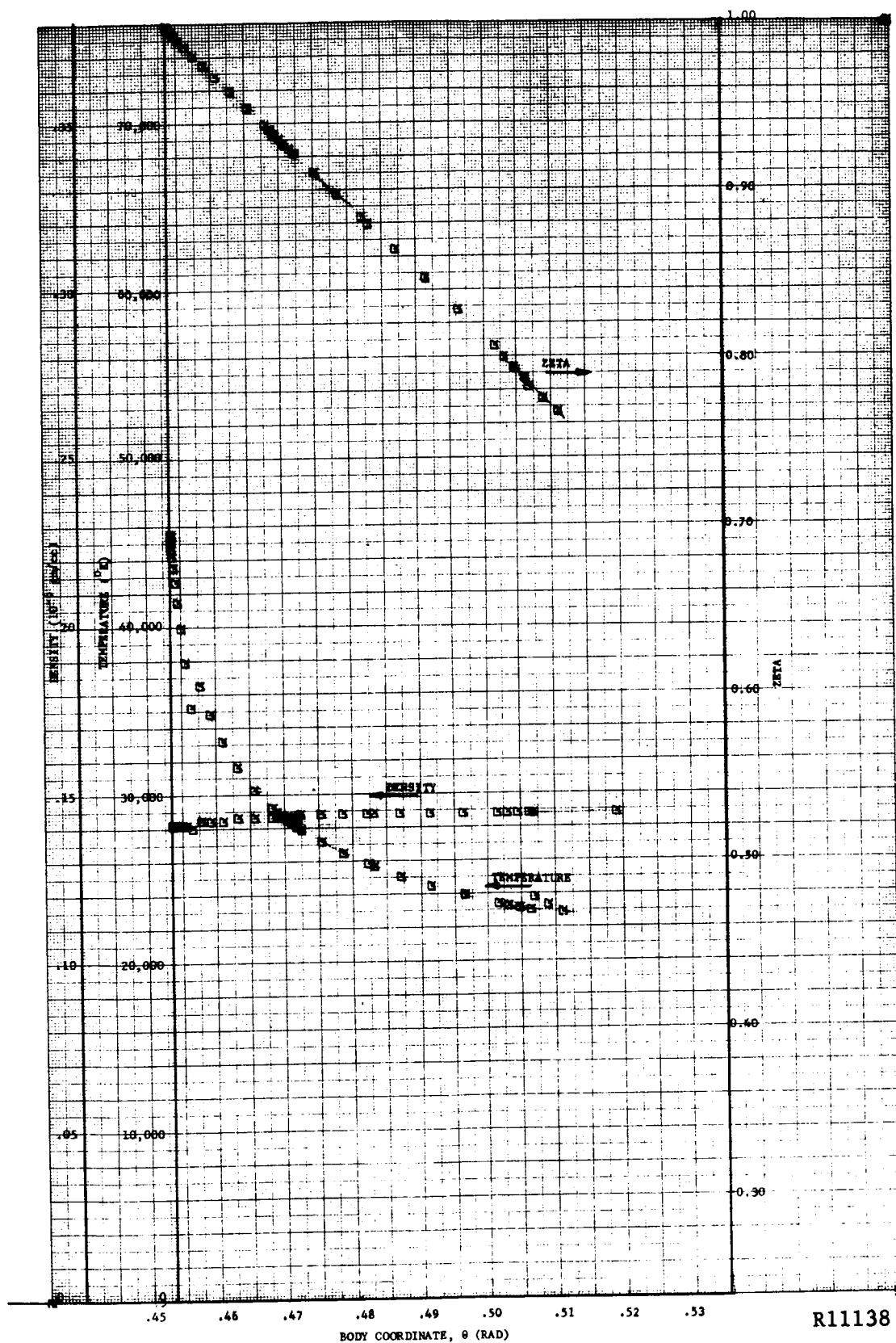


FIGURE 54. TEMPERATURE, DENSITY, AND LOCATION DISTRIBUTIONS ALONG THE $\theta_1 = .4535$ STREAMLINE AS A FUNCTION OF θ , THE BODY COORDINATE (CASE III)

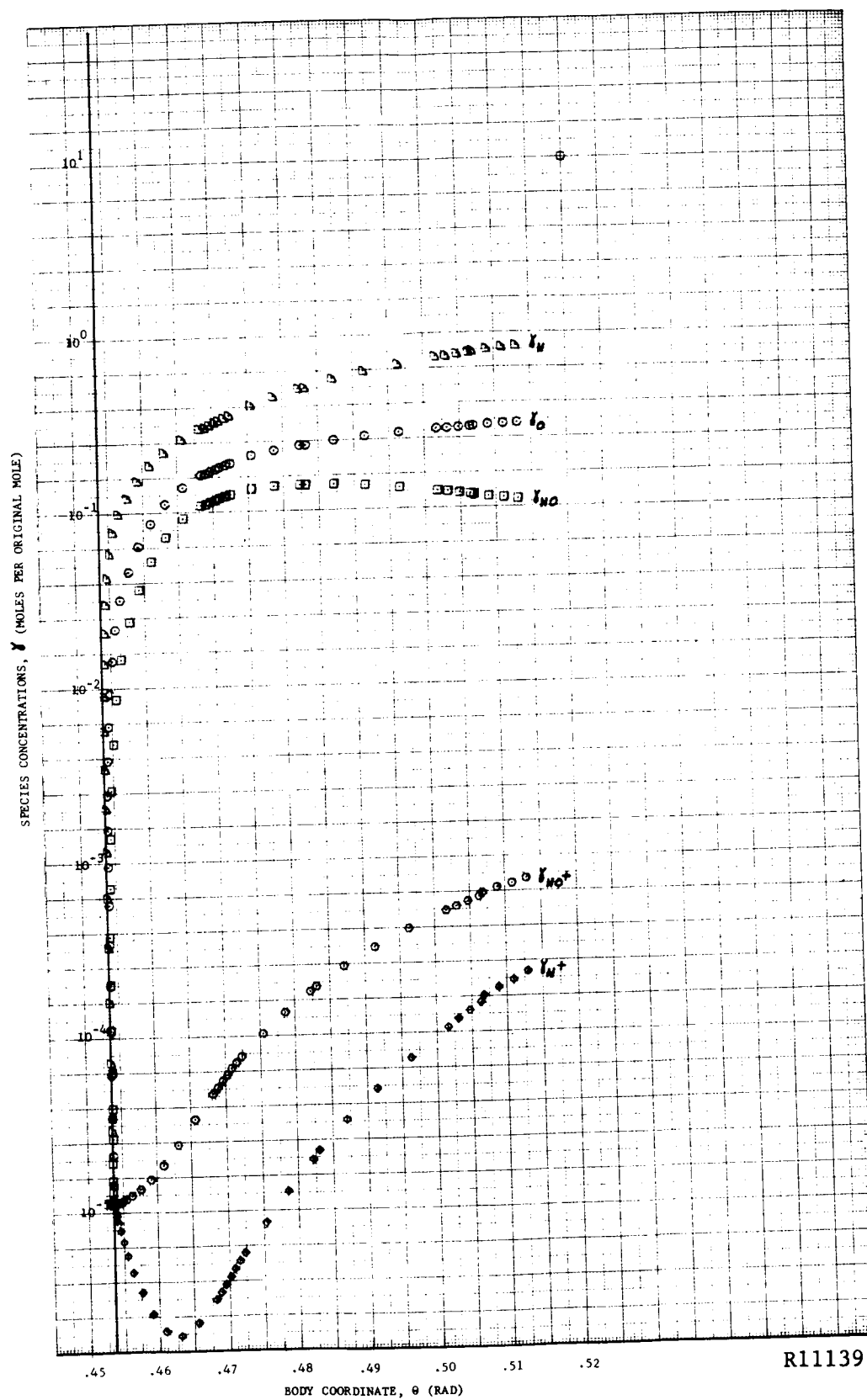


FIGURE 55. Y_N , Y_O , Y_{N+} , Y_{NO} , Y_{O+} DISTRIBUTIONS ALONG THE $\theta_1 = 0.4535$ STREAMLINE AS A FUNCTION OF θ , THE BODY COORDINATE (CASE III)

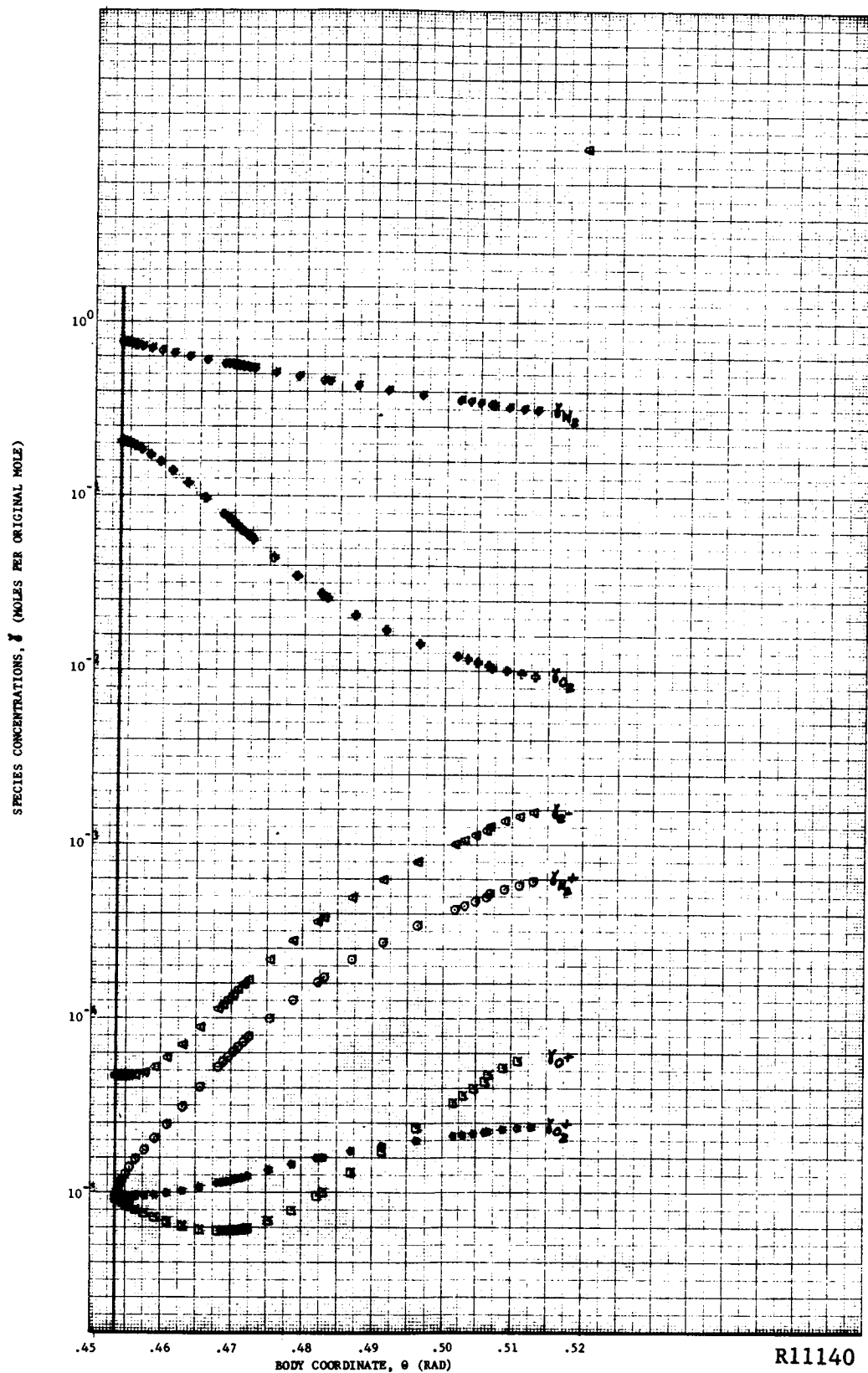
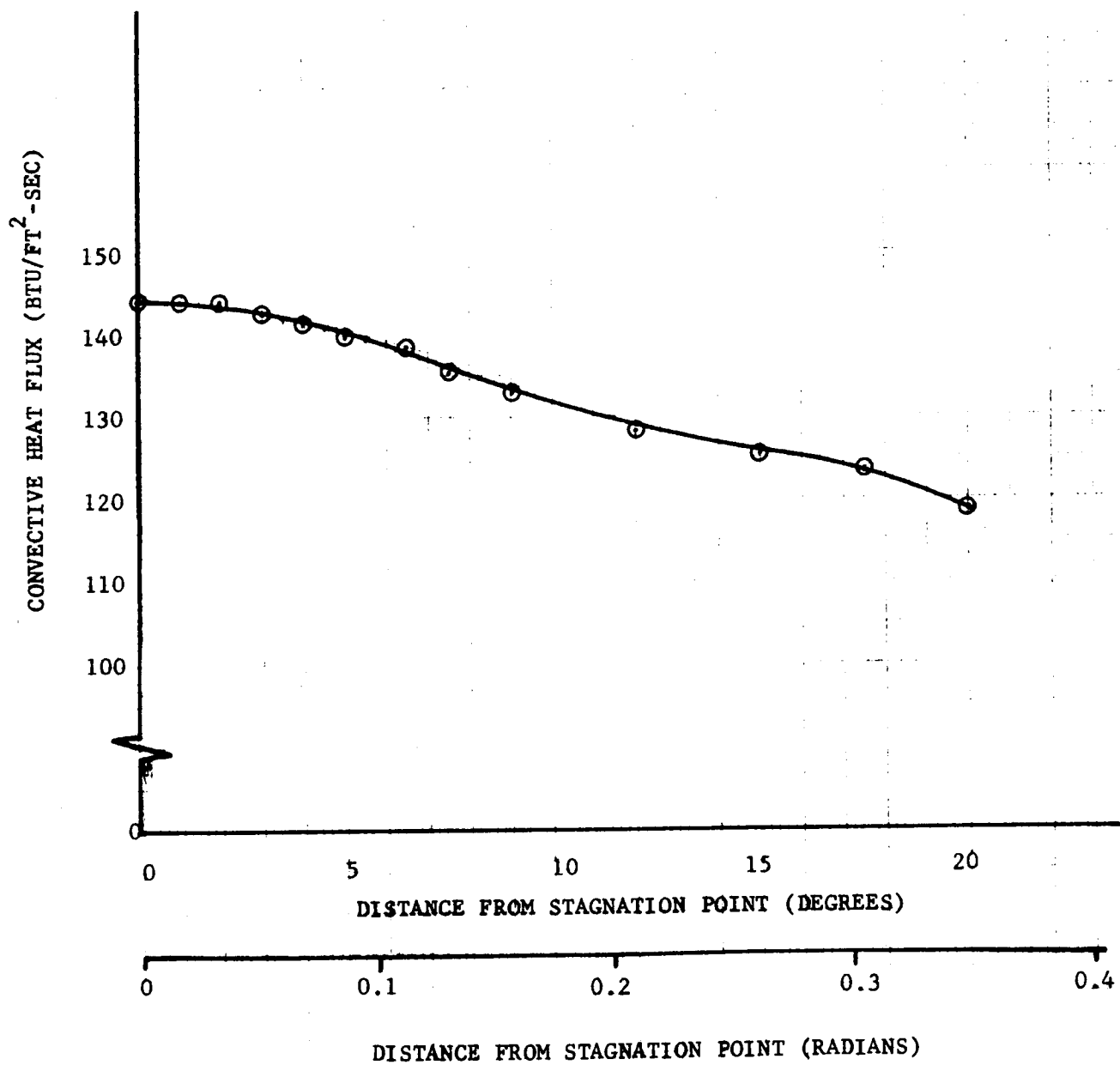
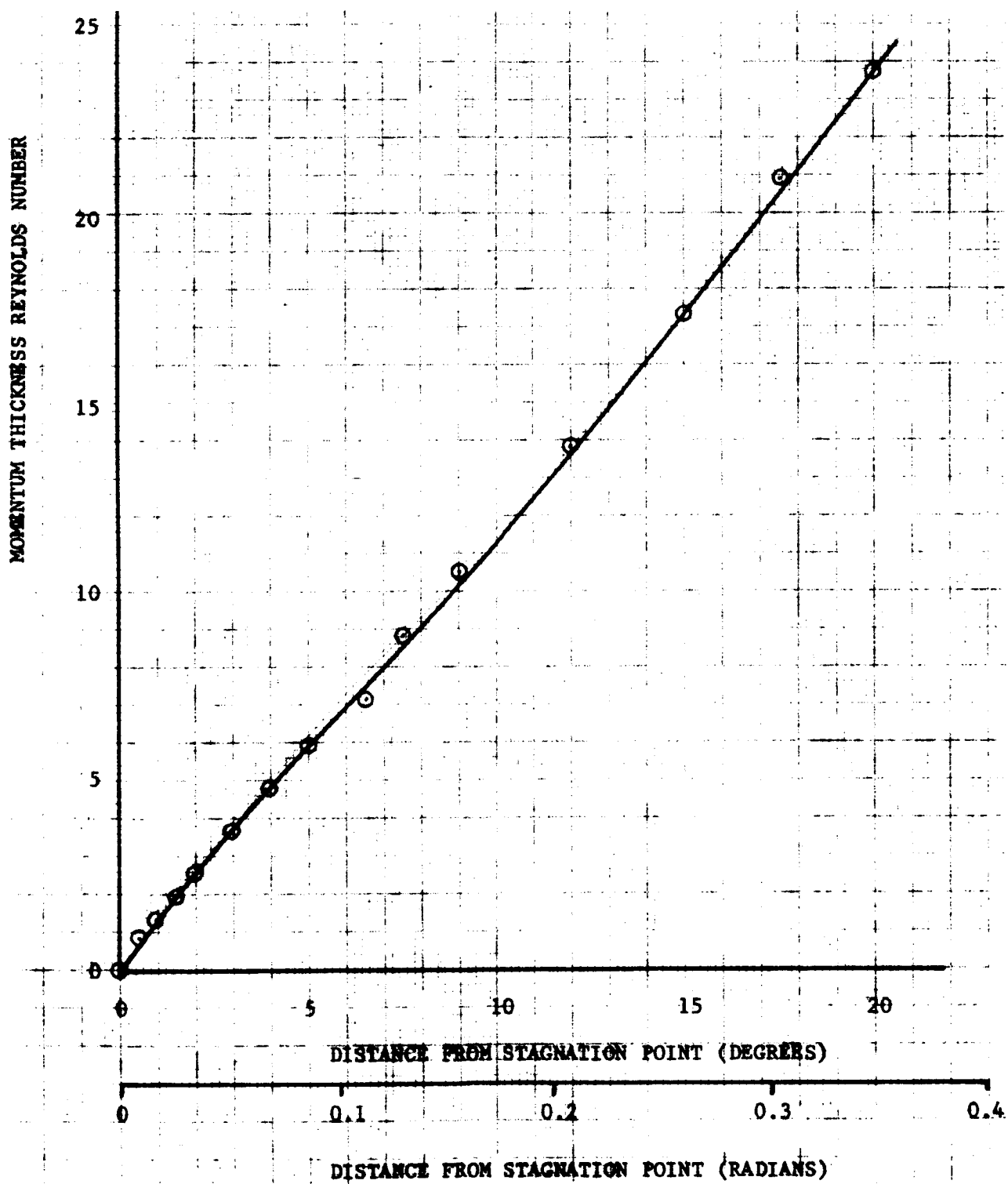


FIGURE 56. γ_{e^-} , γ_{N_2} , $\gamma_{N_2^+}$, γ_{O_2} , $\gamma_{O_2^+}$, γ_{O^+} DISTRIBUTIONS ALONG THE $\theta_1 = .4535$ STREAMLINE AS A FUNCTION OF θ , THE BODY COORDINATE (CASE III)



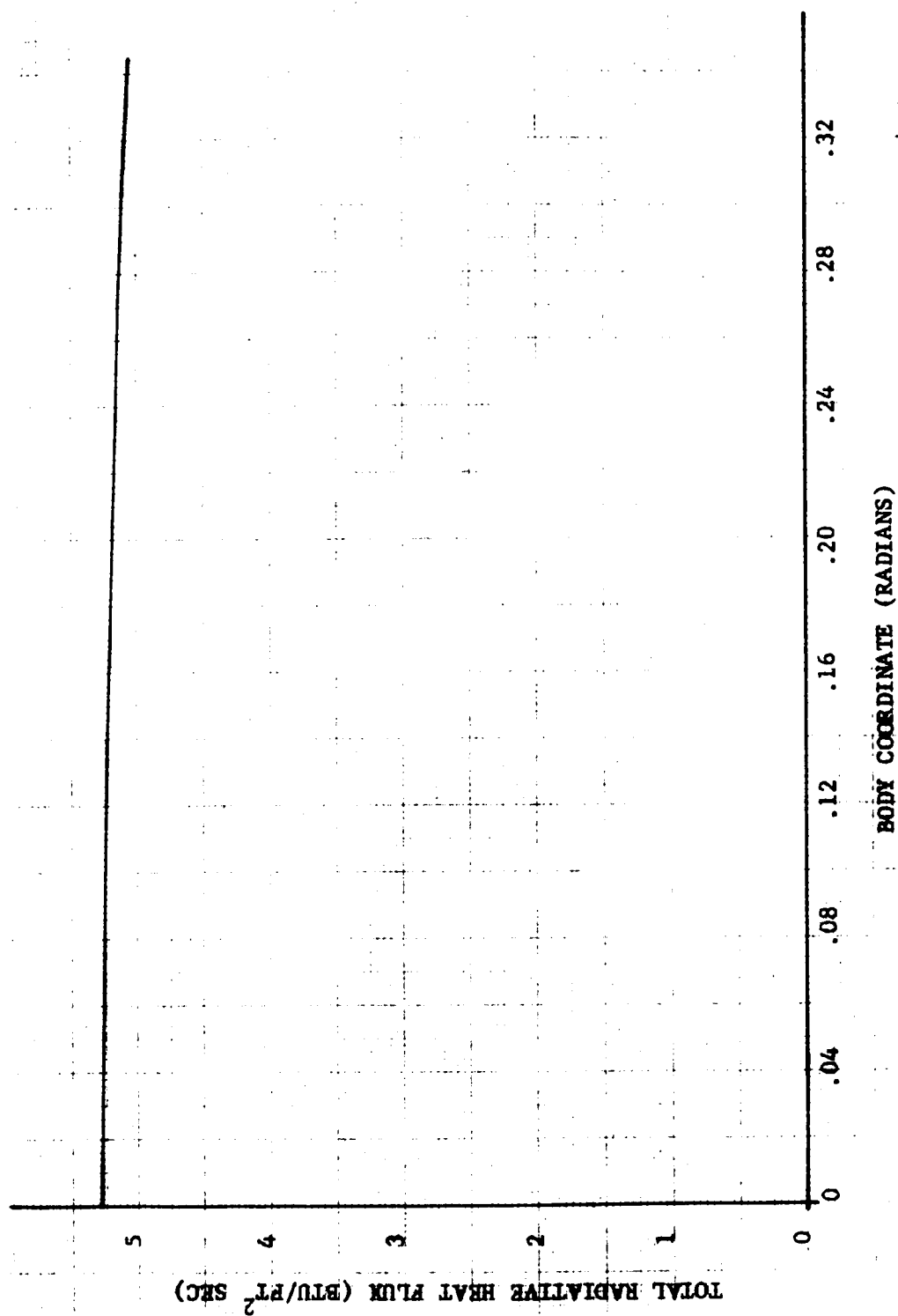
R11141

FIGURE 57. CONVECTIVE HEAT FLUX DISTRIBUTION ON BLUNT FACE, PROJECT FIRE, (CASE III)



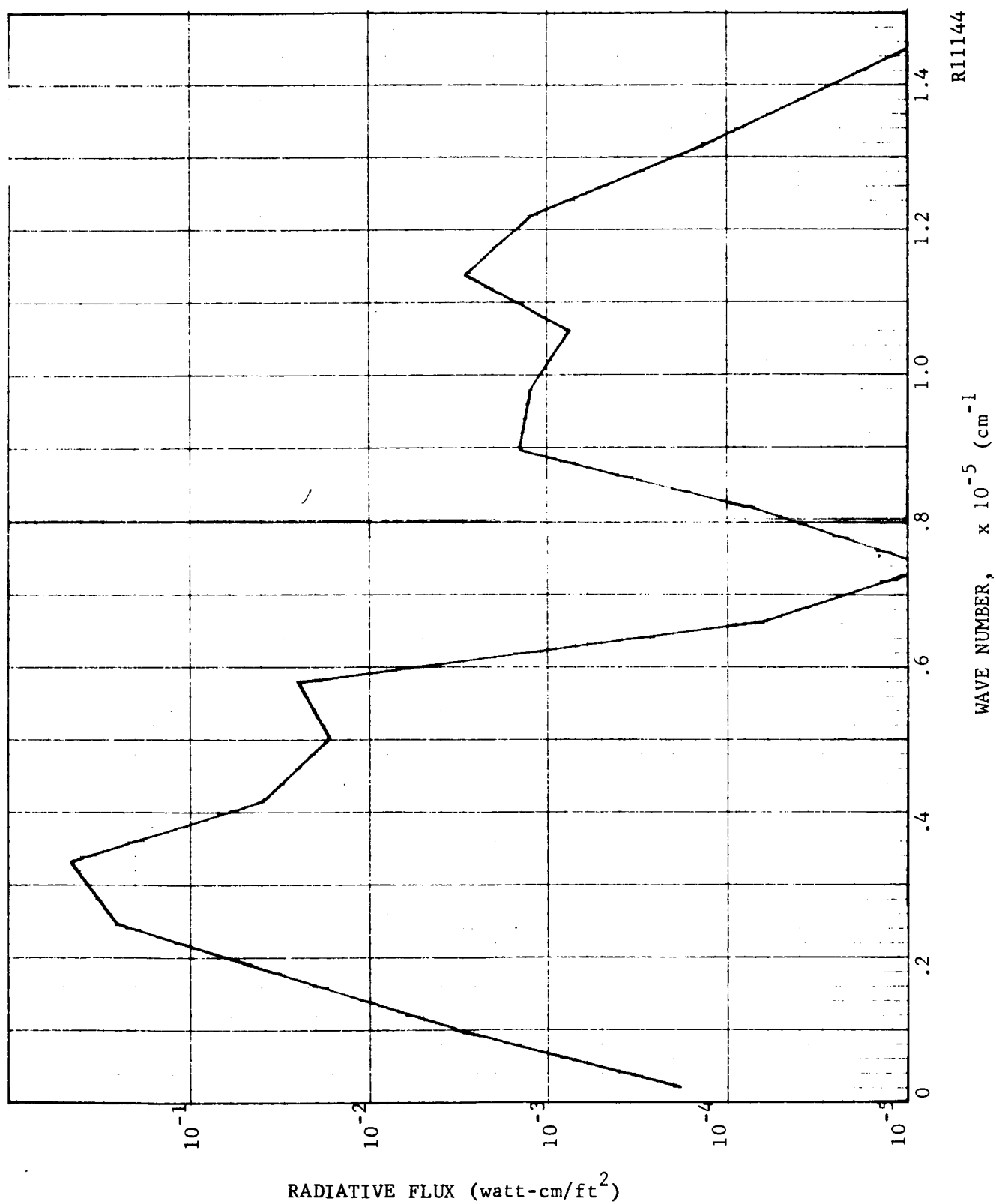
R11142

FIGURE 58. REYNOLDS NUMBER DISTRIBUTION ON BLUNT FACE, PROJECT FIRE, (CASE III)



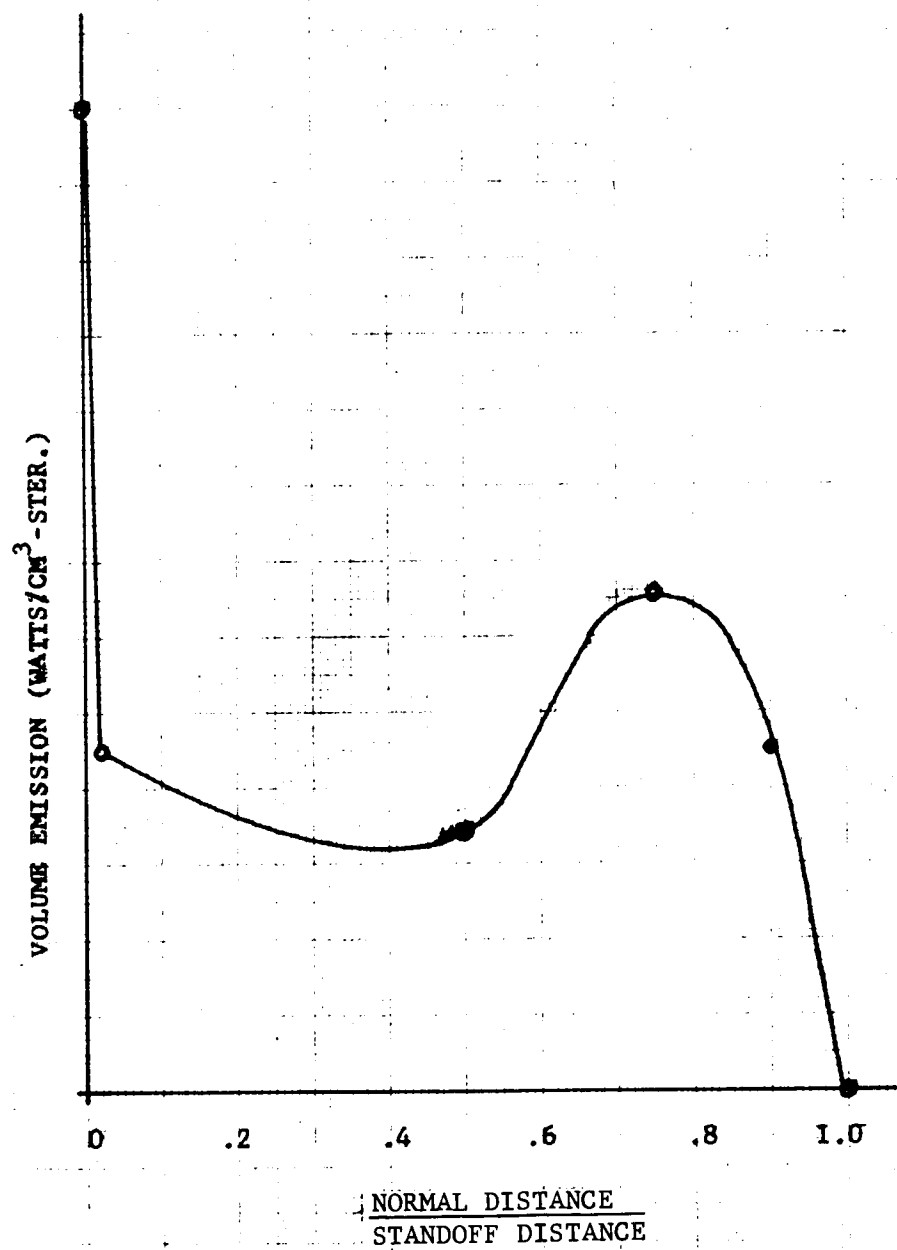
R11143

FIGURE 59. DISTRIBUTION OF RADIATIVE FLUX OVER RE-ENTRY BODY



R11144

FIGURE 60. SPECTRAL INTENSITY OF RADIATION TO STAGNATION POINT



R11152

FIGURE 61. NORMAL DISTRIBUTION OF VOLUME EMISSION FOR CASE III

PHILCO CORPORATION

A SUBSIDIARY OF *Ford Motor Company*

INTRA-COMPANY COMMUNICATION

AERONUTRONIC DIVISION

TO: S. Kravitz

FROM: R. Foster

SUBJECT: Thermodynamic Air Properties for the
Equilibrium Blunt Body Program

October 31, 1963

cc: S. Byron
W. Kuby
E. R. Buley

The approximate analytic expressions of the caloric and thermal equations of state for air required for the equilibrium blunt body have been formulated by Naumova in Ref. 1. The approximate relations give enthalpy, h (cal/gm) and density, ρ (gm/cm³) as functions of pressure, p (atm) ($.001 \text{ atm} \leq p \leq 1000 \text{ atm}$) and temperature, T ($^{\circ}\text{K}$) (to 16800°K). The relative error of the approximate functional relations to the tabular data of Predvoditelev (Ref. 2,3) is reported to be less than 1%.

The form of approximate functions are different for temperatures above and below 2000°K . In the temperature range between 2000°K and 16800°K , the polynomial relationships describing the properties are divided into several temperature intervals. The required functional relationships are as follows:

1. For air temperatures to 2000°K and pressures between $.001$ - 1000 atm ,

$$\rho = \frac{p}{T} R$$

$$h = T \left(U + \frac{V\theta}{e^{\theta} - 1} + \frac{W\phi}{e^{\phi} - 1} \right) + D(A\alpha + B\beta)$$

where

$$\alpha = \frac{2\eta}{\zeta + \sqrt{(1+\eta)^2 + a\eta(p/T)\exp(A/T)}}$$

$$\beta = \frac{1 - \eta^2}{\eta + \sqrt{1 + b(1 - \eta^2)(p/T)\exp(B/T)}}$$

$$\theta = \frac{3373}{T}$$

$$\phi = \frac{2256}{T}$$

$R = 0.3530$, $U = 0.2394$, $V = 0.06179$, $W = 0.01657$, $D = 0.06874$, $A = 59400$, $B = 113300$,
 $\eta = 0.21$, $\zeta = 0.79$, $a = 0.0101$, $b = 0.00252$

2. For air temperatures between $2000^\circ\text{K} \leq T \leq 16800^\circ\text{K}$ and pressures between $.001 \text{ atm} \leq p \leq 1000 \text{ atm}$,

$$\rho = (p/T) R(p, T) = (p/T) R_M \bar{R}$$

$$h = h_M \bar{h}$$

where

$$R_M = 1/\bar{D}(1 + \alpha + \beta + 2\gamma)$$

$$h_M = D \left[(4 + \alpha + \beta + 5\gamma)T + A\alpha + B\beta + 2C\gamma \right]$$

$$\gamma = 1/\sqrt{1 + c \frac{p}{T^{5/2}} \exp \frac{C}{T}},$$

$$\bar{D} = 2838$$

$$c = 1100000$$

$$C = 166500$$

and

$$\bar{R} = \sum_{m=0}^M \sum_{n=0}^N u_{mn} x^m y^n$$

$$\bar{h} = \sum_{m=0}^M \sum_{n=0}^N v_{mn} x^m y^n$$

$$x = (1/3) \ln p$$

The polynomial coefficients, the exponents and the appropriate value of $y(T)$ for a given temperature range are given in the following tables.

Values of u_{mn} at $2000 \leq T \leq 6000$, $y = -2 + 0.0005T$

$\begin{matrix} m \\ n \end{matrix}$	0	1	2	3	4	5
0	1.0153	0.0067	-0.0273	-0.0179	0.0167	0.0114
1	0.0171	0.0859	-0.0211	-0.1770	0.0075	0.0978
2	-0.0329	0.0363	0.1714	-0.0258	-0.1336	-0.0108
3	-0.0300	-0.1994	0.1620	0.4999	-0.1213	-0.3126
4	0.0260	-0.0448	-0.1321	0.0793	0.1080	-0.0265
5	0.0176	0.1218	-0.1243	-0.3145	0.1019	0.2055

Values of u_{mn} at $6000 \leq T \leq 12000$, $y = -3 + 0.0003333T$

$\begin{matrix} m \\ n \end{matrix}$	0	1	2	3	4	5
0	1.0067	0.0052	0.0043	0.0095	0.0085	0.0060
1	-0.0050	-0.0184	-0.0246	0.0368	0.0124	-0.0294
2	0.0062	0.0012	-0.0352	0.0035	0.0412	-0.0191
3	-0.0008	0.0618	0.0356	-0.2320	-0.0243	0.1674
4	-0.0058	-0.0040	0.0571	0.0105	-0.0696	-0.0053
5	0.0035	-0.0444	-0.0343	0.1619	0.0317	-0.1082

Values of u_{mn} at $12000 \leq T \leq 16800$, $y = -6 + 0.0004167T$

$\begin{matrix} m \\ n \end{matrix}$	0	1	2	3	4	5
0	1.0105	-0.0154	-0.0110	0.0371	0.0052	-0.0255
1	0.0098	-0.0015	-0.0419	0.0105	0.0348	-0.0095
2	0.0000	0.0280	-0.0072	-0.0930	0.0074	0.0719
3	-0.0025	0.0009	0.0220	-0.0078	-0.0256	0.0082
4	0.0014	-0.0076	-0.0012	0.0308	-0.0002	-0.0226
5	0.0001	0.0019	-0.0019	-0.0061	0.0012	0.0053

Values of v_{mn} at $2000 \leq T \leq 4000$, $y = -3 + 0.001T$

$\begin{matrix} m \\ n \end{matrix}$	0	1	2	3	4	5
0	1.0474	0.0482	-0.0452	-0.0142	0.0293	-0.0022
1	0.0039	0.1668	-0.0149	-0.2393	0.0501	0.1098
2	-0.0917	0.0416	0.2839	-0.2517	-0.1842	0.1841
3	-0.0113	-0.2471	0.2574	0.3980	-0.2921	-0.1513
4	0.0422	-0.0719	-0.1773	0.3054	0.1151	-0.2154
5	0.0141	0.1069	-0.1785	-0.1475	0.2047	0.0254

Values of v_{mn} at $4000 \leq T \leq 6000$, $y = -5 + 0.001T$

$\begin{matrix} m \\ n \end{matrix}$	0	1	2	3	4	5
0	1.0064	-0.0406	-0.0125	0.1517	0.0500	-0.0625
1	0.0169	0.0363	-0.1986	-0.2031	0.1541	0.1568
2	-0.0102	0.0953	0.0916	-0.1934	-0.0901	0.0655
3	-0.0153	-0.0578	0.1100	0.1604	-0.0779	-0.1081
4	0.0092	-0.0148	-0.0390	-0.0004	0.0281	0.0323
5	0.0018	0.0120	-0.0129	-0.0184	0.0035	0.0082

Values of v_{mn} at $6000 \leq T \leq 12000$, $y = -3 + 0.0003333T$

$n \backslash m$	0	1	2	3	4	5
0	1.0265	-0.0052	0.0028	0.0134	-0.0089	-0.0137
1	0.0383	0.0294	-0.0135	-0.0645	-0.0045	0.0653
2	-0.0125	0.0465	0.0322	-0.0197	-0.0559	0.0105
3	-0.0132	-0.1051	-0.0744	0.4375	0.0994	-0.3517
4	0.0133	0.0015	-0.0908	-0.0667	0.1219	0.0590
5	-0.0072	0.0822	0.1065	-0.3216	-0.1207	0.2351

Values of v_{mn} at $12000 \leq T \leq 16800$, $y = -6 + 0.0004167T$

$n \backslash m$	0	1	2	3	4	5
0	1.0330	0.1089	0.0369	-0.1403	-0.0193	0.0808
1	-0.0278	0.0068	0.1431	0.0145	-0.1080	-0.0150
2	-0.0013	-0.0703	-0.0015	0.2160	0.0051	-0.1577
3	0.0132	0.0080	-0.0720	-0.0229	0.0576	0.0128
4	-0.0004	0.0131	0.0078	-0.0530	-0.0032	0.0371
5	-0.0062	-0.0048	0.0217	0.0193	-0.0018	-0.0176

References

1. Naumova, I. N., "Approximation of Thermodynamic Functions of Air," Zh. Vychist. Matem. i Matem. Fiz., V. 1, No. 2, 1961, pp 295-300.
2. Mikhaylov, V. V., "Analytical Representation of Thermodynamic Functions of Dissociated Air," Collection of Papers, V. 28, 1960, p. 36-43.
3. Mikhaylov, V. V., "Analytical Representation of Thermodynamic Functions of Air," Collection of Papers, V. 31, 1960, p. 206-216.

PHILCO CORPORATION

A SUBSIDIARY OF *Ford Motor Company*.

INTRA-COMPANY COMMUNICATION

TO: R. Foster

AERONUTRONIC DIVISION

December 27, 1963

FROM: R. A. DuPuis

cc: W. Kuby

E. Buley

SUBJECT: Thermodynamic Air Properties for the
Equilibrium Blunt Body

S. Kravitz

The following equations represent the results of calculations made in response to a request from R. Foster.

The functional relations expressing the thermodynamic air properties (ρ , h , as functions of P and T) for the equilibrium blunt body program have been presented in a Philco Corporation Intracompany Communication, No. FFF-102 (Oct. 31, 1963) from R. Foster to S. Kravitz. In reference to these relationships, the quantities

$$\left(\frac{\partial \rho}{\partial P}\right)_T, \left(\frac{\partial \rho}{\partial T}\right)_P, \left(\frac{\partial h}{\partial P}\right)_T, \text{ and } \left(\frac{\partial h}{\partial T}\right)_P$$

have been calculated and are presented. In order to facilitate future computations, all partial derivatives have been expressed with respect to P only, i.e.

$$\left(\frac{\partial}{\partial P}\right)_T \text{ only.}$$

The results are as follows.

Case 1. For air temperature such that $2000^\circ\text{K} \leq T$, and for pressures between 0.001 and 1000 atmospheres,

$$(a) \quad \left(\frac{\partial \rho}{\partial P}\right)_T = \frac{R}{T}$$

$$(b) \quad \left(\frac{\partial \rho}{\partial T}\right)_P = -\frac{PR}{T^2} = -\frac{P}{T} \left(\frac{\partial \rho}{\partial P}\right)_T$$

$$(c) \quad \left(\frac{\partial h}{\partial P}\right)_T = D \left\{ A \left(\frac{\partial \alpha}{\partial P}\right)_T + B \left(\frac{\partial \beta}{\partial P}\right)_T \right\}$$

$$\text{where, } \left(\frac{\partial \alpha}{\partial P}\right)_T = -\frac{a\eta^2 \exp(A/T)}{T\sqrt{\alpha'} \left\{ \gamma + \sqrt{\alpha'} \right\}^2}$$

and,
$$\left(\frac{\partial \beta}{\partial P}\right)_T = - \frac{b(1-n^2)^2 \exp(B/T)}{2T \sqrt{\beta'} \{n + \sqrt{\beta'}\}^2}$$

and where,
$$\alpha' = \frac{2n}{\alpha} - \epsilon$$

and,
$$\sqrt{\beta'} = \frac{(1-n^2)}{\beta} - n.$$

Note that α' and β' are not derivatives, but are defined as

$$\alpha' = (1+n^2) + a n \left(\frac{P}{T}\right) \exp\left(\frac{A}{T}\right), \text{ and}$$

$$\beta' = 1 + b(1-n^2) \left(\frac{P}{T}\right) \exp\left(\frac{B}{T}\right).$$

$$\begin{aligned} \text{(d)} \quad \left(\frac{\partial h}{\partial T}\right)_P &= v\theta \left[\frac{\theta e^\theta - (e^\theta - 1)}{(e^\theta - 1)^2} \right] + w\phi \left[\frac{\phi e^\phi - (e^\phi - 1)}{(e^\phi - 1)^2} \right] \\ &+ \left[U + \frac{v\theta}{(e^\theta - 1)} + \frac{w\phi}{(e^\phi - 1)} \right] + D \left[A \left(\frac{\partial \alpha}{\partial T}\right)_P + B \left(\frac{\partial \beta}{\partial T}\right)_P \right] \end{aligned}$$

or, substituting for $\left(\frac{\partial \alpha}{\partial T}\right)_P$ etc., gives,

$$\begin{aligned} \left(\frac{\partial h}{\partial T}\right)_P &= v\theta \left[\frac{\theta e^\theta - (e^\theta - 1)}{(e^\theta - 1)^2} \right] + w\phi \left[\frac{\phi e^\phi - (e^\phi - 1)}{(e^\phi - 1)^2} \right] \\ &+ \left[U + \frac{v\theta}{(e^\theta - 1)} + \frac{w\phi}{(e^\phi - 1)} \right] - D \left[\frac{AP(A+T)}{T^2} \left(\frac{\partial \alpha}{\partial P}\right)_T + \frac{BP(B+T)}{T^2} \left(\frac{\partial \beta}{\partial P}\right)_T \right] \end{aligned}$$

since,
$$\left(\frac{\partial \alpha}{\partial T}\right)_P = - \frac{P(A+T)}{T^2} \left(\frac{\partial \alpha}{\partial P}\right)_T$$

and,
$$\left(\frac{\partial \beta}{\partial T}\right)_P = - \frac{P(B+T)}{T^2} \left(\frac{\partial \beta}{\partial P}\right)_T.$$

The numerical values for all of the constants shown are presented in the aforementioned memorandum.

Case 2. For air temperatures in the range $2000^\circ\text{K} \leq T \leq 16,800^\circ\text{K}$, and for pressures ranging from 0.001 atmospheres to 1000 atmospheres.

(a)
$$\left(\frac{\partial \rho}{\partial P}\right)_T = \frac{P}{T} \left\{ R_M \sum_{m=0}^M \sum_{n=0}^N u_{mn} y^n \frac{m-1}{3P} \textcircled{a} - \bar{R} R_M^2 D \left[\left(\frac{\partial \alpha}{\partial P}\right)_T + \left(\frac{\partial \beta}{\partial P}\right)_T + 2 \left(\frac{\partial \gamma}{\partial P}\right)_T \right] \right\} + \frac{R_M \bar{R}}{T}$$

$\textcircled{a} = .43429448$

where the expressions for $\left(\frac{\partial \alpha}{\partial P}\right)_T$ and $\left(\frac{\partial \beta}{\partial P}\right)_T$ are the same as those shown previously, and

$$\left(\frac{\partial \gamma}{\partial P}\right)_T = - \frac{\gamma(1-\gamma^2)}{2P}.$$

(b)
$$\left(\frac{\partial \rho}{\partial T}\right)_P = \frac{P}{T} \left\{ R_M \sum_{m=0}^M \sum_{n=0}^N u_{mn} x^m y^{n-1} K - \bar{R} R_M^2 D \left[\left(\frac{\partial \alpha}{\partial T}\right)_P + \left(\frac{\partial \beta}{\partial T}\right)_P + 2 \left(\frac{\partial \gamma}{\partial T}\right)_P \right] \right\} - \frac{R_M \bar{R} P}{T^2},$$

which, after substitution for $\left(\frac{\partial}{\partial T}(\alpha, \beta, \gamma)\right)_P$ gives,

$$\begin{aligned} \left(\frac{\partial \rho}{\partial T}\right)_P = \frac{P}{T} \left\{ R_M \sum_{m=0}^M \sum_{n=0}^N u_{mn} x^m y^{n-1} K + \bar{R} R_M^2 D \left[\frac{P(A+T)}{T^2} \left(\frac{\partial \alpha}{\partial P}\right)_T + \frac{P(B+T)}{T^2} \left(\frac{\partial \beta}{\partial P}\right)_T \right. \right. \\ \left. \left. + \frac{P}{T} \left(5 + 2 \frac{C}{T}\right) \left(\frac{\partial \gamma}{\partial P}\right)_T \right] - \frac{R_M \bar{R}}{T} \right\} \end{aligned}$$

where K is a constant which is a function of the temperature under consideration. K is as follows:

for $2000^\circ\text{K} \leq T \leq 6000^\circ\text{K}$, $K = 0.0005$;

for $6000^\circ\text{K} \leq T \leq 12,000^\circ\text{K}$, $K = 0.0003333$;

and for $12,000^\circ\text{K} \leq T \leq 16,800 \text{ K} = 0.0004167$. $\textcircled{a} = .43429448$

$$(c) \left(\frac{\partial h}{\partial P} \right)_T = h_M \sum_{m=0}^M \sum_{n=0}^N v_{mn} y^n \frac{mx^{m-1}}{3P} \textcircled{a} + \bar{h}R \left\{ T \left[\left(\frac{\partial \alpha}{\partial P} \right)_T + \left(\frac{\partial \beta}{\partial P} \right)_T + 5 \left(\frac{\partial \gamma}{\partial P} \right)_T \right] + A \left(\frac{\partial \alpha}{\partial P} \right)_T + B \left(\frac{\partial \beta}{\partial P} \right)_T + 2C \left(\frac{\partial \gamma}{\partial P} \right)_T \right\} \text{ and } \left(\frac{\partial}{\partial P} (\alpha, \beta, \gamma) \right)_T$$

are again as previously defined.

$$d) \left(\frac{\partial h}{\partial T} \right)_P = h_M \sum_{m=0}^M \sum_{n=0}^N v_{mn} x^m y^{n-1} K + \bar{h}R \left\{ T \left[\left(\frac{\partial \alpha}{\partial T} \right)_P + \left(\frac{\partial \beta}{\partial T} \right)_P + 5 \left(\frac{\partial \gamma}{\partial T} \right)_P \right] + A \left(\frac{\partial \alpha}{\partial T} \right)_P + B \left(\frac{\partial \beta}{\partial T} \right)_P + 2C \left(\frac{\partial \gamma}{\partial T} \right)_P + (4 + \alpha + \beta + 5\gamma) \right\}$$

After the appropriate substitution for $\left(\frac{\partial}{\partial T} (\alpha, \beta, \gamma) \right)_P$ has been made, we have,

$$\begin{aligned} \left(\frac{\partial h}{\partial T} \right)_P = & h_M \sum_{m=0}^M \sum_{n=0}^N v_{mn} x^m y^{n-1} K - \bar{h}R \left\{ T \left[\frac{P(A+T)}{T^2} \left(\frac{\partial \alpha}{\partial P} \right)_T + \right. \right. \\ & + \frac{P(B+T)}{T^2} \left(\frac{\partial \beta}{\partial P} \right)_T + \frac{5P}{2T} \left(5 + 2 \frac{C}{T} \right) \left(\frac{\partial \gamma}{\partial P} \right)_T \left. \right] + \frac{AP(A+T)}{T^2} \left(\frac{\partial \alpha}{\partial P} \right)_T + \frac{BP(B+T)}{T^2} \left(\frac{\partial \beta}{\partial P} \right)_T \\ & \left. + \frac{CP}{T} \left(5 + 2 \frac{C}{T} \right) \left(\frac{\partial \gamma}{\partial P} \right)_T - (4 + \alpha + \beta + 5\gamma) \right\} \end{aligned}$$

where K is the same temperature dependent constant as that previously defined.

PHILCO CORPORATION

A SUBSIDIARY OF *Ford Motor Company*

INTRA-COMPANY COMMUNICATION

TO: E. Buley

AERONUTRONIC DIVISION

March 5, 1964

FROM: R. Foster

cc: W. Kuby
M. Holt
S. Kravitz
D. PiperSUBJECT: Equilibrium Properties behind a
Normal Shock and at the Stagnation
Point of a Blunt Body Using Naumova's¹
Thermodynamic Property Expressions1. Properties behind the Normal Shock

The equilibrium properties behind a normal shock will be obtained by an iterative procedure in which ρ_1 is assumed and p_1 and h_1 are calculated from the normal shock momentum and energy equation. The initial value of ρ_1 will always be assumed to be 6.0 (valid for hypersonic flow) and subscript ∞ quantities are given as input. The equations for calculating p_1 and h_1 are:

$$\bar{p}_1 (\text{atm}) = \bar{p}_\infty (\text{atm}) + \frac{\bar{\rho}_\infty (\text{lb/ft}^3) \bar{q}_\infty^2 (\text{ft/sec})}{68080.184} \left(1 - \frac{1}{\rho_1}\right) \quad (1)$$

$$\bar{h}_1 (\text{cal/gm}) = \frac{\bar{q}_\infty^2}{9.010876 \times 10^4} \left[\frac{1}{\left(\frac{\bar{\rho}_\infty}{\rho_1}\right)^2} - \left(\frac{1}{\rho_1}\right)^2 \right] \quad (2)$$

where

$$\rho_1 = \frac{\bar{\rho}_1 (62.43)}{\bar{\rho}_\infty} \quad (3)$$

Ideally, the calculated \bar{p}_1 and \bar{h}_1 would then be directly inputted into thermodynamic property functions and a new estimate of ρ_1 would be obtained. This new ρ_1 would then be substituted into the normal shock momentum and energy equations and the procedure would be repeated until the iteration gives a ρ_1 consistent to +0.1%. Unfortunately it is not possible to input \bar{h}_1 directly into Naumova's equations since \bar{p} and \bar{T} are the independent variables in these functions. Therefore, given h and p , it is necessary to iterate for T from the equation

$$\bar{h} = \bar{h}(\bar{p}, \bar{T})^* \quad (4)$$

This iteration should be accomplished by bracketing the required \bar{T} by upper and lower bounds and converging to the final answer by a quadratic interpolation. These upper and lower bounds on T , if necessary, can be supplied as input.

¹Superscript numbers refer to references on the last page.

*The functions have been programmed and checked out. See S. Kravitz for the program call sequence.

Once the \bar{T} corresponding to the given \bar{h} and \bar{p} is found, \bar{T} and \bar{p} are substituted into the given equation

$$\bar{\rho} = \bar{\rho}(\bar{p}, \bar{T})^* \quad (5)$$

This new $\bar{\rho}_1$ is substituted into equation (3) to obtain ρ_1 and ρ_1 is in turn substituted into equations (1) and (2) and the procedure is repeated until ρ_1 is consistent to $\pm 0.1\%$.

2. Properties at the Stagnation Point

At the stagnation point, the known thermodynamic properties are entropy ($S_0 = S_1$) and enthalpy, h_0 , where

$$S(\text{cal/gm}^\circ\text{K}) = 1.735 + \int_{p=1(\text{atm})}^P \left(\frac{1}{T} \left[\frac{\partial h}{\partial p} - \frac{1}{\rho} \right]_{T=273.16} dp + \int_{T=273.16}^T \left(\frac{1}{T} \frac{\partial h}{\partial T} \right)_P dT \quad (6)$$

and $K = 41.31506$

where

$$S_\infty = 1.73500 + \int_1^{P_\infty} \left(\frac{1}{T} \left[\frac{\partial h}{\partial p} - \frac{1}{\rho} \right]_{T_\infty} dp + \int_{273.16}^{T_\infty} \left(\frac{1}{T} \frac{\partial h}{\partial T} \right)_{P=1} dT \quad (7)$$

$$S_1 = S_0 = 1.735 + \int_{p=1(\text{atm})}^{P_1} \left(\frac{1}{T} \frac{\partial h}{\partial p} - \frac{1}{\rho} \right)_{T=273.16} dp + \int_{T=273.16}^{T_1} \left(\frac{1}{T} \frac{\partial h}{\partial T} \right)_P dT \quad (8)$$

and

$$h_0(\text{cal/gm}) = \frac{\bar{q}_m^2}{9.010876 \times 10^4} \quad (9)$$

The problem is to find the values of \bar{p} and \bar{T} that correspond to the given \bar{h}_0 and \bar{S}_0 . The first step in the solution is to bracket the actual \bar{p}_0 and \bar{T}_0 with upper and lower bounds. p_0 will be slightly greater than p_1 and for hypersonic problems, $p_0 \leq 1.2 p_1$ and hence an upper and lower bound on p_0 can be established. An upper and lower bound for \bar{T}_0 corresponding to the p_0 bounds can be obtained from the equation

$$h_0 = h_0(\bar{p}, \bar{T})$$

in a manner similar to the normal shock calculation discussed in Section 1.

*The functions have been programmed and checked out. See S. Kravitz for the program call sequence.

After obtaining the \bar{p}_0 and \bar{T}_0 bounds, it is necessary to devise a convergence scheme to find the actual temperature (T_a) and pressure (p_a) at the stagnation point. There are several possible convergence schemes that might be utilized and one scheme suggested by E. Buley is noted here.

Find the mean T and p from their upper and lower bounds using these values as a first guess for T_q and p_q . These values are substituted in the following Taylor series for S and h in which only first order terms are retained.

$$S_0 = S(T_q, p_q) + \frac{\partial S}{\partial p}(T_q, p_q) [p_a - p_q] + \frac{\partial S}{\partial T}(T_q, p_q) [T_a - T_q]$$

$$h_0 = h(T_q, p_q) + \frac{\partial h}{\partial p}(T_q, p_q) [p_a - p_q] + \frac{\partial h}{\partial T}(T_q, p_q) [T_a - T_q]$$

where S_0 and h_0 are given and $S(T_q, p_q)$ and $\frac{\partial S}{\partial p}$, $\frac{\partial S}{\partial T}$ are obtained from (6)

and h , $\frac{\partial h}{\partial p}$, $\frac{\partial h}{\partial T}$ are already programmed.*

Therefore we have two linear simultaneous equations for T_a and p_a which can be solved simultaneously to obtain the next guess for pressure and temperature. The iteration procedure is repeated until p_0 and T_0 are consistent to $\pm 0.1\%$.

References

1. I. N. Naumova, "An Approximation to the Thermodynamic Functions of Air," J. of Computing Mathematics and Mathematical Physics, USSR, 1,2, March-April, 1962.

*The functions have been programmed and checked out. See S. Kravitz for the program call sequence.